Leicester School of Pharmacy

De Montfort University

Leicester

Development of a new actinometric method for polychromatic light irradiation.

Application to photochromes, drugs and stilbenoids

A thesis submitted in partial fulfilment of the requirements for the degree of Doctor of Philosophy (PhD) to be awarded by De Montfort University

Mohammed Ahmed Alqarni

December 2019

Declarations

This thesis contains original work undertaken by the author for the award of Doctor of Philosophy at De Montfort University (Leicester), except where due reference is made to other authors.

No part of the material presented in this thesis has been submitted for any other academic degree or qualification in this or any other higher education institution.

Abstract

The photostability data of chemical species is usually described based upon models using equations applicable to standard zero-, first- or second-order kinetics (classical thermal order kinetics) and other such models. These thermal order kinetic models have certain limitations, however, regarding parameter representation of the photoreaction and the reproducibility of associated results. The other models available in the literature use approximation and expansion methods to solve the photochemical rate law but are unfortunately unable to provide robust models to describe the photochemical reaction itself.

This research resolves many of the drawbacks typically encountered within the photokinetics domain by improving upon an existing model and designing new models that describe photochemical reactions in solution. These models are the Φ- and η-order kinetics. The former reduces the number of elucidation method steps whilst the latter is designed to describe photochemical reactions under irradiation by polychromatic light for three chosen AB reaction systems.

In the development of the above-mentioned methodologies, this research selects species based on their photochemical reaction mechanisms to study their photodegradation, starting from a simple to a complex mechanism. These compounds are: C-DAE for unimolecular AB $(1\Phi)_{\varepsilon_{B=0}}$, nifedipine and dacarbazine for unimolecular AB$(1\Phi)_{\varepsilon_{B\neq 0}}$, and the stilbenoids group, axibinib and O-DAE for photoreversible AB (2Φ) reactions.

The results obtained in this research show that the Φ-order kinetics approach offers a good description of the photodegradation of these species under continuous monochromatic irradiation. It has been established that both the forward ($\Phi_{A\rightarrow B}^{\lambda_{irr}}$) and reverse ($\Phi_{B\rightarrow A}^{\lambda_{irr}}$) quantum yields increased with increasing irradiation wavelength according to a sigmoid pattern. Additionally, this study presents a methodology to calculate the $\beta_{\lambda_{irr}}$ factor, which is used to obtain the photoreactivity of the species, in a method that offers a much simpler and faster approach to this determination than

traditional methods. The stilbenoids group shows higher photoreactivity than the other species studied according to the $\beta_{\lambda_{irr}}$ factor ranking scale.

Other methods were designed to overcome the drawbacks to describing a photochemical reaction under irradiation by polychromatic light. The validity of the new mathematical models (Φ- and η-order) were verified using simulation studies through numerical integration methods (NIMs) to generate simulated cases for each photochemical reaction system considered. In addition, the Φ- and η-order models were examined and validated using experimental HPLC and spectrophotometry photodegradation data obtained for different species under irradiation by polychromatic light. Results obtained in this study confirm the model's predictions, as both photoreaction rate constant and initial reaction velocity (υ_0) were observed to remain constant with variable initial concentrations of the species considered.

Furthermore, actinometric methods were developed and applied to study the photochemical reaction of species in solution under irradiation by monochromatic and polychromatic light. The former and latter were developed to determine the light intensity of unknown light sources. Monochromatic light has a much smaller wavelength distribution than polychromatic, which are determined based on the associated $\beta_{\lambda_{irr}}$ factors. The results show that each method can be used independently to quantify the light intensities from different light sources.

Acknowledgement

I would like to thank Allah for supporting me with the power and patience to conduct and complete this research.

I would also like to express my sincere gratitude and thanks to my supervisors Dr. Mounir Maafi for the continues support of my PhD research, for his patience, motivation, and immense knowledge. His guidance helped me in all time of research and writing of the thesis. I always believed that this work would not have been possible without him.

Thank you to Dr Michael Goodman, my second supervisor, for his time and commitment.

I would also like to express my special appreciation and thanks to Unmesh Desai and Nasmin Juma, for always being available when I need them. Their academic support and personal cheering are greatly appreciated.

A special thanks to Taif University in Saudi Arabia, Saudi Ministry of Education and the Saudi Arabian Cultural Bureau in London for sponsoring my PhD project.

Also, I find no words that can adequately express my love and respect to my father, mother, sisters, brothers and friends for their encouragement, support and prayers.

Finally, my beloved wife, I would like to express my gratitude to your love and support in taking care of our kids, Seba, Lama and Lana. Your support was always the source of my success. This research would not have been possible without your love, care and your permanent support. Sharing my life with you is a real joy.

Journal publications and awarded

A list of publications from this PhD:

Maafi, M., and Al-Qarni, M. A. (2018). Φ-order spectrophotokinetic characterisation and quantification of trans-cis oxyresveratrol reactivity, photodegradation and actinometry. Spectrochimica Acta Part A: Molecular and Biomolecular Spectroscopy, 188, 64-71.

Maafi, M., and Al-Qarni, M. A. (2019). Dependence of Pinosylvin photochemical quantum yield on excitation wavelength. Manuscript under consideration.

A list of awarded from this PhD:

Best poster of the conference Award at 2nd International Conference on Pharmaceutical Chemistry during October 02-04, 2017 Barcelona, Spain

Glossary and abbreviations

STIL	Stilbene
PINO	Pinosylvin
RVT	Resveratrol
ORVT	Oxyresveratrol
PTERO	Pterostilbene
NIF	Nifedipine
DBZ	Dacarbazine
AXI	Axitinib
DAE	1,2-Bis[2-methylbenzo[b]thiophen-3-yl]-3,3,4,4,5,5-hexafluoro-1-cyclopentene
AB (1Φ)	A unimolecular photoreaction mechanism, where the initial species (A) photo-transforms into a product (B) with an efficiency $\Phi_{A\rightarrow B}$
AB (2Φ)	A mechanism which involves two reversing photochemical reactions between the drug and its photoisomer.
$A_{tot}^{\lambda_{irr}}$	The measured total absorbance of the medium.
λ_{irr}	Wavelength of Irradiation, the wavelength used to irradiate the sample
λ_{obs}	Wavelength of Observation, the wavelength at which the sample was observed
$P_{\lambda_{irr}}$	The radiant power value
$\Phi_{A\rightarrow B}^{\lambda_{irr}}$	Forward quantum yield of photochemical reaction realised at the irradiation wavelength (λ_{irr})
$\Phi_{B\rightarrow A}^{\lambda_{irr}}$	Reverse quantum yield of photochemical reaction realised at the irradiation wavelength (λ_{irr})
$A_{tot}^{\lambda_{irr}/\lambda_{obs}}(t)$	The total absorbance of the reaction medium at reaction time ($t = 0, \infty$) when irradiated at certain wavelength and observed at another wavelength
$A_{tot}^{\lambda_{irr}/\lambda_{irr}}(t)$	The total absorbance of the reaction medium at reaction time ($t = 0, \infty$) when irradiated at certain wavelength and at the same wavelength
$C_x(t)$	The concentration of compound (x) at any time
$F_{\lambda_{irr}}(t)$	The time-dependent photokinetic factor

$l_{\lambda_{irr}}$	The optical path length of the irradiation beam
$l_{\lambda_{obs}}$	The optical path length of the monitoring beam
$\varepsilon_x^{\lambda_{irr}}$	The absorption coefficient of compound (x) at the irradiation wavelength (λ_{irr})
$k_{A \leftrightharpoons B}^{\lambda_{irr}}$	The overall reaction rate-constant
$v_{0\ (n)}^{\lambda_{irr}/\lambda_{obs}}$	The reaction's initial velocity, where n is cld. (calculated from theoretical equation) or mod. / exp. (determined from differential equation of the order kinetic model equation).
$K_{\leftrightharpoons}^{\lambda_{irr}}$	the equilibrium constant which expresses the ratio of species' concentrations at pss
ΔC	The change between concentrations
$\beta_{\lambda_{irr}}$	Proportionality factor between the overall rate-constant and the radiant power
N_A	Avogadro's number
N	photon count
F	The mean fraction of light absorbed at the irradiation wavelength
ΔA	the change in the absorbance of compound
h	Planck constant
v	frequency
E_{XS}	excess vibration energy
V	the solution volume
g_λ	Energy density distribution function of the lamp
E_λ	is the spectral irradiance
v_x	wavenumbers of the polychromatic beam emitted by the source
J_i	relative intensity
$T_{f,i}$	The transmittance of filter f
S	The irradiated area
T_x	The transmittance

List of Figures

List of Tables

List of Schemes

Contents

Chapter 1

Introduction and aims

1.1. Introduction

Till date, the usage of thermal kinetics and related models for the photoreactions study have not been reported to treat an accurate interpretation for the photokinetic data set. Widely, this method has been adopted because lack of many reactions integrated includes photoreactions rate-laws. Also, it is worth and needs to define the alternative methods to analysing the photokinetic data set. However, this thesis aimed to develop and validate kinetic models which are an accurate and use for specific photoreactions. Furthermore, a new methodology which disobeys mathematical integration.

In addition, the following three photoreactions typed were selected for development of the kinetic model and data validation purposes such as unimolecular and photoreversible as reported in Chapters from five to eight. Then, this thesis, aim to test the validity of these models experimentally by using drug molecules will be later explained in these chapters.

Throughout the research, the design of experiment used in this project clearly stated in the objectives which provide a standard, acceptable and comparable photostability and experimental kinetic study that was dealing with the reproducibility and lack of experimental concurrency issues.

Also, the developed models accepted to the critical aim of functioning an entire kinetic elucidation of the parameters determining the photoreactions under study and that can be implemented widely and continued in other drug molecules as explained in chapters from five to eight.

The next objective of this thesis, palliating the lack of rate-constant analytical expression for photoreactions that will be explained in early chapters. Then, this parameter could be analysed and compared with the study effects of variable factors include light intensity and initial concentration on photoreactions kinetics, which provide another objective of this thesis.

At last, these studies then also were performed with the additional aim of estimating the drug and compound potential which acts as actinometers thereby currently, the identified limitations with the recommendation as explained at the end of the chapter of this thesis.

The irradiation is divided into two types, namely, monochromatic and polychromic irradiation. Already monochromatic irradiation was studied by Maafi group. I developed the methodology was developed by using non-isosbestic irradiation. Also, I developed new order kinetics for polychromatic irradiation for three types of photochemical reaction. The simulation study was reported in Chapter 6 and an application reported in Chapter 7 and 8 respectively.

Chapter from 1 to 3 describes an introduction and aim of this project to be presented, literature review of the subject accumulated in this part and material and methods employed in this thesis.

Chapter 4 describes the drugs and compounds characterisations.

Chapter 5 describes the photokinetic study under monochromatic irradiation.

Chapter 6 describes the develop or design kinetic model for photochemical reaction (Stimulation part)

Chapter 7 describes the photokinetic study under polychromatic for a unimolecular AB $(1\Phi)_{\varepsilon_{B=0}}$ system.

Chapter 8 describes the photokinetic study under polychromatic for the unimolecular AB $(1\Phi)_{\varepsilon_{B\neq 0}}$ system and photoreversible AB (2Φ) system.

Chapter 9 describes the development of actinometric method under mono and polychromatic light.

The last chapter (Chapter 10) describes the overall conclusions and limitation from the present work.

Chapter2

Literature review

2.1. Introduction

Human life is surrounded by a constant interaction between light and matter. The interaction between light and matter occur in our surroundings and within the human system. A simple example is the biochemistry of vitamin D which is made in the human skin via a series of biochemical processes triggered by the ultraviolet B (280 – 320 spectrum) radiation from the sun [1]. Another example of the interaction of light and matter is seen in the process of photosynthesis, a process vital for the balance of oxygen and carbon dioxide in our atmosphere and the production of carbohydrate [2,3]. The indirect use of light from the sun is seen in cellular respiration which occurs via the breakdown of products produced by the use of sunlight for example photosynthesis for the production of the energy required for survival as seen in humans. This phenomenon has contributed to the development of numerous fields of science including medicine, technology and chemistry. However, to fully appreciate and utilise the phenomena involving light absorption, the study of the interaction between light absorption and matter is essential to further understand its associated advantages and disadvantages [4–6]. Thus, to date, there are different branches of science involved in the study of light including photobiology, photophysics and photochemistry among others. The present review is on the chemical effect of light irradiation on the properties of matter, which is term as photochemistry.

Photochemistry is a field discovered out of observed curiosity, for instance, the bleaching effect of sunlight on pigment and dye observed in cloth manufacturing, painting and even photography. Thus, sunlight was observed to result in colour change, the development of precipitates as photoproducts and in some liquid the development

of gas bubbles. One of the earliest photoreactions recorded in the 18th century was the conversion of nitric oxide to nitrogen dioxide conducted by Joseph Priestley. Another contributing photochemical experiment is that conducted by J. W. Dobereiner which involved the exposure of aqueous oxalic acid and iron (II) oxide to sunlight; a landmark in ferrioxalate actinometry. By the end of the 19th century, the field of photochemistry reported different photoreactions such as the photoreaction of santonin, photodimerization of anthracene and photoreaction of olefin among others [7]. These findings contribute to the multidisciplinary approach to research in modern photochemistry to date.

2.2. Basic of Photochemistry

The absorption of light by a matter affects the properties of that matter, and this interaction is by electromagnetic radiation. Light is an electromagnetic wave which can be classified by wavelength and frequencies; for instance, the visible light is made up of different types of radiation thus having different colours. Matter on the, on the other hand, is made up of elements which have unique chemical and physical properties. An element is made up of atoms which in turn contain protons, electrons and neutrons. Thus, a matter is made up of protons, electrons and neutrons. Therefore the reaction that occurs between the properties of matter and light is term photochemistry.

Photochemistry studies the mechanism of the photochemical reactions, which occurs when a change in the electronic structure of a molecule is observed due to the absorption of a photon of the light, resulting in photochemical changes in the said molecule or adjacent molecules (which is called primary process) [8]. The nature of the

photochemical reaction depends on the wavelength of light absorbed, i.e. visible light (400nm – 700nm) or ultraviolet light (200 nm – 400 nm). Moreover, photochemical changes occur when the absorption of light provides enough energy capable of breaking a bond or twisting the double bond in the molecule, therefore enhancing the molecule to excite from ground state to an excited state. Once the molecule returns to the ground state, the energy will be disposed of in the form of a heat or light (fluorescence or phosphorescence), accompanied by changes in the molecular characterisation [8]. Hence, a photochemical reaction is governed by three basic principles:

- The first law states that a system must absorb light of a particular wavelength for photochemical reaction to occur.
- The second law states that only a single molecule is activated for a photochemical reaction at normal intensities due to a single photon of light absorbed by the system.
- Finally, the third law, also known as the Bunsen-Roscoe Law of Reciprocity, states that "a photochemical effect is directly relational to the total energy dose, regardless of the time required to deliver the dose [9]."

Furthermore, the photochemical processes involving the absorption and emission of a photon in photochemical reaction has been simplified and illustrated by Aleksander Jablonski. This illustration, the Jablonski diagram (Figure 2-1), shows possible schematic consequences of the irradiation of a molecule by the visible spectrum of light. The diagram is a combination of straight and curved lines which represent the possible occurring quantum mechanical transitions experienced by a molecule when exposed to

a specific wavelength of light. The curved lines represent the transition of electrons without light interactions (non-radiative processes) while the straight lines represent the conversion between the energy of an electron and a photon of light (radiative processes). The energy acquired from the light enhance an electron when a molecule absorbs a photon, to excite to a higher energy state called excited state. The Jablonski Diagram has explained the electronic transition process from one electronic energy level to another. Furthermore, each electronic energy state in the Jablonski Diagram is designated by different symbols. These symbols include “S0” ground electronic state, “S1” is first excited singlet state, “T1” is first excited triplet state, “T2” is second excited triplet state and “T3” is third excited triplet state [9].

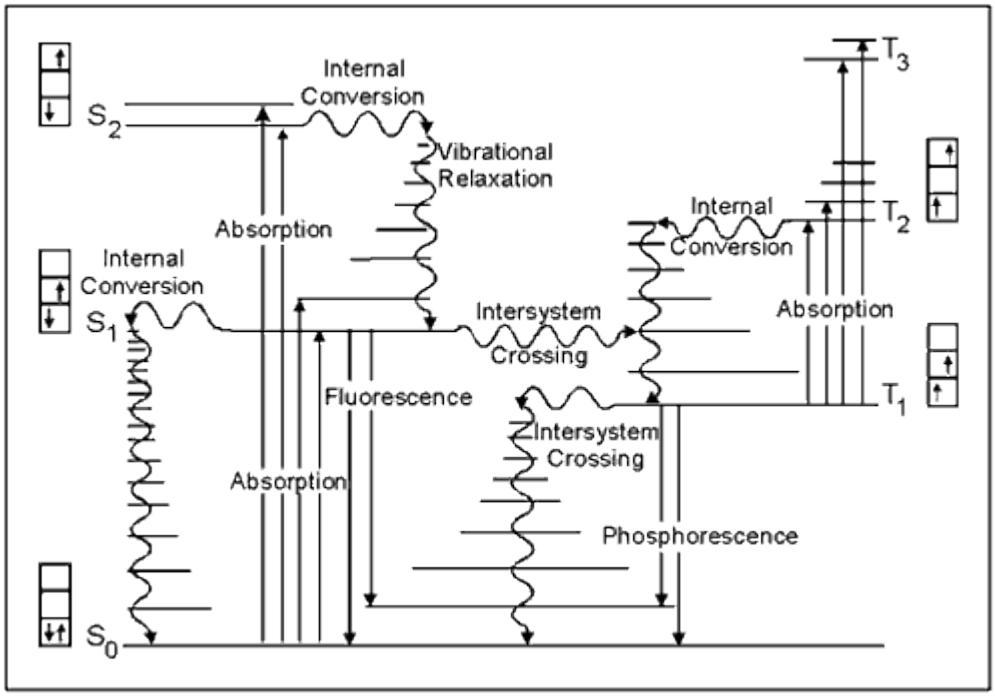

Figure 2- 1: The Jablonski Diagram [9].

The non-radiative processes are represented by internal conversion, inter-system crossing and vibrational relaxation. The vibrational relaxation (VR) is said to occur

immediately after absorbance of a photon. VR occurs when energy deposited into the electron by the photon is transferred to other vibrational modes as kinetic energy. Also, this kinetic energy might remain in the same molecule, or the energy is transferred to neighbouring molecules surrounding the excited molecule. However, an overlap between the vibrational energy and the electronic energy level could result in the transition of the excited electron from a vibration level in an electronic state to another vibration level in a lower electronic state; this occurrence is called the interval conversion (IC). The inter-system crossing (ISC) occurs when there is a change in an electron spin from an excited singlet state to an excited triplet state.

Emission that occur differ during the photochemical reaction, the fluorescence emission occurs between the same spin states (S_1 to S_0), while the phosphorescence emission occurs between the different spin state (T_1 to S_0). In the case of the phosphorescence emission, the wavelength is longer (low energy) with long radiative lifetime compared to the fluorescence emission [9].

2.3. Photodegradation

Photochemistry is of great importance in the pharmaceutical industry; this is because most active pharmaceutical ingredients (API) and excipients are light sensitive. Thus the absorption of light by drug formulations could lead to degradation during manufacturing, storage or administration. Consequently, resulting in loss of drug potency, bye photoproduct formation, altered efficacy and altered side effects which could be harmful to patients. For this reason, it is important to know the photochemical behaviour of drugs to ensure safety and efficacy. To date, many drugs are labelled as

light sensitive (photoreactive or photolabile) by the European Pharmacopoeia [39], and this number is increasing due to new drugs being discovered and old drugs being re-examined. Photochemical reactions take place with the following spectra regions: UV light (UVC = 200 – 290 nm; UVB = 290 – 320 nm; UVA = 320 – 400 nm), visible light (400 – 700 nm) and solar light which include UVA, UVB and visible wavelengths. However, most of the photochemical reactions involved the UVA, UVB or visible light[10]. Light sensitivity among drugs varies and contributing photodegradation factors include radiation (intensity and wavelength), concentration, temperature, water composition, humid, viscosity and pH [11]. Therefore, drug sensitive to light do not necessarily have the same degradative outcome. For instance, riboflavin was reported to degrade in 7.5 minutes when exposed to UV radiation (240 – 366nm) whereas when exposed to visible radiation (400 – 500 nm) it degraded in 150 – 330 minutes [12].

Photodegradation is the process of decomposition caused by the absorption of photons. This process depends on the absorption spectrum of the drug molecule, thus shifting the molecule from its ground state to its excited state. The excited state of the drug molecule is less stable; hence the molecule could undergo different transitions such as phosphorescence, fluorescence, IC, ISC, or photoionization which is the removal of an electron from the molecule. Also, photosensitive drugs could result in different phototoxic response which includes photogenotoxicity, photoallergy, photostability and photoirritation [11,13] as summarised in Figure 2-2.

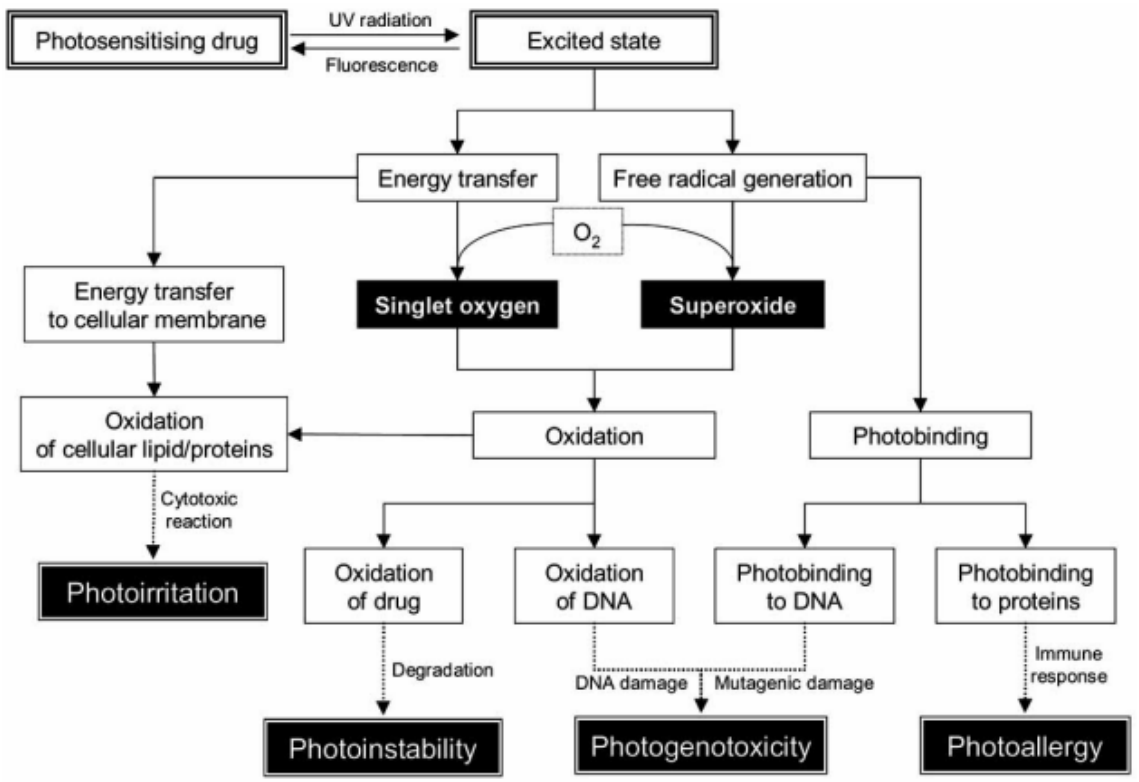

Figure 2- 2: Possible phototoxic responses that could be induced by photosensitive drugs (modified from *[11,13]*)

It is important to know the type of photochemical degradation that can affect the APIs and excipients, in order to protect photosensitive drugs. There are different types of photochemical reaction and example include photodecarboxylation (e.g. Ketoprofen [15–17]), photodehalogenation (e.g. fluoroquinolones [18,19]), photoreduction and photoaddition (e.g. riboflavin[20,21]) . The knowledge of the photochemical associated with photosensitive drugs will provide appropriate formulation strategies to protect said drugs. Different photodegradation effects have been reported for different drug dosage forms and are not necessarily similar for all drugs. However, the most common physical photodegradation effects among all dosage form reported include discolouration and a change in appearance, especially observed in oral solutions, tablets, emulsions and

creams [11]. Therefore, it is important to protect drugs from photodegradation to ensure safety and efficacy.

In general, drugs are exposed to either natural light or artificial light at some point during manufacturing, transportation, storage and usage. Besides, in the hospitals, some drugs are stored in unit-dose containers usually on open shelves, and some drugs are removed from their package. Thus, repackaged drugs are left exposed to fluorescence tubes and daylight for days and in some cases for weeks. Moreover, the FDA (Food and Drug Administration's) Compliance Policy recommended that repackaged drugs have six months from the day of repackaging without the need for photostability testing.

2.4. Photostability

The photostability of a drug is the response of drug to the exposure of UV, solar and visible light that results in physical and/or chemical changes. Photostability of drugs could be examined through photodegradation reaction and is expressed as a drug`s shelf life and an expiration date which are provided based on a drug`s pre-formulation studies. The common physical change in drug after exposure to light is a change in colour, however that alone is not enough to determine the extent of the photodegradation.

In pharmaceutical companies, it is important to maintain drug stability during manufacturing (handling, packaging and labelling), transportation and administration. Moreover, to maintain drug safety, efficacy and stability, different strategies have been used to protect dosage forms from photodegradation. For example, many drugs are

white to reduce light absorption because the white colour reflect the light. However, this does not provide appropriate protection against photodegradation [22].

Some methods used for photostability of drugs include the use of vesicular carriers e.g. liposomes and noisomal gels; lipid nanoparticles e.g. solid lipid nanoparticles; complex formation e.g. complexation with cyclodextrin; microspheres e.g. tristearin – and phosphatidylcholine - based microspheres; and microcapsules e.g. methacrylic copolymers, among others [10,11,23]. Also, the use of appropriate primary and secondary packaging material used can provide protection from light exposure. The most commonly used method is the use of amber-coloured glass or plastic containers, this is because these containers can absorb UV light at about 470nm [11].

2.5. Photostability testing

The importance of photostability studies is to obtain information on the photostability properties of a drug such as the physical and chemical changes observed upon exposure to light, the mechanism and pathways of drug photodegradation, and drug shelf life among other [10]. The photostability studies are conducted to ensure drug safety, efficacy, potency, and possible side effects associated with light exposure. This is conducted according to the guidelines provided by the International Conference on Harmonisation of Technical Requirements for Registration of Pharmaceuticals for Human Use (ICH) for all new drug licenses application [24]. The ICH Q1B guideline provides a chart flow on the photostability testing of new drugs which include forced degradation testing to determine photodegradation pathway and necessary

information on handling, packaging and labelling. For photostability testing, two light sources are recommended by ICH Q1B which include simultaneous exposure of drugs to (1) outdoor daylight and indoor indirect widow glass-filtered daylight and (2) direct indoor light which include cool white fluorescent lamp and near UV fluorescent lamp (with a spectral distribution of 320 – 400 nm and a maximum energy emission of 350 – 370 nm) [24]. Although the ICH Q1B guideline, a 22-year-old guideline, is still used to collect photostability data of drugs, it did not provide a clear guide concerning the analysis and determination of the necessary kinetic data to establish drug photostability [24].

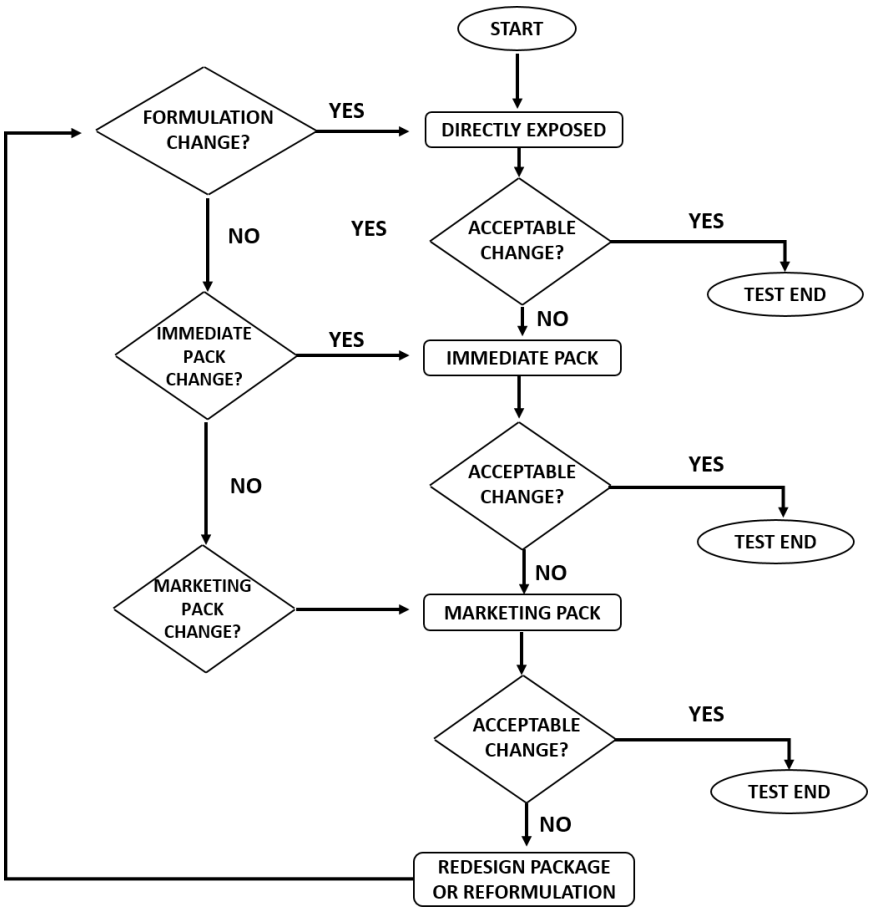

Figure 2- 3: A decision flow chart for photostability testing of drug products [24]

2.6. Photosafety testing

Although photostability testing is conducted to evaluate photodegradation, it does not provide in-vivo details of drug phototoxicity such as drugs associated with light-exposed tissues. Therefore, the European Agency for the Evaluation of Medicinal Products provided guidelines on phototoxicity and photosafety testing in 2002 [25]. These guidelines provided a work-flow on assessing photosafety of drugs. Also, the FDA in collaboration with ICH, the CDER (Centre for Drug Evaluation and Research) and the CBER (Centre for biologics Evaluation and Research) provided a scientific approach for photosafety testing of topical and administered drugs in 2003 [26]. In general, the FDA guidelines encourage the use of old methods and the development of new methods in evaluating human safety. Furthermore, the M3 (R2) guideline on non-clinical safety studies was also provided by FDA in collaboration with ICH, CDER and CBER in 2010. The guidelines focused on the following studies phototoxicity, immunotoxicity, juvenile animal toxicity and abuse potential. And the guideline also provided maximum dose selection options for general toxicity studies [27].

An in-depth guideline on conducting photosafety studies was further released by ICH in 2013 and titled ICH Harmonised Tripartite Guideline: Photosafety Evaluation of Pharmaceuticals [28]. The aim is to evaluate tissue response induced by light interaction with APIs, excipients, dermal clinical formulation and photodynamic therapy products. In addition, an outline on photosafety testing route for both systemic and dermal route was provided.

Both in-vivo and in-vitro nonclinical photosafety testing aims at detecting potential phototoxicity. There are different types of in-vitro assays used; some of these assays depend on drug sample solubility while others involve the direct application of topical tested sample on tissues[28]. The most commonly used in-vitro assay is the 3T3 Neutral Red Uptake phototoxicity test (3T3 NRU-PT) and is used for soluble compounds with light absorption range of 290 – 700nm [28,29]. The principle of 3T3 NRU-PT assay is to determine the cytotoxicity of chemicals on mouse fibroblast cell line (Balb/c 3T3 cells) with and without exposure to a non-cytotoxic dose of simulated solar light ($5J/cm^2$). Cytotoxicity is then expressed as the concentration-dependent reduction of the uptake of the Neutral red dye after a 24 hours treatment with both chemical and irradiation [29]. Apart from the use of mouse model for phototoxicity testing, assays involving the human reconstructed skin models are also used such as the reconstructed human epidermis model and the sensitivity of this assay was reported to be above 90% [30]. On the other name, there is no standard in-vivo phototoxicity testing, instead animal models such as mice, rats and guinea pigs are used. With regards to ocular phototoxicity testing, there are no standard assays, rather recent research shows the development of new models such as the in-vitro human corneal epithelial model [31].

2.7. Limitations associated with the guidelines

In general, both photostability and photosafety testing guidelines aim to determine the adverse effects of photosensitive drugs when exposed to light on human health. Moreover, Data obtained is used to provide necessary strategies to protect light-sensitive drugs from photodegradation reaction and to prevent phototoxicity. However, these regulatory guidelines are associated with limitations with regards to the practical

interpretation, experimental design, analytical and data interpretation [32–35]. Some of these limitations include:

2.7.1. Irradiation source

The ICH Q1b guidelines provided irradiation conditions which are not complimenting the illumination conditions. The guideline used the term light which has a broad definition. Therefore, Baertschi et al., (2010) [32] recommended the use of scientifically correct terms such as radiation, photon or photolysis source. As previously mentioned, option (2) which involve exposure to UVA and cool white fluorescent did not mention a clear statement with regards to either the exposure should be conducted sequentially in an orderly manner or simultaneously.

Moreover, the guideline mentioned the use of either D65 or ID65 light source in option (1). However, D65 and ID65 are two different standards; thus the photoreactions might vary between the two different light source [32]. Furthermore, the near UV fluorescent lamp was recommended in option (2) but emission guideline provided is not specific. The guideline stated that 'spectral distribution from 320 to 400 nm with a maximum energy emission between 350 and 370 nm; a significant proportion of UV should be in both bands of 320–360 nm and 360–400 nm.'' This guideline can be interpreted as radiation below 320nm is not recommended in the ICH Q1b guidelines photostability testing, in contrast, the literature showed that most approved drugs absorb both UVA and UVB regions of the spectrum [33,36,37]. Also, the ICH Q1b and M3 (R2) guidelines included the use of 290-320 nm UVB radiation range in the photosafety testing which clearly shows a lack of agreement between the two guidelines.

In addition, the UVA doses mentioned in photostability testing varies from that mentioned in photosafety testing. In photosafety testing, the UVA dose recommended was 5 – 20 J/cm^2 [28] while that recommended for photostability testing is not less than 200 watt hours/m^2 which is equivalent to 72 J/cm^2 [24]. This discrepancy also needs to be addressed [32].

2.7.2. Actinometry

The photochemical reaction related to the number of photons absorbed. The number of photons absorbed is obtained by using the actinometry. The actinometry is a term that defines the use of a chemical or physical system to determine the photon flux or light dose exposed to a photoreactive sample [38]. The chemical actinometric system, such as ferrioxalate, photochromic, uranyl oxalate, Reinecke's salt, involves exposing a chemical entity to a specific wavelength, resulting in a light-induced reaction. The number of photons absorbed per unit time per unit area is then calculated using the reaction rate (Eq.1-1) [38]. However, physical actinometry involves the use of physical instruments, such as radiometer, that can convert the photons to a quantifiable electric signal [39].

$$Rate\ of\ light\ absorption\ by\ the\ photoreactive\ substance = \frac{Rate\ of\ the\ reaction\ of\ interest}{quantum\ yield}$$

Eq.1-1

Radiometer is a physical instrument used to measure light intensity. The radiometers are contained several types of the photocells which produce the current once photons fall on the cell. It is simple and easy to be used, but it needs to change the photodiode

after used for long times [39]. Also, It regularly needs to calibrate due to the variation in the performance of photodiode and the filter [39].

The chemical actinometry is doing in the same conditions of the experiment of photoreaction when investigation and irradiation and quantification [40].

There are different types of chemical actinometry such as potassium ferrioxalate, photochromic actinometer, Uranyl oxalate and Reinecke's salt actinometer.

The popular and widely used in the liquid phase chemical actinometer is the potassium ferrioxalate due to the wide wavelength range up to 578 nm [38,39,41].

There is another actinometer called photochromic actinometer as azobenzene depends on the photoreversible or photochromatic reaction. The azobenzene actinometer is simple and uniform reaction. It is cover the wavelength range 230-460 nm [38]. The azobenzene was independent on wavelength and temperature except cis-trans was thermally regenerated at 60 °C [38]. The Fulgide Aberchrome 540 is one of the photochromic actinometers, and it is widely used [38,41]. This type of actinometer was used in the region of near UV and visible (310-370 nm and 435-545 nm) due to the reversible photocyclization [38,41].

On the other hand, the cis-trans stilbenes photoisomerization was used as chemical actionmeter for wavelength range 254-366 nm, which the quantum yield depend on the substitution of the stilbene and solvent [38].

Uranyl oxalate actinometer as photosensitiser and cover range between 208-426 nm. This type of actionmeter depends on the pH [38,41].

The type classified as photosubstitution reaction is Reinecke's salt actinometer, which is work in aqueous solution. It is quantum yield wavelength dependent. It is covered the range 316-750 nm [38,41]. This type is not recommended due to extensive error and complex handling [38]. In table (1-1) shows examples of the selected list of liquid phases actinometry.

Table 2- 1: *Examples of selected liquid phase actinometers*

Compound	nm	Solvent	Analytical method	Ref.
cis-Cyclooctene	172, 185	n-Pentane	GC	[38,41]
Iodide/iodate	214-330	Water	Abs. 352 nm	
Azoxybenzene	250-350	EtOH	Abs. 458 nm	
1,2-Dimethoxy-4-nitrobenzene	254-366	Water	Abs. 450 nm	
o-Nitrobenzaldehyde	300-410	CH_2Cl_2, H_2O/EtOH	GC, pH-metry	
trans-2-Nitrocinnamaldehyde	313, 366	MeOH	Abs. 440,	
DCM styrene dye	410-540	$CHCl_3$, MeOH	HPLC	

4-Dicyanomethylene-2-methyl-6-[*p*-(dimethylamino)styryl]-4H-pyran (DCM)

The potassium ferrioxalate mechanism is irradiated using UV, or visible light lead to the reduction of the ferric (Fe^{+3}) and oxidation the oxalate. The reaction is observed at 510 nm through the determination of the ferrous (Fe^{+2}) by using as a complex with 1,10-phenanthroline. The complex does not absorb the light at 510 nm; that's mean the back reaction does not happen [38,41]. So, the potassium ferrioxalate undergoes as direct photoreaction. The number of photons absorbed is determined by using Eq.1-2.

$$\Phi = \frac{The\ number\ of\ molecules\ formed}{No.of\ photons\ absorbed} \qquad \text{Eq.1-2}$$

The analytical method of the azobenzene actinometer is used the HPLC to determine the trans-cis photostationary state.

The Fulgide Aberchrome 540, the fulgide photoreversible reaction is used for the UV region (310-370 nm). The absorbance of Fulgide is measured at 494 nm before and after irradiation [38]. The mole of the photon absorbed is determined by using the Eq.1-3 [41]

$$N_A hv/t = \frac{\Delta A\, V}{\Phi\, \varepsilon\, t} \qquad \text{Eq.1-3}$$

Where N_A is Avogadro's number, ΔA is the increase in the absorbance of the fulgide at 494 nm, V is the volume of the irradiated solution (L), Φ is the quantum yield of the fulgide between 310-370 nm, ε is the molar absorptivity, t is the irradiation time and $(NAhv/t)$ is the mole of the photons absorbed.

For the visible region (435-545 nm) is used the back reaction of the close from to open form cyclization of fulgide and read the different of the absorbance before and after irradiation [38]. The volume of the red solution of the close form of fulgide is known. The mole of the photon absorbed is determined by using the Eq.1-4 [41]:

$$N_A hv/t = \frac{\Delta A\, V}{\Phi\, \varepsilon\, t\, F} \qquad \text{Eq.1-4}$$

Where ΔA is the decrease in the absorbance of the fulgide at 494 nm and F is the mean fraction of light absorbed at the irradiation wavelength.

The Uranyl oxalate actinometer, the oxalic acid in present the uranyl and light irradiation will give the carbon dioxide and monoxide and water. The oxalate ions are determined before and after the irradiation using titration by the potassium permanganate [38,41].

$$H_2C_2O_4 \xrightarrow{h\nu, UO_2^{2+}} CO_2 + CO + H_2O$$

Reinecke's salt actinometer is determined the number of the photon absorbed through release the (SCN^-) after irradiated $[Cr(NH_3)_2(SCN)_4]^-$ by light in present water. The ions released determined by complexation with ferric. The complex of ions with the ferric result as blood red colour, and it is measured the absorbance at 450 nm. The number of photons absorbed is obtained by using the Eq1-1 [41].

In order to apply chemical actinometry, some requirements must be met, which is [38]:

1- It must be a simple system, easy to control the experimental conditions.
2- It must be accurate in quantum yield value for wide number of wavelengths. The quantum yield must be wavelength independent.
3- The chemical material must be thermally stable.
4- It should be sensitive.
5- Simple analytical methods.
6- Easy to synthesise and purify.

However, There are some factors affect in the chemical actinometry as temperature, photoproducts absorption and the chemical actinometry degree of absorption, which lead to developed new actinometry [38].

The temperature might effect in the change of concentration of the compound and lead to a change in chemical conversion of the compound. This will result inaccurate of the number of photons absorbs by the compound [38].

The photoproduct of actinometer should not be absorbed light. In case, if it is absorbed light, it will lead to a decreased range of conversion, and it is difficult to expect the number of photons absorbed [38].

Some chemical actinometry developed for some cases such as the excess volume of high photons intensity was used to irradiate the sample. This type of actinometer is characterized as incomplete absorption of the actinic light. The benefit of this type is to avoid problems of inhomogeneity through photoreaction [38].

There are some advantages for each the chemical actinometry. The potassium ferrioxalate actinometer is sensitive, reliable, simple, inexpensive and constant quantum yield [42–44]. Trans- Azobenzene is commercially available, soluble in different organic solvents, easy to determine without need to complexation, reusable and reversible due to the photoreversible reaction in case the thermal step of cis-trans is neglected [45,46].

However, there are some disadvantages or limitations of the chemical actinometry, and that's lead to developed new actinometry. The potassium ferrioxalate; due to the range of light absorbed for ferrioxalate is visible light, the reaction must be happening in dark condition. Also, the photooxidation reaction of phenanthroline occurs during the slow complex reaction of ferrous (Fe^{+2}) with 1,10-phenanthroline and lead to ferric (Fe^{+3}) with phenanthroline and this it will result in analytical interference [42–44]. The limitation of

the Azobenzene actinometer is needed to quantify the photochemical parameters of cis isomer when used the spectrophotometer [45]. Also, the o-nitrobenzaldehyde actinometer (photoisomerization) is used to determine the photons flux by using a pH meter. The sensitivity of pH metre will effect on the accuracy of o-nitrobenzaldehyde actinometer, and the accuracy of the actinometer will be limited.

The ICH guideline recommended the use of quinine actinometry system for the measurement of chemical exposure to a near UV region of the light source in photostability testing of new drugs [24]. However, the quinine actinometry system (QAS) is not without limitations, for instance, the spectral power distribution used for the calibration of quinine in the ICH guideline was not provided [32].

Moreover, the study de Azevedo Filho *et al.*, [47] showed that this actinometric system depends on the concentration of quinine in the solution and its location in the irradiation chamber. Another limitation associated with QAS is that the absorbance of quinine at 400 nm was shown to continuously increase for more than 60 hours even after the irradiation was stopped which affects the results obtained significantly [32]. Also, the QAS was shown as not compatible with option (1) light sources, according to ICH Q1B guideline. For instance, Baertschi et al., [32] reported the sensitivity of quinine to temperature and oxygen when exposed to a xenon lamp.

2.7.3. Quantum yield

The photochemical reaction is the interaction or the relationship between the light and the molecule. This interaction leads to a change in chemical or physical properties [48].

In the photochemical process the light excited the molecule from ground state to excited state, in this case there are different in structures configurations between the two states [48]. Also, the basis of photobiology is photochemistry [48,49]. The photoreaction is responsible for many phototherapies such as neonatal jaundice [50], psoriasis treatment and cancer treatment as photodynamic therapy [39,49]. Bertelsen and Skibsted (1987) found that exposing meat to the light will change the colour of that, the change of colour gave indicate about the required details of the photochemistry, which are necessary to raise the storage condition of the food. So, it is important to know how many compounds degradable per a photon absorbed. This is lead to the definition of quantum yields (Φ) for photoreaction, it is the number of the compound or molecules decomposed divided by the number of the photon absorbed. Moreover, The quantum yield is the possibility of absorption of one photon at a given wavelength will lead to observe photochemical reaction [48]. The quantum yield is one of the useful quantity to evaluated any photochemical reaction [48]. Also, the quantum yield is used to quantify the photochemical reaction [41]. Skillman, (2008) state that the quantum yield is determined the efficiency of light after absorbed and it is produced a certain effect. The rate of the photodegradation of the compounds depends on the reaction quantum yields, the light intensity, the molar absorptivity at the irradiation wavelength, the path length, and the concentration of the compounds [52].

The quantum yield of the photochemical reaction is independent on the wavelength [53,54]. Also, it is independent on the experimental conditions [39,55]. It is mean that the similarity of the results of the quantum yield of the compounds should be found. So, if it is determined in different labs should be found the same results [39].

However, Several studies have confirmed that the reaction quantum yield is a wavelength dependent [56,57,66–70,58–65]. Sumi et al. [71] reported that many of the photochromic reaction quantum yields were wavelength dependent. Moreover, the quantum yields of Azobenzene as well were dependent on the wavelengths [72]. Greenberg et al. [73] have found that the quantum yield had increased at long wavelength, and that has been confirmed by McDonagh *et al.* in 1989 [50]. However, Bertelsen and Skibsted [52] have reported that the quantum yield has decreased with increasing the irradiation wavelength for Oxymyoglobin in aqueous solution. Moreover, Kim et al. [56] had corrected the statement that stated that the quantum yield in vision is a wavelength independent after they have done several experiments on the 11-cis-retinal chromophore. Klán and Wirz [74] were found that the quantum yield of the ferrioxalete actinometer is wavelength dependent and it is the different values at one wavelength in different labs.

There is no specific or clear reason to explain the change in the quantum yield values with change the irradiation wavelength because it is attributed to different reasons. The first reason, the increase in the quantum yield at end of the uv spectra (long wavelength) of the compound has happened in the weak absorption region due to accidental excitation beam from the monochromator [73]. Second one, this dependence is related to the photoproduct or the different excitation (both, low and high) of the weakly interaction molecule, which leads to producing different photoproducts [64], this might be different wavelength produce different photoproduct and that result to the change of the quantum yield. The exited compound might be exited to separate state that lead to give different photoproduct. Third , it might be contributed to present more than one

isomer or interconverting conformers [68], and it might be attributed to effect of excess vibration energy (E_{xs}), this explained by Kim [76] who is reported that the when the excess vibration energy increased the quantum yield will increased regarding to the Landau Zener model ($\Phi_{\lambda_{irr}} = e^{-k/\sqrt{E_{xs}}}$) [68,75,76]. Fifth, Nakamura et al., [66] have reported that it might be a relationship between the structure of the molecule and the quantum yield, and also, it might be effective in the value of the quantum yield. Bandara and Burdette [69] have stated that the difference in the quantum yield related to remaining the isomerization pathways after exited the molecule because semi-rigid steric constraints such as bridge between the two phenyl rings this block the pathway of deactivation of photoisomerzation accessible following $S_2 \leftarrow S_0$, thus lead to increase the quantum yields [69]. In addition, the change in quantum yield might be resulted of increasing in the excitation energy, the quantum yield will be decreased (i.e. increasing vibrational energy of the S_1 state) even within the $S_1 \leftarrow S_0$ excitation, which the S_1 state has been long lifetime than S_2 [69].

Other studies have reported that the quantum yield is wavelength dependent, but no reasons have been given [50,56,67,71,72,77,78].

2.7.4. Data collection and analysis

The nature of the ICH Q1b guidelines is mainly qualitative, and data analysis is somewhat subjective with regards to the inspection of physical drug changes due to irradiation such as appearance, colour and clarity [24]. However, photodegradation could occur without noticeable physical changes. Furthermore, the guidelines lack analytical methods for assessing other components present in the drugs such as excipients, thus affecting

evaluations and effective comparisons among studies [32]. Besides, kinetic methods (zero, first and second order kinetics) are widely used for analysing and interpreting data obtained from photoreactions, irrespective of their limitations in photochemistry.

2.8. Kinetics treatments overview

2.8.1. Introduction

The purpose of the photostability studies is to provide data that give information on the stability and quality of drugs under different conditions and allow us to expect the shelf life. This study must contain the manufacturing process requirements, such as handling, labelling and packaging, to make sure and protect the potency, quality of product and finally patient safety. Therefore, the photostability is needed to design a specific and accurate method to treat the data, and this is the main requirement before beginning of photostability study.

2.8.2. Reactions kinetics

Kinetic is the study of how a system changes as a function of time, whereas, the reaction kinetics is the study of the rate of a chemical change and how the conditions of the concentration of reactants and products, solvent and temperature influence this rate [79]. The rate of reaction is the rate or speed of change in the concentration of the compound due to the degradation or production of new molecules. The rate of reaction given by Eq.1-5 [80]

$$Rate\ of\ chemical\ reaction\ = \pm \frac{dc}{dt} \qquad \text{Eq.1-5}$$

Where dc indicate a change in concentration with time (dt), and ± the increase or decrease of the product and reactant concentrations.

$$aA \ + \ bB \rightarrow Product$$

Where A and B are the reactant, and the number of moles of reactants A and B is represented by *a* and *b*, respectively, as elementary reaction.

Classification of the order of the reaction depends on the rates quantified for each compound (reactant) [80].

$$Reaction\ rate = \pm \frac{dC_A(t)}{dt} \ = \ k\ {C_A}^a\ {C_B}^b \qquad \text{Eq.1-6}$$

Where *a* and *b* are the orders of reaction. If a= 1 and b=2

$$Reaction\ rate \ = \ k\ {C_A}^1\ {C_B}^2 \qquad \text{Eq.1-7}$$

The reaction is first order concerning A and second order concerning B [80].

The overall order is the sum of the exponents, i.e. third order. The proportionality constant k is termed the rate constant; its value reflects the rate or speed of the reaction [80].

The benefit of the integrated rate law is to give information about the rate of the reaction. It represents a valuable tool to quantify the change of the reaction species over time. The data achieved from the kinetic order is essential for the drug research and development where it is important to predict the shelf life of the drugs and describe the mechanism of the reaction.

Therefore, illustrate the kinetic performance of the degradation of the drug via understanding the integrated rate law is important to understand the fundamental of the photoreaction kinetics and the pharmaceutical application as well. So, thermal kinetic or study, it is used to obtained the shelf life and reported the requirement on the stability while the photostability study is mainly used to developed the analytical method and determined the protective requisites depend on the analytical protocols [39].

In the photochemical reaction, AB (1Φ) is compound A, which transforms to compound B through light irradiation. The differential equations rely on three parameters which include quantum yields (Φ) of the compound at a specific wavelength, the absorbance coefficient (ε) and the irradiated power value (P). The definition of quantum yields (Φ) for photoreaction is the number of the compound or molecules decomposed divided by the number of photons absorbed. These parameters are essential parameters when determining the photochemical reactions.

The differential equations are given by [81]:

$$\frac{dC_A(t)}{dt} = -\Phi_{A\to B}^{\lambda_{irr}} \times \varepsilon_A^{\lambda_{irr}} \times C_A(t) \times l_{\lambda_{irr}} \times P_{\lambda_{irr}} \times F_{\lambda_{irr}}(t) \qquad \text{Eq.1-8}$$

Where $P_{\lambda_{irr}}$ is the radiant power value, $C_A(t)$ is the concentration of A at any time, $\Phi_{A\to B}^{\lambda_{irr}}$ is the quantum yield of photochemical reaction realised at the irradiation wavelength (λ_{irr}), $l_{\lambda_{irr}}$is the optical path length of the irradiation beam, $\varepsilon_A^{\lambda_{irr}}$ is the absorption coefficient of compound A at the irradiation wavelength (λ_{irr}) and $F_{\lambda_{irr}}(t)$ the time-dependent photokinetic factor is given by [81]

$$F_{\lambda_{irr}}(t) = \frac{1-10^{-\left(A_{tot}^{\lambda_{irr}}(t)\right)}}{A_{tot}^{\lambda_{irr}}(t)}$$ Eq.1-9

Where $A_{tot}^{\lambda_{irr}}$ represent the measured total absorbance of the medium.

The time-different of photokinetic factor is to be dependent on the total absorbance of the medium at the irradiation wavelength. Thus equation Eq.1-8 cannot be integrated. Recently, Maafi and Maafi (2014) discovered the differential equation to generate a new kinetic order called Φ-order kinetics. It was reported that unimolecular photodegradation processes of the form AB (1Φ), where A is the initial compound that degraded due to irradiation to compound (B) with a quantum yield (Φ). This novel kinetic approach was found to be a satisfactory description of the whole set of AB (1Φ) photodegradation data under investigation. Consequently, the determination of such a reaction's photochemical quantum yield can be obtained from the overall rate constant of the reaction.

2.8.3. Problematic

2.8.3.1. Introduction

The thermal order kinetics are widely used to treat the data of the kinetics. However, there is number of limitation when it is used for photostability studies. This limitation such as lack to represent all parameters of the photoreaction and reproducibility of the results and other limitations will describe here.

2.8.3.2. Method of data analysis

The photodegradation or photochemical reactions applied the classical zero, 1st and 2nd order kinetic methods to analyse the photodegradation data. [82,83,92,93,84–91].

However, these classical methods depend on the thermal reaction, and some compounds were thermally stable but unstable in light.

In addition, there is no clarity about which order kinetic that photochemical reaction follows when used the thermal kinetic method with photochemical reaction since there are several conclusions and explanations about the kinetic of the photoreaction.

In some cases, it was noted that no accurate kinetics (obeys to different kinetic order) method could be applied to some drug photodegradation [94–97].

Moreover, another study demonstrated that the photodegradation reaction Data (photokinetic traces) of tetracycline was fitted with two types of thermal order kinetic methods [98,99]. However, Maafi and Brown (2007) noted a poor fitting for the photodegradation date when treated by classical thermal (not photo) kinetic methods. Some studies were used two-stage method to treat the photokinetics data where one part of the data fitted with one type of the thermal kinetic order and the other part of data fitted with another type [39,100,101]. However, this way led to ask questions about why there is a change in the kinetic order of the photoreaction of the same reaction under the same process. Also, the photoreaction depends on the concentration, whereas the first order kinetic is widely applied for the treatment of the photoreaction, which is concentration independent [102].

Some studies described equations and parameters, as light intensity, absorption coefficient and quantum yield, that required to photolysis reaction [87–93]. These studies reported that the photodegradation pattern follows the first order kinetics.

The general rate of photodegradation reaction was given in Eq.1-10 [103,104]

$$-\frac{dC(t)}{dt} = \Phi P_{0,\lambda_{irr}} \left(1 - 10^{-A_{tot}^{\lambda_{irr}}(t)}\right) = 2.303\, \Phi P_{0,\lambda_{irr}} \varepsilon_A^{\lambda_{irr}} C_A(t) l_{\lambda_{irr}} \quad \text{Eq.1-10a}$$

By integrated the Eq. 1-10a as first order given by:

$$\ln\left(\frac{C_t}{C_0}\right) = -kt \quad \text{Eq.1-10b}$$

Where the Φ is the quantum yield of the reaction, $P_{0,\lambda_{irr}}$ is incident light intensity and A is absorbance of the molecule. According to Beer-Lambert law the $A_{tot}^{\lambda_{irr}}(t)$ equal to $\varepsilon_A^{\lambda_{irr}} C_A(t) l_{\lambda_{irr}}$.

So, this equation (1-10a) shows that the rate of photodeagradtion is following to the first order.

In these studies, the values of the quantum yields were assumed constant. The photodegradation takes place under monochromatic light irradiation expect some reactions happen under polychromatic light irradiation [90–93] and they were used the same Eq.10a, but in case the photolysis under polychromatic light, they have added the sum in the equation given in Eq.11

$$-\frac{dC(t)}{dt} = 2.303\, \Phi C_A(t) l_{\lambda_{irr}} \sum P_{0,\lambda_{irr}} \varepsilon_A^{\lambda_{irr}} \quad \text{Eq.1-11a}$$

$$\ln\left(\frac{C_t}{C_0}\right) = 2.303\, l_{\lambda_{irr}} \Phi \sum\left(P_{0,\lambda_{irr}} \varepsilon_A^{\lambda_{irr}}\right) t = -kt \quad \text{Eq.1-11b}$$

However, there are some studies reported that mathematical models to describe the photoreaction kinetics [105–108]. These studies have described the kinetics of photoisomerization reaction. The photolysis studies occurred under monochromatic light irradiation, which is used polychromatic light with filter [106–108] and one study was used monochromator [105]. Also, the light intensity was determined by using chemical actinometry. The limitation of these studies will be discussed in the following chapter five, seven and eight.

2.8.3.3. Rate constant determination

The traditional thermal kinetic order is widely used for the photochemical reaction due to the difficulty of integrating the rate law. However, it was found that the values of rate constant quantified by using the thermal kinetic were not reproducible [101]. The change on the rate constant for the same studies might happen due to effect some variable on the photoreaction such as pH or some additives on the reaction sample [101]. It will lead to concluding that, in filed photostability, it could not predict the shelf life of the photochemical reaction [40] because the rate constant quantified according to the traditional thermal kinetic order, and the rate for this case is depended on the temperature, where is defined by the Arrhenius equation. Nevertheless, in case of the photoreaction, the reaction depends on different parameters not on the temperature such as molecule's absorptivity, light intensity and wavelength. Therefore, the rate constant quantified by using the thermal kinetic order does not represent the right rate constant in case photoreaction.

2.9. References

1. Webb AR, DeCosta BR, Holick MF. Sunlight regulates the cutaneous production of vitamin D3 by causing its photodegradation. J. Clin. Endocrinol. Metab. 1989; 68:882–887.

2. White AL., Jahnke LS. Contrasting Effects of UV-A and UV-B on Photosynthesis and Photoprotection of β-carotene in two Dunaliella spp. Plant and Cell Physiology. Oxford University Press; August 2002; 43(8): 877–884. Available at: DOI:10.1093/pcp/pcf105

3. Guan W., Gao K. Impacts of UV radiation on photosynthesis and growth of the coccolithophore Emiliania huxleyi (Haptophyceae). Environmental and Experimental Botany. Elsevier; January 2010; 67(3): 502–508. Available at: DOI:10.1016/J.ENVEXPBOT.2009.08.003

4. An M., Colarelli SM., O'Brien K., Boyajian ME. Why We Need More Nature at Work: Effects of Natural Elements and Sunlight on Employee Mental Health and Work Attitudes. PloS one. Public Library of Science; 2016; 11(5): e0155614. Available at: DOI:10.1371/journal.pone.0155614

5. Fomina N., Sankaranarayanan J., Almutairi A., 2012. Photochemical mechasnisms of lighttriggered release from nanocarriers. Advanced Drug Delivery Reviews. 64, 1005-1020.

6. Moan J. Juzenas P., 2004. Biological effects of combinations of drugs and light. In Tonnesen H. H. Photostability of drugs and drug formulations. Second edition. London: CRC Press. p. 189-212.

7. Roth HD. The Beginnings of Organic Photochemistry. Angewandte Chemie International Edition in English. John Wiley & Sons, Ltd; September 1989; 28(9): 1193–1207. Available at: DOI:10.1002/anie.198911931

8. Jaffe HH., Miller AL. The fates of electronic excitation energy. Journal of Chemical Education. Division of Chemical Education ; September 1966; 43(9): 469. Available at: DOI:10.1021/ed043p469

9. Smith KC. Basic photochemistry. Available at: http://photobiology.info/Photochem.html

10. Ahmad I., Ahmed S., Anwar Z., Sheraz MA., Sikorski M. Photostability and Photostabilization of Drugs and Drug Products. International Journal of Photoenergy. Hindawi; May 2016; 2016: 1–19. Available at: DOI:10.1155/2016/8135608

11. Janga KY., King T., Ji N., Sarabu S., Shadambikar G., Sawant S., et al. Photostability Issues in Pharmaceutical Dosage Forms and Photostabilization. AAPS PharmSciTech. Springer US; January 2018; 19(1): 48–59. Available at:

DOI:10.1208/s12249-017-0869-z

12. Ahmad I., Fasihullah Q., Vaid FHM. Effect of light intensity and wavelengths on photodegradation reactions of riboflavin in aqueous solution. Journal of Photochemistry and Photobiology B: Biology. Elsevier; January 2006; 82(1): 21–27. Available at: DOI:10.1016/J.JPHOTOBIOL.2005.08.004

13. Onoue S., Tsuda Y. Analytical Studies on the Prediction of Photosensitive/Phototoxic Potential of Pharmaceutical Substances. Pharmaceutical Research. Springer-Verlag; January 2006; 23(1): 156–164. Available at: DOI:10.1007/s11095-005-8497-9

14. Tokura Y. Drug photoallergy. Journal of Cutaneous Immunology and Allergy. John Wiley & Sons, Ltd; June 2018; 1(2): 48–57. Available at: DOI:10.1002/cia2.12017

15. Xu Y., Chen X., Fang W-H., Phillips DL. pH- and Wavelength-Dependent Photodecarboxylation of Ketoprofen. Organic Letters. American Chemical Society; October 2011; 13(20): 5472–5475. Available at: DOI:10.1021/ol202182k

16. Borsarelli CD., Braslavsky SE., Sortino S., Marconi G., Monti S. Photodecarboxylation of Ketoprofen in Aqueous Solution. A Time-resolved Laser-induced Optoacoustic Study¶. Photochemistry and Photobiology. John Wiley & Sons, Ltd (10.1111); May 2007; 72(2): 163–171. Available at: DOI:10.1562/0031-8655(2000)0720163POKIAS2.0.CO2

17. McTiernan CD., Fasciani C., González-Béjar M., Roca-Sanjuán D., Alarcon EI., Netto-Ferreira JC. Ketorolac beats ketoprofen: lower photodecarboxylation, photohemolysis and phototoxicity. MedChemComm. The Royal Society of Chemistry; November 2013; 4(12): 1619. Available at: DOI:10.1039/c3md00258f

18. Cuquerella MC., Miranda MA., Boscá F. Generation of Detectable Singlet Aryl Cations by Photodehalogenation of Fluoroquinolones. American Chemical Society; 2006; Available at: DOI:10.1021/JP060634D

19. de Guidi G., Bracchitta G., Catalfo A. Photosensitization Reactions of Fluoroquinolones and Their Biological Consequences. Photochemistry and Photobiology. John Wiley & Sons, Ltd (10.1111); November 2011; 87(6): 1214–1229. Available at: DOI:10.1111/j.1751-1097.2011.00978.x

20. Gul W., Vaid FHM., Faiyaz A., Anwar Z., Khurshid A., Ahmad I. Simultaneous photoaddition, photoreduction and chemical reduction of riboflavin by sulfur containing dianions: A kinetic study. Journal of Photochemistry and Photobiology A: Chemistry. Elsevier; May 2019; 376: 22–31. Available at: DOI:10.1016/J.JPHOTOCHEM.2019.02.035

21. Vaid FHM., Gul W., Faiyaz A., Anwar Z., Ejaz MA., Zahid S., et al. Divalent anion catalyzed photodegradation of riboflavin: A kinetic study. Journal of Photochemistry and Photobiology A: Chemistry. Elsevier; February 2019; 371: 59–66. Available at: DOI:10.1016/J.JPHOTOCHEM.2018.10.048

22. EMA. European Medicines Agency: Committee for Medicinal Products for Human Use (CHMP) CHMP assessment report. 2012.

23. Ioele G., De Luca M., Garofalo A., Ragno G. Photosensitive drugs: a review on their photoprotection by liposomes and cyclodextrins. Drug Delivery. Taylor & Francis; November 2017; 24(2): 33–44. Available at: DOI:10.1080/10717544.2017.1386733

24. ICH. International Conference on Harmonisation of Technical Requirements for Registration of Pharmaceuticals for Human Use (ICH) Harmonised Tripartite Guideline Stability Testing: Photostability Testing of New Drug Substances and Products. Q1B Current Step 4 v. 1996.

25. EMEA. The European Agency for the Evaluation of Medicinal Products Evaluation of Medicines for Human Use COMMITTEE FOR PROPRIETARY MEDICINAL PRODUCTS (CPMP) NOTE FOR GUIDANCE ON PHOTOSAFETY TESTING DISCUSSION IN THE SWP DATE FOR COMING INTO OPERATION. 2002.

26. FDA. Guidance for Industry Q1A(R2) Stability Testing of New Drug Substances and Products. 2003.

27. FDA. Guidance for Industry M3(R2) Nonclinical Safety Studies for the Conduct of Human Clinical Trials and Marketing Authorization for Pharmaceuticals Guidance for Industry. 2010.

28. ICH. ICH Harmonised Tripartite Guideline: Photosafety Evaluation of Pharmaceuticals. Current Step 4 version. 2013.

29. OECD. Test No. 432: In Vitro 3T3 NRU Phototoxicity Test, OECD Guidelines for the Testing of Chemicals. Paris; 2004.

30. Rodrigues Neves C., Gibbs S. Progress on Reconstructed Human Skin Models for Allergy Research and Identifying Contact Sensitizers. Springer, Berlin, Heidelberg; 2018. pp. 1–27. Available at: DOI:10.1007/82_2018_88

31. Chacón M., Vázquez N., Berisa S., Persinal M., Sánchez M., Baamonde B., et al. QobuR – A new in vitro human corneal epithelial model for preclinical drug screening. European Journal of Pharmaceutics and Biopharmaceutics. Elsevier; March 2019; 136: 164–173. Available at: DOI:10.1016/J.EJPB.2019.01.023

32. Baertschi SW., Alsante KM., Tønnesen HH. A Critical Assessment of the ICH Guideline on Photostability Testing of New Drug Substances and Products (Q1B): Recommendation for Revision. Journal of Pharmaceutical Sciences. Elsevier; July 2010; 99(7): 2934–2940. Available at: DOI:10.1002/JPS.22076

33. Baertschi SW., Clapham D., Foti C., Jansen PJ., Kristensen S., Reed R., et al. Implications of In-Use Photostability: Proposed Guidance for Photostability Testing and Labeling to Support the Administration of Photosensitive Pharmaceutical Products, Part 1: Drug Products Administered by Injection.

Journal of Pharmaceutical Sciences. Elsevier; November 2013; 102(11): 3888–3899. Available at: DOI:10.1002/JPS.23717

34. Baertschi SW., Clapham D., Foti C., Kleinman MH., Kristensen S., Reed RA., et al. Implications of In-Use Photostability: Proposed Guidance for Photostability Testing and Labeling to Support the Administration of Photosensitive Pharmaceutical Products, Part 2: Topical Drug Product. Journal of Pharmaceutical Sciences. Elsevier; September 2015; 104(9): 2688–2701. Available at: DOI:10.1002/JPS.24396

35. Allain L., Baertschi SW., Clapham D., Foti C., Lantaff WM., Reed RA., et al. Implications of In-Use Photostability: Proposed Guidance for Photostability Testing and Labeling to Support the Administration of Photosensitive Pharmaceutical Products, Part 3. Oral Drug Products. Journal of Pharmaceutical Sciences. Elsevier; May 2016; 105(5): 1586–1594. Available at: DOI:10.1016/J.XPHS.2016.02.035

36. Khandpur S., Porter RM., Boulton SJ., Anstey A. Drug-induced photosensitivity: new insights into pathomechanisms and clinical variation through basic and applied science. British Journal of Dermatology. John Wiley & Sons, Ltd (10.1111); April 2017; 176(4): 902–909. Available at: DOI:10.1111/bjd.14935

37. Drucker AM., Rosen CF. Drug-Induced Photosensitivity. Drug Safety. Springer International Publishing; October 2011; 34(10): 821–837. Available at: DOI:10.2165/11592780-000000000-00000

38. Kuhn HJ., Braslavsky SE., Schmidt R. Chemical actinometry (IUPAC Technical Report). Pure and Applied Chemistry. De Gruyter; January 2004; 76(12): 2105–2146. Available at: DOI:10.1351/pac200476122105

39. Tønnesen HH. Photostability of Drugs and Drug Formulations, Second Edition. Photostability of Drugs and Drug Formulations, Second Edition. 2010. Available at: DOI:10.1201/9781420023596

40. Tønnesen HH (Hanne H. Photostability of drugs and drug formulations. CRC Press; 2004. 435 p. Available at: https://www.crcpress.com/Photostability-of-Drugs-and-Drug-Formulations/Tonnesen/p/book/9780415303231 (Accessed: 21 May 2019)

41. Montalti M., Credi A., Prodi L., Teresa Gandolfi M. Handbook of Photochemistry, Third Edition. CRC Press; 2006. Available at: DOI:10.1201/9781420015195 (Accessed: 5 April 2019)

42. Lee J., Kim J., Choi W. Ferrioxalate-polyoxometalate system as a new chemical actinometer. Environmental Science and Technology. 2007; 41(15): 5433–5438. Available at: DOI:10.1021/es070474z

43. Li H., Betterton EA., Arnold RG., Ela WP., Barbaris B., Grachane C. Convenient new chemical actinometer based on aqueous acetone, 2-propanol, and carbon

tetrachloride. Environmental Science and Technology. 2005; 39(7): 2262–2266. Available at: DOI:10.1021/es050046y

44. Kirk AD., Namasivayam C. Errors in Ferrioxalate Actinometry. Analytical Chemistry. 1983; 55(14): 2428–2429. Available at: DOI:10.1021/ac00264a053

45. El Achi N., Bakkour Y., Chausset-Boissarie L., Penhoat M., Rolando C. Rapid and facile chemical actinometric protocol for photo-microfluidic systems using azobenzene and NMR spectroscopy. RSC Advances. 2017; 7(47): 29815–29820. Available at: DOI:10.1039/c7ra01237c

46. Gauglitz G., Hubig S. Chemical actinometry in the UV by azobenzene in concentrated solution: A convenient method. Journal of Photochemistry. 1985; 30(2): 121–125. Available at: DOI:10.1016/0047-2670(85)85018-8

47. de Azevedo Filho CA., de Filgueiras Gomes D., de Mélo Guedes JP., Batista RMF., Santos BS. Considerations on the quinine actinometry calibration method used in photostability testing of pharmaceuticals. Journal of Pharmaceutical and Biomedical Analysis. Elsevier; March 2011; 54(4): 886–888. Available at: DOI:10.1016/J.JPBA.2010.11.012

48. Pottier RH., Russell DA. Quantum Yield of a Photochemical Reaction. Photobiological Techniques. 2011; : 45–57. Available at: DOI:10.1007/978-1-4615-3840-0_4

49. Ben-Hur E., Song P-S. The Photochemistry and Photobiology of Furocoumarins (Psoralens). Advances in Radiation Biology. Elsevier; 1 January 1984; 11: 131–171. Available at: DOI:10.1016/B978-0-12-035411-5.50009-5 (Accessed: 16 April 2019)

50. McDonagh AF., Agati G., Fusi F., Pratesi R. Quantum Yields for Laser Photocyclization of Bilirubin in the Presence of Human Serum Albumin. Dependence of Quantum Yield on Excitation Wavelength. Photochemistry and Photobiology. 1989; 50(3): 305–319. Available at: DOI:10.1111/j.1751-1097.1989.tb04164.x

51. Skillman JB. Quantum yield variation across the three pathways of photosynthesis: Not yet out of the dark. Journal of Experimental Botany. 2008; 59(7): 1647–1661. Available at: DOI:10.1093/jxb/ern029

52. Bertelsen G., Skibsted LH. Photooxidation of oxymyoglobin. Wavelength dependence of quantum yields in relation to light discoloration of meat. Meat Science. 1987; 19(4): 243–251. Available at: DOI:10.1016/0309-1740(87)90070-2

53. Kistiakowsky GB., Sternberg JC. Primary photochemical process in bromine. The Journal of Chemical Physics. 1953; 21(12): 2218–2223. Available at: DOI:10.1063/1.1698816

54. Higgins CM., Evans LA., Lloyd-Jones GC., Shallcross DE., Tew DP., Orr-Ewing AJ.

Quantum yields for photochemical production of NO2 from organic nitrates at tropospherically relevant wavelengths. Journal of Physical Chemistry A. 2014; 118(15): 2756–2764. Available at: DOI:10.1021/jp501517t

55. Moore DE. Principles and practice of drug photodegradation studies. Journal of Pharmaceutical and Biomedical Analysis. 1987; 5(5): 441–453. Available at: DOI:10.1016/0731-7085(87)80053-5

56. Kim JE., Tauber MJ., Mathies RA. Wavelength dependent cis-trans isomerization in vision. Biochemistry. 2001; 40(46): 13774–13778. Available at: DOI:10.1021/bi0116137

57. Malacarne M., Protti S., Fagnoni M. A Visible-Light-Driven, Metal-free Route to Aromatic Amides via Radical Arylation of Isonitriles. Advanced Synthesis and Catalysis. 2017; 359(21): 3826–3830. Available at: DOI:10.1002/adsc.201700619

58. Fast DE., Lauer A., Menzel JP., Kelterer AM., Gescheidt G., Barner-Kowollik C. Wavelength-Dependent Photochemistry of Oxime Ester Photoinitiators. Macromolecules. 2017; 50(5): 1815–1823. Available at: DOI:10.1021/acs.macromol.7b00089

59. Marugán J., Vega B., van Grieken R., Pablos C., Martín-Sómer M. Wavelength dependence of the efficiency of photocatalytic processes for water treatment. Applied Catalysis B: Environmental. Elsevier; 2017; 221(September 2017): 258–265. Available at: DOI:10.1016/j.apcatb.2017.09.032

60. Kim JK., Kang DJ., Bae BS. Wavelength-dependent photosensitivity in a germanium-doped sol-gel hybrid material for direct photopatterning. Advanced Functional Materials. 2005; 15(11): 1870–1876. Available at: DOI:10.1002/adfm.200500171

61. Nunes CM., Reva I., Pinho E Melo TMVD., Fausto R. UV-laser photochemistry of isoxazole isolated in a low-temperature matrix. Journal of Organic Chemistry. 2012; 77(19): 8723–8732. Available at: DOI:10.1021/jo301699z

62. Hansen MJ., Velema WA., Lerch MM., Szymanski W., Feringa BL. Wavelength-selective cleavage of photoprotecting groups: Strategies and applications in dynamic systems. Chemical Society Reviews. Royal Society of Chemistry; 2015; 44(11): 3358–3377. Available at: DOI:10.1039/c5cs00118h

63. Singh B., Zweig A., Gallivan JB. Wavelength-Dependent Photochemistry of 2-Aroyl-3-aryl-2H-azirines. Mechanistic Studies. Journal of the American Chemical Society. 1972; 94(4): 1199–1206. Available at: DOI:10.1021/ja00759a028

64. Bogdanova A., Popik V V. Wavelength-dependent photochemistry of diazo Meldrum's acid and its spirocyclic isomer, diazirino Meldrum's acid: Wolff rearrangement versus isomerization. Journal of the American Chemical Society. 2003; 125(6): 1456–1457. Available at: DOI:10.1021/ja029528p

65. PROTTI S., Ravelli D., Photobiological MF-P&., 2019 U. Wavelength-dependence and wavelength-selectivity in photochemical reactions. pubs.rsc.org. 2019.

66. Nakamura S., Kobayashi T., Takata A., Uchida K., Asano Y., Murakami A., et al. Quantum yields and potential energy surfaces: a theoretical study. Journal of Physical Organic Chemistry. John Wiley & Sons, Ltd; 1 November 2007; 20(11): 821–829. Available at: DOI:10.1002/poc.1245 (Accessed: 1 April 2019)

67. Diau EWG. A New Trans-to-Cis Photoisomerization Mechanism of Azobenzene on the S 1(n,π*) Surface. Journal of Physical Chemistry A. 2004; 108(6): 950–956. Available at: DOI:10.1021/jp031149a

68. Ern J., Bens AT., Martin HD., Kuldova K., Peter Trommsdorff H., Kryschi C. Ring-opening and -closure reaction dynamics of a photochromic dithienylethene derivative. Journal of Physical Chemistry A. 2002; 106(9): 1654–1660. Available at: DOI:10.1021/jp012614b

69. Bandara HMD., Burdette SC. Photoisomerization in different classes of azobenzene. Chemical Society Reviews. 2012; 41(5): 1809–1825. Available at: DOI:10.1039/c1cs15179g

70. Holzwarth AR., Schaffner K. WAVELENGTH DEPENDENCE OF QUANTUM YIELDS AND PRODUCT DISTRIBUTION IN THE ANAEROBIC PHOTOCHEMISTRY OF BILIRUBIN DIMETHYL ESTER. Photochemistry and Photobiology. John Wiley & Sons, Ltd (10.1111); 1 May 1981; 33(5): 635–639. Available at: DOI:10.1111/j.1751-1097.1981.tb05469.x (Accessed: 11 April 2019)

71. Sumi T., Takagi Y., Yagi A., Morimoto M., Irie M. Photoirradiation wavelength dependence of cycloreversion quantum yields of diarylethenes. Chemical Communications. The Royal Society of Chemistry; 18 March 2014; 50(30): 3928. Available at: DOI:10.1039/c4cc00396a (Accessed: 2 April 2019)

72. Gagliardi L., Orlandi G., Bernardi F., Cembran A., Garavelli M. A theoretical study of the lowest electronic states of azobenzene: The role of torsion coordinate in the cis-trans photoisomerization. Theoretical Chemistry Accounts. 2004; 111(2–6): 363–372. Available at: DOI:10.1007/s00214-003-0528-1

73. Greenberg JW., Malhotra V., Ennever JF. Wavelength Dependence of the Quantum Yield for the Structural Isomerization of Bilirubin. Photochemistry and Photobiology. 1987; 46(4): 453–456. Available at: DOI:10.1111/j.1751-1097.1987.tb04794.x

74. Klán P., Wirz J. Photochemistry of organic compounds : from concepts to practice. Wiley; 2009. 563 p. Available at: https://www.wiley.com/en-ar/Photochemistry+of+Organic+Compounds%3A+From+Concepts+to+Practice-p-9781405161732 (Accessed: 17 April 2019)

75. Hanazawa M., Sumiya R., Horikawa Y., Irie M. Thermally irreversible photochromic systems. Reversible photocyclization of 1,2-bis (2-

methylbenzo[b]thiophen-3-yl)perfluorocyclocoalkene derivatives. Journal of the Chemical Society, Chemical Communications. 1992; (3): 206–207. Available at: DOI:10.1039/C39920000206

76. Kim JE., Tauber MJ., Mathies RA. Analysis of the mode-specific excited-state energy distribution and wavelength-dependent photoreaction quantum yield in rhodopsin. Biophysical Journal. 2003; 84(4): 2492–2501. Available at: DOI:10.1016/S0006-3495(03)75054-1

77. Agati G., Fusi F., Pratesi R., McDonagh AF. WAVELENGTH-DEPENDENT QUANTUM YIELD FOR Z → E ISOMERIZATION OF BILIRUBIN COMPLEXED WITH HUMAN SERUM ALBUMIN. Photochemistry and Photobiology. John Wiley & Sons, Ltd (10.1111); 1 February 1992; 55(2): 185–190. Available at: DOI:10.1111/j.1751-1097.1992.tb04226.x (Accessed: 2 April 2019)

78. Hansen E., Skibsted LH. Light-induced oxidative changes in model dairy spread. Wavelength dependence of quantum yields. Journal of Agricultural and Food Chemistry. 2000; 48(8): 3090–3094. Available at: DOI:10.1021/jf991232o

79. Mahato RI., Narang AS., Narang AS. Pharmaceutical Dosage Forms and Drug Delivery, SECOND EDITION. CRC Press; 2011. Available at: DOI:10.1201/b12122 (Accessed: 21 May 2019)

80. Connors KA (Kenneth A., Amidon GL., Stella VJ. Chemical stability of pharmaceuticals : a handbook for pharmacists. Wiley; 1986. 847 p. Available at: https://www.wiley.com/en-us/Chemical+Stability+of+Pharmaceuticals%3A+A+Handbook+for+Pharmacists%2C+2nd+Edition-p-9780471879558 (Accessed: 21 May 2019)

81. Maafi M., Brown RG. The kinetic model for AB(1φ) systems. Journal of Photochemistry and Photobiology A: Chemistry. April 2007; 187(2–3): 319–324. Available at: DOI:10.1016/j.jphotochem.2006.10.030 (Accessed: 23 May 2019)

82. Takara A., Kobayashi K., Watanabe S., Okuyama K., Shimada Y., Goto S. Dibucaine inhibits ketoprofen photodegradation via a mechanism different from that of antioxidants. Journal of Photochemistry and Photobiology A: Chemistry. Elsevier B.V.; 2017; 333: 208–212. Available at: DOI:10.1016/j.jphotochem.2016.10.026

83. Li C., Zhang D., Peng J., Li X. The effect of pH, nitrate, iron (III) and bicarbonate on photodegradation of oxytetracycline in aqueous solution. Journal of Photochemistry and Photobiology A: Chemistry. Elsevier B.V.; 2018; 356: 239–247. Available at: DOI:10.1016/j.jphotochem.2018.01.004

84. Passeport E., Zhang N., Wu L., Herrmann H., Sherwood Lollar B., Richnow HH. Aqueous photodegradation of substituted chlorobenzenes: Kinetics, carbon isotope fractionation, and reaction mechanisms. Water Research. Elsevier Ltd; 2018; 135: 95–103. Available at: DOI:10.1016/j.watres.2018.02.008

85. Megerle U., Lechner R., König B., Riedle E. Laboratory apparatus for the accurate,

facile and rapid determination of visible light photoreaction quantum yields. Photochemical and Photobiological Sciences. 2010; 9(10): 1400–1406. Available at: DOI:10.1039/c0pp00195c

86. Voigt M., Jaeger M. On the photodegradation of azithromycin, erythromycin and tylosin and their transformation products – A kinetic study. Sustainable Chemistry and Pharmacy. Elsevier; 1 June 2017; 5: 131–140. Available at: DOI:10.1016/J.SCP.2016.12.001 (Accessed: 7 May 2019)

87. Nassar R., Trivella A., Mokh S., Al-Iskandarani M., Budzinski H., Mazellier P. Photodegradation of sulfamethazine, sulfamethoxypiridazine, amitriptyline, and clomipramine drugs in aqueous media. Journal of Photochemistry and Photobiology A: Chemistry. Elsevier B.V.; 2017; 336: 176–182. Available at: DOI:10.1016/j.jphotochem.2016.12.008

88. Zepp RG. Quantum Yields for Reaction of Pollutants in Dilute Aqueous Solution. Environmental Science and Technology. 1978; 12(3): 327–329. Available at: DOI:10.1021/es60139a010

89. Calisto V., Domingues MRM., Esteves VI. Photodegradation of psychiatric pharmaceuticals in aquatic environments - Kinetics and photodegradation products. Water Research. 2011; 45(18): 6097–6106. Available at: DOI:10.1016/j.watres.2011.09.008

90. Apell JN., McNeill K. Updated and validated solar irradiance reference spectra for estimating environmental photodegradation rates. Environmental Science: Processes & Impacts. Royal Society of Chemistry; 2019; : 427–437. Available at: DOI:10.1039/c8em00478a

91. Yassine M., Fuster L., Dévier MH., Geneste E., Pardon P., Grélard A., et al. Photodegradation of novel oral anticoagulants under sunlight irradiation in aqueous matrices. Chemosphere. 2018; 193: 329–336. Available at: DOI:10.1016/j.chemosphere.2017.11.036

92. Oliveira C., Lima DLD., Silva CP., Calisto V., Otero M., Esteves VI. Photodegradation of sulfamethoxazole in environmental samples: The role of pH, organic matter and salinity. Science of the Total Environment. Elsevier B.V.; 2019; 648: 1403–1410. Available at: DOI:10.1016/j.scitotenv.2018.08.235

93. Mazellier P., Méité L., De Laat J. Photodegradation of the steroid hormones 17β-estradiol (E2) and 17α-ethinylestradiol (EE2) in dilute aqueous solution. Chemosphere. Elsevier Ltd; 2008; 73(8): 1216–1223. Available at: DOI:10.1016/j.chemosphere.2008.07.046

94. Roman J., Breier AR., Steppe M. Stability indicating LC method to determination of sodium montelukast in pharmaceutical dosage form and its photodegradation kinetics. Journal of Chromatographic Science. 2011; 49(7): 540–546. Available at: DOI:10.1093/chrsci/49.7.540

95. MATSUURA I., IMAIZUMI M., SUGIYAMA M. Method of kinetic analysis of photodegradation: Nifedipine in solutions. Chemical & Pharmaceutical Bulletin. 2011; 38(6): 1692–1696. Available at: DOI:10.1248/cpb.38.1692

96. de Haro Moreno A., Regina Nunes Salgado H. Stability Study and Degradation Kinetics of Ceftazidime in Pharmaceutical Preparations. Advances in Analytical Chemistry of Scientific & Academic Publishing. 2012; 2(1): 1–5. Available at: DOI:10.5923/j.aac.20120201.01

97. Ji Y., Zeng C., Ferronato C., Chovelon JM., Yang X. Nitrate-induced photodegradation of atenolol in aqueous solution: Kinetics, toxicity and degradation pathways. Chemosphere. Elsevier Ltd; 2012; 88(5): 644–649. Available at: DOI:10.1016/j.chemosphere.2012.03.050

98. Kakavandi B., Takdastan A., Jaafarzadeh N., Azizi M., Mirzaei A., Azari A. Application of Fe<inf>3</inf>O<inf>4</inf>@C catalyzing heterogeneous UV-Fenton system for tetracycline removal with a focus on optimization by a response surface method. Journal of Photochemistry and Photobiology A: Chemistry. Elsevier B.V.; 2016; 314: 178–188. Available at: DOI:10.1016/j.jphotochem.2015.08.008

99. Ahmadi M., Ramezani Motlagh H., Jaafarzadeh N., Mostoufi A., Saeedi R., Barzegar G., et al. Enhanced photocatalytic degradation of tetracycline and real pharmaceutical wastewater using MWCNT/TiO2nano-composite. Journal of Environmental Management. 2017; 186: 55–63. Available at: DOI:10.1016/j.jenvman.2016.09.088

100. Albini A., Fasani E (Elisa). Drugs, photochemistry and photostability. Royal Society of Chemistry; 1998. 326 p. Available at: https://books.google.co.uk/books?hl=en&lr=&id=S3UoDwAAQBAJ&oi=fnd&pg=PR7&dq=Albini+A.%3B+Fasani+E.,+1998.+Drugs+Photochemistry+and+Photostability.+The+Royal+Society+of+Chemistry:+Cambridge&ots=NhbnU2uMou&sig=dUKcCZg4GHs7WPImb7jYtQiVPqM#v=onepage&q=Albini A.%3B Fasani E.%2C 1998. Drugs Photochemistry and Photostability. The Royal Society of Chemistry%3A Cambridge&f=false (Accessed: 21 May 2019)

101. Piechocki JT., Thoma K. Pharmaceutical photostability and stabilization technology. Informa Healthcare; 2007. 445 p. Available at: https://books.google.co.uk/books?hl=en&lr=&id=SU-mzz55oPIC&oi=fnd&pg=PP1&dq=Piechocki+JT,+Thoma+K.+Pharmaceutical+Photostability+and+Photostabilisation+Technology.+Informa+Healthcare:+London%3B+2010.&ots=SNGFgRS0-Y&sig=lKT-KDpTmD71ESgA018s0YXCZWU#v=onepage&q&f=false (Accessed: 21 May 2019)

102. Moore D. Standardization of Kinetic Studies of Photodegradation Reactions. Photostability of Drugs and Drug Formulations, Second Edition. CRC Press; 2004. pp. 41–65. Available at: DOI:10.1201/9781420023596.ch3 (Accessed: 23 May 2019)

103. Moore DE. Kinetic treatment of photochemical reactions. International Journal of Pharmaceutics. 1990; 63(1): R5.

104. Shaw H., Toby S. Light absorption in photochemistry. Journal of Chemical Education. Division of Chemical Education ; August 1966; 43(8): 408. Available at: DOI:10.1021/ed043p408 (Accessed: 20 May 2019)

105. Nakashima H., Irie M. Synthesis of silsesquioxanes having photochromic diarylethene pendant groups. Macromolecular Rapid Communications. 1997; 18(8): 625–633. Available at: DOI:10.1002/marc.1997.030180801

106. Bayda M., Hug GL., Lukaszewicz J., Majchrzak M., Marciniec B., Marciniak B. Kinetics of reversible photoisomerization: Determination of the primary quantum yields for the E-Z photoisomerization of silylenephenylenevinylene derivatives. Photochemical and Photobiological Sciences. 2009; 8(12): 1667–1675. Available at: DOI:10.1039/b907242j

107. Aillet T., Loubière K., Dechy-Cabaret O., Prat L. Microreactors as a Tool for Acquiring Kinetic Data on Photochemical Reactions. Chemical Engineering and Technology. 2016; 39(1): 115–122. Available at: DOI:10.1002/ceat.201500163

108. Micheau JC., Coudret C., Kobeleva OI., Barachevsky VA., Yarovenko VN., Ivanov SN., et al. Quantitative study of photochromic transformations of diarylethene derivatives with either perhydrocyclopentene or oxazolone or lactone units. Dyes and Pigments. Elsevier Ltd; 2014; 106: 32–38. Available at: DOI:10.1016/j.dyepig.2014.02.013

Chapter 3

Materials and methods

3.1. Chemicals and solvents

The chemicals that used in photochemical studies listed in the table (2-1).

Table 3- 1: *Chemicals and solvents details.*

Compounds	Symbol	Chemical names	Company supplier
E-Stilbene	*E*-STIL	trans-1,2-Diphenylethylene.	Sigma Aldrich (UK)
Pinosylvin	PINO	trans-3,5-Dihydroxystilbene.	
Resveratrol	RVT	3,4’,5-Trihydroxy-trans-stilbene	
Oxyresveratrol	ORVT	2,3’,4,5’-Tetrahydroxy-trans-stilbene	
Pterostilbene	PTERO	3,5-Dimethoxy-4’-hydroxystilbene	
Nifedipine	NIF	1,4-Dihydro-2,6-dimethyl-4-(2-nitrophenyl)-3,5-pyridinedicarboxylic acid dimethyl ester.	
Dacarbazine	DBZ	5-(3,3-Dimethyl-1-triazenyl)imidazole-4-carboxamide.	
Axitinib	AXI	N-Methyl-2-((3-((1E)-2-(pyridin-2-yl)ethenyl)-1H-indazol-6-yl)sulfanyl)benzamide.	
DAE	DAE	1,2-Bis[2-methylbenzo[b]thiophen-3-yl]-3,3,4,4,5,5-hexafluoro-1-cyclopentene	Tokyo Chemical Industry (UK)
Ethanol absolute (analytical reagent grade)			Fisher Scientific
methanol (HPLC grade)			
acetonitrile (HPLC grade)			
Double distilled water	Fistreem cyclone		Fistreem International, UK

3.2. Instruments

3.2.1. Spectrophotometers

In the monochromatic irradiation studies, a diode array spectrophotometer (Agilent 8453), using Agilent 8453 Chemstation kinetics-software, equipped with a 1-cm cuvette sample holder was used to record the absorption spectra of the compounds. The spectrophotometer was equipped with a Peltier system model Agilent 8453 for temperature control.

A Helios Gamma spectrophotometer (ThermoScientificTM) with 600 nm/min speed scan at 0.5 nm interval was used in the polychromatic studies to record the absorption spectra of the compounds. The absorbance data was measured by using VISIONliteTM software.

3.2.2. Irradiation set-up

3.2.2.1. Monochromatic continuous irradiation

The system for irradiation made by PTIC (Photon Technology International Corporation), contains a Ushio 1000 W xenon arc-lamp. This lamp was used to irradiate the sample. The source of light was kept in a housing shell model A6000 and was power-driven by a power supply model LPS-1200, which was cooled with tap water via a pipe circulation system. The lamp housing and monochromator model 101 was attached together, that allows the selection of specific irradiation wavelengths. It consists of a specific f/2.5 monochromator with a 1200 groove/300 nm blaze grating. The excitation beam was directed from the top of the sample cuvette through an optical fibre. The excitation and the analysis light beams were perpendicular to each other.

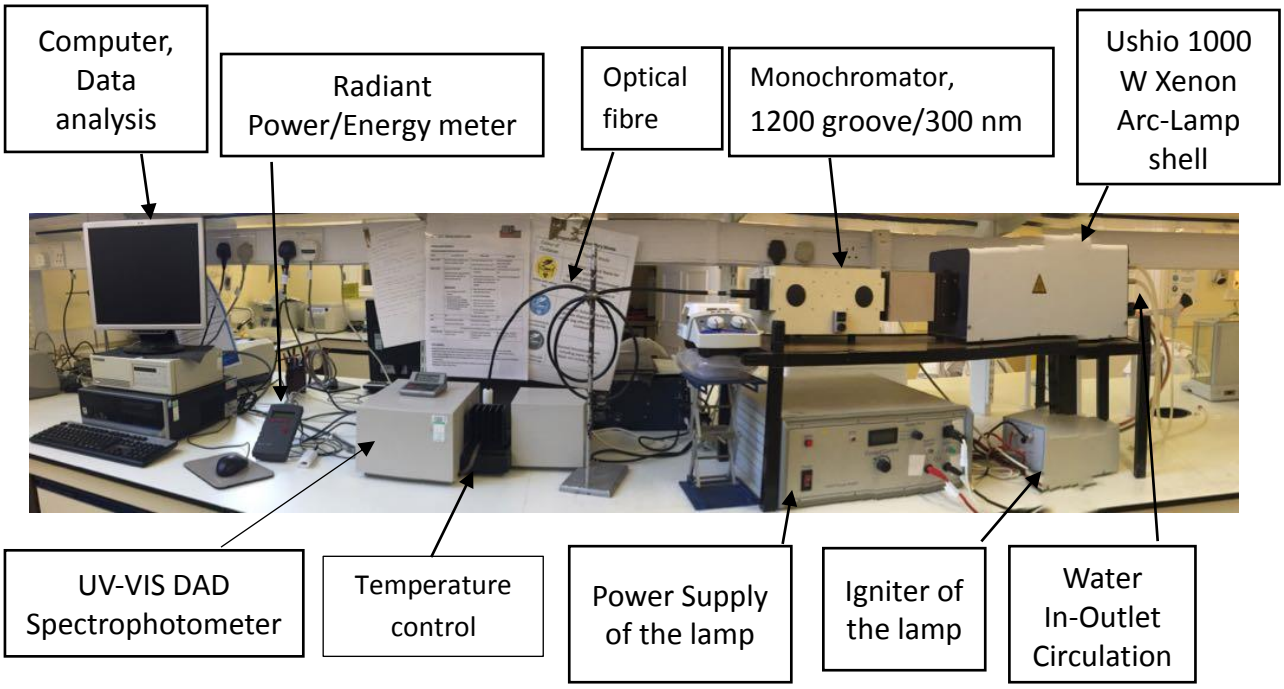

Figure 3- 1: Monochromatic photolysis set-up for continuous irradiation.

3.2.2.2. Polychromatic steady-state irradiation

Two different light sources were used in this study, the light source used in the visible range (400-600 nm) and for unimolecular photoreaction AB $(1\Phi)_{\varepsilon_{B=0}}$ is LED Torch (Light way, model: wk-699b/wk-99g, 5000-8300K, China). The second lamp is the UV handheld lamp (model: UVGL-55, A/C powered, manufactured by Analytikjena, lamp model: G6T5HC, λ=200-400 nm), and was used at UV range (200-400 nm) and for both unimolecular AB $(1\Phi)_{\varepsilon_{B\neq0}}$ and photoreversible reaction AB (2Φ).

The Light cabinet (UV-Light cabinet model: C-10E6, Fisher Scientific, UK) was rectangular enclosure (height = 305 mm, width = 229 mm and Depth = 267 mm) equipped with removable UV handheld lamp, while in the other lamp (LED Torch) will cover the area of the removable UV hand lamp with cardboard carton with small circle hole to pass the light through it. The small circle hole was covered by the woven metallic mesh to reduce

the light intensity of the LED Torch lamp when the experiment is running; meanwhile the experimental off will be covered with foil to protect the sample from the light. The emitted light of the both lamp sources was directed on the top of a 1-cm quartz cuvette. This way of light beams excitation was vertical to the top surface of the sample, which is similar to the monochromatic irradiation setup and to make design as same irradiation way. The sample was stirred continuously using ultra flat compact magnetic stirrer plate, 1.2 cm in hight, (model: AMC-FS-01, Novarli, Czech).

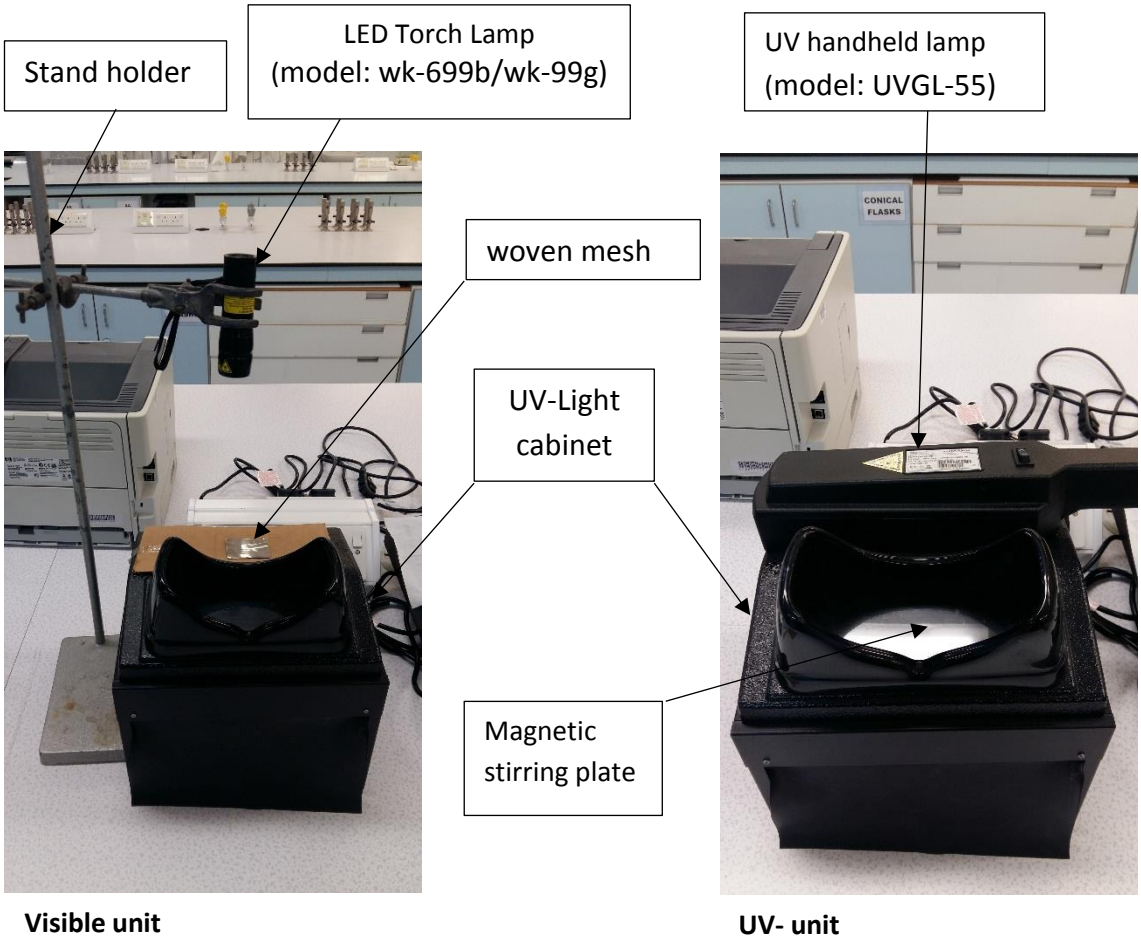

Figure 3- 2: polychromatic photolysis set-up for steady-state irradiations.

3.2.3. Power meters

The radiant power/energy meter model 70260 was adopted to quantify the radiant power of the monochromatic incident excitation beams, and the expressed light power (P_w) that measured by the radiant power meter or spectroradiometer is mW/cm^2.

Avantes spectroradiometer (AvaSpec-ULS2048CL-EVO-UA-50), UA-grating (200-1100nm), slit-25 with a 400um fibre and in-line cosine corrector (FC-UVIR400-1-BX and CC-UV/VIS), was used to measure the radiant power of the polychromatic incident beams, the expressed light power (P_w) that measured by the spectroradiometer is mW/cm^2/nm.

Figure 3-1 show that the light profiles of different light sources. The light sources are sunlight (in July), LED Torch (visible light), Fluoresce light (room light), and UV light sources as short-wave lamp (model: G6T5/SW; 254nm), mid-range wave lamp (model: G6T5E; 302nm), long wave lamp (model: F6T5; BLACK LIGHT; 365nm) and short and long wave lamp (model: G6T5HC; 254/365 nm).

The removable UV hand lamp was provided by filter from the manufacturer to filter and switch between the light if we used lamp contain two wavelengths as short and long wave lamp. When take the light profile without that filter, all the UV light sources were giving same light profile in the range 450 nm to 1100 nm as described in the figure (3-3). While, if the filter is on all the peaks between the 450-1100 will be removed. The UV lamps were giving different light profiles, the mid-range wave lamp was clearly characterised by a broad band in the range 270 to 400 with maxima at ≈302 nm,

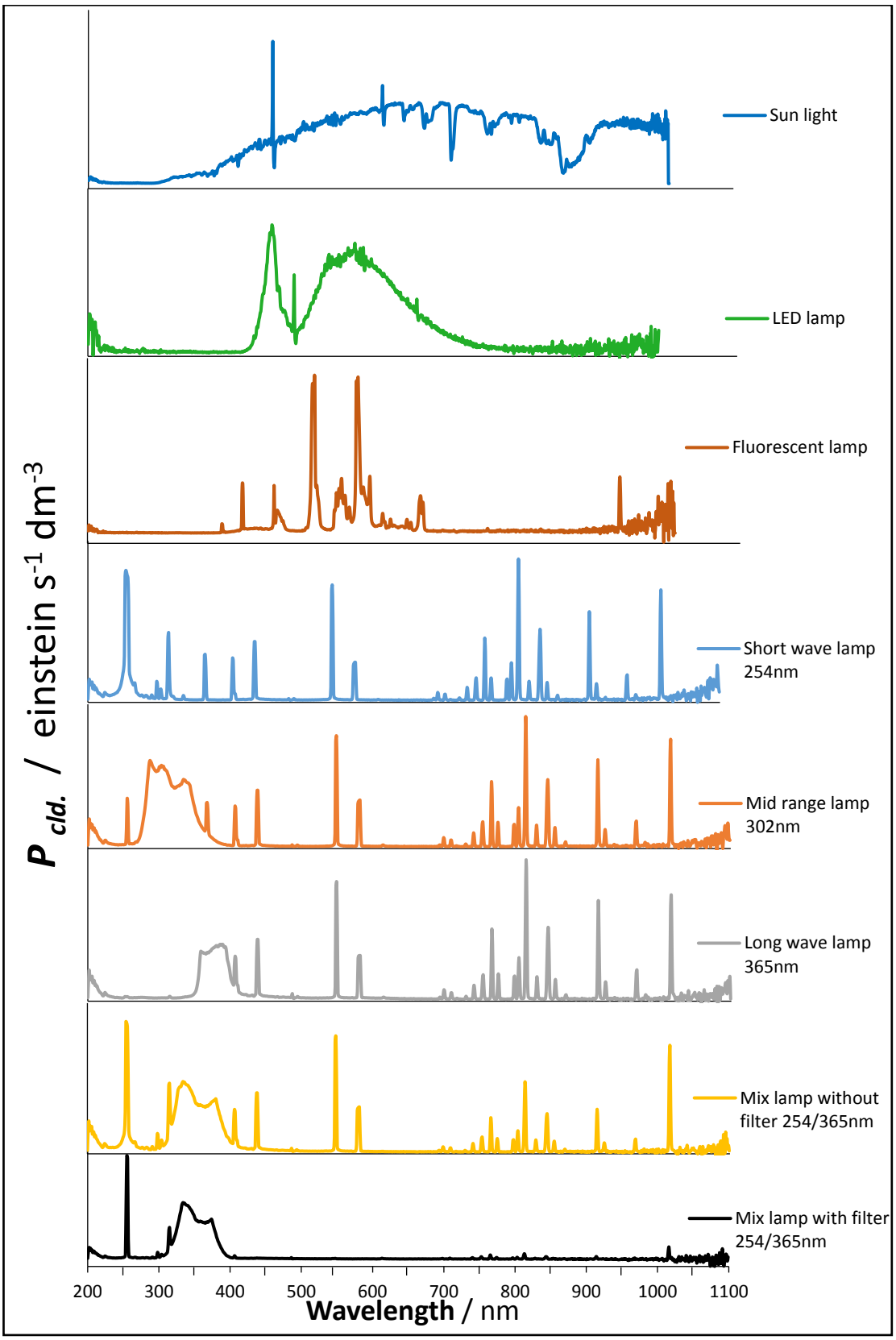

Figure 3- 3: Light profile of different light sources measured by using Avantes spectroradiometer.

long wave lamp was only giving a band after 350 to 400 nm without any bands in the range 200 to 350 nm. However, the short-wave lamp was described by single sharp intensity peak at 254, 313 and 365 nm. On other hands, the visible light as LED Torch and Fluoresce light were clearly do not show any UV light in them profiles, nevertheless the UV and visible light was obviously shown in the sun light but the UV light is much less than visible.

3.2.4. HPLC apparatus

HPLC Analysis was conducted using the Perkin Elmer type Chromatography Interface 600 series equipped with a UV/Vis detector, vacuum degasser and Perkin Elmer Series 200 pump. The analytical separation was obtained by Kinetex C18, 150 X 4.6 mm, 5µm analytical column.

3.3. Methods

3.3.1. Solutions

3.3.1.1. Preparation of solutions

The stock solutions were prepared by weighing ≈1 mg of each compound and dissolved in 1 mL of ethanol. The molar concentrations of these compounds were calculated using the equation below:

$$Concentration\ (M) = \frac{mass\ of\ compound\ (g)}{\text{Molecular weight of compound}\left(\frac{g}{mole}\right) \times \text{Final volume (L)}} \qquad \text{Eq.3-1}$$

The working solutions were freshly prepared by diluting the stock solutions to analysis the irradiation tests at different wavelengths, as shown in Table 2. The concentrations of the working solutions were obtained using the dilution equation:

$$C_1 \times V_1 = C_2 \times V_2$$ Eq.3-2

Both stock and working solutions were wrapped with aluminium foil and stored in the fridge at T < 5°C

3.3.1.2. Calibration graphs

For spectrophotometric, the calibration graphs were obtained by plotting the absorbances (at a specific wavelength), the sum of the absorbances (solutions at time 0 for compound A and compound B as mention below), or peak area (of HPLC) versus concentrations of working standard solutions (Table 3-2).

The HPLC calibration was used to determine the concentration of compound A at the pss; therefore, it was useful to quantify the absorption coefficients (ε) of photoproducts as described in the elucidation method (Eq. 5-13, chapter five, section 5.2.3.1).

In the instance of reaction type AB $(1\Phi)_{\varepsilon_{B\neq 0}}$, A_∞ is equal to A_B because all mother compounds (A) react to form the photoproduct, (B). The calibration graphs of $\sum A_\infty$, which can be found as the gradient of the calibration curves. However, for AB (2Φ), the $\sum \varepsilon_B$ was determined after determining the concentration of the compound in the photostationary state as well. The spectral evolution of the compound is obtained using the spectrophotometer after exposing it to polychromatic light. Once the A_∞ have been obtained, $A_{B\,(pss)}$ can be quantified using Eq.3-3.

$$A_{B\,(pss)} = A_\infty - \left(\varepsilon_A \times C_{A\,(pss)}\right)$$ Eq. 3-3

Once $A_{B\,(pss)}$ is obtained, the sum of $A_{B\,(pss)}$ can be calculated from the individual absorbances, and then the $\sum \varepsilon_B$ was quantified as the above but by using calibration graph of $\sum A_{B\,(pss)}$.

ε_B for both systems is also determined as described in chapter five, section 5.2.3.1, but after irradiation under polychromatic light it will take the form of sum of the individual ε_B. The difference between the sum of the individual ε_B and the predicted $\sum \varepsilon_B$ from the calibration curve should be less than 5%.

The linearity range of calibration graphs imposes the concentration range useful for performing consistent photokinetic studies.

Table 3- 2: The linear range of studied compounds in ethanol, the equation of the line and correlation coefficient (r^2)

Compounds	MWt g/mole	Linearity range x 10^5 / M	Calibration Equation	correlation co-efficient /r^2
Spectrophotometer (single absorbance)				
E-STIL	180.25	0.544 – 8.19	A_{300} = 28272 x C - 0.0244	0.999
PINO	212.244	0.465 – 8.63	A_{300} = 24581 x C - 0.0195	0.999
RVT	228.25	0.465 – 7.00	A_{320} = 33325 x C - 0.0254	0.999
ORVT	244.24	0.426 – 9.28	A_{313} = 22874 x C - 0.0254	0.999
PTERO	256.296	0.386 – 7.16	A_{310} = 19877 x C – 0.0138	0.999
AXI	386.469	0.257 – 5.61	A_{330} = 19773 x C - 0.0096	0.999
DBZ	182.18	1.5 – 10.74	A_{280} = 4996 x C + 0.0007	0.999
NIF	346.335	1.50 – 13.2	A_{240} = 22545x C - 0.0628	0.999
O-DAE	468.48	0.211 – 6.20	A_{260} = 12311 x C - 0.0085	0.999
C-DAE		0.322 – 1.52	A_{520} = 11244 x C – 0.0028	0.999
Spectrophotometer (sum of absorbances)				
E-STIL	**∑A**	0.959 – 7.36	$\sum A_A$ = 2200282.07 xC - 0.97 $\sum A_B$ = 1658419.73 xC + 20.26	0.999
PINO	**∑A**	0.607 -8.18	$\sum A_A$ = 2092358.58 xC + 3.05 $\sum A_B$ = 1363326.76 xC + 16.77	0.999
RVT	**∑A**	0.560 – 5.63	$\sum A_A$ = 3317695.56 xC - 1.65 $\sum A_B$ = 2391333.67 xC + 21.65	0.999
ORVT	**∑A**	1.80 – 9.86	$\sum A_A$ = 1932689.06 xC - 0.78 $\sum A_B$ = 1501918.59 xC + 12.47	0.999

Compounds	MWt g/mole	Linearity range x 10^5 / M	Calibration Equation	correlation co-efficient /r^2
PTERO	**∑A**	0.464 – 6.96	$\sum A_A$ = 1917192.83 xC + 0.84 $\sum A_B$ = 1588207.63 xC + 25.45	0.999
AXI	**∑A**	0.575 – 4.46	$\sum A_A$ = 3276859.34 xC + 45.70 $\sum A_B$ = 3981269.48 xC - 2.19	0.999
DBZ	**∑A**	1.5 – 10.74	$\sum A_A$ = 1150804.81 x C + 0.16 $\sum A_B$ = 345940 x C + 0.041	0.999
NIF	**∑A**	1.50 – 13.2	$\sum A_A$ = 1920969.95x C - 4.79 $\sum A_B$= 1937923.35x C - 4.68	0.999
O-DAE	**∑A**	0.463 – 6.00	$\sum A_A$ = 2386621.40 xC + 1.18 $\sum A_B$ = 2806892.78 xC+ 2.40	0.999
C-DAE	**∑A**	0.322 – 1.52	$\sum A_A$ = 1323914.19x C + 0.07	0.999

HPLC

Compounds	Linearity range x 10^5 / M	Calibration Equation	correlation co-efficient /r^2
E-STIL	0.344-55.0	PA= 2 x 10^{10} x C – 74586	0.999
PINO	0.734-23.5	PA= 3 x 10^{10} x C - 41299	0.999
RVT	0.672-21.5	PA= 3 x 10^{10} x C - 47056	0.999
ORVT	0.475-24.0	PA = 4 x 10^9 x C - 30694	0.999
PTERO	0.305-19.5	PA = 2 x 10^{10} x C - 60644	0.999
AXI	0.650-91.0	PA = 3 x 10^{10} x C - 12986	0.999
DBZ	1.72 – 27.5	PA = 4 x 10^9 x C - 18040	0.999
NIF	0.9 – 50.0	PA = 2 x 10^9 x C – 10810	0.999
DAE	0.107-7.46	PA = 4 x 10^9 x C – 2489.5	0.999

3.4. Photolysis Procedure

3.4.1. Monochromatic continuous Irradiation

In monochromatic, a specific wavelength was set to irradiation, specific volume of compounds (µL) was added to a blank (2mL of ethanol), the sample at 22°C was homogenizing and continuously stirred using magnetic flea. The UV spectra was measured every 30 seconds. To determine light intensity, leave light released through the end of optical fiber optic and then, placed it on the top of photodiode sensor (1 cm^{-2}), which is directly connected to radiometer before and after the photolysis.

3.4.2. Polychromatic Steady-State

The sample cuvette was set inside the UV-Light cabinet to shield it from the light. Also, the experimental sample was set at different height levels inside the cabinet using tiles of 0.6 cm of height. All side of the sample cuvette, except the top part, were covered by aluminium foil. During the lamp off, the top of the sample cuvette was covered by plastic lid to prevent evaporated the sample and protected from light as well.

In order to measure the light intensity by using the spectroradiometer, it takes places inside UV-cabinet at the same level of the sample and light emitted directly towards the on the top of fibre-optic which is connected to spectroradiometer.

The sample would be removed from the cabinet at regular time intervals, and the UV-Visible spectra, and the HPLC peak measured.

In both photolysis studies, The sample was homogenized and stirred continuously during the measurement using magnetic stirrer plate. The kinetic profile of the irradiation samples was recorded until the reaction completed, which was shown by no changing in the absorption spectra and the concentration against time reach to the plateau.

3.5. Chromatographic Conditions

In order to separate the compounds, the combination of two solvents was used (Table 3-3). The volume of injection is 20 µL and the detector was set to detect the sample at specific wavelengths.

3.6. Simulation software

Based on the type of the mechanism of the photochemical reaction, the differential equation was obtained. This equation was input into the MathCad software (MathCad

2000 Professional), which was used the fifth-order Runge-Kutta to generate values based on the photochemical mechanism. The generated values were described the photochemical reaction behaviour through change in the concentrations over time. In this thesis will describe how can treat the data under monochromatic and polychromatic light irradiation in chapter 5 and 6, respectively.

Table 3- 3: *HPLC conditions for the separation of the compounds and their photoproducts.*

Compounds		Mobile phase A Acetonitrile %	Mobile phase B Double deionized H_2O %	Flow rate mL/min	λ / nm	Retention t-isomer / min	Retention c-isomer / min
Stilbinoids	t-STIL	65	35	1	300	5.85	6.24
	PINO	40	60	1	300	5.15	5.76
	RVT	30	70	1	310	4.02	5.36
	ORVT	15	85	1.5	328	11.3	10.3
	PTERO	50	50	1	320	5.40	5.93
Drug	AXI	50	50	1	332	2.41	3.32
	DBZ	5	95	1	330	5.09	-
		Methanol	Double deionized H2O %				
Drugs	NIF	55	45	1	326	6.86	5.28
photochrome	DAE	90%	10 %	1.2	299	(O-DAE) 3.69	(C-DAE) 5.56

3.7. Actinometry study

Monochromatic actinometric studies, by exposing the same working solutions to specific wavelengths with a sequence of various power intensities for each wavelength.

Φ-order equations are used to fit the kinetic traces that are observed at irradiation wavelength.

Polychromatic actinometric studies were used the same method of monochromatic actinometric above but expose solutions to a full range of UV and visible allowed by the lamp (Fig. 3-3) with a sequence of different power intensities. The different light intensities were obtained by using several distances to the lamp using tiles or reducing the intensity by placing woven metallic mesh on the top of the sample cuvette. Φ- and η-order equations (Chapter nine) were used to fit the kinetic traces that were observed.

This study was conducted by using three independent experiments solutions of each studies compounds.

Chapter 4
Selected photoactive systems

4.1. Photochemical reaction mechanism

In this study, we wish to study three types of photochemical reaction mechanisms. The photochemical reaction contains the mother compounds A and the photoproduct B, the photokinetic behaviour of the mother compounds A when subjected to the light will result in different AB systems.

When exposed the mother compound to the light, the photoproduct is formed (B) which characterised by it does not absorb the irradiation light (ε_B = 0), and the reaction is a direct reaction, which the photochemical reaction mechanism is called a unimolecular photodegradation AB $(1\Phi)_{\varepsilon_{B=0}}$. In this study, the close form of DAE (C-DAE) (Scheme 4-1) is selected compound.

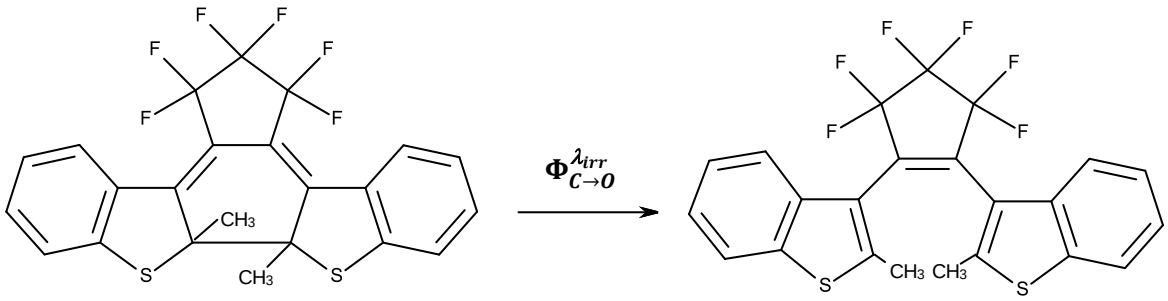

A DAE B

CLOSE Under visible irradiation OPEN

Scheme 4- 1: *The unimolecular AB $(1\Phi)_{\varepsilon_{B=0}}$ degradation mechanism of C-DAE under visible irradiation (A the main compound and B the photoproduct)*

The photochemical reaction of DAE is photocyclization or opening of the cycle [1]. The O-DAE is colourless and C-DAE is pink colour. When exposing the commercial form of the DAE (O-DAE) to UV light irradiation, the reaction is reversible. Whereas, the close form of DAE, when irradiation by visible light transfers to open form in an irreversible

reaction [2]. The isomers of DAE are thermally stable (at 80° C for a long time) [3–5]. In this study, we chosen the C-DAE as example of AB $(1\Phi)_{\varepsilon_{B=0}}$ due to the photoproduct form O-DAE does not absorb the visible light, which mean ε_B = 0. While, the O-DAE was used as example for the AB (2Φ), we will describe the AB (2Φ) system later, due to the photoreversible reaction.

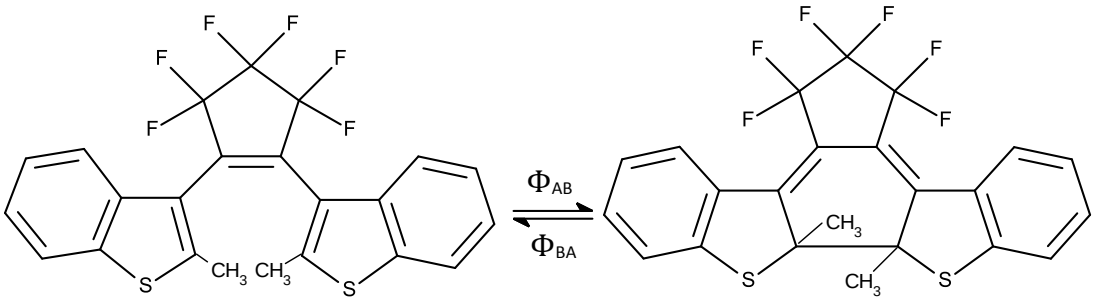

A

OPEN

DAE

Under UV irradiation

B

CLOSE

Scheme 4- 2: *AB (2Φ) photoreversible reaction of O-DAE (A the main compound (open-form) and B the photoproduct (close-form)*

As shown in scheme 4-3, when the photochemical reaction is a direct reaction but, in this case, the compound is formed by the light (B) does absorb the light ($\varepsilon_B \neq 0$). This AB system is called unimolecular photodegradation AB $(1\Phi)_{\varepsilon_{B\neq 0}}$ as well. In this study, we are chosen the NIF and DBZ as examples.

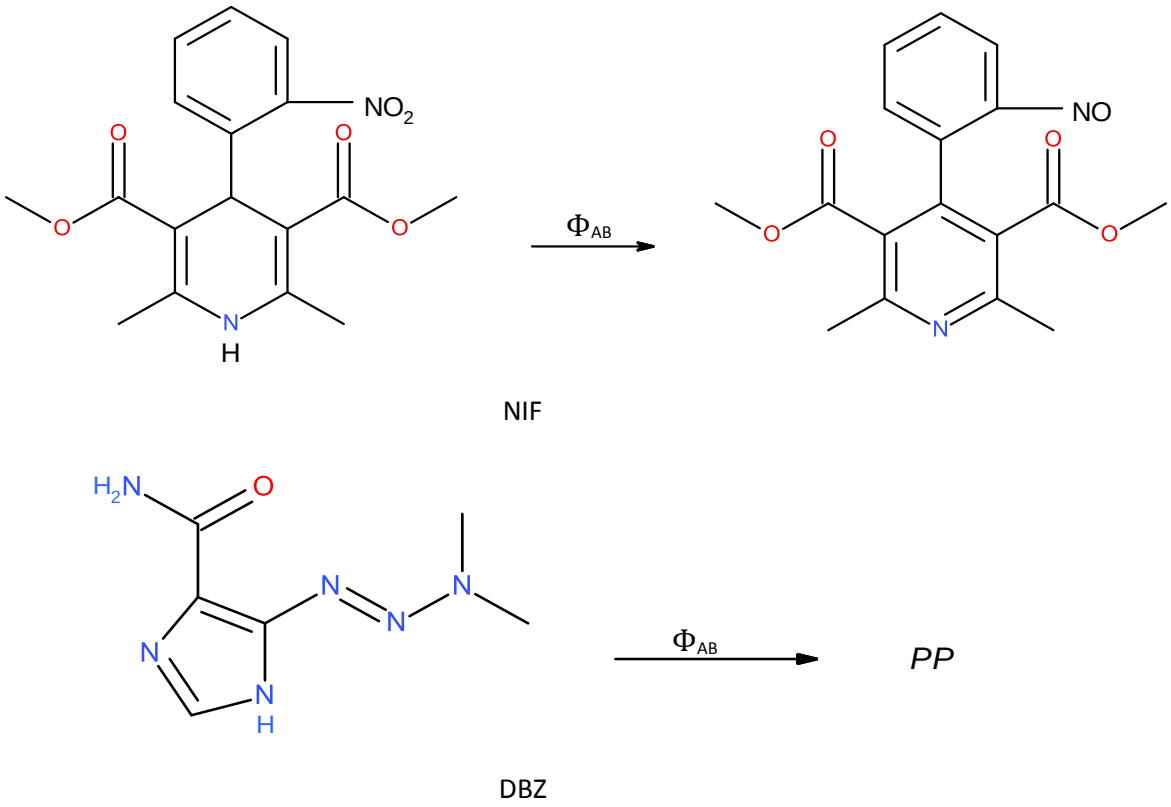

Scheme 4- 3: *The unimolecular AB* $(1\Phi)_{\varepsilon_{B\neq 0}}$ *degradation mechanism of DBZ and NIF.*

Some of the antihypertensive drugs knowns as calcium channel blockers, in particular, and certain dihydropyridine groups have been indicated as being photosensitive and as giving one photoproduct after irradiation by UV/VIS light, such as nifedipine (NIF).

Dacarbazine (DBZ) is an anti-cancer drug known as imidazole carboxamide. It is used to treat melanoma, Hodgkin's lymphoma [6], and soft tissue sarcoma in combination with other anti-cancer drugs [7].

The chemical structure of NIF containing a nitro group in ortho position in the phenyl ring. This nitro group was responsible for classified the NIF as sensitive to the light. The

photoconversion, which is reduction the nitro to nitroso group in the NIF [8]. This reduction leads to the loss of the therapeutic efficiency of the NIF [9].

The photodegradation of the DBZ under natural and fluorescence light was studied in aqueous solutions. These studies founded that after a day exposed the DBZ to the fluorescence light induces a 10 % loss, while a higher loss was observed when direct exposure to sunlight. The photoproduct produced from the exposed the DBZ to light was found to be the main reason to cause the major side effect of the DBZ, a local venous pains [10–12].

The third type of the kinetics that we are interested in is the photoreversible reaction. It involves the mother compounds, A, and its photoproduct, B. This reaction is pure opposed photochemical reaction. Thus, it is labelled as AB (2Φ) photoreaction. In this study, we used t-STIL, PINO, RVT, PTERO, ORVT, AXI and O-DAE to represent the AB (2Φ) system as shown in scheme 4-2, 4-4 and 4-5.

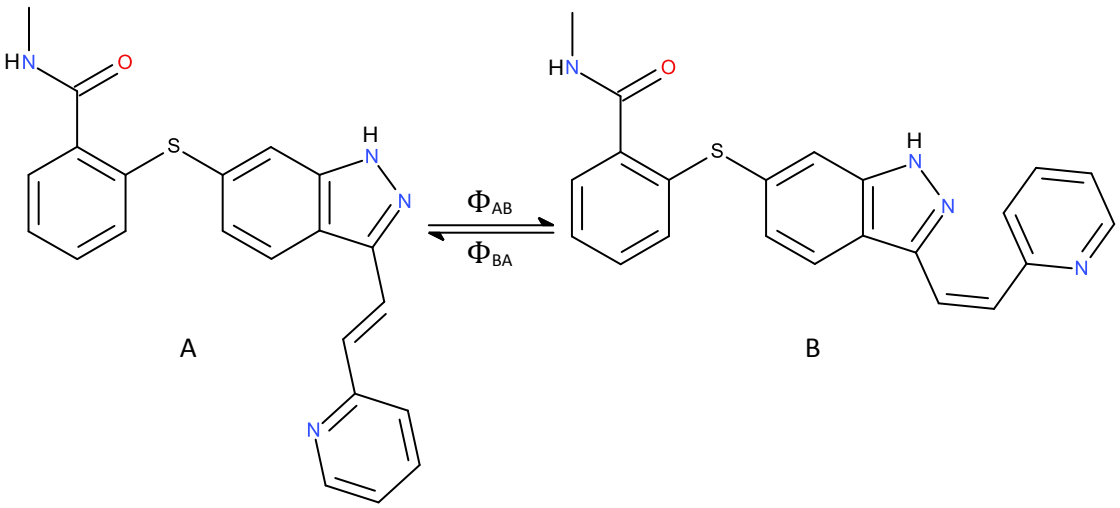

Scheme 4- 4: *AB (2Φ) photoreversible reaction of AXI (A the main compound (trans-form) and B the photoproduct (cis-form)*

Axitinib (AXI) is indazole derivative, which is anticancer agent classified as tyrosine kinase inhibitor [13], it is used as selective, potent and orally active to treat the advanced renal cell carcinoma due to it is a selective inhibitor of vascular endothelial growth factor (VEGF) receptors 1, 2, and 3 [13,14]

There are several studies reported that when exposure the AXI to the light-induced the photoisomers (*Z* and *E*). However, there are no photokinetic studies published on the AXI [15,16]. The biological activity of the *Z* and *E* of the AXI was investigated [15]. The *Z*-isomer was less active by 43 times than trans-isomer in vascular endothelial growth factor receptor 2 (VEGFR2) [15]. In vitro, it is possible to restore the biological activity of the *E*-AXI through irradiate the *Z*-AXI under UV light (365 nm). However, *vice versa* restored the biological activity in aqueous solution was not possible for *E* to *Z*- AXI due to the irreversible photocycloaddition, which formed a biologically inactive axitinib [15].

Stilbenes are a category as a polyphenolic compound. *E*- stilbene (*E*-STIL), Pinosylvin (PINO), Resveratrol (RVT), Oxyresveratrol (ORVT) and Pterostilbene (PTERO) are compounds of the stilbenoids group (scheme 1) and reported to be present in several plants such as peanut, raspberries, blueberries, and tea. More so, it is reported to highly concentrated in grapes and wine [17–19]. These compounds are a natural antioxidant [18,19] with neuroprotective properties useful in the protection of cerebral ischemia and with trauma cells, leading to significant inhibition of neuronal death [20–23]. Other biological functions associated with stilbenoids group include tyrosinase inhibition, anti-inflammatory, anti-herpetic, anti-HIV and anti-tumor activities [24–30]. Stilbene is

considered as a model compound, and it is used to understand the photoresponse of *Z* and *E* reactions [31] because it was well known the photoisomerization of stilbene and it had been studied in detail [32]

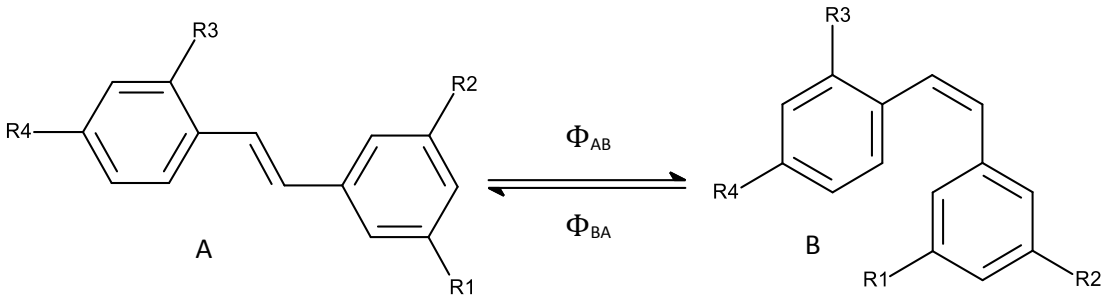

Compound	R1	R2	R3	R4
E-STIL	H	H	H	H
PINO	OH	OH	H	H
RVT	OH	OH	H	OH
PTERO	OCH_3	OCH_3	H	OCH_3
ORVT	OH	OH	OH	OH

Scheme 4- 5: *AB(2Φ) photoreversible reaction of stilbenoid group (A the main compound (E-form) and B the photoproduct (Z-form)*

Few photochemical studies have been reported for compounds belonging to the stilbenoid group such as RVT. However, none have been reported for ORVT, PTERO and PINO [22,25–27]. Previous studies reported that compounds belonging to the stilbenoids group are mostly present in *Z* and *E* isomerism, where the latter is said to be more stable than the former [17,33]. Photochemical analysis on *E*-RVT by Silva et al., (2013) concluded that under different irradiation conditions including UV (monochromatic ultraviolet light, 254nm), Vis (polychromatic light, ≥365nm) and UV-Vis (polychromatic light, 200-600nm), the *Z*-RVT was the main compound with maximum absorption spectra of 286 nm [34]. Although the reaction is slower when irradiated at

254 nm, the rate constant increased with an irradiation wavelength [34]. Similarly, the study of Iva, Pedzinski and Mihaljevi, (2015) found that the cis-RVT form was formed when *E*-RVT was irradiated at range 400-600 nm. However, the transformation reaction was slow [35]. Both studies used the first-order rate law to calculate the kinetics rate constant and quantum yield of RVT [34,35].

In another study, Zheng et al., (2014) reported that other products with fluorescence properties are produced in concomitant with *Z*-RVT from a *E*-RVT when exposed to UV/sunlight at length [36–40]. However, Iva, Pedzinski and Mihaljevi, (2015) indicates that according to low fluorescence quantum yield value, the RVT deactivated in excited singlet state due to internal conversion to the ground state and/or isomerisation rather than fluorescence. Thus, they found that the isomerisation was most efficient in the deactivated process of RVT in excited singlet state [35].

4.2. References

1. Maafi M., Brown RG. Kinetic analysis and elucidation options for AB(1k,2ϕ) systems. new spectrokinetic methods for photochromes. Photochemical and Photobiological Sciences. 2008; 7(11): 1360–1372. Available at: DOI:10.1039/b807556e
2. Yamamoto S., Matsuda K., Irie M. Absolute asymmetric photocyclization of a photochromic diarylethene derivative in single crystals. Angewandte Chemie - International Edition. 2003; 42(14): 1636–1639. Available at: DOI:10.1002/anie.200250417
3. Kuldová K., Tsyganenko K., Corval A., Trommsdorff HP., Bens AT., Kryschi C. Photo-switchable dithienylethenes: Threshold of the photoreactivity. Synthetic Metals. 2000; 115(1): 163–166. Available at: DOI:10.1016/S0379-6779(00)00327-1
4. Irie M. Photochromic diarylethenes for optical data storage media. Molecular Crystals and Liquid Crystals Science and Technology. Section A. Molecular Crystals

and Liquid Crystals. 1993; 227(1): 263–270. Available at: DOI:10.1080/10587259308030979

5. Irie M. Photochromic diarylethenes for photonic devices. Pure and Applied Chemistry. 2007; 68(7): 1367–1371. Available at: DOI:10.1351/pac199668071367

6. Bonifazi E., Angelini G., Meneghini CL. Adverse photo reaction to dacarbazine (DTIC). Contact Dermatitis. John Wiley & Sons, Ltd (10.1111); 1 June 1981; 7(3): 161–161. Available at: DOI:10.1111/j.1600-0536.1981.tb04600.x

7. Nussbaumer S., Bonnabry P., Veuthey J-L., Fleury-Souverain S. Analysis of anticancer drugs: A review. Talanta. Elsevier; 15 October 2011; 85(5): 2265–2289. Available at: DOI:10.1016/J.TALANTA.2011.08.034

8. Maafi W., Maafi M. Modelling nifedipine photodegradation, photostability and actinometric properties. International Journal of Pharmaceutics. Elsevier B.V.; 2013; 456(1): 153–164. Available at: DOI:10.1016/j.ijpharm.2013.07.075

9. Pizarro-Urzúa NA., Núñez-Vergara LJ. Nifedipine and nitrendipine reactivity toward singlet oxygen. Journal of Photochemistry and Photobiology A: Chemistry. 2005; 175(2–3): 129–137. Available at: DOI:10.1016/j.jphotochem.2005.04.027

10. Shetty B V., Schowen RL., Slavik M., Riley CM. Degradation of dacarbazine in aqueous solution. Journal of Pharmaceutical and Biomedical Analysis. 1992; 10(9): 675–683. Available at: DOI:10.1016/0731-7085(92)80096-6

11. Weissman MM., Haven N. units/ml). 1962; : 2150.

12. El Aatmani M., Poujol S., Astre C., Malosse F., Pinguet F. Stability of dacarbazine in amber glass vials and polyvinyl chloride bags. American Journal of Health-System Pharmacy. 2002; 59(14): 1351–1356.

13. Mirzaei MS., Taherpour AA. Tautomeric preferences of the cis and trans isomers of axitinib. Chemical Physics. 2018; 507(April): 10–18. Available at: DOI:10.1016/j.chemphys.2018.04.006

14. Rini BI., Escudier B., Tomczak P., Kaprin A., Szczylik C., Hutson TE., et al. Comparative effectiveness of axitinib versus sorafenib in advanced renal cell carcinoma (AXIS): A randomised phase 3 trial. The Lancet. Elsevier Ltd; 2011; 378(9807): 1931–1939. Available at: DOI:10.1016/S0140-6736(11)61613-9

15. Schmidt D., Rodat T., Heintze L., Weber J., Horbert R., Girreser U., et al. Axitinib: A Photoswitchable Approved Tyrosine Kinase Inhibitor. ChemMedChem. 2018; 13(22): 2415–2426. Available at: DOI:10.1002/cmdc.201800531

16. Bouchet S., Chauzit E., Ducint D., Castaing N., Canal-Raffin M., Moore N., et al. Simultaneous determination of nine tyrosine kinase inhibitors by 96-well solid-phase extraction and ultra performance LC/MS-MS. Clinica Chimica Acta. 2011; 412(11–12): 1060–1067. Available at: DOI:10.1016/j.cca.2011.02.023

17. Cacho JI., Campillo N., Viñas P., Hernández-Córdoba M. Stir bar sorptive extraction with gas chromatography-mass spectrometry for the determination of resveratrol, piceatannol and oxyresveratrol isomers in wines. Journal of Chromatography A. 2013; 1315: 21–27. Available at: DOI:10.1016/j.chroma.2013.09.045

18. Fan GJ., Liu X Da., Qian YP., Shang YJ., Li XZ., Dai F., et al. 4,4'-Dihydroxy-trans-stilbene, a resveratrol analogue, exhibited enhanced antioxidant activity and cytotoxicity. Bioorganic and Medicinal Chemistry. Elsevier Ltd; 2009; 17(6): 2360–2365. Available at: DOI:10.1016/j.bmc.2009.02.014

19. Xu L., Liu C., Xiang W., Chen H., Qin X., Huang X. Advances in the study of oxyresveratrol. International Journal of Pharmacology. 2014. pp. 44–54. Available at: DOI:10.3923/ijp.2014.44.54

20. Chibrikova L., Fekkes D., Weber JT., Slemmer JE., Vlug AS., Lamont M., et al. Potential neuroprotective effects of oxyresveratrol against traumatic injury. European Journal of Pharmacology. Elsevier B.V.; 2012; 680(1–3): 55–62. Available at: DOI:10.1016/j.ejphar.2012.01.036

21. Andrabi SA., Lorenz P., Wolf G., Horn TFW., Breuer C. Blood–brain barrier permeability to the neuroprotectant oxyresveratrol. Neuroscience Letters. 2005; 393(2–3): 113–118. Available at: DOI:10.1016/j.neulet.2005.09.081

22. Ashraf MI., Shahzad M., Shabbir A. Oxyresveratrol ameliorates allergic airway inflammation via attenuation of IL-4, IL-5, and IL-13 expression levels. Cytokine. Elsevier Ltd; 2015; 76(2): 375–381. Available at: DOI:10.1016/j.cyto.2015.09.013

23. Dvorakova M., Landa P. Anti-inflammatory activity of natural stilbenoids: A review. Pharmacological Research. October 2017; 124: 126–145. Available at: DOI:10.1016/j.phrs.2017.08.002 (Accessed: 28 May 2019)

24. Huang H., Zhang J., Chen G., Lu Z., Wang X., Sha N., et al. High performance liquid chromatographic method for the determination and pharmacokinetic studies of oxyresveratrol and resveratrol in rat plasma after oral administration ofSmilax china extract. Biomedical Chromatography. April 2008; 22(4): 421–427. Available at: DOI:10.1002/bmc.950 (Accessed: 28 May 2019)

25. Che CT., Zheng Z., Xu DD., Wong CCM., Li H., Sung JJY., et al. 3,3',4,5,5'-Pentahydroxy-Trans-Stilbene, a Resveratrol Derivative, Induces Apoptosis in Colorectal Carcinoma Cells Via Oxidative Stress. European Journal of Pharmacology. Elsevier B.V.; 2010; 637(1–3): 55–61. Available at: DOI:10.1016/j.ejphar.2010.04.009

26. Mouihate A., Horn TF., Pittman QJ. Oxyresveratrol dampens neuroimmune responses in vivo: a selective effect on TNF-α. American Journal of Physiology-Regulatory, Integrative and Comparative Physiology. 2006; 291(5): R1215–R1221. Available at: DOI:10.1152/ajpregu.00250.2006

27. Chuanasa T., Phromjai J., Lipipun V., Likhitwitayawuid K., Suzuki M., Pramyothin P., et al. Anti-herpes simplex virus (HSV-1) activity of oxyresveratrol derived from Thai medicinal plant: Mechanism of action and therapeutic efficacy on cutaneous HSV-1 infection in mice. Antiviral Research. 2008; 80(1): 62–70. Available at: DOI:10.1016/j.antiviral.2008.05.002

28. Galindo I., Hernáez B., Berná J., Fenoll J., Cenis JL., Escribano JM., et al. Comparative inhibitory activity of the stilbenes resveratrol and oxyresveratrol on African swine fever virus replication. Antiviral Research. Elsevier B.V.; 2011; 91(1): 57–63. Available at: DOI:10.1016/j.antiviral.2011.04.013

29. Jagtap UB., Bapat VA. Artocarpus: A review of its traditional uses, phytochemistry and pharmacology. Journal of Ethnopharmacology. Elsevier Ireland Ltd; 2010; 129(2): 142–166. Available at: DOI:10.1016/j.jep.2010.03.031

30. Guengerich FP., Chun YJ., Kim D., Gillam EMJ., Shimada T. Cytochrome P450 1B1: A target for inhibition in anticarcinogenesis strategies. Mutation Research - Fundamental and Molecular Mechanisms of Mutagenesis. 2003; 523–524: 173–182. Available at: DOI:10.1016/S0027-5107(02)00333-0

31. Suzuki M., Momotake A., Kanna Y., Nishimura Y., Hirota K., Morihashi K., et al. Photochemistry of arylacetylenyl-substituted stilbenes. Journal of Photochemistry and Photobiology A: Chemistry. Elsevier; 15 January 2013; 252: 203–210. Available at: DOI:10.1016/J.JPHOTOCHEM.2012.11.019 (Accessed: 28 May 2019)

32. Moore WM., Morgan DD., Stermitz FR. The Photochemical Conversion of Stilbene to Phenanthrene. The Nature of the Intermediate. Journal of the American Chemical Society. March 1963; 85(6): 829–830. Available at: DOI:10.1021/ja00889a050 (Accessed: 28 May 2019)

33. Chen X., He H., Wang G., Yang B., Ren W., Ma L., et al. Stereospecific determination of cis-and trans-resveratrol in rat plasma by HPLC: application to pharmacokinetic studies. Biomed. Chromatogr. 2007; 21: 257–265. Available at: DOI:10.1002/bmc (Accessed: 28 May 2019)

34. Silva CG., Monteiro J., Marques RRN., Silva AMT., Martínez C., Canle L. M., et al. Photochemical and photocatalytic degradation of trans-resveratrol. Photochemical and Photobiological Sciences. 2013; 12(4): 638–644. Available at: DOI:10.1039/c2pp25239b

35. Iva D., Pedzinski T., Mihaljevi B. Journal of Photochemistry and Photobiology A : Chemistry Photophysical and photochemical properties of resveratrol. 2015; 299: 118–124. Available at: DOI:10.1016/j.jphotochem.2014.11.019

36. Zheng X-Q., Ye J-H., Zhao Y., Lu J-L., Shi M., Liang Y-R. Photo-induced chemical reaction of trans-resveratrol. Food Chemistry. Elsevier Ltd; 2014; 171: 137–143. Available at: DOI:10.1016/j.foodchem.2014.08.130

37. López-Hernández J., Paseiro-Losada P., Sanches-Silva AT., Lage-Yusty MA. Study of the changes of trans-resveratrol caused by ultraviolet light and determination of trans- and cis-resveratrol in Spanish white wines. European Food Research and Technology. 2007; 225(5–6): 789–796. Available at: DOI:10.1007/s00217-006-0483-x

38. Rodríguez RÁ., Lahoz IR., Faza ON., Cid MM., Lopez CS. Theoretical and experimental exploration of the photochemistry of resveratrol: Beyond the simple double bond isomerization. Organic and Biomolecular Chemistry. 2012; 10(46): 9175–9182. Available at: DOI:10.1039/c2ob26241j

39. Han H., Yang I., Kim SK., Kang J., Kim E., Sul S., et al. Photochemical generation of a new, highly fluorescent compound from non-fluorescent resveratrol. Chemical Communications. 2012; 48(32): 3839. Available at: DOI:10.1039/c2cc30940h

40. Yan Wang †., Florentina Catana †., Yanan Yang †., Robin Roderick ‡ and., Richard B. van Breemen* †. An LC-MS Method for Analyzing Total Resveratrol in Grape Juice, Cranberry Juice, and in Wine. American Chemical Society ; 2002; Available at: DOI:10.1021/JF010812U (Accessed: 28 May 2019)

Chapter 5

Photokinetic some stilbenoid and diarylethene derivatives under monochromatic light

5.1. Introduction

Recently in the literature, Φ-order kinetics were shown to be a better tool to describe the behaviour of photochemical reactions and to quantify their parameters [1–5]. Previous studies proposed a method to analyse the photokinetic data of unimolecular and photoreversible compounds based on the isosbestic irradiation point [1–5]. The strategy used on Φ-order kinetics allows a description of the photokinetic data, and a determination of the overall rate constant, the molar absorptivity, and quantum yields. This leads to no possibility for the same data to allow for interpretations with different orders for one reaction. This study has developed a new method to investigate the photokinetic data for unimolecular and photoreversible reactions driven by non-isosbestic irradiation (UV or visible). For the purposes of describing this new method, E-stilbene, widely used as a photoreversible and model compound, its derivatives and diarylethene derivative (DAE) have been selected.

5.2. The mathematical background

5.2.1. General equation

The Φ–order model is used to describe the transformation of a photoreversible compound (A) and photoproduct (B), which are respectively driven by a forward quantum yield ($\Phi_{A\to B}^{\lambda_{irr}}$) and a reverse quantum yield ($\Phi_{B\to A}^{\lambda_{irr}}$). In the case of the use of non-isosbestic wavelengths (λ_{irr}) (continuous irradiation), A and B absorb different amounts of light ($P_{\lambda_{irr}}$). This is due to the difference in their absorption coefficients (ε)

($\varepsilon_A^{\lambda_{irr}} \neq \varepsilon_B^{\lambda_{irr}} \neq 0$). In this case, the unimolecular photodegradation reactions ($A \xrightarrow{\Phi_{AB}} B$) $\varepsilon_B^{\lambda_{irr}}$ is either equal to zero or otherwise.

$$\frac{dC_A(t)}{dt} = -\frac{dC_B(t)}{dt} = \left(\Phi_{B\to A}^{\lambda_{irr}} \times \varepsilon_B^{\lambda_{irr}} \times C_B(t) - \Phi_{A\to B}^{\lambda_{irr}} \times \varepsilon_A^{\lambda_{irr}} \times C_A(t)\right) \times l_{\lambda_{irr}} \times P_{\lambda_{irr}} \times F_{\lambda_{irr}}(t) \quad \text{Eq.5-1}$$

Where $P_{\lambda_{irr}}$ is the radiant power value, $\Phi_{A\to B}^{\lambda_{irr}}$ and $\Phi_{B\to A}^{\lambda_{irr}}$ are the forward and reverse quantum yields of the photochemical reaction as realised at the irradiation wavelength (λ_{irr}), $l_{\lambda_{irr}}$is the optical path length of the irradiating beam inside the sample, and $F_{\lambda_{irr}}(t)$ the time-dependent photokinetic factor given by [5]

$$F_{\lambda_{irr}}(t) = \frac{1-10^{-(A_{tot}^{\lambda_{irr}/\lambda_{irr}}(t)\times l_{\lambda_{irr}}/l_{\lambda_{obs}})}}{A_{tot}^{\lambda_{irr}/\lambda_{irr}}(t)\times l_{\lambda_{irr}}/l_{\lambda_{obs}}} \quad \text{Eq.5-2}$$

Where $A_{tot}^{\lambda_{irr}/\lambda_{irr}}$ is the measured total absorbance of the medium at λ_{obs}, and $l_{\lambda_{obs}}$is the optical path length of the monitoring beam ($l_{\lambda_{irr}} \neq l_{\lambda_{obs}}$).

$$A_{tot}^{\lambda_{irr}/\lambda_{obs}}(t) = A_{tot}^{\lambda_{irr}/\lambda_{obs}}(pss) + \frac{A_{tot}^{\lambda_{irr}/\lambda_{obs}}(0) - A_{tot}^{\lambda_{irr}/\lambda_{obs}}(pss)}{A_{tot}^{\lambda_{irr}/\lambda_{irr}}(0) - A_{tot}^{\lambda_{irr}/\lambda_{irr}}(pss)} \times \frac{l_{\lambda_{obs}}}{l_{\lambda_{irr}}} \times \log[1 + \left(10^{[(A_{tot}^{\lambda_{irr}/\lambda_{irr}}(0) - A_{tot}^{\lambda_{irr}/\lambda_{irr}}(pss))\times \frac{l_{\lambda_{obs}}}{l_{\lambda_{irr}}}]} - 1\right) \times e^{-k_{A\leftrightharpoons B}^{\lambda_{irr}} \times t}] \quad \text{Eq.5-3}$$

The cumulative total absorbance of the medium at the initial time (t = 0) and at the photostationary state (t = ∞), is measured under observation conditions ($l_{\lambda_{obs}}$), not the excitation condition ($l_{\lambda_{irr}}$)). The optical path lengths ($l_{\lambda_{irr}}$and$l_{\lambda_{obs}}$) are not necessarily equal. The medium absorbance under the excitation conditions (i.e., corresponding to a measurement along $l_{\lambda_{irr}}$) can be indirectly accessed.

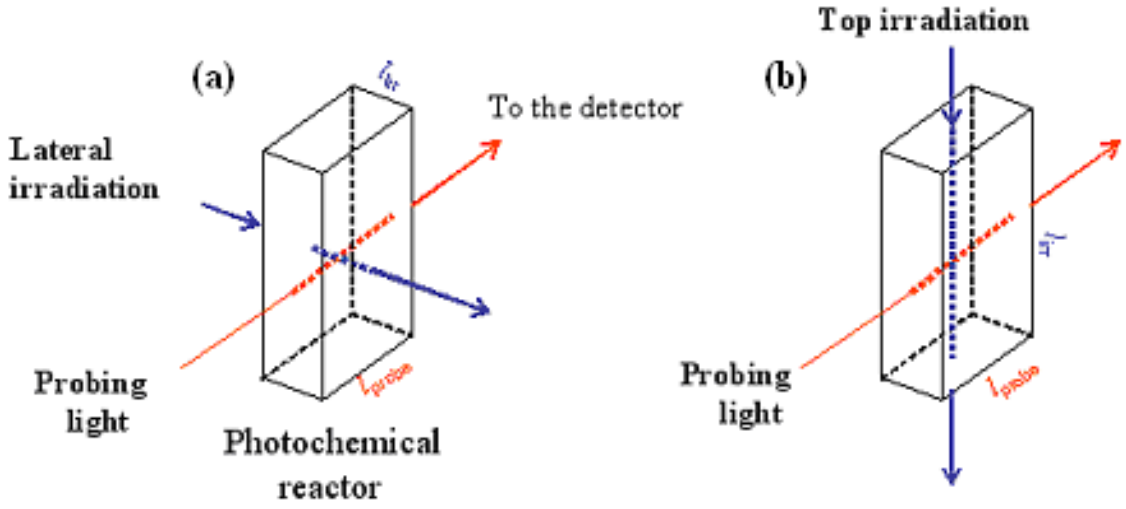

Scheme 5- 1: *The sample cuvettes and the possible paths of irradiation and probing lights* [6].

The analytical expression for the exponential factor, $k_{A\leftrightharpoons B}^{\lambda_{irr}}$, in Eq. (5-3), which represents the overall reaction rate constant, is expressed as [5]:

$$k_{A\leftrightharpoons B}^{\lambda_{irr}} = \left(\Phi_{A\to B}^{\lambda_{irr}} \times \varepsilon_{A}^{\lambda_{irr}} + \Phi_{B\to A}^{\lambda_{irr}} \times \varepsilon_{B}^{\lambda_{irr}}\right) \times l_{\lambda_{irr}} \times P_{\lambda_{irr}} \times F_{\lambda_{irr}}(pss) = P_{\lambda_{irr}}\, \beta_{\lambda_{irr}} \quad \text{Eq.5-4}$$

With $F_{\lambda_{irr}}(pss)$ is the same Eq. (5-2) but where $A_{tot}^{\lambda_{irr}/\lambda_{irr}}(pss)$ replaces $A_{tot}^{\lambda_{irr}/\lambda_{irr}}(t)$.

Where $A_{tot}^{\lambda_{irr}/\lambda_{obs}}(t)$, $A_{tot}^{\lambda_{irr}/\lambda_{obs}}(0)$, $A_{tot}^{\lambda_{irr}/\lambda_{obs}}(pss)$, $A_{tot}^{\lambda_{irr}/\lambda_{irr}}(0)$ and $A_{tot}^{\lambda_{irr}/\lambda_{irr}}(pss)$ in Eq. (5-3) are the measured total absorbance of the medium at the time of reaction (0 and ∞), and $\lambda_{irr}/\lambda_{irr}$ and $\lambda_{irr}/\lambda_{obs}$ are when irradiated and observed at the same and different wavelengths, respectively.

The numerical value of the reaction's initial velocity ($v_0^{\lambda_{irr}/\lambda_{obs}}$) can be derived from Eq. (5-1) [5].

$$v_0^{\lambda_{irr}/\lambda_{obs}}(cld) = \left(\varepsilon_B^{\lambda_{obs}} - \varepsilon_A^{\lambda_{obs}}\right) \times l_{\lambda_{obs}} \times \Phi_{A\to B}^{\lambda_{irr}} \times \varepsilon_A^{\lambda_{irr}} \times l_{\lambda_{irr}} \times P_{\lambda_{irr}} \times F_{\lambda_{irr}}(0) \times C_0$$

Eq.5-5

Furthermore, it can be extracted from the differentiation of Eq. (5-3) (at t = 0), as [5]

$$v_0^{\lambda_{irr}/\lambda_{obs}}(mod.) = \left(\frac{dA_{tot}^{\lambda_{irr}/\lambda_{obs}}}{dt}\right)_0 = \frac{A_{tot}^{\lambda_{irr}/\lambda_{obs}}(0) - A_{tot}^{\lambda_{irr}/\lambda_{obs}}(pss)}{A_{tot}^{\lambda_{irr}/\lambda_{obs}}(0) - A_{tot}^{\lambda_{irr}/\lambda_{obs}}(pss)} \times \frac{k_{A\leftrightarrows B}^{\lambda_{irr}}(mod.)}{l_{\lambda_{irr}}/l_{\lambda_{obs}} \times Ln(10)} \times \left(10^{[(A_{tot}^{\lambda_{irr}/\lambda_{irr}}(pss) - A_{tot}^{\lambda_{irr}/\lambda_{irr}}(0)) \times l_{\lambda_{irr}}/l_{\lambda_{obs}}]} - 1\right)$$

Eq.5-6

5.2.2. Elucidation method

5.2.2.1. Elucidation methods of the study compounds

There are three unknown parameters: the $\Phi_{A\to B}^{\lambda_{irr}}$ and $\Phi_{B\to A}^{\lambda_{irr}}$ quantum yields, and the absorption coefficient of the photoproduct ($\varepsilon_B^{\lambda_{irr}}$). It was difficult to predict these parameters from the kinetic traces alone (fitting parameter $k_{A\leftrightarrows B}^{\lambda_{irr}}$ Eq.5-3) because this cannot be solved by equation (5-3). In addition, to avoid degeneracy of the kinetic solution [36-38] (see section 5.3), an elucidation method was devised. This work will propose a method based on non-isosbestic irradiation.

The elucidation method for the photoreversible reaction can be realised in three steps.

(i) The first step involves determination of the concentrations of A and B at the photostationary state (pss). In this step, the photodegradation reaction under monochromatic and non-isosbestic irradiation is monitored by HPLC.

(ii) The second step involves reconstructing the absorption spectra of the photoproduct. Once the $C_A(0)$, $C_A(pss)$ and $C_B(pss)$ are known, $\varepsilon_B^{\lambda_{irr}}$ can be calculated using Eq. 5-7, as:

$$\varepsilon_B^{\lambda_{irr}} = \frac{A_{pss}^{\lambda_{irr}} - C_A(pss) \times \varepsilon_A^{\lambda_{irr}} \times l_{\lambda_{obs}}}{(C(0) - C_A(pss)) \times l_{\lambda_{obs}}} \quad \text{Eq.5-7}$$

(iii) Finally, the number of unknown factors is reduced to two ($\Phi_{A\to B}^{\lambda_{irr}}$and $\Phi_{B\to A}^{\lambda_{irr}}$) whose absolute values at any irradiation wavelength can be determined by Eqs. 5-6, 5-8 and 5-9, respectively.

$$\Phi_{A\to B}^{\lambda_{irr}} = \frac{v_0^{\lambda_{irr}/\lambda_{obs}}(mod)}{\left(\varepsilon_B^{\lambda_{irr}} - \varepsilon_A^{\lambda_{irr}}\right) \times l_{\lambda_{obs}} \times \varepsilon_A^{\lambda_{irr}} \times l_{\lambda_{irr}} \times P_{\lambda_{irr}} \times F_{\lambda_{irr}}(0) \times C_0} \quad \text{Eq.5-8}$$

$$\Phi_{B\to A}^{\lambda_{irr}} = \frac{1}{\varepsilon_B^{\lambda_{irr}}} \left[\left(\frac{k_{A \leftrightharpoons B}^{\lambda_{irr}}}{l_{\lambda_{irr}} \times P_{\lambda_{irr}} \times F_{\lambda_{irr}}(pss)} \right) - \left(\Phi_{A\to B}^{\lambda_{irr}} \times \varepsilon_A^{\lambda_{irr}} \right) \right] \quad \text{Eq.5-9}$$

This approach was introduced for the first time here and circumvents the exclusive requirement of the previous approach for isosbestic irradiation [2].

5.2.3. Method to determine the percentage of A and B

The degradation percentage is used to determine the composition of pss. The quantities of $C_A(pss)$ and $C_B(pss)$ at each irradiation wavelength are obtained by HPLC.

Taking into account the mass balance equation, $C_B(pss) = C_A(0) - C_A(pss)$, the percentage of compound at pss for each λ_{irr} (% A_{pss}) can be calculated by Eq. (5-10).

$$\%\, A_{pss} = \frac{C_A(pss)}{C_A(0)} \times 100 \quad \text{Eq.5-10}$$

Otherwise, the degradation percentage at each irradiation wavelength can be obtained as Eq. (5-11).

$$A_{Deg} = 100 - C_A(pss)\ \%$$ Eq.5-11

5.3. Identifiability issue

5.3.1. The issue of the goodness of fitting versus reliability of fitting information

Identifiability is basically a question of the uniqueness of solutions for certain types of mathematical models for specific attributes [7,8]. The identifiability problem usually has meaning in the context of unknown model parameters. The usual question is whether or not a unique solution can be found for unknown model parameters, from real experiments data collected. It is clear that the modelling process is a critical aspect, especially if the parameters are analogous to the physical attributes of interest and need to be quantified by the model [7,8]. So, when a degeneration of the kinetic solution as a direct result of lack of data is detected, the identifiability issue arises. Identifiability is a concern in reaction kinetics since different sets of possible values (kinetic solutions) can be determined for the series of unknowns of the reaction. This is the case when one takes into consideration the kinetic data of a reactive process, or even a single kinetic trace. Each of the different solutions means the experimental data are ideally suited, and therefore it is impossible to determine the real solution (with these logical solutions). The following is an example of identifiability for the ORVT case.

This study discusses the problem of kinetic methods in terms of fitting and the utility of this type of reaction. Therefore, equation formula (Eq. 5-12) describes this kind of photokinetic reaction, where this formula can be determined by rearranging Eq. (5-3) and combining it with the mass balance. To conduct this study, it is necessary to implement variable numbers to unknown, variable parameters in this equation with

other parameters that are being held constant; this confirms whether the data fits or otherwise. After that, a comparison of these fittings is required. Moreover, using a known variable value parameter (α), $\varepsilon_B^{\lambda_{irr}}$ can be easily calculated (Eq. 5-13) because $\varepsilon_A^{\lambda_{irr}}$ is known, where a comparison between the $\varepsilon_B^{\lambda_{irr}}$ can be made according to Eq. 5-7 and calculated from Eq.5-13.

Table 5- 1: The constant values of fitting parameters used in equation (5-12)

Δc × 10^5/ M	$A_{tot}^{\lambda_{irr}/\lambda_{irr}}$ **(0)**	$A_{tot}^{\lambda_{irr}/\lambda_{irr}}$ **(pss)**	$\varepsilon_A^{\lambda_{irr}}$ /M^{-1} cm^{-1}	$l_{\lambda_{obs}}$ /cm	$l_{\lambda_{irr}}$ /cm	$F_{\lambda_{irr}}(0)$	$F_{\lambda_{irr}}(pss)$	$P_{\lambda_{irr}}$ **× 10^7** /einstein s^{-1} dm^{-3}
1.68	0.486	0.239	28261.8	1	2.01	0.92	1.39	2.01

There are two unknown parameters in Eq. (5-12), which are α and the overall rate constant ($k_{A\leftrightharpoons B}^{\lambda_{irr}}$).

$$C_A(t) = C_A(pss) + \frac{\log[1+(10^{\alpha\times\Delta C}-1)\times e^{-k_{A\leftrightharpoons B}^{\lambda_{irr}}\times t}]}{\alpha} \quad \text{Eq.5-12}$$

Where the α parameter is given by

$$\alpha = (\varepsilon_A^{\lambda_{irr}} - \varepsilon_B^{\lambda_{irr}}) \times l_{\lambda_{irr}} \quad \text{Eq.5-13}$$

The change in concentration ΔC is calculated by

$$\Delta C = C_A(0) - C_A(pss) \quad \text{Eq.5-14}$$

Firstly, this work shows that the concentration was well fitted with equations 5-12, 5-13 and 5-14 (Fig. 5-1).

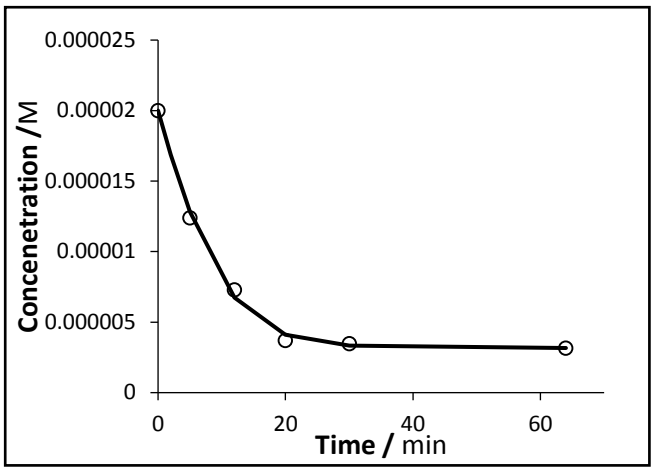

Figure 5- 1: Evolution of E-ORVT concentration (C_A (0) = 2 × 10^{-5}M, C_A (pss) = 3.2×10^{-6} M) monitored by HPLC when irradiated continuously with a monochromatic beam at 328 nm (2.01 × 10^{-7} einstein $s^{-1}dm^{-3}$, 22°C) and fitted by Eq.5-12.

To confirm if this equation can be used or otherwise, low and highly variable values of α need to be chosen. Results were obtained and fitted using equation 5-12 (Fig.5-2) (Table 5-1 and 5-2). Moreover, a comparison between $\varepsilon_B^{\lambda_{irr}}$ value was calculated by Eq. (5-7) and $\varepsilon_B^{\lambda_{irr}}$ value was calculated via Eq. (5-13). Using variable numbers, it was found that there are significant variations in the $\varepsilon_B^{\lambda_{irr}}$values. This means that it is difficult to state which $\varepsilon_B^{\lambda_{irr}}$ value is true. In addition, there are variations in the values of $\Phi_{\mathrm{E}\to\mathrm{Z}}^{\lambda_{\mathrm{irr}}}$and $\Phi_{\mathrm{Z}\to\mathrm{E}}^{\lambda_{\mathrm{irr}}}$, which are calculated by Eq. (5-15) and (5-16) (Table 5-2). These confirm that the results from this equation cannot be used in this instance because different $\varepsilon_B^{\lambda_{irr}}$ values are found and, consequently, it is impossible to choose which one right.

Thus, this section will describe the inability of the kinetic method to describe the photochemical reaction. Moreover, this study shows that the value of some parameters could be predicted using Eq. (5-12), such as α and $k_{A\leftrightharpoons B}^{\lambda_{irr}}$. However, there are similar fittings for the data (Fig. 5-2), and this work indicates the disadvantages associated with

this species as regards the kinetic method. In addition, there are several parameter values that have the same fitting (Fig. 5-2 and Appendix I), meaning there are different possibilities that can fit the HPLC traces with different results in each case. Thus, in this instance, the results cannot be held to be either true or false. This study confirms that the classical kinetics model cannot be used to calculate $\varepsilon_B^{\lambda_{irr}}$, $\Phi_{\mathrm{A\rightarrow B}}^{\lambda_{\mathrm{irr}}}$and $\Phi_{\mathrm{A\rightarrow B}}^{\lambda_{\mathrm{irr}}}$. Also, this study shows that this kind of fitting is not sufficiently powerful to support or to be used as a reference when determining $\varepsilon_B^{\lambda_{irr}}$, $\Phi_{\mathrm{A\rightarrow B}}^{\lambda_{\mathrm{irr}}}$ and $\Phi_{\mathrm{A\rightarrow B}}^{\lambda_{\mathrm{irr}}}$. Thus, this work has confirmed that the elucidation method (section 5.2.2) was the best approach to solving this problem.

$$\Phi_{\mathrm{A\rightarrow B}}^{\lambda_{\mathrm{irr}}} = \frac{C_B(pss)\times k_{A\leftrightharpoons B}^{\lambda_{irr}}}{\varepsilon_A^{\lambda_{irr}}\times l_{\lambda_{irr}}\times P_{\lambda_{irr}}\times F_{\lambda_{irr}}(pss)\times C_0} \qquad \text{Eq.5-15}$$

$$\Phi_{\mathrm{B\rightarrow A}}^{\lambda_{\mathrm{irr}}} = \frac{C_A(pss)\times k_{A\leftrightharpoons B}^{\lambda_{irr}}}{\varepsilon_B^{\lambda_{irr}}\times l_{\lambda_{irr}}\times P_{\lambda_{irr}}\times F_{\lambda_{irr}}(pss)\times C_0} \qquad \text{Eq.5-16}$$

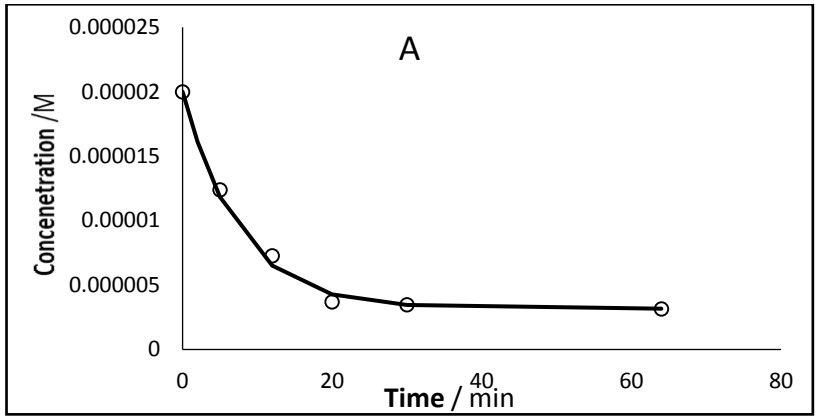

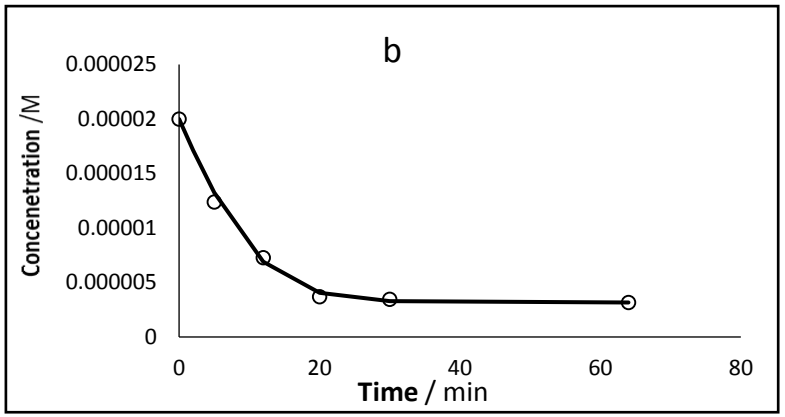

Figure 5- 2: a,b. The E-ORVT concentration monitored by HPLC when irradiated continuously with a monochromatic beam at 328 nm (2.01×10^{-7} einstein $s^{-1}dm^{-3}$, 22°C) and fitted by Eq.5-12 using variable numbers, which in Fig (A) and (B) the α values at case 1 and case 4 respectively.

Table 5- 2: *Examples of fitting parameters and calculated unknowns for the reaction of ORVT in ethanol.*

Case #→ / **Parameters↓**		**Case #0**[a]	**Case # 1**[b]	**Case # 2**[c]	**Case # 3**[d]	**Case # 4**[e]	**Case # 5**[f]	**Case # 6**[g]
Variable value	α	35391.74	2500	35586	49256	52145	75000	100000
	$k^{\lambda_{irr}}_{A\leftrightharpoons B}$/min^{-1}	0.3	0.138	0.18	0.185	0.2	0.267	0.32
	$k^{\lambda_{irr}}_{A\leftrightharpoons B}$/ s^{-1}	0.005	0.0023	0.003	0.0031	0.0033	0.0046	0.0053
Calculated value	$\varepsilon^{\lambda_{irr}}_{B}$/M^{-1} cm^{-1}	10653.97	27018.02	10557.33	3756.33	2319.02	-9051.63	-21489.44
	$\Phi^{\lambda_{irr}}_{A\rightarrow B}$	0.23	0.13	0.17	0.17	0.19	0.29	0.35
	$\Phi^{\lambda_{irr}}_{B\rightarrow A}$	0.21	0.025	0.084	0.24	0.29	-0.17	-0.09

a: Using elucidation method to determined quantum yields and $\varepsilon^{\lambda_{irr}}_{B}$ calculated using Eq.5-7. **b-g:** $\varepsilon^{\lambda_{irr}}_{B}$ calculated using Eq.5-13 after α is knowin

5.4. Stability of compounds in ethanolic solution

5.4.1. Electronic spectral characteristics of the drugs

The UV electronic spectra of the stilbinoid group studied show two main bands (250-400 (A-band) and 200-250 nm (B-band)) with the maxim between 295 and 328 nm, ($4.47 \geq \log\varepsilon \geq 5.17$) (Table 5-3, Fig. 5-3a). The four or five peaks characterising the electronic spectra of stilbinoids are attributed to π,π^* transitions corresponding to the extended π system which might have a minor contribution from the n,π^* transitions due to the presence of hydroxyl groups [9]. The bathochromic shift in the spectra of stilbene derivatives are due to the presence of electron donating groups, in the form of hydroxyl and methoxy groups substituted on the benzene rings [10,11]. This will influence the conjugated system and to move the absorption peak at long wavelength than stilbene. The location of the substituent will effect on the spectra, the *para* position show increase in the red shift while the *meta* has a little effect on the spectrum [12]. We notice that the subsitued on *orthro* and *para* positions is greater red shift in the A-band than *meta* (Fig. 5-3a, Table 5-3). In other words, the bathochromic shift of a specific band was significantly affected by the substituent position, m, m, o',p'- tetrahydroxy stilbene (ORVT) has shown the effect of the substituent position on the move the A-band to longer wavelength compare to others. However, the m, m'- dihydroxy stilbene (PINO) show a little effect on the spectra 5 nm move toward in the A-band compare to stilbene. In addition, When the number of substituents on the benzene rings increases to between two to four substitutes, then ≈5-33 nm bathochromic shifted in the spectra (ORVT > PTERO,RVT >PINO) compare to stilbene (Table 5-3). Continuous monochromatic

irradiation (Fig. 5-3a) of the *E*-STIL and its derivatives demonstrate an increase in intensity of spectral features in some sections of the spectrum and a decrease in others. This change in the spectrum indicates that a chemical transformation has occurred. From the experimental observations, the colour of the solution did not change, and no precipitation was present in the solutions during the transformation, and no cyclization products could subsequently be identified.

The electronic spectrum of DAE in open form is characterised by three peaks, while the closed form is characterised by five (Table 5-3). The photochemical reaction of the O-DAE lead to a new band at the visible region, which related to the closed form (coloured). C-DAE (cyclic) is formed under UV light in range (200-400nm). In the closed cyclic form, the π-electrons are delocalized, causing the energy gap to become small [13], and hence the change in colour of the solution[13]. The absorption spectrum of the open form was in the UV range with a max at 225 nm. The red shift, observed in the open form absorption spectrum, is shown by a band at 520 nm.

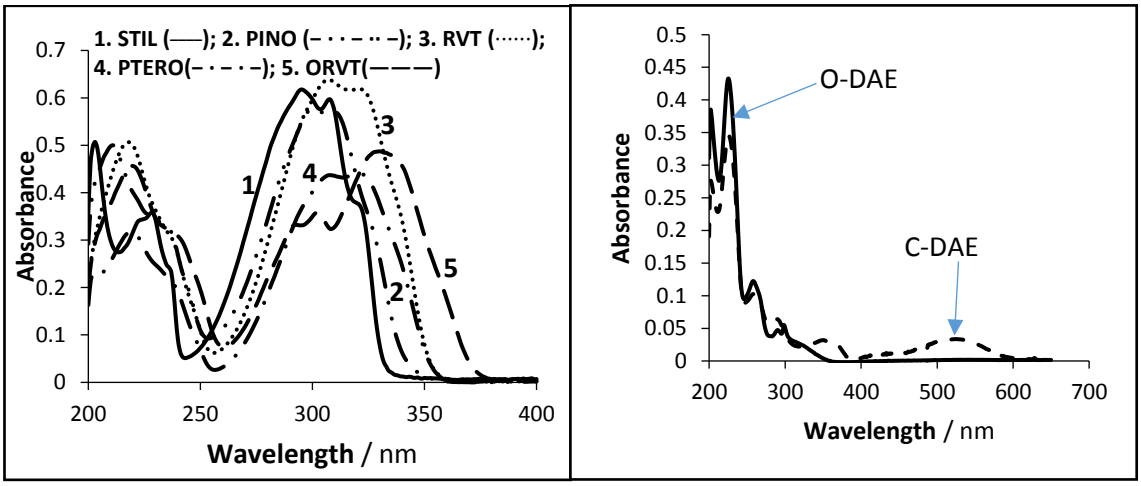

*Figure 5- 3: UV/Vis Spectrum in pure ethanolic solution before degradation of (**a**) E- isomer of STIL, PINO, RVT, PTERO and ORVT (5.5×10^{-6}, 2.35×10^{-5}, 1.88×10^{-5}, 1.95×10^{-5} and 2×10^{-5} M, respectively (b) DAE (O-DAE and C-DAE) (5.26×10^{6} and 3.42×10^{6} M), respectively.*

Table 5- 3: Features of the studied compounds and photoproducts.

Compound	Features of the compound (*E)*		Features of the Photoproduct (Z)		Isosbestic λ	$\Delta\lambda_{max}$ from STIL /nm
	λ /nm	**Log ε**	**λ** /nm	**Log ε**		
STIL	205 (216) 229 237 (244) 295 (304) 307 (318) 322	4.37 (4.11) 4.21 3.98 (3.33) 4.47 (4.44) 4.45 (4.25) 4.23	205 (216) 223 (240) 252 (257) 283 293 (304) 308 (320) 322	4.55 (4.27) 4.28 (4.08) 4.18 (403) 3.96 389 (3.52) 3.38 (2.78) 2.45	230 264	-
Pino	212 (227) 231 (236) 237 (255) 300 (305) 311	4.33 (4.18) 4.16 (4.13) 4.13 (3.60) 4.39 (4.38) 4.38	210 (252) 261 (266) 272 295 (308) 313	4.33 (3.96) 4.02 (4.00) 3.99 3.84 (3.54) 3.37	230 241 276	5 m, m- OH
RVT	(210) 215 238 (257) 307 (316) 323	(4.49) 4.29 4.33 (3.72) 4.52 (4.50) 4.50	204 (217) 235 (255) 263 (273) 300 325	4.63 (4.46) 4.33 (4.16) 4.22 (4.15) 4.07 3.62	280	12 m, m, p'-OH
PTERO	(206) 220 239 (258) 308 (316) 323	(4.16) 4.24 4.03 (3.33) 4.30 (4.29) 4.29	(210) 220 235 (253) 264 (272) 302 323	(4.27) 4.26 4.19 (4.05) 4.10 (3.98) 3.81 3.32	280	13 m, m, p'-OCH_3
ORVT	222 (233) 241 (261) 291	4.39 (4.26) 4.22 (3.49) 4.27	205 (217) 222 (259) 292	4.58 (4.45) 4.40 (3.85) 4.09	240 255 280	33 m, m, o',p'-OH

Compound	Features of the compound (*E*)		Features of the Photoproduct (Z)		Isosbestic λ	$\Delta\lambda_{max}$ from STIL /nm
	λ /nm	**Log ε**	**λ** /nm	**Log ε**		
ORVT	(297) 304 (309) <u>328</u>	(4.28) 4.31 (4.27) 4.45	(299) 307 (309) <u>325</u>	(4.06) 4.07 (4.07) 4.06		
DAE	204 (217) 227 (247) 261 (282) 293 (297) <u>300</u>	4.49 (4.45) 4.59 (3.98) 4.06 (3.62) 3.66 (3.69) 3.72	204 (212) 227 (249) 261 (282) 293 (300) (317) 354 (393) 437 (450) <u>520</u>	3.85 (4.17) 4.14 (3.96) 3.88 (4.09) 4.04 (3.79) (3.43) 4.07 (3.41) 3.64 (3.61) 4.01	240 255 280	

*The underline represents the maxima wavelength, the wavelength between the bracket represent the shoulders

5.4.2. Photostability of the study compounds in Ethanol

The spectral evolutions of the *E*-RVT and *E*-PTERO produced just one isosbestic point, where the other compounds produced three and *E*-STIL produced two. These isosbestic points meant no secondary reactions occurs during the transformation reaction (Fig. 5-4 and Appendix I).

The chromatographic analyses of the irradiated sample showed only two peaks (the main compounds and its photoproduct) for all the tested compounds. The HPLC chromatograms show that there is no complete depletion of the starting derivatives, indicating the equilibrium state between the A and B. These characteristics are related

to photoreversible mechanism AB (2Φ). However, the chromatogram of C-DAE is completely depleted as the ring opening reaction mechanism AB $(1\Phi)_{\varepsilon_{B=0}}$ regenerates A.

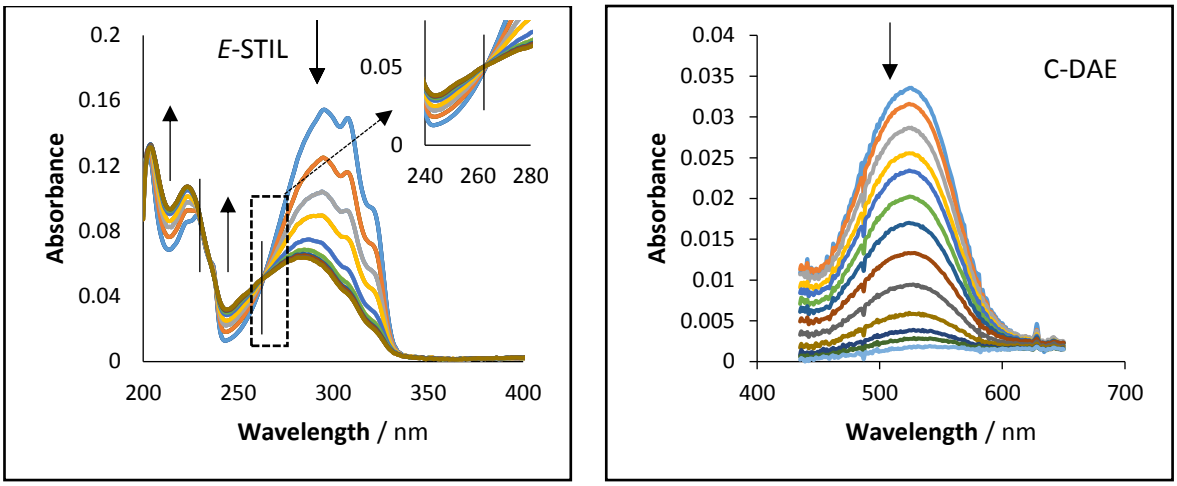

Figure 5- 4: Evolution the electronic absorption spectra of E- STIL and C-DAE (5.5 × 10^{-6} and 3.42x 10^{-6} M, respectively) in ethanol solutions subjected to continuous irradiation with a monochromatic beam at 325 and 520 nm (4.79 ×10^{-7} and 1.46 × 10^{-6} einstein s^{-1} dm^{-3}), respectively. The arrows indicate the direction of the evolution of absorption maxima during photoreaction and vertical line cross the spectra at the isosbestic point.

5.4.3. Effect of irradiation wavelength on photodegradation traces

The light distribution spectral and the compounds spectral properties play a role in the compounds' photodegradation [14,15].

Similarity of the absorption spectra of the compounds is not sufficient to predict the relevant wavelength range, hence not all absorbed light lead to photodecomposition [16].

The study compounds were thermally stable in ethanol at 22°C but react to light at different rates. For instance, the reactions of STIL, ORVT and PINO were all reach to pss within forty minutes, whereas those of PTERO and C-DAE required only ten minutes.

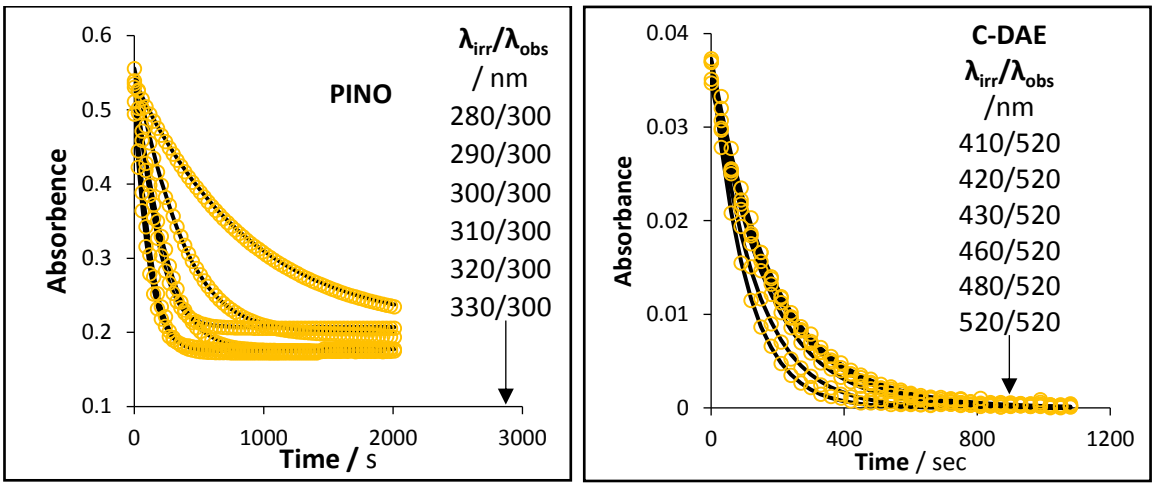

Figure 5- 5: Photokinetic traces of E-PINO (2.16 × 10^{-5} M) and C-DAE (3.42x 10^{-6} M) in ethanol solutions at different irradiation wavelengths (λ_{irr}) and λ_{obs}= 300 and 520 nm, respectively. The circles represent the exp. data while the lines represent the fitting traces using Eq.5-3.

The ethanolic solutions of the compounds studied under illumination at various monochromatic wavelengths was selected from the main absorption spectrum of these compounds. The kinetic traces of the study compounds' degradation were monitored at specific observation wavelengths for these compounds, and were fitted into Equation (5-3) (Fig. 5-5 and Appendix I).

Eq. (5-3) used to fit all experimental traces (Fig. 5-5) related to the *E-Z* overall rate constant values ($k_{A\leftrightharpoons B}^{\lambda_{irr}}$) of the study compounds' photodegradation reaction. It was found that the $k_{A\leftrightharpoons B}^{\lambda_{irr}}$ values increased and then decreased with increasing wavelength (Table 5-4). However, these values must be considered with some caution because of the inconsistency in the $k_{A\leftrightharpoons B}^{\lambda_{irr}}$ values that was observed as wavelength increased. Hence, they all depend on different factors such as quantum yields (Φ) of the drug at specific wavelengths, the extinction coefficients of both species ($\varepsilon_A^{\lambda_{irr}}$and $\varepsilon_B^{\lambda_{irr}}$), and the intensity of the radiation ($P_{\lambda_{irr}}$), as shown clearly by Eq. (5-4). Therefore, it is important to

measure all the parameters, especially the quantum yield, to allow for an even-handed comparison.

This argument is even more critical when the kinetic data are treated by classical thermal order kinetics and/or when polychromatic light is used [2].

Table 5- 4: *Overall photoreaction rate constant, spectroscopic and kinetic parameter values of studies compounds for a set of monochromatic irradiations performed in ethanol at 22° C.*

Compound	λ_{irr} /nm	λ_{obs} /nm	$A_{tot}^{\lambda_{irr}/\lambda_{obs}}(0)$	$A_{tot}^{\lambda_{irr}/\lambda_{obs}}(pss)$	$P_{\lambda_{irr}}\times10^{7}$ /einstein s^{-1} dm^{-3}	$k_{A\leftrightarrows B}^{\lambda_{irr}}$ / s^{-1}
E-STIL	220	300	0.144	0.0570	3.29	0.00055
	240		0.143	0.0580	4.39	0.0007
	270		0.142	0.0516	4.07	0.00245
	280		0.141	0.0530	2.79	0.0032
	290		0.146	0.0550	2.79	0.0055
	300		0.142	0.0492	3.19	0.0088
	310		0.141	0.0496	3.48	0.011
	325		0.144	0.0482	4.79	0.014
E-PINO	280	300	0.539	0.209	3.40	0.00128
	290		0.556	0.200	4.16	0.00405
	300		0.530	0.179	5.45	0.0069
	310		0.536	0.207	6.29	0.01
	320		0.511	0.174	6.09	0.012
	330		0.494	0.177	6.99	0.012
E-RVT	235	310	0.620	0.114	2.08	0.0009
	270		0.610	0.271	4.65	0.0015
	290		0.622	0.277	2.81	0.0049
	300		0.627	0.278	3.39	0.0084
	310		0.626	0.278	3.94	0.0125
	320		0.627	0.277	4.07	0.0148
	330		0.625	0.276	5.18	0.017
	340		0.627	0.272	7.03	0.017
E-ORVT	260	328	0.474	0.222	1.79	0.0004
	295		0.492	0.270	2.52	0.0015
	310		0.474	0.219	2.10	0.0025
	320		0.489	0.240	5.41	0.0085
	328		0.486	0.240	2.39	0.0047
	340		0.498	0.216	2.83	0.0068
	350		0.480	0.215	3.21	0.0080
	360		0.468	0.175	4.60	0.0150

Compound	λ_{irr} /nm	λ_{obs} /nm	$A_{tot}^{\lambda_{irr}/\lambda_{obs}}(0)$	$A_{tot}^{\lambda_{irr}/\lambda_{obs}}(pss)$	$P_{\lambda_{irr}} \times 10^7$ /einstein s^{-1} dm^{-3}	$k_{A \leftrightarrows B}^{\lambda_{irr}}$ / s^{-1}
E-PTERO	220	320	0.476	0.189	9.31	0.001
	250		0.453	0.195	8.86	0.002
	280		0.466	0.195	8.75	0.007
	290		0.456	0.201	7.99	0.001
	300		0.441	0.165	7.67	0.020
	320		0.439	0.141	10.60	0.042
	330		0.431	0.128	12.66	0.043
	350		0.431	0.123	16.81	0.036
O-DAE	280	350	0.010	0.035	3.61	0.002
	290		0.011	0.035	3.99	0.003
	330		0.011	0.034	5.4	0.0042
	350		0.010	0.034	10.06	0.0074
	360		0.011	0.031	13.20	0.0081
C-DAE	410	520	0.036	0	16.70	0.0052
	420		0.036	0	15.30	0.0055
	430		0.037	0	16.70	0.0055
	460		0.037	0	18.60	0.0063
	480		0.037	0	18.00	0.008
	520		0.037	0	14.60	0.0101

5.5. Kinetic elucidation

5.5.1. Determination of the photostationary state's composition

The photostationary state solutions of all compounds were analysed by HPLC.

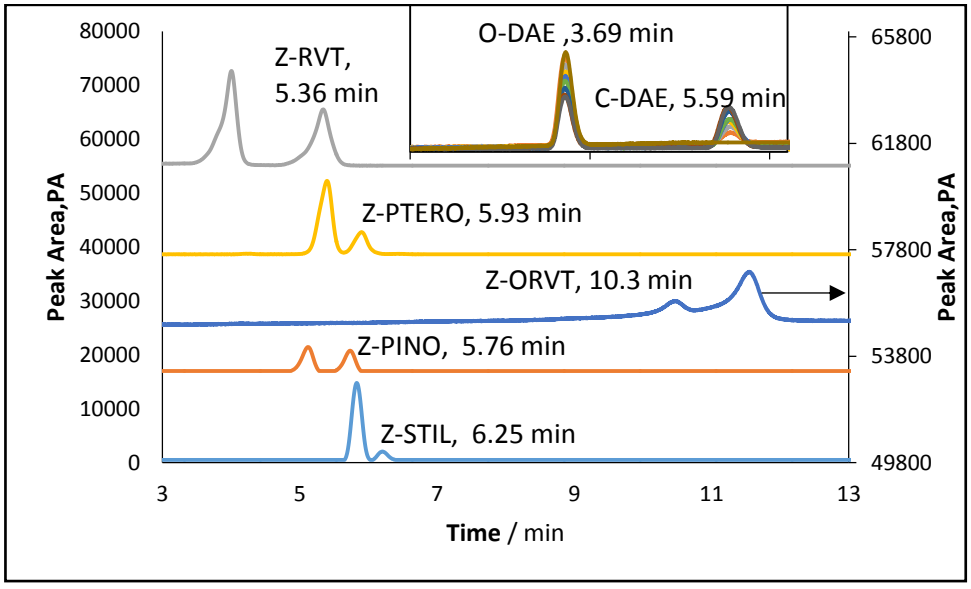

Figure 5- 6: Chromatograms of the studied compounds.

5.5.2. Reconstruction of the whole spectrum of the photoproduct

The absorption spectrum of the photoproduct ($\varepsilon_B^{\lambda_{irr}}$) can be reconstructed using Eq. (5-7) (Fig.5-7) and the absorption spectra of the reaction medium at the initial time and at the photostationary state (the reconstruction is carried out without physically separating the photoproducts of the study compounds from the reaction medium).

Photoisomers have more vibrational structure than the starting material.

For all the study compounds, the new peaks related to photoproducts were observed regardless of the irradiation wavelength. These attributes indicate that a photochemical mechanism does not change with irradiation.

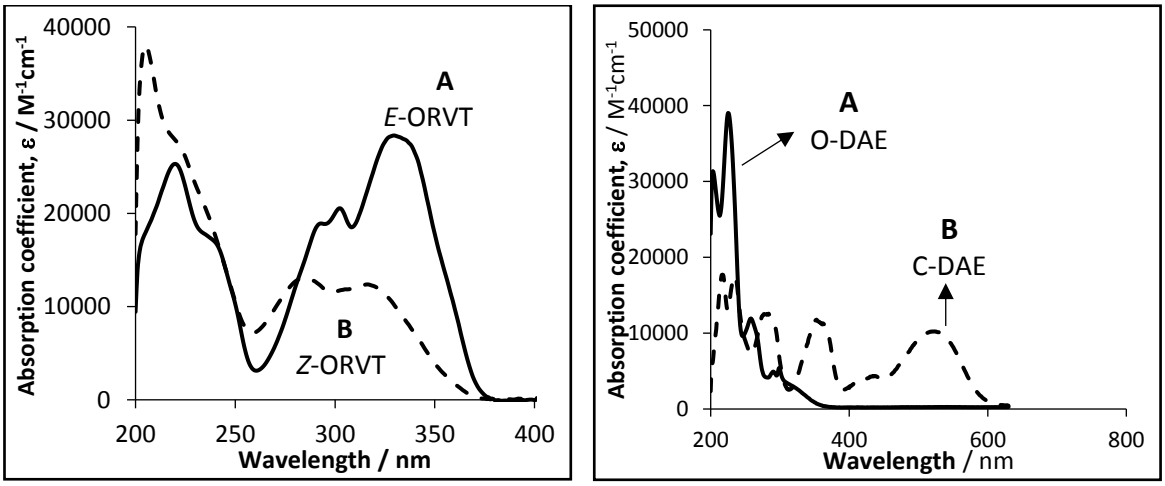

Figure 5- 7: Native and reconstructed electronic absorption spectra (absorption coefficient units) of E-isomers and its Z- isomers photoproduct of ORVT and DAE at open and close form.

5.5.3. Determination of the Reaction quantum yields

Once the absorption coefficients of the photoproduct were known, the individual absolute values of the quantum yield at any irradiation wavelength were calculated

using Equations (5-6) and (5-4). The numerical value of the reaction's initial velocity (ν_0) can be determined using Eq. (5-7). Both forward and reverse quantum yields have been found to be wavelength dependent (Fig.5-8). Increases of between two- and 17-fold have been recorded for the $\Phi_{A\rightarrow B}^{\lambda_{irr}}$values of *E*-stilbenoids in the wavelengths range 220 nm – 350nm (Fig. 5-8, Table 5-5). However, the variation in the $\Phi_{B\rightarrow A}^{\lambda_{irr}}$ values within the same wavelength range were much more important, ranging between a factor of seven and 166. This result suggests that the reverse reaction ($\Phi_{B\rightarrow A}^{\lambda_{irr}}$) was more highly affected by the variation of the irradiation wavelength.

In contrast, the reverse quantum yield of the $C \rightarrow O$ reaction of DAE is less affected by the different irradiation wavelengths between 280-380 nm, whereas, in the same wavelength range, the forward quantum yield reaction undergoes a six-fold increase.

In case the ORVT, the phototransformation of *Z*-isomer is less efficient than *E*-isomer, this might be due to the geometric strain, when the two big groups in the *E*-isomer forms are opposite side to each other, then they interact less with each other than with the *Z*-form, where larger groups in *Z*-isomer are less separate and have lower independence.

Table 5- 5: *Quantum yields, overall rate-constant, absorption coefficients and initial velocity values for studies compounds photodegradation reactions under different monochromatic irradiations.*

λ_{irr} /nm	$P_{\lambda_{irr}}$ × 10^7 / einsteins^{-1} dm^{-3}	$A_{tot}^{\lambda_{irr}/\lambda_{irr}}(pss)$	$k_{A\rightleftharpoons B}^{\lambda_{irr}}$ / s^{-1}	$v_0^{\lambda_{irr}/\lambda_{irr}}$ x 10^4 / s^{-1}	$\varepsilon_A^{\lambda_{irr}}$ / $M^{-1}cm^{-1}$	$\varepsilon_B^{\lambda_{irr}}$ / $M^{-1}cm^{-1}$	$F_{\lambda_{irr}}(0)$	$(\Phi_{A\rightarrow B}^{\lambda_{irr}}$ ± SD) x 10^2	$(\Phi_{B\rightarrow A}^{\lambda_{irr}}$ ± SD) x 10^2
t-STIL									
220	3.29	0.063	0.00062	0.13	15291.73	20136.40	2.08	2.26± 0.05	0.53± 0.01
240	4.39	0.023	0.0007	-0.37	3288.49	12100.97	1.95	4.11± 0.04	5.46± 0.06
270	4.07	0.057	0.002	-0.44	15233.66	10641.09	1.91	7.18± 0.07	0.31± 0.08
280	2.79	0.058	0.0032	-1.41	22887.44	9745.44	1.79	9.49± 0.03	5.56± 0.06
290	2.79	0.063	0.0055	-3.62	28107.85	7874.21	1.67	12.85± 0.06	14.69± 0.42
300	3.19	0.049	0.0088	-6.57	28556.52	4881.19	1.67	17.50± 0.14	28.76± 0.76
310	3.48	0.039	0.012	-9.68	25574.18	2008.46	1.67	23.74± 0.32	88.09± 0.53
325	4.79	0.015	0.014	-6.76	12995.59	215.29	1.95	38.35± 0.41	590.16± 0.38
PINO									
280	3.40	0.287	0.0023	-1.24	14639.63	9373.60	1.07	10.49 ± 0.29	12.54 ± 3.68
290	4.16	0.229	0.0038	-5.48	20798.74	8123.77	0.92	11.28 ± 1.57	9.65 ± 1.27
300	5.45	0.179	0.0069	-11.66	24570.59	5683.90	0.82	12.36 ± 0.90	14.93 ± 1.27
310	6.29	0.089	0.0105	-18.78	24309.56	2981.40	0.85	14.24 ± 0.73	25.93 ± 5.33
320	6.09	0.043	0.0112	-18.14	18158.69	1376.58	1.19	19.73 ± 1.09	45.45 ± 13.90
330	6.99	0.044	0.011	-14.70	11202.53	579.21	1.31	27.69 ± 1.68	87.98 ± 3.47
RVT									
235	2.79	0.359	0.00057	0.25	19103.93	21583.61	1.21	5.94± 0.35	0.27± 0.13
270	4.65	0.214	0.0016	1.19	8911.25	14637.99	1.66	8.93± 0.56	2.59± 0.25
290	2.81	0.334	0.0038	-3.95	25842.63	14399.99	0.93	13.86± 0.45	15.13± 0.99
300	3.39	0.315	0.0075	-11.29	31183.23	11877.18	0.81	18.59± 0.43	27.82± 1.33
310	3.94	0.279	0.0125	-21.66	32541.43	8452.25	0.75	24.18± 0.34	51.69± 0.59
320	4.07	0.222	0.0148	-26.89	32092.79	5628.32	0.76	26.51± 0.34	72.68± 2.39

λ_{irr} /nm	$P_{\lambda_{irr}}$ × 10^7 / einsteins^{-1} dm^{-3}	$A_{tot}^{\lambda_{irr}/\lambda_{irr}}(pss)$	$k_{A\rightleftharpoons B}^{\lambda_{irr}}$ / s^{-1}	$v_0^{\lambda_{irr}/\lambda_{irr}}$ x 10^4 / s^{-1}	$\varepsilon_A^{\lambda_{irr}}$ / $M^{-1}cm^{-1}$	$\varepsilon_B^{\lambda_{irr}}$ / $M^{-1}cm^{-1}$	$F_{\lambda_{irr}}(0)$	($\Phi_{A\rightarrow B}^{\lambda_{irr}}$ ± SD) x 10^2	($\Phi_{B\rightarrow A}^{\lambda_{irr}}$ ± SD) x 10^2
RVT									
330	5.18	0.147	0.017	-30.72	26408.03	3099.77	0.86	27.82± 0.85	79.36± 3.03
340	7.03	0.074	0.017	-26.09	18080.62	1941.63	1.16	29.03± 0.44	48.69± 1.87
ORVT									
260	1.95	0.097	0.00028	0.13	3137.99	7239.39	2.03	6.90 ± 0.86	2.30 ± 1.02
295	2.25	0.227	0.0016	-1.29	18858.67	11834.99	1.18	10.50 ± 0.17	4.30 ± 0.42
310	2.29	0.232	0.0026	-1.84	18800.78	12053.62	1.21	15.40 ± 1.32	9.10 ± 1.72
320	4.68	0.252	0.009	-11.17	25047.97	12150.87	0.99	21.34 ± 0.14	13.97 ± 0.11
328	2.01	0.239	0.005	-7.35	28261.80	10654.78	0.92	23.30 ± 1.57	21.91 ± 3.21
340	4.02	0.148	0.015	-23.44	26490.31	7110.86	1.01	35.01 ± 1.32	26.34 ± 5.77
350	4.55	0.096	0.015	-21.94	17801.98	3912.45	1.16	43.80 ± 1.60	26.26 ± 1.4
360	7.64	0.031	0.015	-14.94	9783.39	1690.81	1.61	45.38± 0.67	6.87 ± 1.6
PTERO									
230	9.07	0.327	0.00108	0.51	20246.15	24384.63	1.25	1.90± 0.049	0.53± 0.049
240	9.52	0.235	0.005	0.29	14861.53	19238.98	1.39	1.11± 0.37	1.01± 1.27
250	8.87	0.107	0.00098	0.28	6410.26	15328.07	1.91	1.20± 0.076	1.50± 0.088
260	8.92	0.099	0.0021	1.12	3471.79	18320.34	2.04	4.10 ± 0.29	2.72± 0.47
270	9.39	0.156	0.0036	1.89	7133.33	15117.01	1.79	6.44± 0.18	4.74± 0.17
290	7.99	0.243	0.012	-8.60	22246.15	13784.55	1.15	16.63± 0.12	13.20± 0.27
300	7.67	0.208	0.018	-22.59	27174.36	10446.67	1.02	20.53± 0.73	23.09± 1.18
310	8.95	0.184	0.026	-37.98	28979.49	7146.59	0.96	23.10± 0.37	39.11± 3.12
320	10.61	0.139	0.037	-58.12	28979.49	4202.95	0.96	26.32± 2.53	64.43± 7.06
DAE								($\Phi_{O\rightarrow C}^{\lambda_{irr}}$ ± SD) x 10^2	$\Phi_{C\rightarrow O}^{\lambda_{irr}}$ ± SD) x
280	3.61	0.0878	0.0021	7.29	12482.99	4176.56	2.03	11.0± 0. 2	9.0± 0. 70
290	3.99	0.0926	0.0035	7.71	11637.17	4926.17	1.98	11.0± 0.07	15.0± 2.70

λ_{irr} /nm	$P_{\lambda_{irr}}$ × 10^7 / einsteins^{-1} dm^{-3}	$A_{tot}^{\lambda_{irr}/\lambda_{irr}}(pss)$	$k_{A\rightleftharpoons B}^{\lambda_{irr}}$ / s^{-1}	$v_0^{\lambda_{irr}/\lambda_{irr}}$ x 10^4 / s^{-1}	$\varepsilon_A^{\lambda_{irr}}$ / $M^{-1}cm^{-1}$	$\varepsilon_B^{\lambda_{irr}}$ / $M^{-1}cm^{-1}$	$F_{\lambda_{irr}}(0)$	($\Phi_{O\rightarrow C}^{\lambda_{irr}}$ ± SD) x 10^2	$\Phi_{C\rightarrow O}^{\lambda_{irr}}$ ± SD) x 10^2
DAE									
330	5.4	0.0508	0.0041	5.84	5779.46	2274.52	2.14	23.04± 0.5	22.40± 0.40
350	10.02	0.0340	0.0074	18.70	11666.94	869.58	2.25	38.0± 0.06	12.0± 2.70
360	10.06	0.0211	0.008	13.20	11262.89	479.617	2.28	52.0± 0.1	14.0± 0.2
380	13.20	0.0033	0.007	1.76	4561.76	229.51	2.29	63.0± 2.0	22.0± 0.11
410	16.70	0	0.0052	-5.67	4139.072	162.00	2.24	-	16.30± 0.08
420	15.30	0	0.049	-3.40	4536.28	162.00	2.26	-	15.40± 0.04
430	16.70	0	0.0055	-8.20	4847.36	219.45	2.22	-	14.70± 0.02
450	16.47	0	0.005	-5.36	4667.02	215.58	2.24	-	14.10± 0.006
460	18.60	0	0.0061	-8.98	5087.53	221.64	2.22	-	13.90 ± 0.04
480	18.00	0	0.0086	-21.50	7483.98	246.44	2.17	-	13.80± 0.005
520	14.60	0	0.0101	-34.39	10905.79	256.5075	2.12	-	13.80± 0.09
535	18.70	0	0.0125	-44.75	10550.33	267.01	2.11	-	13.80± 0.02

It is also interesting to notice that the quantum yields of $Z \rightarrow E$ were larger than those of the E-isomers with the exception of ORVT (Table 5-5). The difference in quantum yileds between two isomers (*E*- and *Z*-) suggest that it may be a difference in the photoisomers' exited- state of each species, that does not support the hypothesis that both isomers are decay from a common intermediate.

The calculated percentage of photodecomposition of studied compounds in ethanol were found in the 240–380 nm range to be between 25 and 97% (Figure 5-8, Appendix I, Table 1). In general, the degradation percentage increase with irradiation wavelength (Figure 5-8). These findings show that the photoreaction supports the phototransformation of *E*-isomers, in which the *Z*-isomers contributes significantly to the composition of the pss species. This finding implies that this method makes it easy to determine the degradation percentage (without need to use HPLC), and also it shows that the degradation percentage is dependent on wavelength. This means that exposure of the study compounds to light (UVA and/or visible) lead to the complete depletion these compounds, and so it is strongly recommended to protect the study compounds from exposure to light (Fig.5-9). The percentage degradation would also help to decide about the appropriate dosage of the API in the formulation.

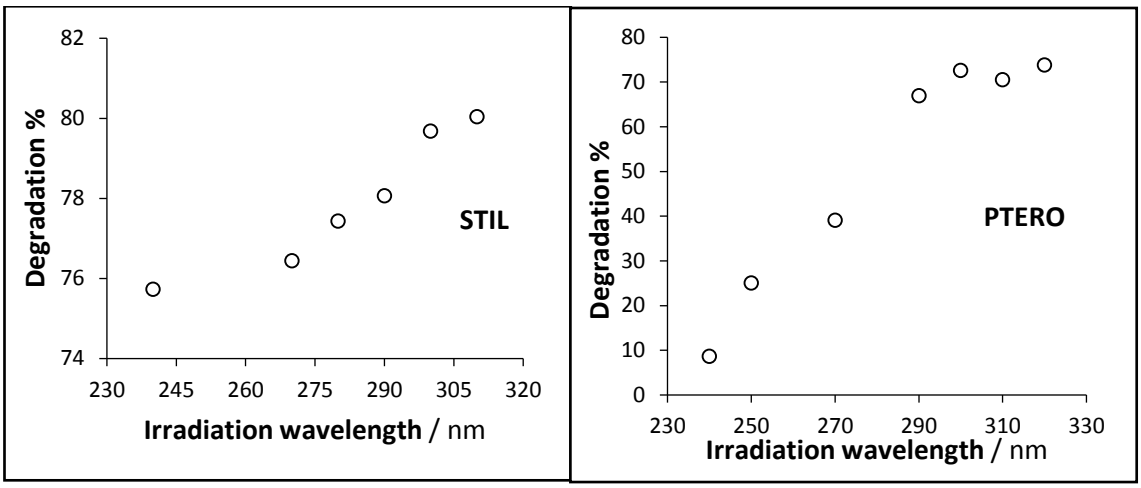

Figure 5- 8: Relationship between $Degradation\ \%$ with irradiation wavelength (λ_{irr}) of E-STIL and E-PTERO.

Good sigmoid correlations of the experimental values ($\mathbf{\Phi_{exp.}}$) for these irradiation wavelengths (Fig. 5-9, and Table 5-6) were found. Eq. (5-17) can be used to calculate the quantum yield at any wavelength. In contrast, the linear correlation in two ranges (330-350 and 350-380 nm) of the Φ_{exp} of C-DAE were found (Eqs. 5-18 and 5-19).

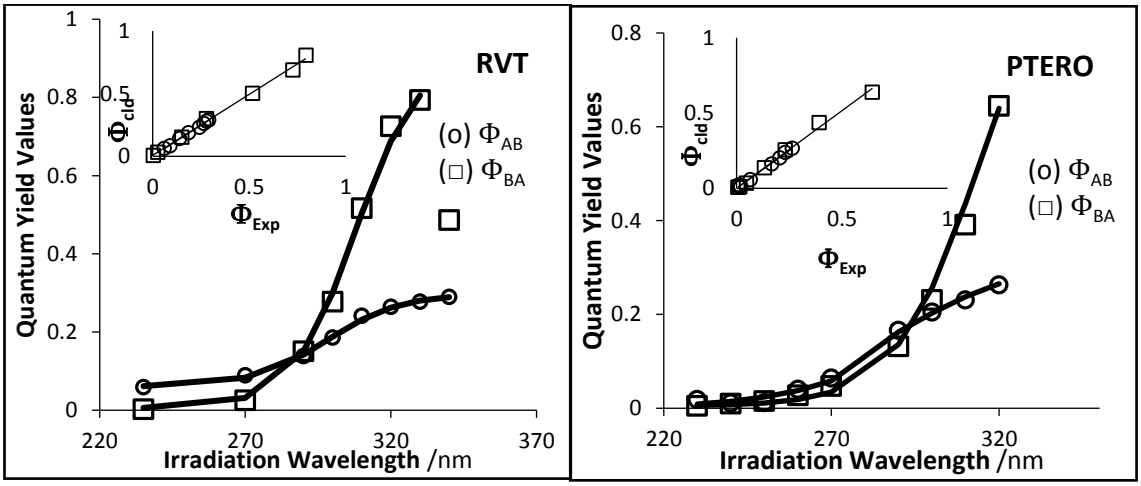

Figure 5- 9: RVT and PTERO forward $\Phi_{A\to B}^{\lambda_{irr}}$ and reverse $\Phi_{B\to A}^{\lambda_{irr}}$ photochemical quantum yield values determined at different irradiation wavelengths. Inset: the linear- relationship of the experimental and calculated (Eq.5-17) values of the forward ($\Phi_{A\to B}^{\lambda_{irr}}$) and the reverse ($\Phi_{A\to B}^{\lambda_{irr}}$) quantum yields.

$$\Phi_{A\to B\ (X)}^{\lambda_{irr}} = A + \frac{B}{1+C\times e^{-D(\lambda_{irr}-E)}} \qquad \text{Eq. 5-17}$$

$$\Phi^{\lambda_{irr}}_{DAE\ C\rightarrow O\ (330-350)} = -0.0053 \times \lambda_{irr} + 1.9915 \quad \text{(UV irradiation)} \qquad \text{Eq. 5-18}$$

$$\Phi^{\lambda_{irr}}_{DAE\ C\rightarrow O\ (350-380)} = 0.0035 \times \lambda_{irr} - 1.1197 \quad \text{(UV irradiation)} \qquad \text{Eq. 5-19}$$

Where the equation parameters represent in Table 5-6.

Table 5- 6: *The values of (A, B, C, D and E) in sigmoid equation (5-17).*

Compound (X)	Reaction	A	B	C	D	E
t-STIL	$A \rightarrow B$	0.021	1.125	39	0.045	260
	$B \rightarrow A$	0.004	4.15	26	0.1145	293
PINO	$A \rightarrow B$	0.1	0.5	210	0.0921	278
	$B \rightarrow A$	0.1	1.8	270	0.106	280
RVT	$A \rightarrow B$	0.06	0.237	14	0.08	265
	$B \rightarrow A$	0.005	0.901	21	0.098	275
ORVT	$A \rightarrow B$	0.068	0.417	440	0.0826	254
	$B \rightarrow A$	0.025	0.28	135	0.0925	270
PTERO	$A \rightarrow B$	0.4	0.45	85	0.051	219
	$B \rightarrow A$	0.005	1.03	70	0.08	261
DAE (280-380)	$O \rightarrow C$	0.09	0.57	105	0.049	259
DAE (280-330)	$C \rightarrow O$	0.0615	0.165	80	0.192	266
C-DEA (vis)	$C \rightarrow O$	0.138	0.068	1.7	0.061	410

Thus, the quantum yield of *E*/*Z* photoreversible systems should, *a priori*, be considered wavelength dependent. These results confirm the utility of the easy-to-implement and reliable Φ-order model. It allows the determination of quantum yield values and identifies their dependence on wavelength.

5.6. Pseudo Constants

The $\beta_{\lambda_{irr}}$ factor values were calculated from the experimental data for $k^{\lambda_{irr}}_{A\rightleftharpoons B}$ and $P_{\lambda_{irr}}$, as described in Table 5-4, based on Eq. 5-4. By plotting the $\beta_{\lambda_{irr}}$factor values against the

corresponding wavelengths, a sigmoid-shaped graph is obtained (Fig. 5-9, Eq. 5-20), except for the O-DAE graph which is triangle-shaped. Moreover, the $\beta_{\lambda_{irr}}$ factor methodology was used previously by Maafi group [1,4,5,17–20] and provided the scale of the photoreactivities through the $\beta_{\lambda_{irr}}$ factor (Table 5-7), which is the value of the $\beta_{\lambda_{irr}}$ factor relative to fast and slow photoreactivity due to this factor being light intensity independent. Because it is difficult to replicate light intensities between different laboratories [17,21], this leads to inaccuracies in the overall rate constant in this comparison. Therefore, it might be this factor can help to solve the difficulties inherent to comparing the photodecomposition results achieved under different circumstance [20].

$$\beta_{\lambda_{irr,X}} = A + \frac{B}{1+C\times e^{-D(\lambda_{irr}-E)}} \quad \text{Eq. 5-20a}$$

Where the values of A, B, C, D and E are given in Table 5-6.

Table 5- 7: *Values of (A, B, C, D and E) in $\beta_{\lambda_{irr,X}}$ equation 20a.*

Compound (X)	A	B	C	D	E
t-STIL	1550	38900	62	0.1	251
PINO	5500	14400	1.35	0.11	297
RVT	2303	38500	79	0.101	256
ORVT	2220	23900	139	0.088	260
PTERO	700	38500	96	0.084	242
C-DAE	3100	4000	0.12	0.08	510

$$\beta_{\lambda_{irr,O-DAE\,(280-350)}} = 32.32 \times \lambda_{irr} - 3236.1 \quad \text{Eq. 5-20b}$$

$$\beta_{\lambda_{irr,O-DAE\,(350-380)}} = -93.65 \times \lambda_{irr} + 41018 \quad \text{Eq. 5-20c}$$

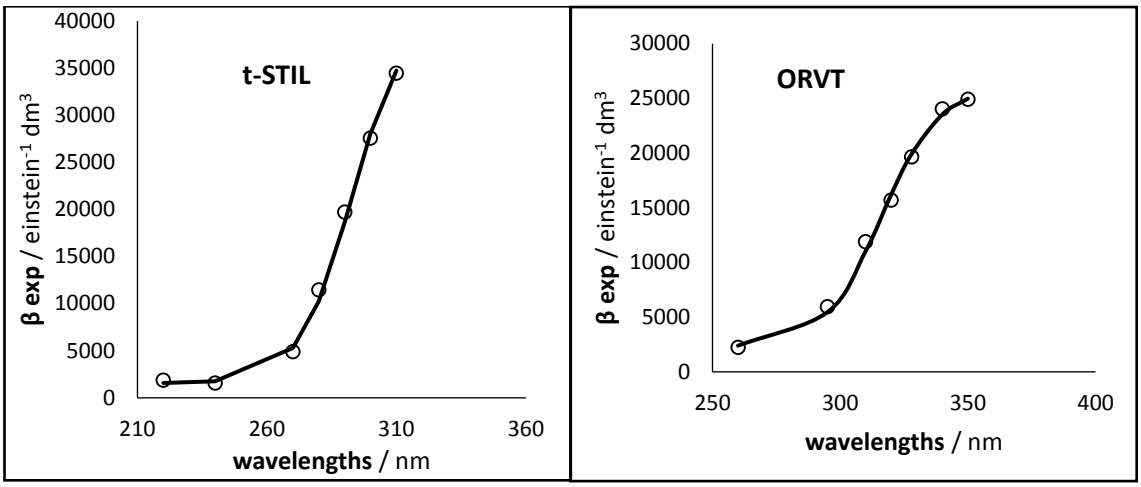

Figure 5- 10: Calculated $\beta_{\lambda_{irr}}$ values (circles) for E-STIL and E-ORVT as examples using Eq. (5-4) and the values of $k_{A\rightleftharpoons B}^{\lambda_{irr}}$ and $P_{\lambda_{irr}}$ provided in Table 5-5. The sigmoid model, Eq. 5-20a (line) was used to fit the experimental data.

***Table 5- 8**: Comparative $\beta_{\lambda_{irr}}$ values for several drugs and a proposal for a ranking scale*

Compound	Pseudo Rate Constant ($\beta_{\lambda_{irr}}$) /einstein^{-1} dm^3	Ranking Group	ref
Monochromatic studies			
Rvt	4207-36582	Group I: $\beta > 10^4$	
tstil	1577-34724		
Ptero	2437-34905		
Montelukast	2251-28069		[5]
Orvt	5454-24970		[18]
Pino	6764-18390		
Axitinib	2193-14552		[22]
Tranlast	1079-10387		
Nifedipone	8117-9776	Group II: $6 > \beta \times 10^3 > 10$	[1]
Nisoldipine	7558-8851		[20]
O-DAE	5812-8074		
C-DAE	3111-6895		
Sunitinib	1560-5847		[3]
Dacarbazine	2121-4013	Group III: $2 > \beta \times 10^3 > 6$	[4]
Fluovoxamine	818-2077	Group IV: $\beta < 2000$	[19]
Riboflavine	226-422		[17]
FMF	4-44		[17]

5.7. Discussion

There are few models, to best of our knowledge, in the literature [23–27] that are used to describe the photochemical reaction for three AB systems. We worked on discussing these models, and comparing them with ours as following.

The photokinetic models of the photochemical reaction AB $(1\Phi)_{\varepsilon_{B=0}}$ system [23–26,28] were taken into consideration by the simple rate equation (5-21) below.

$$-\frac{dC_A}{dt} = \Phi_{A\to B}P_{abs,\lambda_{irr}} = \Phi_{A\to B}P_{0,\lambda_{irr}}\left(1-10^{-\varepsilon_A^{\lambda_{irr}}C_A(t)l}\right) \qquad \text{Eq.5-21}$$

Where the $P_{abs,\lambda_{irr}}$ is the light absorbed by the molecules.

In the AB $(1\Phi)_{\varepsilon_{B=0}}$ system, the Irie group [23] has used the same model proposed by Zepp [23], which was used to describe the closed-ring isomer of the dithienylethene derivative, and the method's limitations will be described briefly later in the model proposed by Zepp [23]. However, in 2014, the Irie group [28] has proposed a model that was different to the model proposed in 1999 by same group [23], which used the same differential equation, Eq. 5-21. The model was given as

$$\log(10^{A_t}-1)-\log(10^{A_0}-1) = -\frac{1000\times\varepsilon_A^{\lambda_{irr}}\times l\times\Phi_{A\to B}P_{0,\lambda_{irr}}}{VN_A}t \qquad \text{Eq.5-22}$$

Where N_A is Avogadro's number, V is the solution volume, which are scaled by a multiple of 1000 to correct the unit in this equation to convert from molecules to molar concentration.

However, Eq. (5-22) is similar to that proposed by Maafi group a long time ago [29]. Where when we use the change of base using the natural log as the base log, as given in Eq. (5-23), then one will get the same equation.

$$\log_a x = \frac{\ln x}{\ln a} \qquad \text{Eq.5-23}$$

In order to change the base in Eq. (5-22), using the natural log as the base log, and if we assume that the concentration was the molar concentration, we can remove the conversion parameters as given in Eq. (5-24).

$$\frac{1}{\ln 10}\ln\frac{(10^{A_t}-1)}{(10^{A_0}-1)} = -\frac{1000\times\varepsilon_A^{\lambda_{irr}}\times l\times\Phi_{A\to B}P_{0,\lambda_{irr}}}{VN_A}t = -\varepsilon_A^{\lambda_{irr}}\times l\times\Phi_{A\to B}P_{0,\lambda_{irr}}t \qquad \text{Eq.5-24}$$

There is a certain similarity in the integration between finding in this study and that of the Irie group [28]. Moreover, an interesting finding in results obtained in this study and those of the Irie group [28] was a similar pattern in the quantum yield with wavelength, where the quantum yield decreased with increasing wavelength (wavelength dependent). The quantum yield values were two-fold greater than the values of the current study; this was due to the solvent effect, where ethanol was used in the current study and n-hexan by the Irie group [28]. In addition, in the previous study [30] it was found that the polarity of the solvent will have an effect on the value of the quantum yield, where the quantum yield was two- to three-fold greater in nonpolar solvents than polar solvents. Also, the slight difference between the quantum yields found by the Irie group [28] ($\Phi_{C\to O}^{\lambda_{517}}$ = 0.28) and that reported by Maafi in hexane for the same molecule [29] ($\Phi_{C\to O}^{\lambda_{517}}$ = 0.242) might be due to the difference in light intensity. However, the Irie

group (1999) [23] reported that the quantum yield values were constant for the reaction in the visible range.

Moreover, Stranius et al. [25] reported that the differential equation [43] was solved using the numerical integration function provided in the Matlab computer programme without mathematical simplification or analytical solutions.

However, for the AB $(1\Phi)_{\varepsilon_{B\neq 0}}$ system, two methods [26,31] have been used to describe this system's photochemical reaction. Mazellier [31] described the equations and parameters for the photochemical reaction, which first was proposed by Zepp [24], and this approach was used in several studies [23,31,32]. The model used the differential equation (5-21), when the total absorbance must be lower than 0.02 [31], which mean that the concentration of the compound is low, thus lead to the light absorption is weak. According to this, a Simpson expansion was allowed on the differential equation (Eq. 5-21), and the associated model is given in Eq. 5-25 (See Appendix VI.A).

$$-\frac{dC_A}{dt} = 2.303\ \Phi_{A\rightarrow B} P_{0,\lambda_{irr}} l \varepsilon_A^{\lambda_{irr}} C_A(t) \qquad \text{Eq. 5-25}$$

Where the quantum yield was considered to be constant during the photoreaction, and by integrated Eq. 5-26 as being pseudo-first order

$$\ln \frac{C_A(t)}{C_A(0)} = -2.303\ \Phi_{A\rightarrow B} P_{0,\lambda_{irr}} l \varepsilon_A^{\lambda_{irr}} t = -kt \qquad \text{Eq.5-26}$$

This method was used to quantify the photodegradation and photostabilisation [23,31,32] of different compounds. We could conclude that the kinetics results of these studies [23,31,32] are that the photokinetic traces treated by first order kinetics, and also the quantum yield, was wavelength independent [23,31,32].

There is a certain deficiency in the differential equation (Eq. 5-25) (See Appendix VI.a), in that since an expansion is used, this will lead to the differential equation does not consider the amount light absorbed by both compounds. However, the differential equation for the photokinetics cannot be simplified in this manner due to $P_{abs,\lambda_{irr}}$ by the molecule, which should be taken into account in the differential equation [33]. In this case the light absorbed by the molecule vary during the photochemical reaction because of the concentration of the starting compound changed. Also, the time dependence of the absorbance factor ($F_{\lambda_{irr}}(t)$) will lead to an inability to integrate the rate equation in a closed form [1,29], where the factor $F_{\lambda_{irr}}(t)$ is dependent on the concentration (total absorbance of the media) [1,29]. Moreover, if the total absorbance, i.e. high concentration, was higher than 0.02, then the expansion was not existing it in this case due to it was not achieved the condition of the expansion.

It is important to note that the k is concentration independent (Eq. 5-26), however, the experimental rate constant of the photodegradation of different compounds [34–37] using this approach (Eq. 5-26) is changed with concentration. This finding lead to the contradiction between the theoretical (Eq. 5-26) and the experimental could be result from the approximation that used in the derivation of Eq. (5-25).

In the model proposed by Stadler et al. [26] was used the same differential equation (Eq. 5-21) to determination the quantum yield by using Eq. (5-28) (See appendix VI.B):

$$\frac{dA_{tot}^{\lambda_{irr}}}{dt} = -\Phi_{A\to B}P_{abs,\lambda irr}\left(\varepsilon_A^{\lambda_{obs}} - \varepsilon_B^{\lambda_{obs}}\right)l_{obs} = -\Phi_{A\to B}P_{abs,\lambda irr}\frac{\left(A_{tot}^{\lambda_{irr}}(0) - A_{tot}^{\lambda_{irr}}(pss)\right)}{C_A(0)} \quad \text{Eq.5-27}$$

$$\Phi_{A\to B} = \frac{k_{fit}C_A(0)}{P_{0,\lambda_{irr}}\left(1-10^{-\varepsilon_A C_A(0) l_{irr}}\right)} \quad \text{Eq.5-28}$$

where k_{fit} represents the rate constant of the initial photokinetic traces using first-order or zero-order model given by:

$$\left(\frac{dA_{tot}^{\lambda_{irr}}}{dt}\right)_{t=0} = -k_{fit}\left(A_{tot}^{\lambda_{irr}}(0) - A_{tot}^{\lambda_{irr}}(pss)\right) \quad \text{Eq.5-29}$$

In order to determine the quantum yield from the slope of the $k_{fit}C_A(0)$ against $P_{0,\lambda_{irr}}\left(1-10^{-\varepsilon_A C_A(0) l_{irr}}\right)$, where k_{fit} was determined from initial slope of the experimental data over time at different light irradiation.

According to deviation proposed above, it is clear that the equation of the rate for the photochemical reaction equation as given by Eq.5-27 is effectively equal to the first order rate equation, since their rate-constant is equal using the value obtained from Eq.5-29. This identity is not valid. Therefore, such an approximation cannot doubt on the validity of the result obtained.

On the other hand, there are two of models that can be used to describe the photochemical reaction of the AB (2Φ) system [23,27]. One of these models has been described by Irie group [23] who reported the rate of the photochemical reversible reaction, this is given by Eq. (5-30) after using the expansion (assuming $\varepsilon_A^{\lambda_{irr}} C_A(t) l$ must be less than 0.02):

$$\frac{dC_B}{dt} = \frac{1000\times P_{0,\lambda_{irr}}}{l}\left(\Phi_{A\to B}^{\lambda_{irr}}\left(1-10^{-\varepsilon_A^{\lambda_{irr}} C_A(t) l}\right) - \Phi_{B\to A}^{\lambda_{irr}}\left(1-10^{-\varepsilon_B^{\lambda_{irr}} C_B(t) l}\right)\right) = 2.303 \times 1000 \times P_{0,\lambda_{irr}}(\Phi_{A\to B}^{\lambda_{irr}}\varepsilon_A^{\lambda_{irr}} C_A(t) - \Phi_{B\to A}^{\lambda_{irr}}\varepsilon_B^{\lambda_{irr}} C_B(t)) \quad \text{Eq.5-30}$$

By using the relationship at the photostationary state, the Eq. 5-30 is concluded

$$\ln\frac{A_{tot}^{\lambda_{irr}}(pss) - A_{tot}^{\lambda_{irr}}(0)}{A_{tot}^{\lambda_{irr}}(pss) - A_{tot}^{\lambda_{irr}}(t)} = -2.303 \times 1000 \times P_{0,\lambda_{irr}} \Phi_{A\to B}^{\lambda_{irr}} \varepsilon_A^{\lambda_{irr}} \frac{C_0}{C_{B(\infty)}} t \quad \text{Eq.5-31}$$

This equation might be correlated to equation represent the AB $(1\Phi)_{\varepsilon_{B=0}}$ system, and it could be taken as an AB $(1\Phi)_{\varepsilon_{B=0}}$ for each reaction (forward and reverse) and then sum the two equations to formalise Eq. (5-30). Indeed, this equation was describing a different mechanism than the photoreversible AB (2Φ) (Appendix VI.C). Then if we applying this equation, it needs to irradiated the sample at different wavelengths at same time, which mean each compound will absorbed the light at specific wavelength than other. Moreover, by using the $\frac{dC_B}{dt}$ or $\frac{dC_A}{dt}$ to introduce the photochemical differential equation of the photoreversible AB (2Φ) mechanism mean that the both compounds absorbed light irradiation with different amount. In addition, there is no match between the integration of Eq. (5-30) with the concluding equation (Eq.5-31).

By analyising the above models [23,26,31], it is evident that the above model has a limitation and lack to describe photochemical reaction due to use of assumption and prediction in the simplified differential equation (5-21).

Ladanyi et al. [27] and Stranius et al. [25] reported that the differential equation of the photoreversible reaction is given by:

$$\frac{dC_A(t)}{dt} = \frac{1}{V}\frac{P_{0,\lambda_{irr}}}{NA}\frac{\left(1-10^{-\left(\varepsilon_A^{\lambda_{irr}}C_A(t)+\varepsilon_B^{\lambda_{irr}}C_B(t)\right)l}\right)}{\left(\varepsilon_A^{\lambda_{irr}}C_A(t)+\varepsilon_B^{\lambda_{irr}}C_B(t)\right)}\left(\Phi_{A\to B}^{\lambda_{irr}}\varepsilon_B^{\lambda_{irr}}C_B(t)-\Phi_{A\to B}^{\lambda_{irr}}\varepsilon_A^{\lambda_{irr}}C_A(t)\right)+ k_{the}C_B(t) \quad \text{Eq.5-32}$$

Where k_{the} is the rate constant for the thermal reaction. This equation describes all the relevant photochemical parameters. Nevertheless, three unknown parameters are existing in this equation, $\varepsilon_B^{\lambda_{irr}}$, $\Phi_{A\to B}^{\lambda_{irr}}$ and $\Phi_{A\to B}^{\lambda_{irr}}$. It is difficult to quantify these unknown parameters. However, to solve this problem, a numerical method was employed using

the Matlab programme suite [24,26]. Where the study [27] has explain that the molar absorption coefficients were obtained using numerical methods for each wavelength [27] whilst the quantum yields were estimated as the analytic least-squares fit the system of (N – 1) equations, and which are similar to the Matlab results [27].

On the other hand, Stranius et al. [25] reported a method to determine the quantum yields. Firstly, the quantum yield of A or B is obtained using a specific wavelength, at this wavelength only the one compound absorbed the irradiatation light, and the quantum yield is quantified as AB $(1\Phi)_{\varepsilon_{B=0}}$ system (this suggestion could be difficult to be achieved due to the reaction is reversible reaction), or using the previous reported quantum yield values. Then, $\varepsilon_B^{\lambda_{irr}}$ is determined through irradiation of the compound until it reachs the photostationary state, at which point the total absorbance of the compound was recorded using a spectrophotometer, and then quantified in terms of the concentrations of each species present using an analytical technique such as HPLC or NMR. This allows the absorption spectrum of B to be recalculated. When the quantum yield is known for one species (A or B), the quantum yield for other species (B or A) can obtained using Eq. (5-32) in Matlab to fit the experimental data. Moreover, the dynamic equilibrium constant ($K_{\leftrightharpoons}^{\lambda_{irr}}$) was used to obtain the quantum yield ($K_{\leftrightharpoons}^{\lambda_{irr}} = \frac{\Phi_{A\to B}^{\lambda_{irr}} \times \varepsilon_A^{\lambda_{irr}}}{\Phi_{B\to A}^{\lambda_{irr}} \times \varepsilon_B^{\lambda_{irr}}} = \frac{C_B(pss)}{C_A(pss)}$).

In this context, this method was used to redetermine the quantum yield of azobenzene in solution [25,27]. The outcome of Ladanyi et al.'s study [27] showed that the quantum yield is wavelength dependent.

In this model [25,27] the thermal rate constant was included due to there being a thermal reaction during the photochemical reaction and which is accordingly taken into account in Eq. (5-32). Nevertheless, Ladanyi et al. [27] and Stranius et al. [25] fitted the data by using a computer software without any mathematical simplification of the Eq. (5-32).

The Φ-order kinetics were developed in this study, it was used to study photodegradation under monochromatic, continuous irradiation at the non-isosbestic point. There is a difference between model present in this study and other models [24,26,38] with regard to the associated differential equation. Whilst the photokinetic factor was involved and considered in the proposed model. The most interesting point about Φ-order model was its significant agreement with the principle of the differential equation of the photochemical reaction.

The rate-constants in model proposed in this work were found to change with changing concentration, where the overall rate constant is given by Eq. (5-4), the change in rate constant with change in concentration is due to all the parameters in Eq. (5-4) being independent of concentration except $F_{\lambda_{irr}}(t)$, which is concentration dependent. $F_{\lambda_{irr}}(t)$ is the photokinetic factor, which represents the fraction of the absorption by this compound in the overall absorption of the reaction mixture. As the concentration of the compound changes during the reaction this will led to a change in P_{abs} (and $F_{(t)}$) [1,2]. If the concentration increases, $F_{\lambda_{irr}}(t)$ will be decreased and then k will be decreased. The same observation and confirmation that the rate constant decreases with increasing

concentration of the molecule in the study of effects of concentration on the rate constants for nifedipine and nisoldipine using Φ-order kinetics were made [1,20].

While, other models [23,24] found that the rate constant, mathematically, was concentration independent. However, experimentally, there are differences when the rate-constant is obtained according to the Zepp model [24] with different concentrations [34–37].

Historically [39], quantum yield is expected to remain constant with irradiation wavelength in agreement with Kasha's rule [40]. Moreover, the quantum yield is considered wavelength independent, as mentioned in the methods above [23,24,26]. However, there are a number of studies that have reported that quantum yields change with wavelength or are not wavelength independent, i.e., that Kasha's rule is not followed [9,27,28,41–56]. In addition, Elisei, Mazzucato and Görner (1989) found that the quantified quantum yield values for stilbene derivatives such as 1-styrylnaphthalene and dinaphthylethylene in methylcyclohexane increased when irradiation wavelength increased within the range 313-366 nm from 0.16 to 0.30 and 0.04 to 0.08, respectively. In contrast, other studies [57–64] have showed the opposite effect in terms of wavelength, where $\Phi^{\lambda_{irr}}_{trans\rightarrow cis}$ and $\Phi^{\lambda_{irr}}_{cis\rightarrow trans}$ decreased with increasing irradiating wavelength (Appendix I, Table I-2). Moreover, the quantum yields of the photochroms (open to closed form) were wavelength dependent, as has been found by various different studies [65–68]. The significant difference between the quantum yields for indolylfugide, as one of the open to closed forms in the photochrom system in toluene, where the associated quantum yields were reported in the Yokoyama study ($\Phi^{\lambda_{405}}_{O\rightarrow C}$ =

0.14 and$\Phi_{C\to O}^{\lambda_{405}}$ = 0.26) [67] and the Wolak study ($\Phi_{O\to C}^{\lambda_{427}}$ = 0.20 and$\Phi_{C\to O}^{\lambda_{427}}$ = 0.10) [66]. In addition, the results obtained in this study showed that the quantum yield of C-DAE in ethanol ($\Phi_{C\to O}^{\lambda_{517}}$ is 0.14) was two-fold lower than in the hexane ($\Phi_{C\to O}^{\lambda_{517}}$ is 0.242) [29], which also confirms the solvent effect on quantum yield.

Also, previous studies [57,69–73] showed that quantum yield is dependent on wavelength where the $\Phi_{trans\to cis}^{\lambda_{irr}}$ and $\Phi_{cis\to trans}^{\lambda_{irr}}$of stilbene in benzene and n-hexane were reported to increase with increasing irradiating wavelength between 313-405 nm and 254-313nm, respectively. The values of the wavelength dependent $\Phi_{trans\to cis}^{\lambda_{irr}}$and $\Phi_{cis\to trans}^{\lambda_{irr}}$ ranged between 0.36 – 0.42 and 0.28 – 0.32, respectively. Similarly, in this study the $\Phi_{trans\to cis}^{\lambda_{irr}}$ and $\Phi_{cis\to trans}^{\lambda_{irr}}$ of t-STIL and its derivatives were found to increase with increasing irradiation wavelength (220-360 nm) (Appendix I).

Moreover, the effect of substitution on the quantum yield was established by several studies for the stilbene group [74–82]. The position of electron donating or withdrawing groups on the aromatic ring has been shown to result in a significant change in the value of the associated quantum yield [74–82]. The *E-Z* quantum yields for stilbene in different solutions were higher in the *para* positions than the *meta* positions (Appendix I, Table I-3) [74–82]. The hydroxy in the *orthro* position shows a higher quantum yield than in the *meta* (Appendix I, Table I-3) [83]. Also, in acetonitrile, the quantum yield when the hydroxy was in the *ortho* position was found to be higher ($\Phi_{trans\to cis}^{\lambda_{irr}}$ = 0.39) than in the *para* ($\Phi_{trans\to cis}^{\lambda_{irr}}$ =0.35) [83]. Moreover, if there are more than one substituent disubstituted on the same benzene ring, the *para* position shows a higher quantum yield

than the *meta* position as well (see Table I-2 case *m,p*-dimethoxy, in appendix I) [81]. The results of this study show that higher quantum yields are observed for the silbenoid compounds is due to the hydroxy substituent being in the *para* and *ortho* positions in the ORVT (ORVT > RVT > PTERO > PINO). This finding is supported by the results discussed above [83]. Substituents in both positions (*para* and *ortho*) might lead to a synergistic effect on the value of the quantum yield.

However, the findings from the previous studies is that there are no systematic studies that describe that the effects of irradiation on the quantum yields of the stilbenoids and the diarylethenes derivatives. Furthermore, these studies confirm that the photoisomerisation of the stilbenoids group and diarylethenes derivative are strongly wavelength dependent.

5.8. Conclusion

The recently proposed Φ-order kinetics model describe well the traces of photokinetics of STIL and its derivatives. The effectiveness of the elucidation method opens a new perspective on modelling photoreactions

This study confirms the dependence on wavelength of quantum yield. The reverse quantum yield increased with the variation irradiating wavelength according to sigmoid patterns. Increases between 7 and 294-fold were recorded between 220 nm and 350 nm. However, the forward ($\Phi_{A\rightarrow B}^{\lambda_{irr}}$) quantum yields were less affected (2-17-fold increase) for same range. A 6-fold increase in the $\Phi_{O\rightarrow C}^{\lambda_{irr}}$ values of O-DAE than C-DAE in the wavelength range 280-380 nm.

It seems that the quantum yield of *E*/*Z* photoreversible systems should be a *priori* considered wavelength dependent, as indicated by these results. Therefore, the average quantum yield values obtained using polychromatic irradiation might be deemed misleading and must be considered with care.

Finally, this study indicates that this new approach using the kinetics model (Φ-order) can easily be applied to many other drugs which have photounstable properties with the AB mechanism, regardless of being a photoreversible or unimolecular system.

5.9. References

1. Maafi W., Maafi M. Modelling nifedipine photodegradation, photostability and actinometric properties. International Journal of Pharmaceutics. Elsevier B.V.; 2013; 456(1): 153–164.
2. Maafi M., Maafi W. Φ-Order Kinetics of Photoreversible-Drug Reactions. International Journal of Pharmaceutics. 2014; 471(1–2): 536–543.
3. Maafi M., Lee LY. Actinometric and Φ-order photodegradation properties of anti-cancer sunitinib. Journal of Pharmaceutical and Biomedical Analysis. Elsevier B.V.; 2015; 110: 34–41.
4. Maafi M., Lee LY. Determination of Dacarbazine Φ-Order Photokinetics, Quantum Yields, and Potential for Actinometry. Journal of Pharmaceutical Sciences. Elsevier Masson SAS; 2015; 104(10): 3501–3509.
5. Maafi M., Maafi W. Montelukast photodegradation: Elucidation of Φ-order kinetics, determination of quantum yields and application to actinometry. International Journal of Pharmaceutics. 2014; 471(1–2): 544–552.
6. Maafi M. Useful spectrokinetic methods for the investigation of photochromic and thermo-photochromic spiropyrans. Molecules. 2008; 13(9): 2260–2302.
7. Maafi M., Brown RG. Photophysics and kinetics of naphthopyran derivatives, Part 2: Analysis of diarylnaphthopyran kinetics. Degeneracy of the kinetic solution. International Journal of Chemical Kinetics. 2005; 37(12): 717–727.
8. Maafi M., Brown RG. Photophysics and kinetics of naphthopyran derivatives, Part

6: A fundamental system of equations to describe ABC(3k,6ϕ) dynamics. A contribution to the elucidation of [2H]-naphthopyran kinetics. International Journal of Chemical Kinetics. May 2008; 40(5): 268–281.

9. Coyle J. Advances in photochemistry, volume 19. Journal of Photochemistry and Photobiology A: Chemistry. J. Wiley; 1996; 94(2–3): 263.

10. R Padhye BM., Rao NR., Venkataraman K. THE EFFECT OF SUBSTITUTION ON THE LIGHT ABSORPTION OF NAPHTHALENE. Available at: https://www.ias.ac.in/article/fulltext/seca/038/04/0297-0306 (Accessed: 28 May 2019)

11. Duvenhage MM., Visser HG., Ntwaeaborwa OM., Swart HC. The effect of electron donating and withdrawing groups on the morphology and optical properties of Alq3. Physica B: Condensed Matter. Elsevier; 2014; 439: 46–49.

12. Waldeck DH. Photoisomerization dynamics of stilbenes in polar solvents. Journal of Molecular Liquids. 1993; 57(C): 127–148.

13. Matsuda K., Matsuo M., Mizoguti S., Higashiguchi K., Irie M. Reversed photoswitching of intramolecular magnetic interaction using a photochromic Bis(2-thienyl)ethene spin coupler. Journal of Physical Chemistry B. 2002; 106(43): 11218–11225.

14. Yoshioka S., Stella VJ. Stability of drugs and dosage forms. Kluwer Academic/Plenum Publishers; 2000. 268 p.

15. Piechocki JT., Thoma K. Pharmaceutical photostability and stabilization technology. Informa Healthcare; 2007. 445 p. Available at:

16. Aman W., Thoma K. Particular features of photolabile substances in tablets. Pharmazie. 2003; 58(9): 645–650.

17. Maafi M., Maafi W. Modeling and Elucidation of the Kinetics of Multiple Consecutive Photoreactions AB4(4Φ) With Φ-order Kinetics. Application to the Photodegradation of Riboflavin. Journal of Pharmaceutical Sciences. Elsevier; 1 December 2016; 105(12): 3537–3548.

18. Maafi M., Al-Qarni MA. Φ-order spectrophotokinetic characterisation and quantification of trans-cis oxyresveratrol reactivity, photodegradation and actinometry. Spectrochimica Acta Part A: Molecular and Biomolecular Spectroscopy. Elsevier; 5 January 2018; 188: 64–71.

19. Maafi M., Maafi W. Quantitative assessment of photostability and photostabilisation of Fluvoxamine and its design for actinometry. Photochemical and Photobiological Sciences. 2015; 14(5): 982–994.

20. Maafi M., Maafi W. Quantification of Unimolecular Photoreaction Kinetics: Determination of Quantum Yields and Development of Actinometers—The

Photodegradation Case of Cardiovascular Drug Nisoldipine. International Journal of Photoenergy. 2015; 2015: 1–12.

21. Tønnesen HH. Photoreactivity of drugs. In Situ. 2008; : 102–113.

22. Yan Lee L. Study Of The Photodegradation And Photostability Of Anti-Cancer Drugs In Different Media Towards The Development Of Both New Actinometers And Liquid Formulations. 2016.

23. Nakashima H., Irie M. Synthesis of silsesquioxanes having photochromic dithienylethene pendant groups. Macromolecular Chemistry and Physics. John Wiley & Sons, Ltd; 1 April 1999; 200(4): 683–692.

24. Zepp RG. Quantum Yields for Reaction of Pollutants in Dilute Aqueous Solution. Environmental Science and Technology. 1978; 12(3): 327–329.

25. Stranius K., Börjesson K. Determining the photoisomerization quantum yield of photoswitchable molecules in solution and in the solid state. Scientific Reports. Nature Publishing Group; 2017; 7(September 2016): 1–9.

26. Stadler E., Eibel A., Fast D., Freißmuth H., Holly C., Wiech M., et al. A versatile method for the determination of photochemical quantum yields: Via online UV-Vis spectroscopy. Photochemical and Photobiological Sciences. Royal Society of Chemistry; 2018; 17(5): 660–669.

27. Ladányi V., Dvořák P., Al Anshori J., Vetráková Ľ., Wirz J., Heger D. Azobenzene photoisomerization quantum yields in methanol redetermined. Photochemical and Photobiological Sciences. 2017; 16(12): 1757–1761.

28. Sumi T., Takagi Y., Yagi A., Morimoto M., Irie M. Photoirradiation wavelength dependence of cycloreversion quantum yields of diarylethenes. Chemical Communications. The Royal Society of Chemistry; 18 March 2014; 50(30): 3928.

29. Maafi M., Brown RG. The kinetic model for AB(1φ) systems. Journal of Photochemistry and Photobiology A: Chemistry. April 2007; 187(2–3): 319–324.

30. Rodier J-M., Myers AB. cis-Stilbene Photochemistry: Solvent Dependence. Journal of the American Chemical Society. 1993; (37): 10791–10795.

31. Nassar R., Trivella A., Mokh S., Al-Iskandarani M., Budzinski H., Mazellier P. Photodegradation of sulfamethazine, sulfamethoxypiridazine, amitriptyline, and clomipramine drugs in aqueous media. Journal of Photochemistry and Photobiology A: Chemistry. Elsevier B.V.; 2017; 336: 176–182.

32. Ahmad I., Ahmed S., Anwar Z., Sheraz MA., Sikorski M. Photostability and Photostabilization of Drugs and Drug Products. International Journal of Photoenergy. Hindawi; May 2016; 2016: 1–19.

33. Mauser H (Heinz)., Gauglitz G (Günter). Photokinetics : theoretical fundamentals

and applications. Elsevier; 1998. 555 p.

34. Chen D., Ray AK. Photodegradation kinetics of 4-nitrophenol in TiO2 suspension. Water Research. 1998; 32(11): 3223–3234.

35. Nansheng D., Feng W., Luo F., Liu Z. Photodegradation of dyes in aqueous solutions containing Fe(III)-oxalato complexes. Chemosphere. 1997; 35(11): 2697–2706.

36. Torniainen K., Tammilehto S., Pharmaceutics VU-I journal of., 1996 U. The effect of pH, buffer type and drug concentration on the photodegradation of ciprofloxacin. Elsevier.

37. Xia X., Li G., Yang Z., Chen Y., Huang GH. Effects of fulvic acid concentration and origin on photodegradation of polycyclic aromatic hydrocarbons in aqueous solution: Importance of active oxygen. Environmental Pollution. Elsevier Ltd; 2009; 157(4): 1352–1359.

38. Nakashima H., Irie M. Synthesis of silsesquioxanes having photochromic diarylethene pendant groups. Macromolecular Rapid Communications. 1997; 18(8): 625–633.

39. Suzuki H. The Spatial Configurations and the Ultraviolet Absorption Spectra of the Stilbene Derivatives. Bulletin of the Chemical Society of Japan. The Chemical Society of Japan; 12 March 1952; 25(3): 145–150.

40. Kasha M. Characterization of electronic transitions in complex molecules. Discussions of the Faraday Society. The Royal Society of Chemistry; 1 January 1950; 9(0): 14.

41. Singh B., Zweig A., Gallivan JB. Wavelength-Dependent Photochemistry of 2-Aroyl-3-aryl-2H-azirines. Mechanistic Studies. Journal of the American Chemical Society. 1972; 94(4): 1199–1206.

42. Bogdanova A., Popik V V. Wavelength-dependent photochemistry of diazo Meldrum's acid and its spirocyclic isomer, diazirino Meldrum's acid: Wolff rearrangement versus isomerization. Journal of the American Chemical Society. 2003; 125(6): 1456–1457.

43. PROTTI S., Ravelli D., Photobiological MF-P&., 2019 U. Wavelength-dependence and wavelength-selectivity in photochemical reactions. pubs.rsc.org. 2019.

44. Nakamura S., Kobayashi T., Takata A., Uchida K., Asano Y., Murakami A., et al. Quantum yields and potential energy surfaces: a theoretical study. Journal of Physical Organic Chemistry. John Wiley & Sons, Ltd; 1 November 2007; 20(11): 821–829.

45. Diau EWG. A New Trans-to-Cis Photoisomerization Mechanism of Azobenzene on the S 1(n,π*) Surface. Journal of Physical Chemistry A. 2004; 108(6): 950–956.

46. Ern J., Bens AT., Martin HD., Kuldova K., Peter Trommsdorff H., Kryschi C. Ring-opening and -closure reaction dynamics of a photochromic dithienylethene derivative. Journal of Physical Chemistry A. 2002; 106(9): 1654–1660.

47. Bandara HMD., Burdette SC. Photoisomerization in different classes of azobenzene. Chemical Society Reviews. 2012; 41(5): 1809–1825.

48. Holzwarth AR., Schaffner K. WAVELENGTH DEPENDENCE OF QUANTUM YIELDS AND PRODUCT DISTRIBUTION IN THE ANAEROBIC PHOTOCHEMISTRY OF BILIRUBIN DIMETHYL ESTER. Photochemistry and Photobiology. John Wiley & Sons, Ltd (10.1111); 1 May 1981; 33(5): 635–639.

49. Görner H., Kuhn HJ. *Cis-Trans* Photoisomerization of Stilbenes and Stilbene-Like Molecules. John Wiley & Sons, Ltd; 2007. pp. 1–117.

50. Kim JE., Tauber MJ., Mathies RA. Wavelength dependent cis-trans isomerization in vision. Biochemistry. 2001; 40(46): 13774–13778.

51. Malacarne M., Protti S., Fagnoni M. A Visible-Light-Driven, Metal-free Route to Aromatic Amides via Radical Arylation of Isonitriles. Advanced Synthesis and Catalysis. 2017; 359(21): 3826–3830.

52. Fast DE., Lauer A., Menzel JP., Kelterer AM., Gescheidt G., Barner-Kowollik C. Wavelength-Dependent Photochemistry of Oxime Ester Photoinitiators. Macromolecules. 2017; 50(5): 1815–1823.

53. Marugán J., Vega B., van Grieken R., Pablos C., Martín-Sómer M. Wavelength dependence of the efficiency of photocatalytic processes for water treatment. Applied Catalysis B: Environmental. Elsevier; 2017; 221(September 2017): 258–265.

54. Kim JK., Kang DJ., Bae BS. Wavelength-dependent photosensitivity in a germanium-doped sol-gel hybrid material for direct photopatterning. Advanced Functional Materials. 2005; 15(11): 1870–1876.

55. Nunes CM., Reva I., Pinho E Melo TMVD., Fausto R. UV-laser photochemistry of isoxazole isolated in a low-temperature matrix. Journal of Organic Chemistry. 2012; 77(19): 8723–8732.

56. Hansen MJ., Velema WA., Lerch MM., Szymanski W., Feringa BL. Wavelength-selective cleavage of photoprotecting groups: Strategies and applications in dynamic systems. Chemical Society Reviews. Royal Society of Chemistry; 2015; 44(11): 3358–3377.

57. Elisei F., Mazzucato U., Görner H. trans→cis Photoisomerization of 1-styrylnaphthalene and its 4′-bromo- and 4′-chloro-derivatives. A fluorimetric and laser flash photolytic study. Journal of the Chemical Society, Faraday Transactions 1: Physical Chemistry in Condensed Phases. The Royal Society of Chemistry; 1 January 1989; 85(6): 1469.

58. Schulte-Frohlinde D., Blume H., Güsten H. PHOTOCHEMICAL cis-trans-ISOMERIZATION OF SUBSTITUTED STILBENES. The Journal of Physical Chemistry. December 1962; 66(12): 2486–2491.

59. Reviews VK-RC., 1966 undefined. Intermolecular energy transfer in photochemical reactions in solutions of organic compounds. adsabs.harvard.edu.

60. Bortolus P., Cauzzo G., Mazzucato U., Galiazzo G. The Photocyclization of Styrylpyridines to Azaphenanthrenes and their Geometrical Photoisomerization. Zeitschrift für Physikalische Chemie. De Gruyter Oldenbourg; 1 January 1969; 63(1_4): 29–38. 9

61. Bortolus P., Cauzzo G., Mazzucato U., Galiazzo G. *Cis-trans* Photoisomerization of Styrylpyridines. Zeitschrift für Physikalische Chemie. De Gruyter Oldenbourg; 1 December 1966; 51(5_6): 264–273.

62. Galiazzo G., Bortolus P., Cauzzo G., Mazzucato U. Geometrical isomerism and photochemical behaviour of α-substituted 2 and 4-styrylpyridines. Journal of Heterocyclic Chemistry. John Wiley & Sons, Ltd; 1 August 1969; 6(4): 465–473.

63. Bartocci G., Bortolus P., Mazzucato U. Excited reactivity of aza aromatics. II. Solvent protonation effects on photoisomerization and luminescence of styrylpyridines. The Journal of Physical Chemistry. March 1973; 77(5): 605–610.

64. Kaganowich M., Fischer G., Fischer E., Goedicke C., Stegemeyer H. Temperature Dependence of Photoisomerisation VIII [1] . l-Phenyl-2-(2-naphthyl)-ethylene. Zeitschrift für Physikalische Chemie. De Gruyter Oldenbourg; 1 October 1971; 76(1_2): 79–84.

65. Wolak MA., Gillespie NB., Thomas CJ., Birge RR., Lees WJ. Optical and thermal properties of photochromic fluorinated adamantylidene indolylfulgides. Journal of Photochemistry and Photobiology A: Chemistry. 2002; 147(1): 39–44.

66. Wolak MA., Thomas CJ., Gillespie NB., Birge RR., Lees WJ. Tuning the optical properties of fluorinated indolylfulgimides. Journal of Organic Chemistry. 2003; 68(2): 319–326.

67. Yokoyama Y., Takahashi K. Trifluoromethyl-substituted photochromic indolylfulgide. A remarkably durable fulgide towards photochemical and thermal treatments. Chemistry Letters. 1996. pp. 1037–1038.

68. Cordes T., Malkmus S., DiGirolamo JA., Lees WJ., Nenov A., De Vivie-Riedle R., et al. Accelerated and efficient photochemistry from higher excited electronic states in fulgide molecules. Journal of Physical Chemistry A. 2008; 112(51): 13364–13371.

69. Valentine D., Hammond GS. Mechanisms of photochemical reactions in solution. LXVII. Energy wastage in photosensitized isomerization of the stilbenes. Journal of the American Chemical Society. May 1972; 94(10): 3449–3454.

70. Saltiel J. Perdeuteriostilbene. The Role of Phantom States in the *cis-trans* Photoisomerization of Stilbenes. Journal of the American Chemical Society. February 1967; 89(4): 1036–1037.

71. SALTIEL J., CHARLTON JL. Cis–Trans Isomerization of Olefins. Organic Chemistry: A Series of Monographs. Academic Press; 1 January 1980; 42: 25–89.

72. Stegemeyer H. ON THE MECHANISM OF PHOTOCHEMICAL cis ↔ trans ISOMERIZATION. The Journal of Physical Chemistry. December 1962; 66(12): 2555–2560.

73. Bylina A., Grabowski ZR. Photo-isomerization and the triplet state of stilbene. Transactions of the Faraday Society. The Royal Society of Chemistry; 1 January 1969; 65(0): 458.

74. Lewis FD., Kalgutkar RS., Yang JS. The photochemistry of trans-ortho-, -meta-, and -para-aminostilbenes. Journal of the American Chemical Society. 1999; 121(51): 12045–12053.

75. Lewis FD., Yang JS. The excited state behavior of aminostilbenes. A new example of the meta effect. Journal of the American Chemical Society. 1997; 119(16): 3834–3835.

76. Lewis FD., Kalgutkar RS. The photochemistry of cis-ortho-, meta-, and para-aminostilbenes. Journal of Physical Chemistry A. 2001; 105(1): 285–291.

77. Lewis FD., Weigel W., Zuo X. Relaxation pathways of photoexcited diaminostilbenes. The meta-amino effect. Journal of Physical Chemistry A. 2001; 105(19): 4691–4696.

78. Lewis FD., Weigel W. Excited State Properties of Donor - Acceptor Substituted trans -Stilbenes : The meta -Amino Effect. 2000; : 8146–8153.

79. Lewis FD., Crompton EM. Hydroxystilbene isomer-specific photoisomerization versus proton transfer. Journal of the American Chemical Society. 2003; 125(14): 4044–4045.

80. Crompton EM., Lewis FD. Positional effects of the hydroxy subtituent on the photochemical and photophysical behavior of 3- and 4-hydroxystilbene. Photochemical and Photobiological Sciences. 2004; 3(7): 660–668. A

81. Roberts JC., Pincock JA. Photophysical Properties and Photoadditions of Alcohols. 2006; (V): 2453–2465.

82. Otolski CJ., Mohan Raj A., Sharma G., Prabhakar R., Ramamurthy V., Elles CG. Ultrafast trans → cis Photoisomerization Dynamics of Alkyl-Substituted Stilbenes in a Supramolecular Capsule [research-article]. Journal of Physical Chemistry A. American Chemical Society; 2019; 123(24): 5061–5071.

83. Murohoshi T., Kaneda K., Ikegami M., Arai T. Photoisomerization and isomer-specific addition of water in hydroxystilbenes. Photochemical and Photobiological Sciences. 2003; 2(12): 1247–1249.

Chapter 6

Mathematical simulations of AB (1Φ) and AB (2Φ) systems driven by polychromatic light

6.1. Introduction

There have been no models, to date, that describe the photodegradation kinetics of drugs under polychromatic irradiation. The photodegradation tests carried out thus far have been modelled using classical thermal kinetics (i.e., zero-, first- and second-order reactions) [2–9]. This clearly represents a gap in the knowledge in the field of photostability [10–15]. Recently, a specific Φ-order representation of the photoreaction behaviour of the specific case of monochromatic light irradiation has been described [10].

This chapter considers the design of new kinetic strategies ($\Phi-$ and η-kinetics) for the photodegradation AB $(1\Phi)_{\varepsilon_{B=0}}$, AB $(1\Phi)_{\varepsilon_{B\neq 0}}$ and photoreversible, AB (2Φ) systems that occur under irradiation by polychromatic light. There properties and features will be determined from a closed-form integration, a numerical integration calculation, and from experiment.

In this chapter, we have rationalized the drugs' photoreaction behaviours by introducing the concept of '$\Phi-$ and η-kinetics', which represent new kinetic orders by which to describe photoreactions (and which are fundamentally different from the known classical reaction orders). The $\Phi-$ and η-kinetics are applicable specifically to photodegradation AB $(1\Phi)_{\varepsilon_{B=0}}$, AB $(1\Phi)_{\varepsilon_{B\neq 0}}$ and photoreversible, AB (2Φ) processes, respectively.

In this study, we designated the photokinetic order under polychromatic light. This mathematical model will describe the time dependency of the reaction.

6.2. Numerical integration methods (NIMs)

Due to the difficulties associated with integrating the rate law differential equation for the photochemical reaction under polychromatic light irradiation, we developed a new methodology to create and validate new order kinetics as Φ-order kinetic to photokinetic study under monochromatic irradiation [10]. In order to solve the difficulty of integrate the rate law, the new order kinetic model for the various systems of the photochemical reaction were first proposed; however, whilst this allowed us to obtain certain models, one cannot simply conclude that such models are correct. Rather, each model needs to be tested using the generated or simulated data. To generate this data, one needs to approximate the values of the integrals of the complex equation through some appropriate tool, which in this instance is NIMs. NIMs is an independent mathematical method used to evaluate the value of an integral when a mathematical solution to the above problem has been found. This is a sensible way to test the validity of the proposal model because the model should be represent or give the same result for the independent mathematical method and the NIMs [16].

The NIMs consist of different methods to find approximate values for such integrals (the function of these values is produced as a table of values). In this study, MathCad was used, which uses NIMs based on the fifth Runge-Kutta. This software makes it easy to generate data over the integral time according to the input values. The values input into the software are related to the photoreaction parameters. These data are created one concentration at a time, and the generated data will show the change in the concentrations over time. From this, the output values illustrate the photochemical

reaction behaviour. Furthermore, the NIMs can generate a large number of photochemical reaction cases as proceed under different conditions. This will cover the more likely possibilities for the photochemical reaction, and can be used it to test the proposed model under different experimental conditions. Once the results of the test model with NIMs data are positive, that meaning the model is applicable to this stage.

The advantages of this tool are that it generates accurate and precise photokinetic traces related to the input values, and identifies or detects any problems with the proposal model because the Runge-Kutta method is extremely precise, as confirmed by Maafi group when they developed the Φ-order kinetics [10,12,16,17].

6.3. Data simulation using MathCad

In order to generate data, different cases that proceed under different experimental conditions need to be proposed. These cases contain photochemical reaction parameters such as C_A , $\sum \varepsilon_A$, $\sum \varepsilon_B$, $\sum \Phi_{AB}$, $\sum \Phi_{BA}$, $l_{\lambda_{irr}}$ and $\sum P$. The process by which data is generated is described in Scheme 6-1.

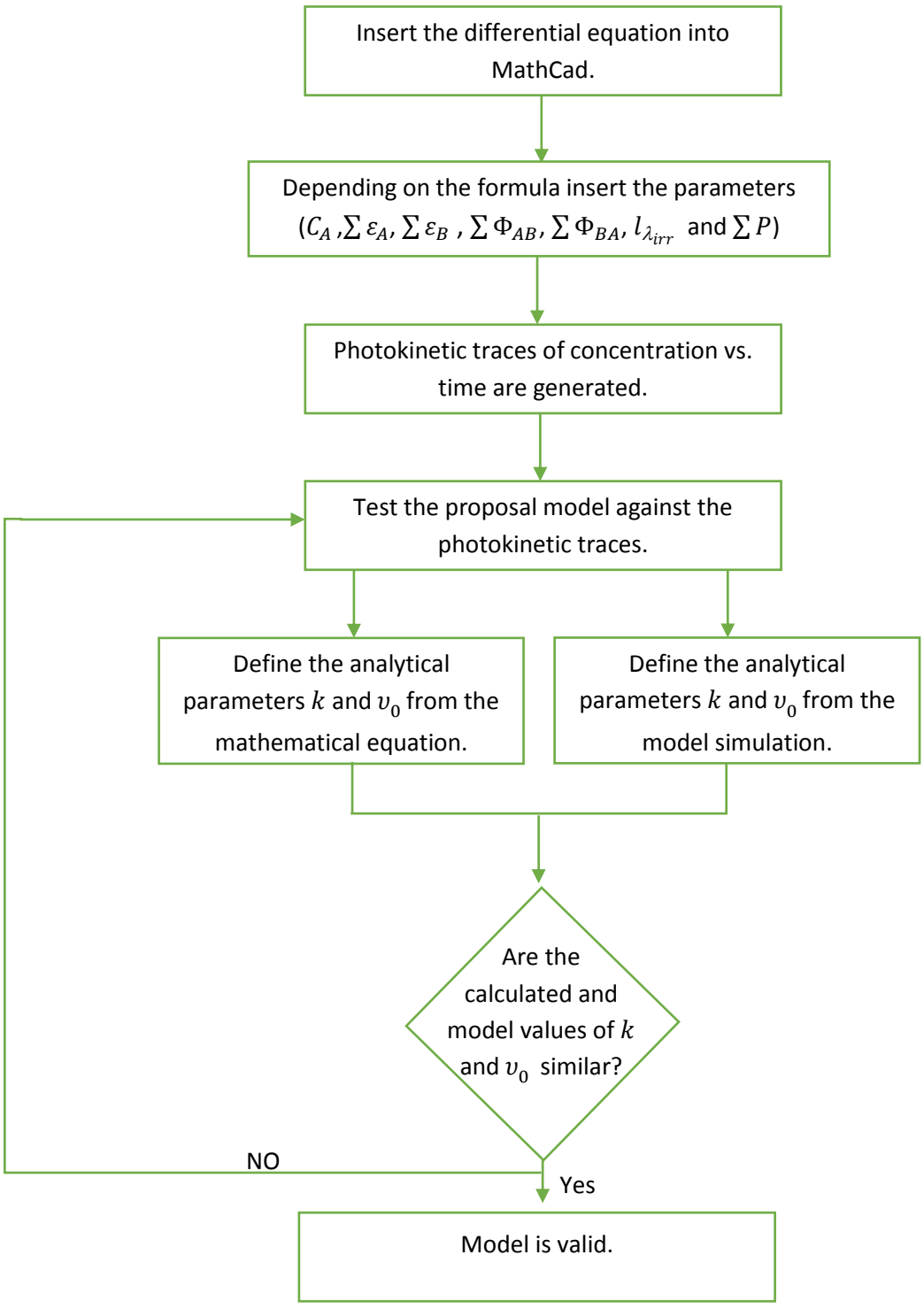

Scheme 6- 1: *Flow chart showing how the data for the new order model under polychromatic light can be generated using MathCad.*

The data generated by MathCad is shown in figure (6-1), which describes the behaviour of three types of photochemical reaction systems. AB $(1\Phi)_{\varepsilon_{B=0}}$ and AB $(1\Phi)_{\varepsilon_{B\neq 0}}$ systems show that the concentration changes with time reach zero. However, AB (2Φ) system, the change in concentration will not entirely (i.e., an equilibrium state will instead be reached).

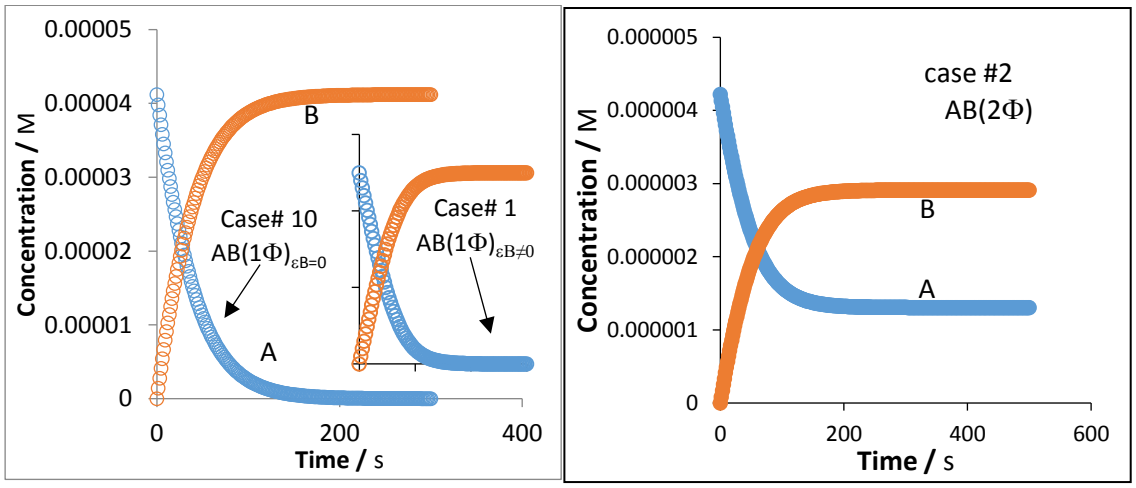

Figure 6- 1: Photokinetic traces generated using MathCad for the three systems, which is related to the cases presented in table 6-1 and 6-3.

6.4. Φ-order kinetic model for AB $(1\Phi)_{\varepsilon_{B=0}}$

The differential equation for AB $(1\Phi)_{\varepsilon_{B=0}}$ was solved using closed-form integration. The photokinetic model for this type of reaction under polychromatic irradiation was found to follow Φ-order kinetics (log-exp kinetics). This kinetic model required only the concentration $(C_A\,(t))$, sum of the absorption coefficients $(\sum\,\varepsilon_A)$ and the sum of the absorbances $(\sum A_0)$ of the species A $(\sum A_0 = C_A\,(0) \times l_{\lambda_{obs}} \times \sum\,\varepsilon_A)$, as given in Eq.6-1 (See appendix II. 1):

$$C_A(t) = \frac{1}{\left(\frac{l_{\lambda_{irr}}}{l_{\lambda_{obs}}} \times \sum \varepsilon_A\right)} \times \log\left(1 + \left(-1 + 10^{\left(\frac{l_{\lambda_{irr}}}{l_{\lambda_{obs}}} \times (C_A(0) \times l_{\lambda_{obs}} \times \sum \varepsilon_A)\right)}\right) \times e^{(-k_{AB}t)}\right) \quad \text{Eq.6-1}$$

The sum of the absorption coefficients and the absorbances were proposed for use in the model, because the reaction proceeded under irradiation by multiple wavelengths, where each wavelength had a different light intensity to the others. The overall rate constant (k_{AB}) represents in equation 6-2 is dependent on the photochemical reaction parameters Φ_{AB}, ε_A, $P_{\lambda_{irr}}$, $l_{\lambda_{irr}}$ and $\ln 10$, but is independent of the initial concentration, as:

$$k_{AB,cld} = \ln 10 \times l_{\lambda_{irr}} \times \sum(\Phi_{AB} \times \varepsilon_A \times P) \quad \text{Eq.6-2}$$

The variation in light intensity was indicated by the overall rate constant, and is proportional to the change in the overall rate constant once the all the experimental conditions are the same.

The initial velocity can be determined experimentally from the graph of the kinetic traces (the early points of the kinetic traces) and is theoretically given as:

$$^1\upsilon_0\, cld. = \frac{k_{AB}}{\sum \varepsilon_A \times l_{\lambda_{irr}} \times \ln 10} \quad \text{Eq.6-3}$$

Where the initial velocity is dependent on the reaction considered but independent of concentration.

6.4.1. Testing the model with generated data

The applicability of the Φ-order kinetics developed under polychromatic light was achieved using independent theoretical simulated data, which was generated using a

fifth-order Runge-Kutta integration (RK) based on AB $(1\Phi)_{\varepsilon_{B=0}}$. More than 100 different synthetic kinetic traces were generated, with each system different to the others. This number of cases are used to check the probability of change in the parameters on the model and cover all possible of the reactions (Table 6-1).

The fitting of the synthetic photokinetic traces was not sufficient to conclude that a model is suitable and applicable to this kind of photoreaction. However, there are two further parameters that can be used to validate the applicability of the model. These parameters are the overall rate constant and initial velocity, because these depend on photochemical reaction parameters such as Φ_{AB}, ε_A, $P_{\lambda_{irr}}$, $l_{\lambda_{irr}}$, and these parameters will indicate any change in the reaction due to the variation in $P_{\lambda_{irr}}$ in the course of the reaction.

In this study, all the synthetic photokinetic traces showed good fits to model Eq.6-1, which is the first stage in determining the applicability of the model. In this regard, the model demonstrates a good fit in all cases in table 1. These fitting and mathematical models illustrate that Φ-order kinetics are useful in terms of describing photoreaction AB $(1\Phi)_{\varepsilon_{B=0}}$ system. The fitting of the synthetics photokinetic traces with the model are described in the figure (6-2).

Table 6- 1: *Example sets of data used to generate unimolecular photokinetic traces using the Φ-order method and to calculate k_{AB} using equation 1.*

Case	$C_A(0)$ **x 10^6** /M	$\sum \varepsilon_A$ / $M^{-1}cm^{-1}$	ℓ_{irr} / cm	$\sum \Phi_{AB}$	$\sum P$ x10^8 /einstein s^{-1} dm^{-3}	$k_{AB,mod}$ / s^{-1}	$k_{AB,cld}$ / s^{-1}
1	2.50	225980	2	0.31	2.50	0.0081	0.0081
2	0.851	601543	2	0.23	1.5	0.0096	0.0096
3	4.32	118970	2	0.78	2.00	0.0085	0.0085
4	9.14	65650	2	0.48	5.5	0.0079	0.0079

Case	$C_A(0)$ x 10^6 /M	$\sum \varepsilon_A$ / $M^{-1}cm^{-1}$	ℓ_{irr} / cm	$\sum \Phi_{AB}$	$\sum P$ x10^8 /einstein s^{-1} dm^{-3}	$k_{AB,mod}$ / s^{-1}	$k_{AB,cld}$ / s^{-1}
5	3.65	151230	2	0.15	7	0.0073	0.0073
6	24.0	24560	2	0.062	150	0.011	0.011
7	3.25	180100	0.5	0.041	80	0.0068	0.0068
8	0.851	601543	2	0.23	3.5	0.0223	0.0223
9	18.9	31520	3	0.023	200	0.01	0.01
10	4.15	136504	3	0.072	25	0.0169	0.0169

* ℓ_{obs} is 1 cm

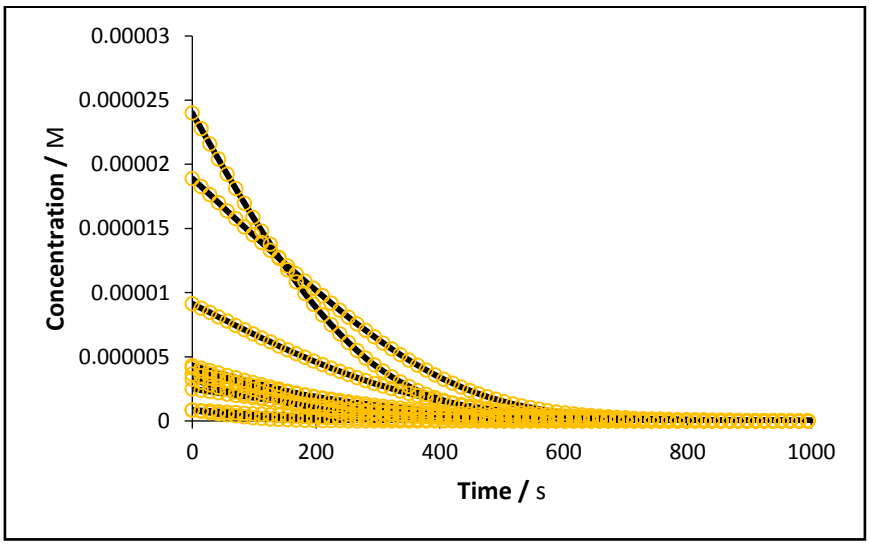

Figure 6-2 Samples of simulated traces (circle) and the corresponding model (Eq.1) traces (line).

A certain similarity in the results was found between the overall rate constant ($k_{AB,mod}$) obtained from the fitting and the theoretical ($k_{AB,cld}$) achieved from equation 6-2 for all different cases, and with same cases but with different light intensity (Fig.6-3).

In addition, a quantitative comparison between the initial velocities $v_{0,mod.}$ and $v_{0,cld.}$ for the photoreactions was made. The initial velocity was quantified theoretically using Eq.6-3, while $v_{0,mod.}$ (model fitting) was obtained graphically from the photokinetic traces as the gradient of the straight line of concentration against time (Fig.6-3).

The percentage errors between the model fitting and theoretical values for both parameters (k_{AB} and v_0) were less than 10% for each (as shown in Fig.6-3b as one example of one case).

The model shows a good correlation between $k_{AB,cld}$ and $v_{0,cld.}$ with $k_{AB,exp}$ and $v_{0,exp.}$, respectively, for all photokinetic cases (Fig.6-3a).

Moreover, the solution concentration effect was used to validate the model. The simulation suggested that k_{AB} and v_0 were independent of concentration, as predicated from Eqs. 6-2 and 6-3. These results confirm the reliability and suitability of the model to describe the photoreaction AB (1Φ) (Fig.6-3b).

The finding results from this simulation indicate the validity and accuracy of the model in terms of describing photochemical reaction AB $(1\Phi)_{\varepsilon_{B=0}}$ under polychromatic light irradiation.

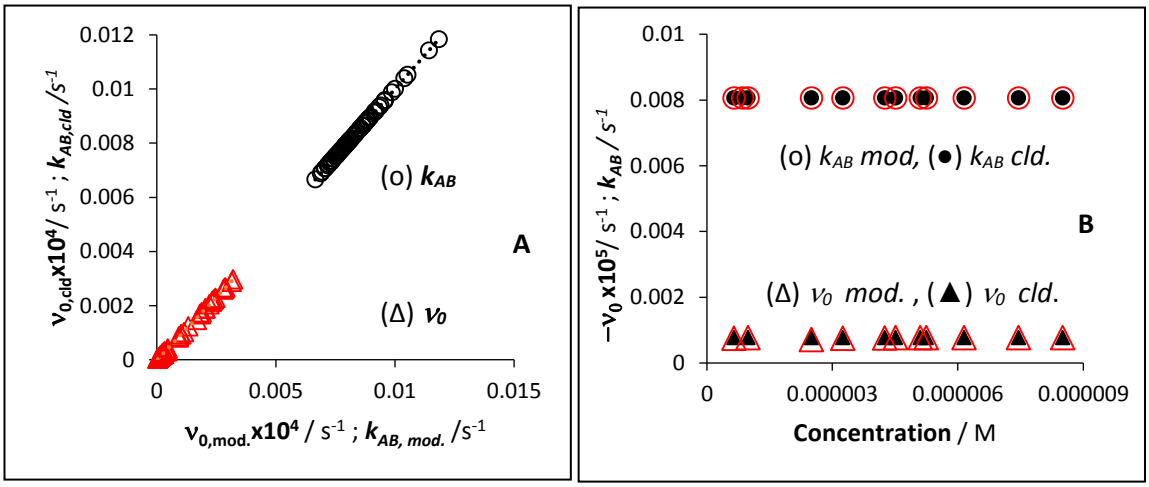

Figure 6-3 ***(a)*** *Good correlation between model and theoretical values for k_{AB} and $^1v_0$. all cases.* ***(b)*** *Constant $k_{AB.mod}$ and $^1v_{0,mod.}$ with different initial concentrations* $\boldsymbol{C_0}$ *for case 1. The open and solid symbols represent the model and calculated values of $k_{\eta,cld}$ and $v_{0,cld.}$, respectively.*

6.5. η-order kinetic model for AB $(\mathbf{1\Phi})_{\varepsilon_{B\neq 0}}$ and AB (2Φ)

The differential equations for photoreaction AB $(1\Phi)_{\varepsilon_{B\neq 0}}$ and AB (2Φ) express the difference in the concentrations of the mother compound (A) and the photoproduct (B) ($C_A(t)$ and $C_B(t)$, respectively); this takes into account the fact that the reaction mix is homogenised and stirred continuously and subject to polychromatic and steady-state irradiation, and is maintained at a constant temperature throughout.

$$\boldsymbol{A \xrightarrow{\Phi_{AB}} B} \qquad , \qquad \boldsymbol{A \underset{\Phi_{BA}}{\overset{\Phi_{AB}}{\rightleftharpoons}} B}$$

Scheme 6- 2: *AB* $(1\Phi)_{\varepsilon_{B\neq 0}}$ *and AB (2Φ) photoreaction*

A closed-form integration of the differential equation for the two photochemical reaction systems given in scheme 6.1 leads to the following integrated rate law (Eq.6-4), where both A and B absorb the polychromatic light (See appendix II. 2).

$$\boldsymbol{\eta(t) = -k_\eta t} \qquad \text{Eq.6-4}$$

η appears to be similar to a zero-order photoreaction linear line, but is actually quite different. η is a function involving both initial and time-based (t) concentrations of the reactant A (C_{A_0},C_{A_t}), the absorption coefficients (ε_A, ε_B), Φ_{AB}, Φ_{BA}, $l_{\lambda_{irr}}$ and P . One of the components of the η function is a logarithm.

$$\boldsymbol{\eta(t) = \left(C_{A_t} - C_{A_0}\right) \times \alpha + \gamma \times Ln\, \frac{C_{A_t}+\delta}{C_{A_0}+\delta}} \qquad \text{Eq.6-5}$$

where $\boldsymbol{\alpha}$, $\boldsymbol{\gamma}$ and $\boldsymbol{\delta}$ are factors that depend on the type of reaction, as seen in table (6-2).

Table 6- 2: *α, γ and δ Factors.*

Photochemical reaction type	α	γ	δ
AB $(\mathbf{1\Phi})_{\varepsilon_{B\neq 0}}$	$\left(\sum_{\lambda_i}^{\lambda_f} \varepsilon_A - \sum_{\lambda_i}^{\lambda_f} \varepsilon_B\right)$	$\left(C_{A_0} \times \sum_{\lambda_i}^{\lambda_f} \varepsilon_B\right)$	0
AB (2Φ)	1	ρ_3	ρ_1

Where ρ_1 and ρ_3 are given by:

$$\rho_1 = \frac{1}{\rho_2} \times \sum_{\lambda_i}^{\lambda_f}\left[\left(\Phi_{BA}(\lambda_i) \times \varepsilon_B(\lambda_i) \times C_{A_0}\right) \times P\ (\lambda_i)\right] \times l_{\lambda_{irr}} \quad \text{Eq.6-6}$$

$$\rho_2 = -\sum_{\lambda_i}^{\lambda_f}\left[\left(\Phi_{BA}(\lambda_i) \times \varepsilon_B(\lambda_i) + \Phi_{AB}(\lambda_i) \times \varepsilon_A(\lambda_i)\right) \times P\ (\lambda_i)\right] \times l_{\lambda_{irr}} \quad \text{Eq.6-7}$$

$$\rho_3 = \theta_{AB} - \rho_1 \quad \text{Eq.6-8}$$

$$\theta_{AB} = C_{A_0} \times \frac{\sum_{\lambda_i}^{\lambda_f} \varepsilon_B(\lambda_i)}{\sum_{\lambda_i}^{\lambda_f}\left(\varepsilon_A(\lambda_i) - \varepsilon_B(\lambda_i)\right)} \quad \text{Eq.6-9}$$

The η-order integrated rate law (Eq.6-4) does not correspond to any of the known kinetic orders (concentration plus logarithm). The analytical parameter k_η (Eq.6-10,6-11) represents the overall rate constant and is dependent on the various photochemical reaction parameters, and is proportional to the photoreaction quantum yields ($\Phi_{A\to B}^{\lambda_{irr}}$, $\Phi_{B\to A}^{\lambda_{irr}}$), ε_A, ε_B and $P_{\lambda_{irr}}$, but it is C_{A_0}- and $l_{\lambda_{irr}}$-independent.

The overall rate constant for AB $(1\Phi)_{\varepsilon_{B\neq 0}}$ $({}^2k_\eta)$ is given as:

$${}^2k_\eta = \sum_{\lambda_i}^{\lambda_f}\left[\left(\Phi_{AB}(\lambda_i) \times \varepsilon_A(\lambda_i)\right) \times P(\lambda_i)\right] \quad \text{Eq.6-10}$$

While the overall rate constant for AB (2Φ) (${}^3k_\eta$) is given as:

$${}^3k_\eta = \frac{\sum_{\lambda_i}^{\lambda_f}\left[\left(\Phi_{BA}(\lambda_i) \times \varepsilon_B(\lambda_i) + \Phi_{AB}(\lambda_i) \times \varepsilon_A(\lambda_i)\right) \times P\ (\lambda_i)\right]}{\sum_{\lambda_i}^{\lambda_f}\left(\varepsilon_A(\lambda_i) - \varepsilon_B(\lambda_i)\right)} \quad \text{Eq.6-11}$$

According to equations 6-10 and 6-11, the rate constant is theoretically constant over the concentrations given. This is one of the model validations used when comparing between the model fitting and theoretical values, and should not differ by more than 10%.

Also, the initial velocity, υ_0, is used to validate the model. The validation comes from the extent of the similarity between the theoretical and the model linear line values. The model initial velocity ($\upsilon_{0,mod.}$) is obtained graphically from the gradient of the concentration against time (using the few of the initial points of the reaction). The theoretical initial velocity ($\upsilon_{0,cld.}$) is derived from equation (6-12) for AB $(1\Phi)_{\varepsilon_{B\neq 0}}$, and from equation (6-13) for AB (2Φ).

$$^{2}\upsilon_{0\,,cld} = -\frac{\left(\sum_{\lambda_i}^{\lambda_f}[(\Phi_{AB}(\lambda_i)\times\varepsilon_A(\lambda_i))\times P(\lambda_i]\right)\times C_{A_0}}{\sum_{\lambda_i}^{\lambda_f}\varepsilon_B(\lambda_i)\times C_{A_0}+\left(\sum_{\lambda_i}^{\lambda_f}(\varepsilon_A(\lambda_i)-\varepsilon_B(\lambda_i))\right)\times C_{A_0}} = -\frac{^{2}k_\eta}{\sum_{\lambda_i}^{\lambda_f}\varepsilon_A(\lambda_i)} \qquad \text{Eq.6-12}$$

$$^{3}\upsilon_{0\,,cld} = -^{3}k_\eta \times \frac{C_{A_0}+\rho_1}{C_{A_0}+\theta_{AB}} \qquad \text{Eq.6-13}$$

The initial velocities of each of the systems ($^{2}\upsilon_{0\,,cld}$ and $^{3}\upsilon_{0\,,cld}$) were independent of the concentration and path length, but still depend on the other photochemical reaction parameters.

6.5.1. Testing of η-order kinetics model

In order to test the η-order kinetics model, the kinetic traces were obtained from a fifth-order Runge-Kutta integration (RK) and were subsequently tested using Eq. 6-4 (Fig. 6-4). More than 250 (involving different ε_A, ε_B, Φ_{AB}, Φ_{BA}, $l_{\lambda_{irr}}$and $P_{\lambda_{irr}}$) synthetic kinetic traces were generated and tested for AB $(1\Phi)_{\varepsilon_{B\neq 0}}$and AB (2Φ) (see Table 6-3).

Excellent agreement was obtained between the 250 synthetic kinetic profiles and model Eq. 6-4 for each system (Fig.6-4). The fitting of the independent mathematical data was taken as a first indication of the validation of the model. This method of validation is

mandatory in terms of evaluating the proposed model against a large amount of generated data. The findings demonstrate that η-order kinetics can be used and is applicable to model a large number of AB $(1\Phi)_{\varepsilon_{B\neq 0}}$ and AB (2Φ) photochemical reactions under polychromatic light.

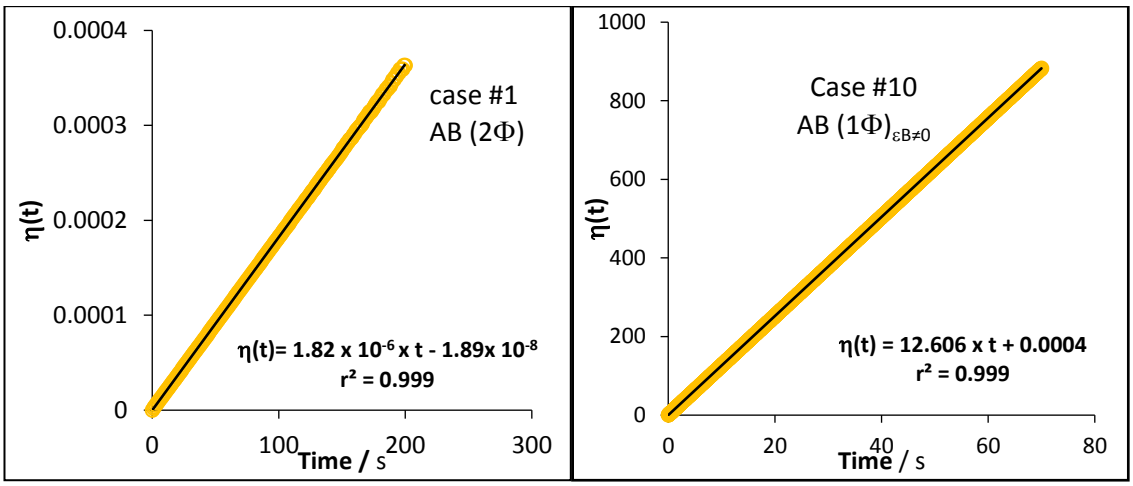

Figure 6-4: Samples of simulated traces after applying the model (Eq.6-4) and the model fitting is given linear line.

The validity of the model was evaluated by comparing the similarity between the model and theoretical values found for the overall rate constant for each of the systems ($^2k_\eta$ and $^3k_\eta$). The photokinetic traces that represent the photochemical reaction were generated as based on the fifth RK with high precision [10]. The calculated values were obtained from Eqs.6- 10 and 6- 11, and it will be depending on the ε_A, ε_B, Φ_{AB}, $\Phi_{\mathrm{BA}}$and $P_{\lambda_{irr}}$, and it independent on the concentration and $l_{\lambda_{irr}}$; the model values were calculated by fitting the model (Eq.6-4) to the synthetic data. The similarity between the results for the theoretical and model values of k_η for AB $(1\Phi)_{\varepsilon_{B\neq 0}}$ and AB (2Φ) is illustrated in (Fig. 6-5a).

Table 6- 3: *Example sets of data used to generate some of AB* $(1\Phi)_{\varepsilon_{B\neq0}}$ *and AB (2Φ) traces using η-order method and to calculate k using equations 6-4.*

Case	$\sum \boldsymbol{\varepsilon_A}$ / $M^{-1}cm^{-1}$	$\sum \boldsymbol{\varepsilon_B}$ / $M^{-1}cm^{-1}$	$\frac{\sum \boldsymbol{\varepsilon_A}}{\sum \boldsymbol{\varepsilon_B}}$	ℓ_{obs} / cm	ℓ_{irr} / cm	$\sum \boldsymbol{P}$ /einstein s^{-1} dm^{-3}	$\sum(\boldsymbol{\Phi_{AB}} \times \boldsymbol{\varepsilon_A} \times \boldsymbol{P})$	$\sum(\boldsymbol{\Phi_{BA}} \times \boldsymbol{\varepsilon_B} \times \boldsymbol{P})$	$\left(\sum \boldsymbol{\varepsilon_A} - \sum \boldsymbol{\varepsilon_B}\right)$ / $M^{-1}cm^{-1}$	Average k_{AB}mod. / s^{-1}	Average ν_0 mod. x10^6 / s^{-1}
$(\mathbf{1\Phi})_{\boldsymbol{\varepsilon_{B\neq0}}}$											
1	1012855.5	743938.3	1.36	1	2	0.0005	0.96	0	268917.1	0.96	-0.94
2	1692277.5	2290528.	0.74	1	2	0.0005	2.21	0	-598251.13	2.21	-1.30
3	1329572.2	1434053.	0.93	1	2	0.00196	4.89	0	-104481.59	4.89	-3.67
4	880339.54	798558.5	1.10	1	2	0.0161	3.63	0	81780.97	3.63	-4.00
5	1578375.5	1141445.	1.38	1	2	0.0083	7.96	0	436930.02	7.96	-5.03
6	1409815.7	1013813.	1.39	1	2	0.0083	6.49	0	396002.76	6.49	-4.61
7	673050.02	727065.4	0.93	1	2	0.0162	4.94	0	-54015.47	4.94	-7.10
8	740465.81	467124.6	1.56	1	2	0.008	1.54	0	273341.21	1.54	-2.08
9	998674.77	940878.8	1.06	1	2	0.047	12.61	0	57795.94	12.61	-12.50
10	705182.11	809532.5	0.87	1	2	0.0005	0.58	0	-104350.46	0.58	-0.82
AB (2Φ)										k_{AB} x10^5	
1	1684678.9	758105.5	2.22	1	2	0.0019	1.04	0.65	926573.44	0.18	-0.61
2	1343694.3	417261.6	3.22	1	2	0.0162	11.04	1.81	926432.69	1.39	-8.20
3	932108.35	335035.4	2.78	1	2	0.0167	2.22	14.69	597072.89	2.83	-2.30
4	795819.61	798558.5	0.99	1	2	0.0090	8.65	11.86	-2738.96	-748.0	-16.0
5	1070863.3	930534.2	1.15	1	2	0.0079	9.45	3.43	140329.08	9.17	-8.72
6	1241520.3	571941.8	2.17	1	2	0.0084	5.91	10.05	669578.48	2.38	-4.64
7	827826.45	372521.9	2.22	1	2	0.00012	0.04	0.02	455304.55	0.13	-0.052
8	658414.37	727065.4	0.91	1	2	0.392	4.16	94.71	-68651.12	-144.0	-6.00
9	1079447.2	1509972.	0.715	1	2	0.0078	10.25	3.21	-430525.37	-3.13	-9.32
10	868338.64	258743.1	3.36	1	2.7	0.0002	0.19	0.03	609595.54	0.036	-0.22

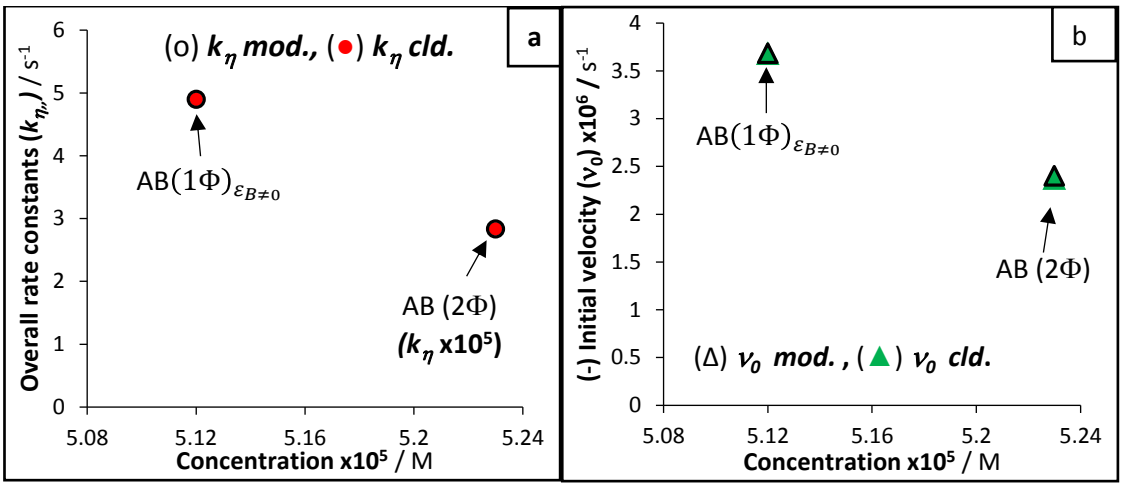

Figure 6-5: (a) The good agreement between $k_{\eta,mod.}$ and $k_{\eta,cld.}$, where open and solid symbols represent $k_{\eta,mod.}$ and $k_{\eta,cld.}$, respectively, for case 3. (b) Good agreement between $v_{0,mod.}$ and $v_{0,cld.}$, where open and solid symbols represent $v_{0,mod.}$ and $v_{0,cld.}$, respectively, for case 3.

The numerical values (υ_0) were obtained graphically from the gradient of the initial stage of the graph of concentration against time, and is compared with the theoretical values given by Eqs. 6-12 and 6-13, and it will be depending on the ε_A, ε_B, Φ_{AB}, $\Phi_{BA}$and $P_{\lambda_{irr}}$, and it is concentration and $l_{\lambda_{irr}}$ independent. So, υ_0 will be constant in each case. Excellent agreement was found between the model and theoretical values of the initial velocities (υ_0) (Fig. 6-5b).

There was good correlation between the model and theoretical values for the parameters k_η and υ_0 for both systems AB$(1\Phi)_{\varepsilon_{B\neq0}}$ and AB (2Φ), with less than 5% error for each of these systems. These findings confirm that the model works.

In order to test further the model, the concentration effect was studied. According to the model, k_η and υ_0 were constant with concentration due to their concentration-independence as expressed in equation (6-10) to (6-13). The two parameters (k_η and

υ_0) were used to detect the change in the photoreaction, once if set same condition of the photoreaction expect one parameter. As expected from the equations for k_η and υ_0 , these parameters were predicted to remain constant with concentration (Fig.6-6). In addition, the theoretical and model values for parameters k_η and υ_0 were very similar to each other less than 5%.

This study is important in terms of evaluating the effect of concentration on the photochemical reaction because concentration can be considered an effective means of classifying the type of kinetic order. For example, we can be explained the change in the photochemical reaction order for studied compounds or drugs, as nisoldpined [18], which the kinetic order was attributed to the initial concentrations of these compounds. So, the first order was apparent with lower initial concentration, in contrast the zero-order kinetic was with higher initial concentration, photoreaction responses may be viewed as slowing down as the initial concentration increases [18]. This would mean that the kinetic traces of the compounds show that the lower initial concentration have been steeper than higher ones, which the former (lower) was fitting with first order (exponential model), while the latter with zero order (linear) [18].

This indicates the need for an appropriate kinetical approach for photodegradation reaction as it is clearly not adequately descriptive to make reasonable conclusions about the relative photochemical reaction to ensure a good fitting with classical method.

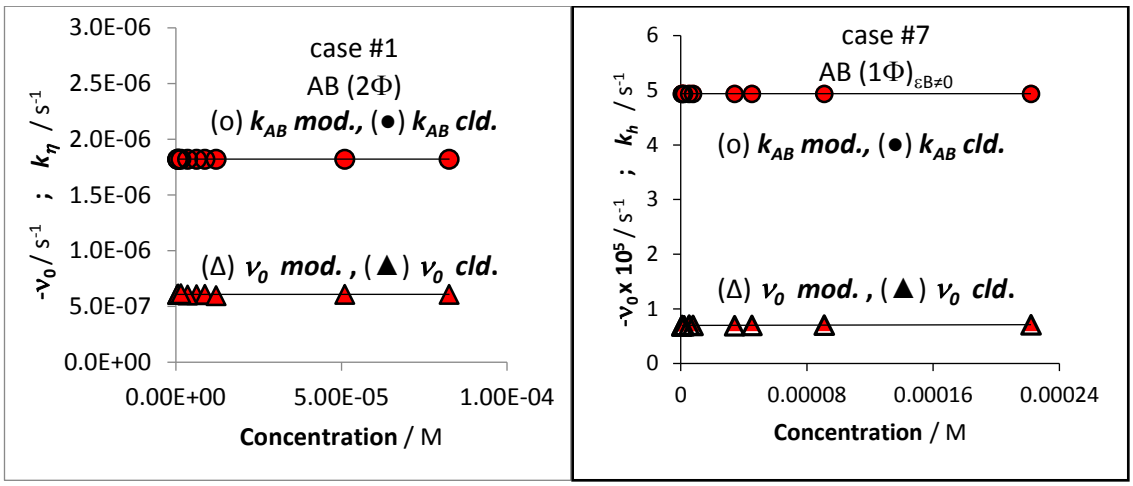

Figure 6-6: Constant $k_{\eta,\,mod.}$ and $\upsilon_{0,mod.}$ of the simulated data of the two photochemical reaction systems with different initial concentrations ($\boldsymbol{C}_A(0)$). The open and solid symbols represent the experimental and calculated values of $k_{\eta,cld}$ and $\upsilon_{0,cld.}$, respectively.

6.6. Actinometry

In both the models presented here, a linear relationship between the overall rate constant and the sum of the light intensity ($\sum P$) can be expected, as predicated by Eq.6-14. This means that the models were offering to indicate the change in the overall rate constant (k) with $\sum P$. The linear relationship for studied molecules can be used to develop an actinometric method for the molecules studied under polychromatic light. The actinometric method allows the total light intensity of the unknown light source to be quantified [11-12,14-15].

$$k = \sum \beta_{AB} \times \sum P(\lambda_i) \qquad \text{Eq.6-14}$$

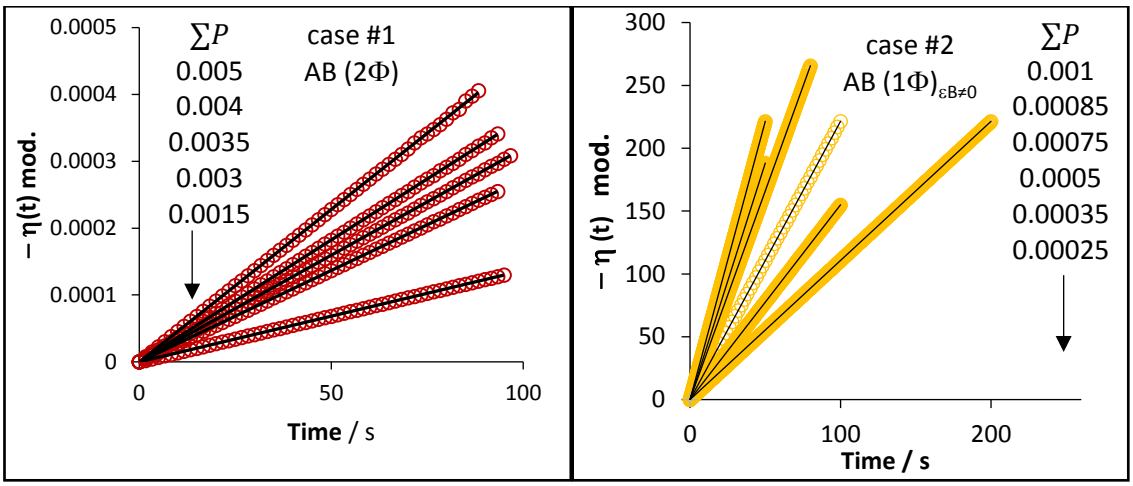

Figure 6-7: Effect of increasing the radiant power of the polychromatic irradiation beam on the photokinetic traces of simulated date at range 200-400nm. The experimental data (circles) were fitted by Eq. 6-4.

In order to test the applicability of the model to developed an actinometric method, by using same set of the cases in table 1 and 2 with change the sum of the light intensity to assume to subject the same solution or case to irradiation using beams of different radiant powers. Then, for each case, simulated kinetic traces for the series radiant power values were obtained and fitted with the proposal model for each system. The effect of the light intensity was evaluated by the overall rate constant (Fig.6-7), which increases with increasing $\sum P$ (Eq. 6-14).

More importantly, a good linear relationship between the $k_{mod.}$ for both models and $\sum P$ (Fig.6-9) with intercepts close to zero unit and the gradient of the equation can be expressed as a factor β_{AB}. The value of the factor β_{AB} will contribute to quantifying the light intensity for any polychromatic light source. Fig. (6-8) shows the excellent agreement between the theoretical values with measurable (model) values of light intensity.

The fact of the actinometric method developed here is easy to apply without any information about the photochemical reaction ($\Phi_{A\to B}^{\lambda_{irr}}$, $\Phi_{B\to A}^{\lambda_{irr}}$, ε_A *and* ε_B) expect the type of the mechanism of the photochemical reaction.

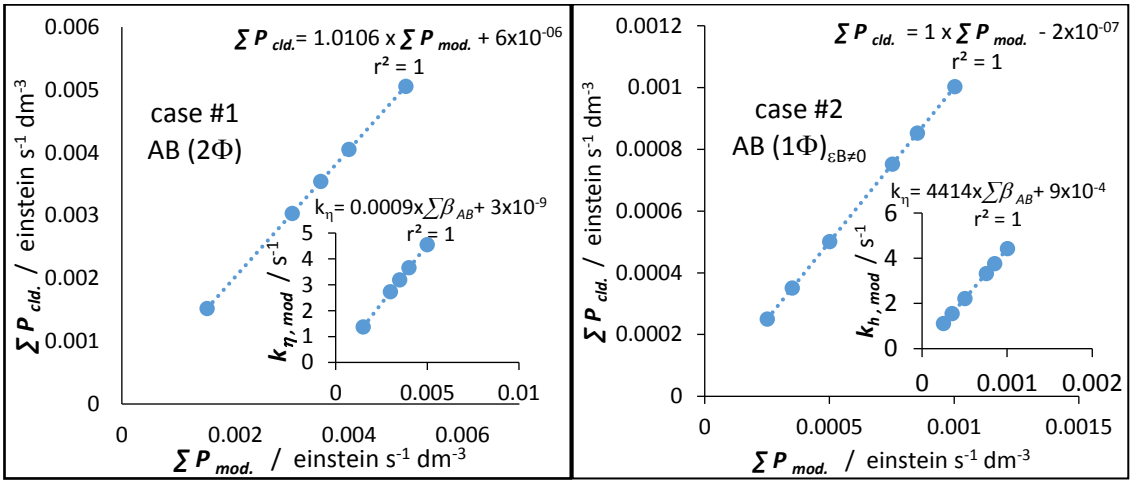

Figure 6-8: Linear correlation of experimental (∑P) and calculated (∑P) values of the radiant power showing simulation cases. Inset: the linear relationship between the $k_{\eta,\,mod.}$ *and* ∑P.

6.7. Simulation of the trace same poly data to mono by using same the poly data for both systems.

In order to compare between rate of reaction for the polychromatic and monochromatic in both AB (1Φ) and AB (2Φ), by using the same simulation conditions of polychromatic study and take the monochromatic data from that data. After that, the Mathcad was used to generate the photokinetic traces of the monochromatic and polychromatic. In addition, the study was used the same case but change the light profile. It was used different lamp profiles with different and similar intensities between each other. In all studies with different and same light intensities (Fig. 6-9), the rate of the reaction in polychromatic was faster than monochromatic at different wavelengths. However, it was found slower than monochromatic at 340 nm, it might be the place of the

wavelength in the UV spectra was contributed to this effect, while which is in the last of the UV spectra with high quantum yield as well.

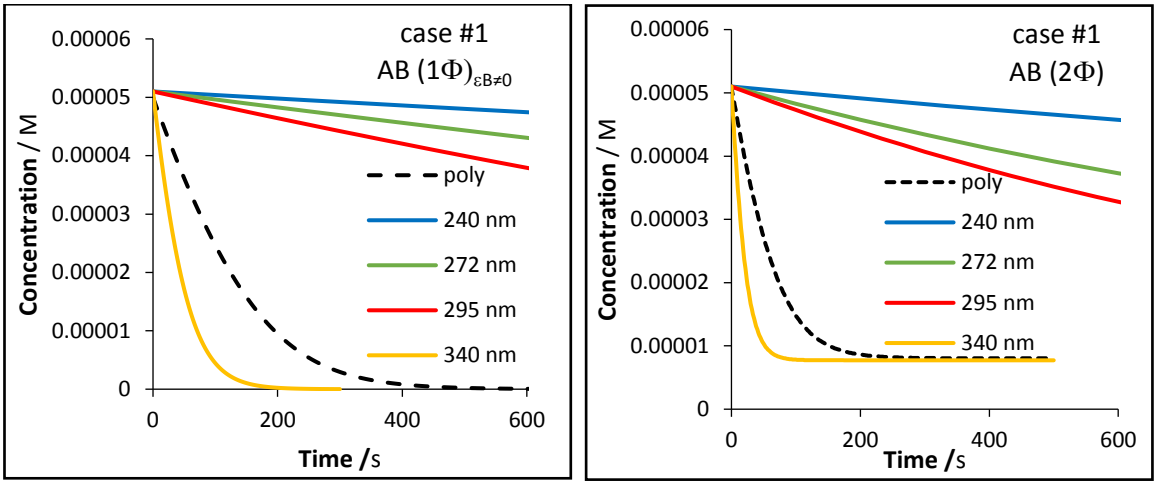

Figure 6-9: Compare between the behaviour one simulation case in polychromatic and monochromatic light irradiation.

6.8. Discussion

The new Φ- and η-order kinetics described above allows the description of photochemical reaction AB systems.

Moreover, the excellent fitting of synthetic kinetic traces for different photochemical systems show that not only is these models suitable for describing these types of photochemical reactions, but also demonstrates the accuracy of the newly developed order kinetics.

The models clearly show that the analytical rate constant k is dependent on the quantum yield of the reaction, the intensity of the light source, and the absorption coefficients (ε_A , ε_B); however, it is independent of concentration, C_{A_0}, and optical path length, $l_{\lambda_{irr}}$. Moreover, in accord with the fact that k is dependent of different

parameters, namely Φ_{AB}, Φ_{BA}, ε_A, ε_B and P, it is difficult to compare the different rate constants found in different laboratories or studies because it is difficult to ensure the same light intensity conditions. The rate constant equation (Eqs. 6-2, 6-10 and 6-11) and the initial velocity equation (Eqs. 6-3, 6-12 and 6-13) contain monochromatic data, indicating the importance of conducting a monochromatic study before the polychromatic study, and can be quantified in terms of $k_{cld.}$ and $\upsilon_{0,cld.}$.

The k in each of the models represent the photokinetic parameters, which is allow to quantify the change of the photochemical reaction with over time rather than rate constant in the thermal order kinetics. That is, the thermal rate constant is defined by Arrhenius equation, where the reaction in this case, by definition, is temperature dependent [19]. Nevertheless, most photoreactions are not dependent on temperature but it is depending on the parameters such as the light intensity and molecular absorptivity. Furthermore, the predicated values for the thermal rate constant did not give a true indication of the rate of the photochemical reaction because the photoreaction parameters as light intensity did not reflect in the Arrhenius equation. Which Arrhenius equation is used to estimate the relation between the temperature and the rate constant of the chemical reaction [19].

6.9. Conclusion

These models contribute to the rationalization and quantification of the features of three types of photochemical reaction. The $\Phi-$ and η-orders fill the gap in the photokinetics of the three AB systems.

The kinetic traces obtained by a fifth order Runge-Kutta integration were well fitted by $\Phi-$ and η-orders. An excellent agreement was obtained between the synthetic kinetic profiles and $\Phi-$ and η-orders model. This demonstrates that the $\Phi-$ and η-orders kinetics can model a large number of photochemical reactions of the three AB systems.

The rate constant and the initial velocity were constant with concentrations and depend on the photokinetics parameters $\Phi_{\mathrm{A}\to\mathrm{B}}$, $\Phi_{\mathrm{B}\to\mathrm{A}}$,$\varepsilon_A^{\lambda_{irr}}$, $\varepsilon_B^{\lambda_{irr}}$, and $P_{\lambda_{irr}}$. The model yielded a good correlation between the model and theoretical of rate constant in both models with less than 5% error. The theoretical rate constant for both models was calculated using only monochromatic irradiation data. This show the important of study the compounds or the drugs under monochromatic light before studying under polychromatic light to verify the result of rate constant.

Also, in this study found that the rate constant and the initial velocity were a function of the light intensity ($P_{\lambda_{irr}}$). In addition, these models represent an excellent tool by which to develop new actinometry.

6.10. References

1. ICH. International Conference on Harmonisation of Technical Requirements for Registration of Pharmaceuticals for Human Use (ICH) Harmonised Tripartite Guideline Stability Testing: Photostability Testing of New Drug Substances and Products. Q1B Current Step 4 v. 1996.
2. Takara A., Kobayashi K., Watanabe S., Okuyama K., Shimada Y., Goto S. Dibucaine inhibits ketoprofen photodegradation via a mechanism different from that of antioxidants. Journal of Photochemistry and Photobiology A: Chemistry. Elsevier B.V.; 2017; 333: 208–212. Available at: DOI:10.1016/j.jphotochem.2016.10.026
3. Li C., Zhang D., Peng J., Li X. The effect of pH, nitrate, iron (III) and bicarbonate on photodegradation of oxytetracycline in aqueous solution. Journal of

Photochemistry and Photobiology A: Chemistry. Elsevier B.V.; 2018; 356: 239–247. Available at: DOI:10.1016/j.jphotochem.2018.01.004

4. Oliveira C., Lima DLD., Silva CP., Calisto V., Otero M., Esteves VI. Photodegradation of sulfamethoxazole in environmental samples: The role of pH, organic matter and salinity. Science of the Total Environment. Elsevier B.V.; 2019; 648: 1403–1410. Available at: DOI:10.1016/j.scitotenv.2018.08.235

5. Mazellier P., Méité L., De Laat J. Photodegradation of the steroid hormones 17β-estradiol (E2) and 17α-ethinylestradiol (EE2) in dilute aqueous solution. Chemosphere. Elsevier Ltd; 2008; 73(8): 1216–1223. Available at: DOI:10.1016/j.chemosphere.2008.07.046

6. Passeport E., Zhang N., Wu L., Herrmann H., Sherwood Lollar B., Richnow HH. Aqueous photodegradation of substituted chlorobenzenes: Kinetics, carbon isotope fractionation, and reaction mechanisms. Water Research. Elsevier Ltd; 2018; 135: 95–103. Available at: DOI:10.1016/j.watres.2018.02.008

7. Megerle U., Lechner R., König B., Riedle E. Laboratory apparatus for the accurate, facile and rapid determination of visible light photoreaction quantum yields. Photochemical and Photobiological Sciences. 2010; 9(10): 1400–1406. Available at: DOI:10.1039/c0pp00195c

8. Voigt M., Jaeger M. On the photodegradation of azithromycin, erythromycin and tylosin and their transformation products – A kinetic study. Sustainable Chemistry and Pharmacy. Elsevier; 1 June 2017; 5: 131–140. Available at: DOI:10.1016/J.SCP.2016.12.001 (Accessed: 7 May 2019)

9. Zepp RG. Quantum Yields for Reaction of Pollutants in Dilute Aqueous Solution. Environmental Science and Technology. 1978; 12(3): 327–329. Available at: DOI:10.1021/es60139a010

10. Maafi W., Maafi M. Modelling nifedipine photodegradation, photostability and actinometric properties. International Journal of Pharmaceutics. Elsevier B.V.; 2013; 456(1): 153–164. Available at: DOI:10.1016/j.ijpharm.2013.07.075

11. Maafi M., Lee LY. Determination of Dacarbazine Φ-Order Photokinetics, Quantum Yields, and Potential for Actinometry. Journal of Pharmaceutical Sciences. Elsevier Masson SAS; 2015; 104(10): 3501–3509. Available at: DOI:10.1002/jps.24568

12. Maafi M., Maafi W. Φ-Order Kinetics of Photoreversible-Drug Reactions. International Journal of Pharmaceutics. 2014; 471(1–2): 536–543. Available at: DOI:10.1016/j.ijpharm.2014.05.017

13. Kawabe Y., Nakamura H., Hino E., Suzuki S. Photochemical stabilities of some dihydropyridine calcium-channel blockers in powdered pharmaceutical tablets. Journal of Pharmaceutical and Biomedical Analysis. Elsevier; 15 July 2008; 47(3): 618–624. Available at: DOI:10.1016/J.JPBA.2008.01.042

14. Lee LY. Study Of The Photodegradation And Photostability Of Anti-Cancer Drugs In Different Media Towards The Development Of Both New Actinometers And Liquid Formulations. De Montfort University; 2016; Available at: https://www.dora.dmu.ac.uk/handle/2086/12188

15. Maafi M., Maafi W. Modeling and Elucidation of the Kinetics of Multiple Consecutive Photoreactions AB4(4Φ) With Φ-order Kinetics. Application to the Photodegradation of Riboflavin. Journal of Pharmaceutical Sciences. Elsevier; 1 December 2016; 105(12): 3537–3548. Available at: DOI:10.1016/J.XPHS.2016.06.030

16. Maafi M. Useful spectrokinetic methods for the investigation of photochromic and thermo-photochromic spiropyrans. Molecules. 2008; 13(9): 2260–2302. Available at: DOI:10.3390/molecules13092260

17. Maafi M., Brown RG. The kinetic model for AB(1φ) systems. Journal of Photochemistry and Photobiology A: Chemistry. 2006; 187(2–3): 319–324. Available at: DOI:10.1016/j.jphotochem.2006.10.030

18. Maafi M., Maafi W. Quantification of Unimolecular Photoreaction Kinetics: Determination of Quantum Yields and Development of Actinometers—The Photodegradation Case of Cardiovascular Drug Nisoldipine. International Journal of Photoenergy. 2015; 2015: 1–12. Available at: DOI:10.1155/2015/454895

19. Maafi W. Modelling and elucidation of photoreaction kinetics - Applications and actinometry using nifedipine, nisoldipine, montelukast, fluvoxamine and riboflavin. De Montfort University; 2016; Available at: https://www.dora.dmu.ac.uk/handle/2086/13110

Chapter 7

The modelling of AB $(1\Phi)_{\varepsilon_{B=0}}$ under polychromatic light.

The case of C-DAE.

7.1. Introduction

Even though everywhere, the classical data treatments were found not efficient to fully and reliably describe photodegradation kinetics [1]. So far, there are some models used to describe the photochemical reaction AB (1Φ). Nevertheless, there is a lack in these models to describe the photochemical reaction [2,3].

This chapter considers the application of the new Φ-order kinetics to a real experiment (C-DAE). The photochemical reaction of this compound occurs under irradiation by polychromatic light in the range 400 to 800 nm. Its properties and features will be determined from a closed-form integration, a numerical integration calculation, and from experiment, as described in chapter 6 (section 6-4).

7.2. Photoselection of C-DAE in Ethanol

C-DAE has a UV-vis spectrum that is characterised by two bands in the visible region. The lowest absorbance band is observed between 390-450 nm whilst the second is between 450-600 nm. This compound has been shown to be thermally stable and its open form is obtained by visible light irradiation (400-600 nm) [4]. The quantum yield of the closed form of C-DAE is wavelength dependent, as described in section 5.5.3 [4,5].

The pink solution of C-DAE was exposed to steady-state polychromatic visible light (cool white light, characterise this by the profile (Fig. 3-3). The temporal evolution of the electronic spectrum shows a smooth decrease in the intensity of the band at 520 nm until it reaches zero (Fig. 7-1), indicating that C-DAE has been fully transformed into the open form (colourless solution).

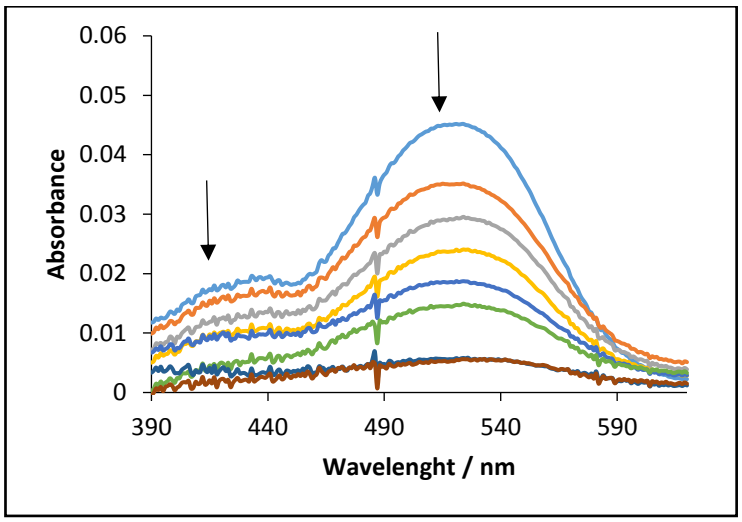

Figure 7- 1: Evolution of C-DAE under irradiation by polychromatic visible light for a solution of C-DAE at a concentration of 4.32 x 10^{-6} M.

The chromatogram showed two peaks (C-DAE and O-DAE). The C-DAE peak vanishes when conversion to the open form was complete, meanwhile the peak for the open form increased in intensity. There were no extra peaks in the chromatogram (Fig. 7-2). This finding shows that no any difference in the behaviour of DAE with polychromatic and monochromatic irradiation.

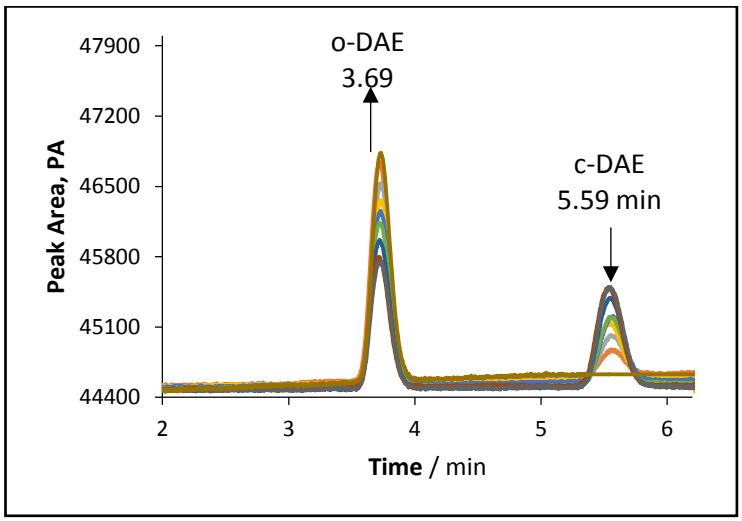

Figure 7- 2: HPLC chromatogram for C-DAE (4.32 x 10^{-6} M solution).

7.3. Φ-order kinetics of C-DAE

The polychromatic visible light irradiation of C-DAE at different concentrations is monitored by measuring concentration with time via HPLC.

To apply the Φ-model, one needs to obtain the $\sum \varepsilon_A$ for C-DAE. First, the C-DAE and O-DAE concentrations are obtained from the commercially available C-DAE HPLC and UV calibration graphs. The concentrations in the photostationary state (pss) of O-DAE were also obtained.

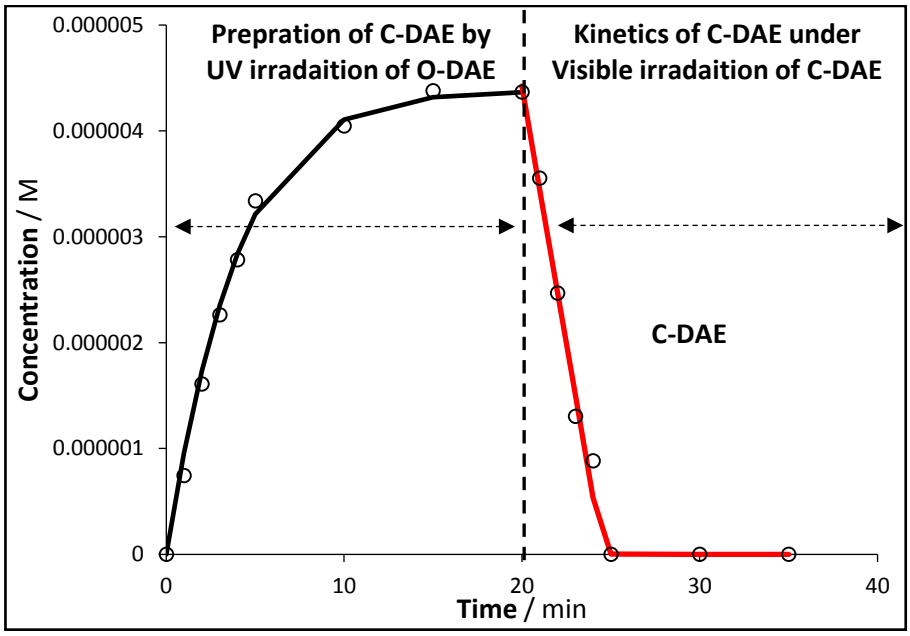

Figure 7- 3: Preparation of C-DAE by using 1.07 x10^{-5}M of O-DAE, Photokinetic traces for C-DEA (red line fitting using Eq.7-1).

Figure 7-3 show that the C-DAE is formed from the O-DAE under UV irradiation by using mix wavelength lamp (254/365 nm), and the irradiation was taken about 20 minutes to reach to the equilibrium, this process is called preparation of C-DAE. When the C-DAE was formed, the solution was irradiated under polychromatic light Visible range (400-

600 nm) by using LED torch lamp. The photokinetic trace of experimental data (in the circle) was fitted (red line) by Φ-order kinetic model (Eq. 7-1).

$\sum \varepsilon_{C-DAE}$ was obtained from the calibration graph of the sum of absorbance against concentration (Fig.7-4). The linearity range shows the workable concentration range for photokinetic studies of C-DAE. Moreover, the percentage difference between $\sum \varepsilon_{C-DAE}$ when obtained graphically, and the sum of the individual absorption coefficients, as described in chapter 5, was less than 10 %. This finding confirms the reliability and applicability of this method in terms of determining $\sum \varepsilon_{C-DAE}$.

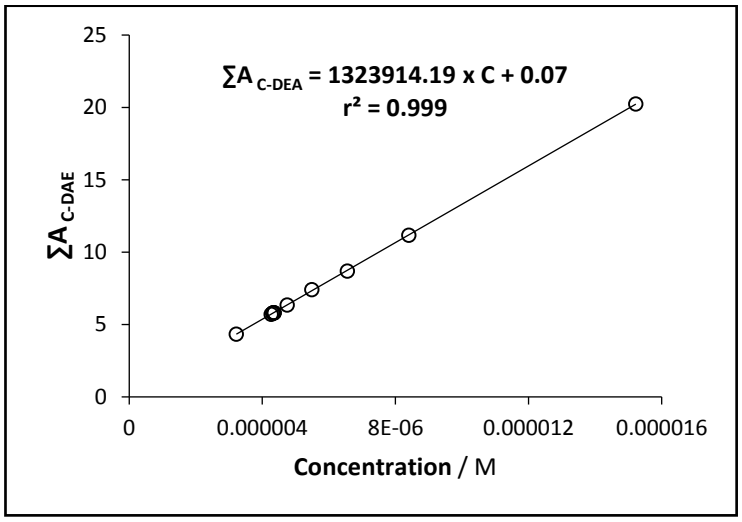

Figure 7- 4: Calibration curve for the sum of the absorption (400-600 nm) for the C-DAE.

7.4. C-DAE photodegradation kinetics

Ethanolic solutions with different concentrations of C-DAE within the linearity range were exposed to steady-state polychromatic visible light.

The Φ-order kinetics model (Eq.7-1), as described in chapter six, was applied to fit all the experimental traces of C-DAE. For each concentration, the experiment was carried out

at the same light intensity. The Φ-order model could be fitted to all the experimental traces gained from the HPLC (Fig.7-5, Table 7-1). These results indicated that the mechanism for the C-DAE closure is $AB(1\Phi)_{\varepsilon_{B=0}}$system, that the C-DAE photodecomposition obeys Φ-order kinetics, and the model equation is a suitable descriptor of this system.

$$C_A(t) = \frac{1}{\left(l_{\lambda_{irr}} \times \sum \varepsilon_A\right)} \times \log\left(1 + \left(-1 + 10^{\left(l_{\lambda_{irr}} \times \sum A_0\right)}\right) \times e^{(-k_{AB}t)}\right) \quad \text{Eq.7-1}$$

Table 7- 1: *Overall rate constant, kinetics and spectroscopic parameter values of study of C-DAE under polychromatic visible light irradiation*

$C_A\ (0)\times 10^6$ / M	$\sum_{400}^{600} A_{co}$	$\sum_{400}^{600} P_{exp.} \times 10^6$ / einstein s^{-1} dm^{-3}	k / sec^{-1}	$-v_{0,exp}\times 10^6$ / sec^{-1}
3.22	4.34	5.95	0.1	0.016
4.32	5.80	6.03	0.11	0.018
4.75	6.35	5.96	0.11	0.018
5.49	7.42	6.04	0.11	0.017
6.65	8.69	6.08	0.11	0.018
8.40	11.17	5.95	0.1	0.017

*$\sum_{400}^{600} \varepsilon_{c-DAE}$ is 1323914.19 M^{-1} cm^{-1}

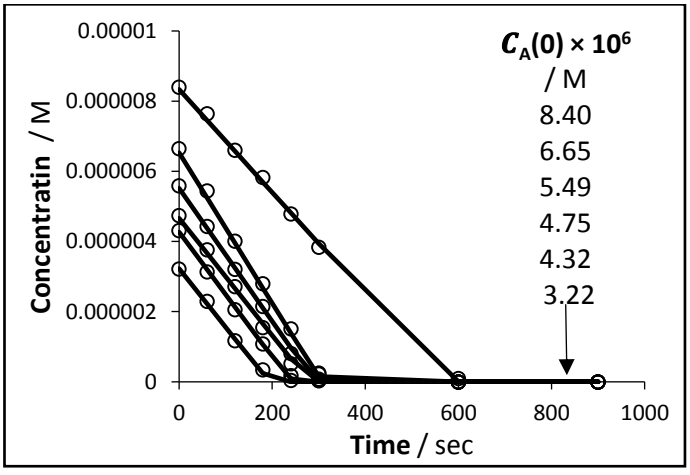

Figure 7- 5: Photokinetic traces of C-DAE in ethanol solutions at irradiation under polychromatic visible light (400-600 nm). The circles represent the exp. data while the lines represent the fitting traces using Eq.7-1.

The observed overall rate-constants (k_{AB}) were independent of the concentration of the sample solution (Fig 7-6). The wavelength-dependent quantum yields quantified in chapter five were used to validate k_{AB} according to Eq. (7-2). This confirms the importance of using monochromatic light to validate the results of the polychromatic study. In addition, the rate constant for the reaction under polychromatic light can be quantified without physical experimental once the monochromatic data study is available. Through, the monochromatic data such as Φ_{AB} was calculated from the represented equation in the chapter 5 (Eq. 5-17), ε_A was obtained as the monochromatic study, and the $P_{\lambda_{irr}}$ was quantified by using the spectroradiometer. Once has achieved all this, then the k_{AB} can be quantified by using Eq. (7-2).

$$k_{AB,cld} = \ln 10 \times l_{\lambda_{irr}} \times \sum(\Phi_{AB} \times \varepsilon_A \times P) \qquad \text{Eq.7-2}$$

Moreover, the experimental initial velocity ($\boldsymbol{v_0}$) was found to be constant with concentration as well (Fig. 7-6).

$$v_0\, cld. = \frac{k_{AB}}{\sum \varepsilon_A \times l_{\lambda_{irr}} \times \ln 10} \qquad \text{Eq.7-3}$$

The similarity between the experimental and theoretical of k_{AB} and $\boldsymbol{v_0}$ is 95% for each parameter. This finding also confirms the results shown in chapter 6.

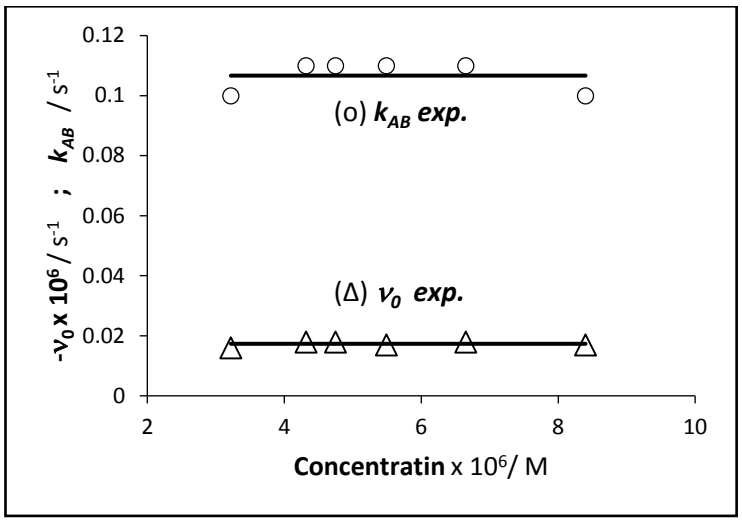

Figure 7- 6: Constant $k_{AB,\,exp.}$ and $\upsilon_{0,exp.}$ for C-DAE for experiments with different initial concentrations ($\boldsymbol{C_A}(0)$). The open symbols represent the experimental values found for $k_{AB,exp}$ and $\upsilon_{0,exp.}$.

7.5. Discussion

The literature offers very few examples of AB $(1\Phi)_{\varepsilon_{B=0}}$ kinetics under polychromatic light. Thus far, this kinetics was described by two methods [6,7].

The most recent was presented by Roibu et al. in 2018 [6]. This approach used the same differential equation proposed by Irie group [8] but with some modification. They introduced the energy density distribution function of the lamp (g_λ) into the differential equation as a quantification of the photons contribution at different energies when transforming the molecule. They used it as a ratio of intensities over the molecule absorption area [6]. The differential equation (7-4) takes the sum of all parameters due to the polychromatic irradiation. The $\sum g_\lambda$ multiplied by $P_{\lambda_{irr}}$ gives the sum value of the $P_{\lambda_{irr}}$.

$$-\frac{dC_A}{dt} = \frac{P_{0,\lambda_{irr}}}{V}\sum_{480}^{620}\Phi_{A\to B}g_\lambda\left(1-e^{-\varepsilon_A^{\lambda_{irr}}C_A(t)l}\right) \qquad \text{Eq.7-4}$$

Where V is volume and g_λ given by

$$g_\lambda = \frac{E_\lambda}{\sum_{480}^{620} E_\lambda} \quad \text{Eq.7-5}$$

with E_λ is the spectral irradiance (W $cm^{-2}nm^{-1}$). There are several approximations used to simplify and to finalise the integration to obtained the same formula as used by the Irie group [8] for study under monochromatic light. However, there are limitations with these approximations. Firstly, the parameter δ_λ, as defined by Eq. (7-6), was added to simplify the integration of Eq. (7-4). The first approximation states that δ_λ is close to zero; if studied under monochromatic irradiation, where g_λ is equal to one, then $\varepsilon_\lambda = \sum \varepsilon_\lambda g_\lambda$ is equal to one (because only one wavelength is determining the reaction). However, in polychromatic irradiation, the $\varepsilon_\lambda = \sum \varepsilon_\lambda g_\lambda$ is difficult to that happen due to $g_\lambda \neq 1$ or zero and $\varepsilon_\lambda \neq \sum \varepsilon_\lambda g_\lambda$ but they were used LED as light source for polychromatic light and it was considered as monochromatic, however they are characterized by a spread with an average at the maximum wavelength. For this reason, they were assumed that the δ_λ is close to zero.

$$\delta_\lambda = \frac{\varepsilon_\lambda}{\sum_{480}^{620} \varepsilon_\lambda g_\lambda} - 1 \quad \text{Eq.7-6}$$

The second approximation used the parameter α, which is defined by Eq. (7-7).

$$\alpha = \frac{\sum_{480}^{620} \varepsilon_\lambda g_{\lambda\delta_\lambda}}{\sum_{480}^{620} \varepsilon_\lambda g_\lambda} \quad \text{Eq.7-7}$$

The α parameter is equal to zero as well due to using the δ_λ parameter in Eq. (7-7). By using the previous approximation of δ_λ of zero, then α accordingly also becomes zero.

However, δ_λ is not equal to zero for the same reason as above. Therefore, the suggestion from this limitation in the integration leads to subsequent problems.

Roibu et al.[6] concluded that the integration of the differential equation was similar to that by the Irie group [8], but with some modification by adding the weighted averages of some of the parameters as summation over the wavelength.

$$\log\left(10^{\varepsilon_{avg} l C_A(0)} - 1\right) - \log\left(10^{\varepsilon_{avg} l C_A(t)} - 1\right) = \varepsilon_{avg} l \Phi_{avg} \frac{P_{0,\lambda_{irr}}}{V} t \qquad \text{Eq.7-8}$$

Where,

$$\varepsilon_{avg} = \sum_{480}^{620} \varepsilon_A^{\lambda_{irr}} \mathrm{g}_\lambda \qquad \text{Eq.7-9a}$$

$$\Phi_{avg} = \sum_{480}^{620} \Phi_{A\to B} \mathrm{g}_\lambda \qquad \text{Eq.7-9b}$$

Where the rate constant (k) is

$$k = \varepsilon_{avg} l \Phi_{avg} \frac{P_{0,\lambda_{irr}}}{V} \qquad \text{Eq.7-10}$$

However, there is no clear relationship between g_λ and $\varepsilon_A^{\lambda_{irr}}$ and $\Phi_{A\to B}$ in the differential equation while there is relationship with $P_{\lambda_{irr}}$, which is used to obtain the sum of the light intensities.

The second method was reported by Hrdina et al. [7], described the rate of the photochemical reaction with equation (7-11) that was unsolvable. So a numerical integration was performed [7].

$$r = \left(\frac{S}{V}\right)\left[\frac{1}{(\tilde{\nu}_m - \tilde{\nu}_n)}\right] \sum_i \Phi_{A\to B} P_{0,\lambda_{irr}} \left(1 - 10^{-\varepsilon_A^{\lambda_{irr}} C_A(t) l}\right) \Delta\tilde{\nu} =$$

$$\left(\frac{S}{V}\right)\left[\frac{1}{(\tilde{\nu}_m - \tilde{\nu}_n)}\right] \sum_i \Phi_{A\to B} T_{f,i} P_{0,\lambda_{irr}} \left(1 - T_{A,i}\right) \Delta\tilde{\nu} \qquad \text{Eq.7-11}$$

Where S is the irradiated area, and $\tilde{\nu}_m$ and $\tilde{\nu}_n$ are the limiting wavenumbers of the polychromatic beam emitted by the source. i is the reference to wavenumber ($\tilde{\nu}$), $T_{f,i}$ is the transmittance of filter f at wavenumber $\tilde{\nu}$ and $T_{A,i}$ is the actinometer transmittance at this wavenumber.

The parameter Δv was an integration step for Eq. (7-11). The transmittance of the filter was used by using the absorption filter because the aim is to determine the intensities of light, and the light absorbed was replaced by filter transmittance Eq. (7-11).

$P_{\lambda_{irr}}$ was replaced by using the relative intensity J_i as

$$J_i = P_{0,\lambda_{irr}}/C \qquad \text{Eq.7-12}$$

Where the C is a constant.

$$r_t = C\left(\frac{S}{V}\right)\left[\frac{1}{(\tilde{\nu}_m-\tilde{\nu}_n)}\right]\sum_i \Phi_{A\to B}T_{f,i}J_i\left(1-T_{A,i}\right)\Delta\tilde{\nu} \qquad \text{Eq.7-13}$$

The authors were assumed that the right side of the equation is time independent (constant), thus meaning the integration of this equation is representative of zero-order kinetics which, if summed, both K and S_t are constant.

$$r_t = \frac{dc_A}{dt} = \left(\frac{S}{V}\right)KS_t \qquad \text{Eq.7-14}$$

This equation (7-14) was solved as being zero order.

$$(c_A(t) - c_A(0)) = \left(\frac{S}{V}\right)KS_t t \qquad \text{Eq.7-15}$$

Where,

$$K = \frac{C}{(\tilde{\nu}_m-\tilde{\nu}_n)} \qquad \text{Eq.7-16}$$

$$S_t = \sum_i \Phi_{A\to B}T_{f,i}J_i\left(1-T_{A,i}\right)\Delta\tilde{\nu} \qquad \text{Eq.7-17}$$

However, $T_{f,i}$ was added without any clarification. Hence, $T = 10^{-A}$. Also, the time independence of the right-hand side of equation (7-13) was an assumption but is not true due to the transmittance being dependent on the number of photons passing or absorbed, where the number of photons absorbed depends on the conversion of the molecule by time of the irradiation. Therefore, the transmittance is time dependent. In addition, K was obtained from the slope of the linear line of concentration against time (Eq. 7-15), but the slope of the straight line should contain $\left(\frac{S}{V}\right) KS_t$ thus leading to the K obtained from slope not being true. Also, as mentioned in this study [7], S_t was calculated using Eq. (7-17). There are two unknown parameters in this equation, Φ_A, J_i, thus also leading to difficulties in calculating S_t.

The most interesting finding in the present results in this study was that the new order kinetics represent a suitable description of the photochemical reaction. Presented model included all criteria that could affect the photochemical reaction. The similarity of the two methods started from the same principle of the differential equation. There was a similarity in the function of proposed model (log-exp) to the function of method one [6]. However, there is a difference between proposed model in this study and the first model [6], where in the first the parameters g_λ, ε_{avg} and Φ_{avg} were included in the model equation, while, there was difference in the model function and proposed model (log-exp) and the second model (zero order) [7].

In the findings of this study, the overall rate constant was dependent on different photochemical parameters, namely Φ_{AB}, ε_A, $l_{\lambda_{irr}}$ and $P_{\lambda_{irr}}$, which is similar to the findings for the first model [6]. In addition, the concentration effect was studied, from

which it was noted that the overall rate constants were constant regardless of initial concentration. This result was similar to that in the first method when studying the concentration effect [6].

In this study, it was found that the quantum yield was wavelength dependent in this study and the first model [6], while the quantum yield in the second model was considered wavelength independent [7]. However, the proposed model in this study used sum values whilst the first model used a weighted average value. For the quantum yield, in the present study there is a logical reason to use the sum of the quantum yields, namely because there is significant variation between the values of the quantum yields; but in the first method [6] was taken a weighted average of the quantum yields (i.e. the sum of light intensities multiplied by g_λ). This clear to suggest that the value of the g_λ is not equal to one. The quantum yield could be used to quantify and validate the overall rate constant, and by comparison between the experimental and the theoretical overall rate constant it was found that the result is similar, with a less than 5% error. The analytical parameter k_{AB} in the polychromatic study was ten-fold greater than in the monochromatic studies, which in this study, under polychromatic light, was 0.1 s^{-1}, while in the monochromatic study reported in chapter 5 was 0.0101 s^{-1} at 520 nm and in a previous study was 0.0105 s^{-1} at 517 nm [4]. This finding might be due to the molecule being exposed to multiple wavelengths, each at a different light intensity, or it might be the light intensity is become bigger in polychromatic light than monochromatic light irradiation.

7.6. Conclusions

The new model applied in this chapter has established photodegradation AB $(1\Phi)_{\varepsilon_{B=0}}$system, as driven by polychromatic light. The new Φ-order kinetics, applied here for C-DAE could quantify and evaluate well the photostability independent of concentration. The overall rate constant and initial velocity were independent on concentration. The overall rate constant is dependent on Φ_{AB}, ε_A, $l_{\lambda_{irr}}$ and $P_{\lambda_{irr}}$, which therefor offers a tool to develop new compound actinometers.

7.7. References

1. Roman J., Breier AR., Steppe M. Stability indicating LC method to determination of sodium montelukast in pharmaceutical dosage form and its photodegradation kinetics. Journal of Chromatographic Science. 2011; 49(7): 540–546. Available at: DOI:10.1093/chrsci/49.7.540

2. Zepp RG. Quantum Yields for Reaction of Pollutants in Dilute Aqueous Solution. Environmental Science and Technology. 1978; 12(3): 327–329. Available at: DOI:10.1021/es60139a010

3. Nakashima H., Irie M. Synthesis of silsesquioxanes having photochromic dithienylethene pendant groups. Macromolecular Chemistry and Physics. 1999; 200(4): 683–692. Available at: DOI:10.1002/(SICI)1521-3935(19990401)200:4<683::AID-MACP683>3.0.CO;2-N

4. Maafi M. The potential of AB(1Φ) systems for direct actinometry. Diarylethenes as successful actinometers for the visible range. Physical Chemistry Chemical Physics. 2010; 12(40): 13248–13254. Available at: DOI:10.1039/c0cp00469c

5. Maafi M., Brown RG. The kinetic model for AB(1φ) systems: A closed-form integration of the differential equation with a variable photokinetic factor. Journal of Photochemistry and Photobiology A: Chemistry. April 2007; 187(2–3): 319–324. Available at: DOI:10.1016/j.jphotochem.2006.10.030 (Accessed: 23 May 2019)

6. Roibu A., Fransen S., Leblebici ME., Meir G., Van Gerven T., Kuhn S. An accessible visible-light actinometer for the determination of photon flux and optical pathlength in flow photo microreactors. Scientific Reports. Springer US; 2018; 8(1): 1–10. Available at: DOI:10.1038/s41598-018-23735-2

7. Hrdina, R., Čepčiansky, I. and Bittová, H. Determination of the intensity of

polychromatic radiation in the reaction compartment as a function of wavenumber. Collection of Czechoslovak chemical communications. 1991, 56(6), pp.1173-1179.

8. Sumi T., Takagi Y., Yagi A., Morimoto M., Irie M. Photoirradiation wavelength dependence of cycloreversion quantum yields of diarylethenes. Chemical Communications. The Royal Society of Chemistry; 18 March 2014; 50(30): 3928. Available at: DOI:10.1039/c4cc00396a (Accessed: 2 April 2019)

Chapter 8

Experimental investigation of AB $(1\Phi)_{\varepsilon_{B\neq 0}}$ and AB (2Φ) systems under polychromatic light.

The η-order kinetics

8.1. Introduction

Using thermal reaction orders to treat the photostability data have been confirmed to be unsuitable for photodegradation studies [2,3]. This lack in procedures is due to the fact that, there are no mathematical models known in the literature that are able to describe the photodegradation kinetics under polychromatic light exposure [2–4]. In fact, this represents a lack of knowledge in the field of photochemistry.

Moreover, there are many photosystems that have been reported to light give a single photoproduct. These types include the photochemical mechanism are known as AB$(1\Phi)_{\varepsilon_{B\neq 0}}$ and AB (2Φ) [5]. Nifedipine (NIF) and Dacarbazine (DBZ) have been selected as real examples for the photochemical reaction AB$(1\Phi)_{\varepsilon_{B\neq 0}}$. While, the stilbinods group, AXI and O-DAE, belong to AB (2Φ) type. The photostabilities studies of these compounds have been established under monochromatic irradiation in Chapter 5 and by Maafi group [6].

The aim of this study is to apply the η-order kinetics model in the characterization and quantitative evaluation of the effects of polychromatic light on the photokinetic behaviour of the selected molecules in ethanolic solutions.

8.2. Photostability of the compounds in Ethanol

For the most part, these compounds mostly absorb in the UVA and UVB region of the spectrum. The band at long wavelength was attributed to $\pi \rightarrow \pi^*$ transitions due to presence of the double bond system [7]. Polychromatic UVA-UVB steady-state irradiation of all the compounds of interest in the present study leads to the smooth

increase and decrease in the UV absorbance spectra (Fig. 8-1). The spectral evolution of these compounds under polychromatic light is similar to those under monochromatic light, as described in chapter 5 for the stilbinods group and DAE, and for AXI, NIF and DBZ as described in the group's research [3,6,8]. The spectral evaluation of these compounds indicated several isosbestic points. These isosbestic points confirm that the reactions are quantitative and that no secondary reaction occurs during the main reaction. The 360 nm and 326 nm bands of NIF and DBZ, respectively, were both completely depleted.

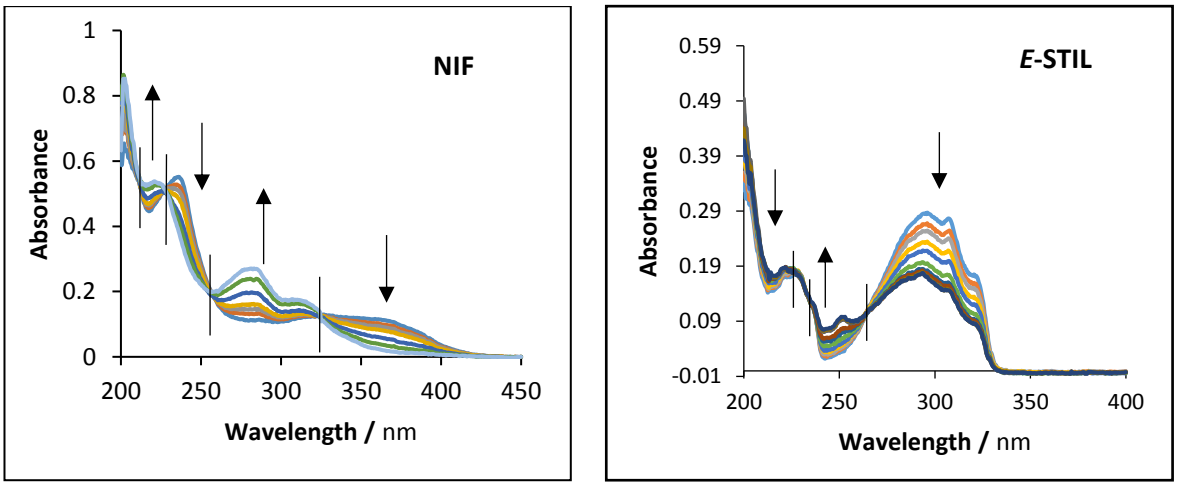

Figure 8- 1: Evolution of the absorption spectra of NIF (2.88×10^{-5} M) and E-STIL (1.25×10^{-5} M) in ethanol, when subjected to a polychromatic steady irradiation using mix wavelength lamp (254/365 nm) (200-400 nm). Arrows indicate direction of evolution; vertical lines cross the spectra at the isosbestic points

The HPLC chromatograms indicated that after exposing the compounds to polychromatic light (irradiation), there were only two peaks (the main species and its photoproduct). At photostationary state, the main peaks of NIF and DBZ were completely depleted, confirming that NIF and DBZ undergo AB $(1\Phi)_{\varepsilon_{B\neq 0}}$

photoreactions; however, complete depletion was not observed for the other compounds proving their AB (2Φ) character.

8.3. η-order kinetics of compounds

The effects of irradiation using polychromatic light on photodegradation will be considered in this study. The kinetics for the compounds studied for both systems (AB $(1\Phi)_{\varepsilon_{B\neq 0}}$ and AB (2Φ)) were obtained when each were irradiated by polychromatic light in various concentrations.

To apply this model and obtain the overall rate constant (k_η), one needs to quantify C_A(t), $\Phi_{A\rightarrow B}^{\lambda_{irr}}$, $\Phi_{B\rightarrow A}^{\lambda_{irr}}$, $\sum \varepsilon_A(\lambda_i)$ and $\sum \varepsilon_B(\lambda_i)$.

The HPLC method was used to obtain the concentration of the main compound and its photoproduct. The HPLC calibration graphs were used to determine with precision the concentrations of the compounds (C_A(0)) and C_A(t) after polychromatic light irradiation for different times.

The total absorbances were measured via spectrophotometry as the sums of individual wavelength absorbances over the range of irradiation at time 0 for the main compounds and photostationary state (pss) of each of the photoproducts. The calibration curves for the total absorbances were used to obtain $\sum \varepsilon_A(\lambda_i)$ and $\sum \varepsilon_B(\lambda_i)$ for each of the studied compounds (Fig.8-2).

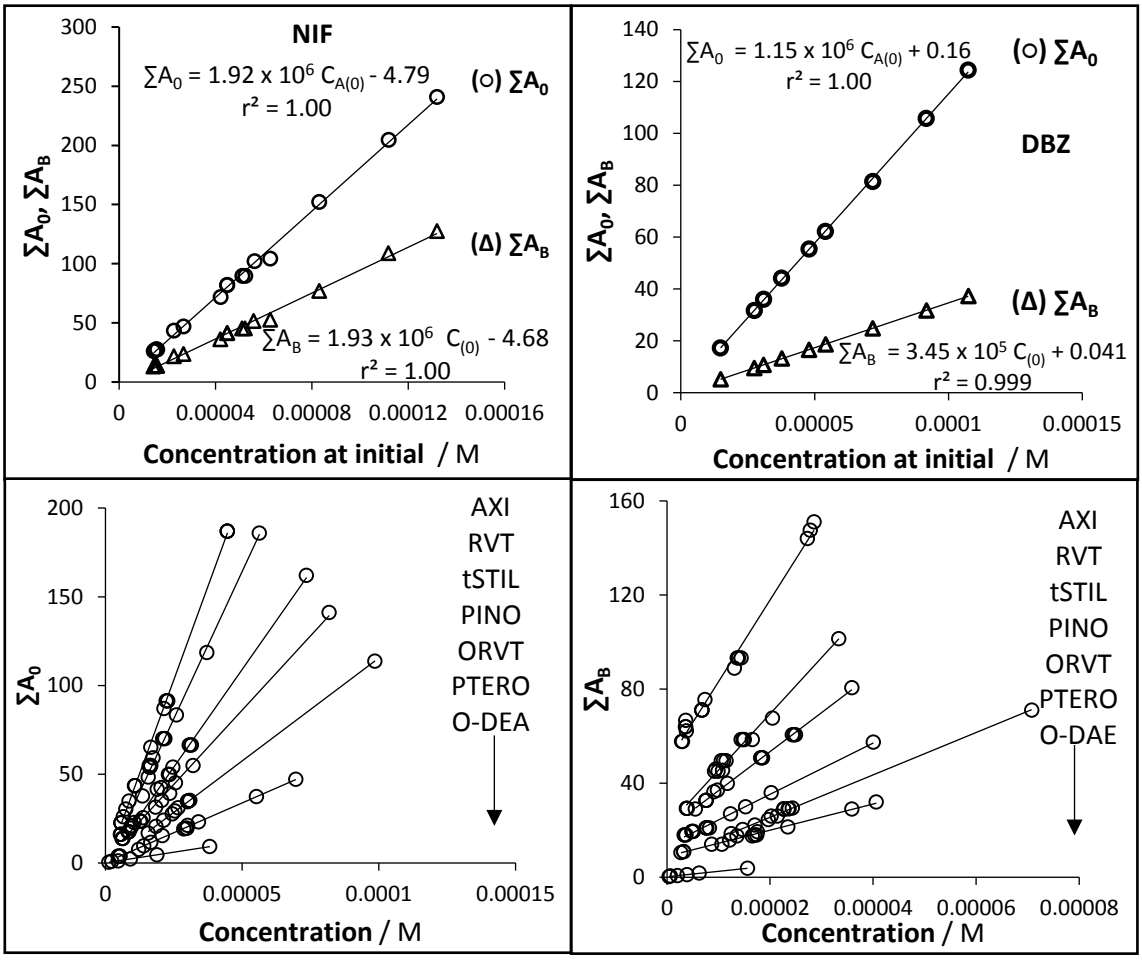

Figure 8- 2: Calibration graphs of studies compounds based on $\sum \boldsymbol{A_0}$ *or* $\sum \boldsymbol{A_\infty}$ *variation with concentration (*$\boldsymbol{C_A}(0)$*)*

The range over which the calibration graphs were linear (Figs. 8-2) is indicative of the useful concentration range for performing consistent photokinetic studies for these compounds in both systems. In addition, the comparison between the magnitudes of $\sum \varepsilon_A(\lambda_i)$ and $\sum \varepsilon_B(\lambda_i)$ (as obtained using the method described in chapter 3, section 3.32.1), and the sum of the individual $\varepsilon_A(\lambda_i)$ and $\varepsilon_B(\lambda_i)$ (when calculated as described in chapter five, section 5.2.2.1) showed that the percentage difference between the two

was less than 10%, which indicates that the method is both valuable and applicable for determining the sums of these parameters.

Figure 8-3 show that the absorption spectra of the initial compound ($\varepsilon_A^{\lambda_{irr}}$)and its photoproduct ($\varepsilon_B^{\lambda_{irr}}$) at initial time and photostationary state. It is noticeable that the absorption spectra behaviour of the all studies compounds under polychromatic light irradiation were same behaviour under monochromatic studied. The quantum yields values were determined using the equation that obtained from the study photodegration of the compounds under monochromatic irradiation, this equation used to represent the sigmoid patterns of the quantum yield values.

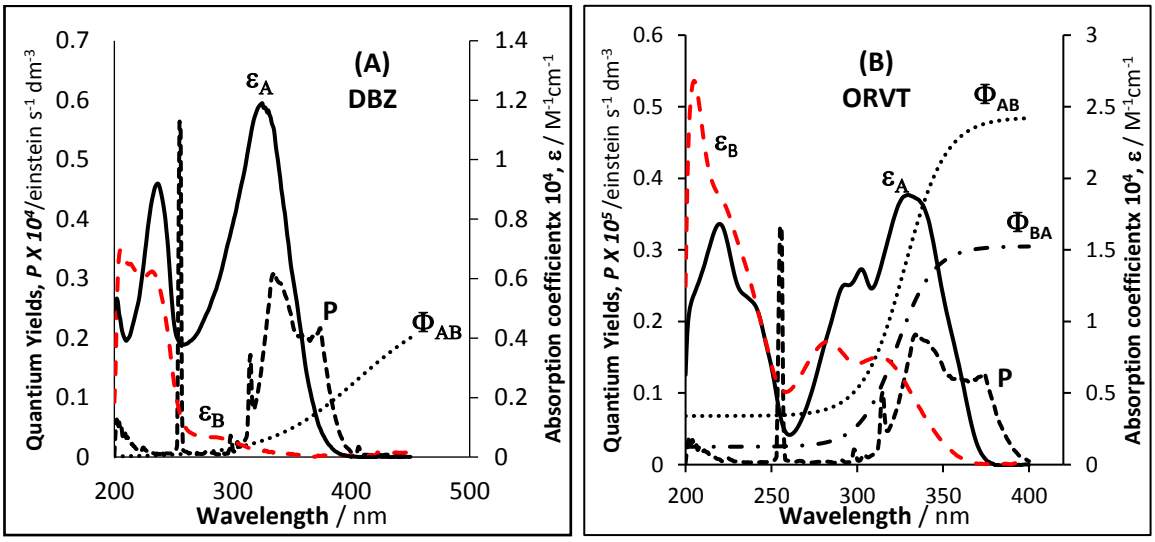

Figure 8- 3: Profiles of experimental ε_A, ε_B, P, Φ_{AB} and Φ_{BA} of DBZ and ORVT using mix wavelength lamp (254/365 nm).

The selective compounds showed that all the compounds were value of $\sum \boldsymbol{\varepsilon_A}(\lambda_i) > \sum \boldsymbol{\varepsilon_B}(\lambda_i)$ expect the O-DAE ($\sum \varepsilon_A(\lambda_i) < \sum \varepsilon_B(\lambda_i)$) and about equal value in the NIF. While, the sum of value of three parameters Φ_{AB}, $\varepsilon_A^{\lambda_{irr}}$ and $P_{\lambda_{irr}}$ is bigger than the reverse value, expect in case the AXI (Table. 8-1).

Table 8- 1: *the summation of absorption coefficients, light intensity and sum of value of three parameters Φ, ε and P for studies compounds photoisomerisation reactions under monochromatic irradiations.*

System	$\sum \varepsilon_A(\lambda_i)$ / $M^{-1}cm^{-1}$	$\sum \varepsilon_B(\lambda_i)$ / $M^{-1}cm^{-1}$	$\sum P(\lambda_i)$ /einstein s^{-1} dm^{-3}	$\sum(\Phi_{AB} \times \varepsilon_A \times P)$	$\sum(\Phi_{BA} \times \varepsilon_B \times P)$
AB $(1\Phi)_{\varepsilon_{B\neq 0}}$	**NIF**				
	1920219.56	1936173.24	0.00022	0.296	0
	DBZ				
	1150028.96	344785.1452	0.00018	0.0386	0
AB (2Φ)	**t-STIL**				
	2201390.92	1627877.93	0.000055	0.272	0.0269
	PINO				
	2084163.89	1325011.57	0.00019	0.546	0.0076
	RVT				
	3319305.86	2368298.35	0.000077	0.628	0.0593
	ORVT				
	1907318.75	1496198.29	0.000077	0.168	0.0592
	PTERO				
	1917082.05	1574316.91	0.000099	0.511	0.0176
	AXI				
	3841612.85	3276331.99	0.00012	0.200	0.277
	O-DAE				
	2396185.03	2723189.77	0.00029	0.501	0.423

* Where ℓ_{obs}=1 cm and ℓ_{irr}= 2 cm

8.4. Photodegradation kinetics

The photodegradation kinetics of NIF, DBZ, AXI, STIL, PINO, RVT, ORVT, PTERO and O-DAE were studied by exposing fresh ethanolic solutions of these species polychromatic steady-state irradiation in the range 200-400 nm. The variations in concentrations over time for each were obtained via HPLC.

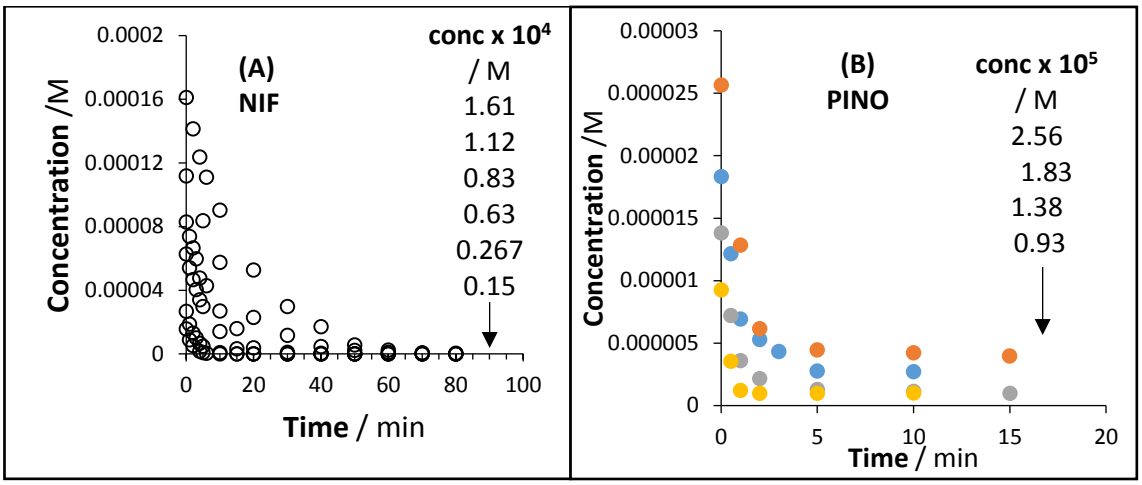

Figure 8- 4: ***a, b.*** *Photokinetic traces of NIF and PINO under polychromatic light* using mix wavelength lamp (254/365 nm).

The application of η-order kinetics to the experimental traces found for these compounds could be accurately fit using Eq. 6-4 (Fig. 8-5). These results confirm that these compounds underwent photodegradation under irradiation by steady-state polychromatic light following η-order kinetics.

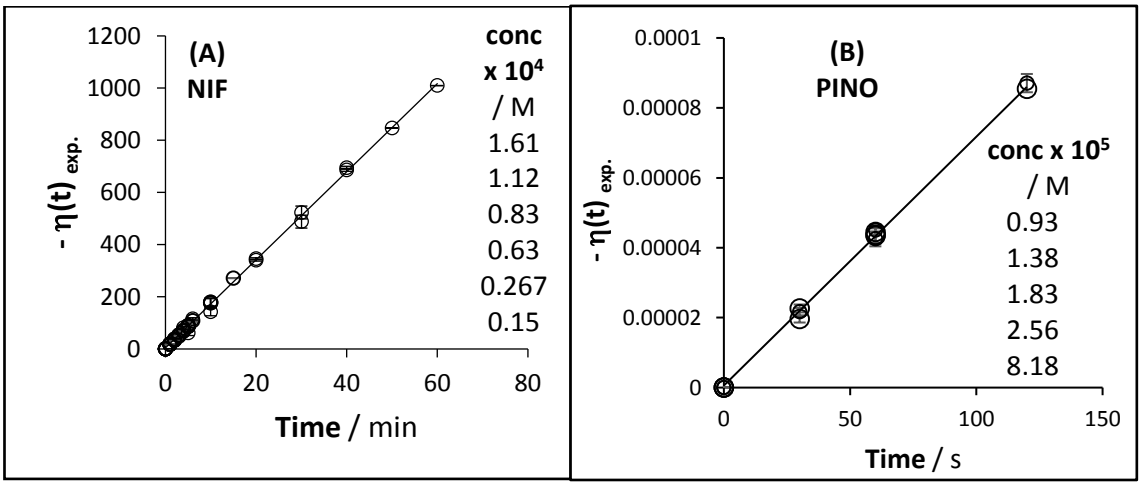

Figure 8- 5: ***a, b.*** *applied η-order on the photokinetic traces of NIF and PINO under polychromatic light* using mix wavelength lamp (254/365 nm)*, circle corresponding to experimental data and line corresponding to the fitting traces using Eq.6-4.*

$$\boldsymbol{\eta(t) = -k_{\eta} t}$$ Eq.6-4

$$\boldsymbol{\eta(t) = \left(C_{A_t} - C_{A_0}\right) \times \alpha + \gamma \times Ln \frac{C_{A_t}+\delta}{C_{A_0}+\delta}}$$ Eq.6-5

where $\boldsymbol{\alpha}$, $\boldsymbol{\gamma}$ and $\boldsymbol{\delta}$ are factors that are dependent on the type of reaction, as described in chapter 6.

Fitting the model to the photokinetic traces allowed the determination of the analytical overall rate constant (k_{η}) for the compounds studied. It was found that k_{η} and v_0 remained constant with concentration for both systems (Fig. 8-6). There is an excellent correlation between the experimental and calculated values of k_{η} and v_0 using Eq. 6-10 and 6-11 and Eq.6-12 and 6-13, respectively, with percentage errors less than 5%. NIF degraded six times faster than DBZ when exposed to polychromatic light. These results are conform to the predication of the η-order as discussed in chapter 6 and therefore $\eta(t)$ fully describe the photodegradation kinetics in solutions of the studied compounds for both systems.

The overall rate constant for AB $(1\Phi)_{\varepsilon_{B\neq 0}}$ (${}^{2}k_{\eta}$) and AB (2Φ) (${}^{3}k_{\eta}$) can be given as:

$${}^{2}k_{\eta} = \sum_{\lambda_i}^{\lambda_f}[(\Phi_{AB}(\lambda_i) \times \varepsilon_A(\lambda_i)) \times P(\lambda_i)]$$ Eq6-10

$${}^{3}k_{\eta} = \frac{\sum_{\lambda_i}^{\lambda_f}[(\Phi_{BA}(\lambda_i)\times\varepsilon_B(\lambda_i)+\Phi_{AB}(\lambda_i)\times\varepsilon_A(\lambda_i))\times P(\lambda_i)]}{\sum_{\lambda_i}^{\lambda_f}(\varepsilon_A(\lambda_i)-\varepsilon_B(\lambda_i))}$$ Eq.6-11

And the initial velocities can be given as:

$${}^{2}v_{0,cld} = -\frac{\left(\sum_{\lambda_i}^{\lambda_f}[(\Phi_{AB}(\lambda_i)\times\varepsilon_A(\lambda_i))\times P(\lambda_i]\right)\times C_{A_0}}{\sum_{\lambda_i}^{\lambda_f}\varepsilon_B(\lambda_i)\times C_{A_0}+\left(\sum_{\lambda_i}^{\lambda_f}(\varepsilon_A(\lambda_i)-\varepsilon_B(\lambda_i))\right)\times C_{A_0}} = -\frac{{}^{2}k_{\eta}}{\sum_{\lambda_i}^{\lambda_f}\varepsilon_A(\lambda_i)}$$ Eq.6-12

$$^{3}\upsilon_{0\,,cld} = -^{3}k_{\eta} \times \frac{C_{A_0}+\rho_1}{C_{A_0}+\theta_{AB}}$$ Eq.6-13

8.5. Effect of the concentration on η- order kinetics

Various initial concentrations of the selected drugs were used to investigate their effects on the rate constant of the new order kinetics (Table 8-2). These concentrations were chosen to lie within the compounds' linearity ranges obtained for $\sum A$ against concentration. The photokinetic traces could be accurately fitted using model Eq.6-4 (Fig. 8-5). Again, the accuracy of the mathematical model is confirmed by the results obtained for the photochemical reaction of AB $(1\Phi)_{\varepsilon_{B\neq 0}}$ and AB (2Φ). The rate constant (k_{η}) and the initial velocity (υ_0) remained constant with changing concentration (Fig.8-6), as predicted in Eqs. (6-10, 6-11) and Eqs (6-12,6-13). Therefore, these results indicated that $\eta(t)$ was concentration independent.

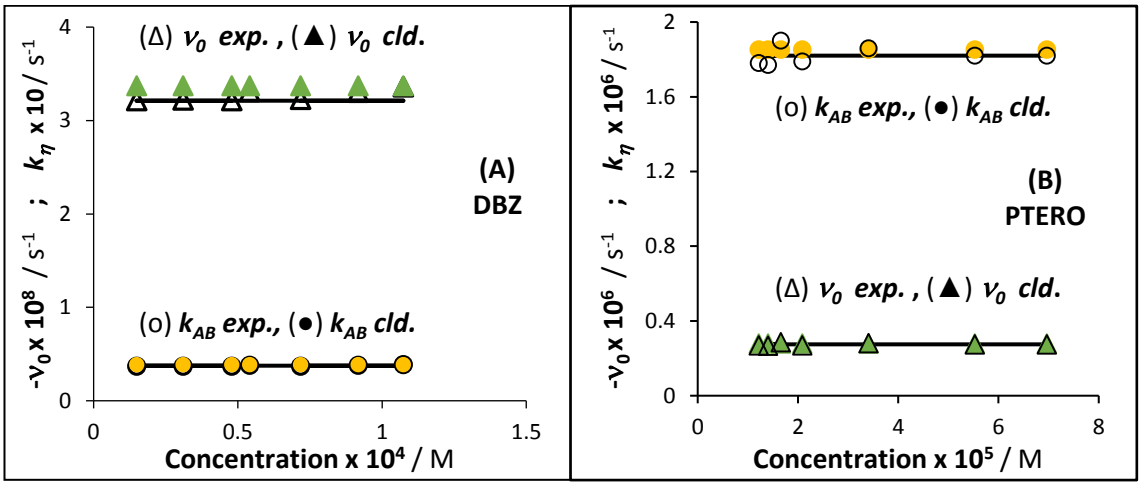

*Figure 8- 6: **a.b.** Constant $k_{\eta,\,mod.}$ and $\upsilon_{0,mod.}$ of DBZ and PTERO with different initial concentration ($\boldsymbol{C_A}(0)$). The open and solid symbols represent the experimental and calculated values of $k_{\eta,cld}$ and $\upsilon_{0,cld.}$, respectively.*

Table 8- 2: *Effect of the concentration on Overall photoreaction rate constant values of studies compounds under polychromatic irradiations performed in ethanol.*

$C_A(0)$ x10^5 /M	$k_{\eta,exp.}$ / s^{-1}	$k_{\eta,cld}$ / s^{-1}	% different	$C_A(0)$ x10^5 /M	$k_{\eta,exp.}$ x10^7 / s^{-1}	$k_{\eta,cld}$ x10^7 / s^{-1}	% different
NIF				**t-STIL**			
1.50	0.287	0.296	3.04	0.964	4.93	5.20	5.19
2.67	0.293	0.296	1.01	1.05	4.91	5.20	5.58
4.50	0.288	0.296	2.70	1.26	5.45	5.20	-4.81
4.80	0.291	0.296	1.69	2.54	5.39	5.20	-3.65
5.20	0.290	0.296	2.03	7.36	5.67	5.20	-9.04
6.30	0.293	0.296	1.01	**PINO**			
8.30	0.293	0.296	1.01	0.926	7.26	7.30	0.55
11.2	0.288	0.296	2.70	1.38	7.38	7.30	-1.09
13.2	0.291	0.296	1.69	1.83	7.32	7.30	-0.27
16.1	0.293	0.296	1.01	2.56	7.23	7.30	0.96
				8.18	7.32	7.30	-0.27
DBZ				**RVT**			
1.49	0.0369	0.0386	4.09	1.36	0.750	0.723	-3.73
3.09	0.0370	0.0386	4.10	1.56	0.725	0.723	-0.28
4.79	0.0369	0.0386	3.96	1.66	0.758	0.723	-4.84
5.41	0.0380	0.0386	1.27	2.17	0.696	0.723	3.73
7.16	0.0371	0.0386	-0.292	2.59	0.694	0.723	4.01
9.17	0.0379	0.0386	1.49	3.71	0.762	0.723	-5.39
10.74	0.0386	0.0386	3.67	5.64	0.723	0.723	0.043
$C_A(0)$ x10^5/M	$k_{AB,exp.}$ x10^7 / s^{-1}	$k_{AB,cld}$ x10^7 / s^{-1}	% different	$C_A(0)$ x10^5/M	$k_{AB,exp.}$ x10^6/ s^{-1}	$k_{AB,cld}$ x10^6/ s^{-1}	% different
ORVT				**O-DEA**			
1.81	5.66	5.52	-2.54	0.705	-2.66	-2.83	5.44
2.36	5.67	5.52	-2.72	0.930	-2.64	-2.83	7.07
3.06	5.62	5.52	-1.81	1.36	-2.78	-2.83	3.12
4.22	5.61	5.52	-1.63	2.40	-2.81	-2.83	0.454
8.65	5.77	5.52	-4.53	5.97	-2.61	-2.83	7.00
AXI				**PTERO**			
0.577	1.90	2.00	5.00	1.22	1.48	1.54	3.96
0.745	1.95	2.00	2.50	1.66	1.57	1.54	-1.88
0.867	1.93	2.00	3.50	2.08	1.48	1.54	3.96
1.09	2.15	2.00	-7.50	3.40	1.50	1.54	2.66
1.66	1.86	2.00	7.00	5.53	1.54	1.54	0.065

$C_A(0)$ x10^5/M	$k_{AB,exp.}$ x10^7 / s^{-1}	$k_{AB,cld}$ x10^7 / s^{-1}	% different	$C_A(0)$ x10^5/M	$k_{AB,exp.}$ x10^6/ s^{-1}	$k_{AB,cld}$ x10^6/ s^{-1}	% different
AXI				**PTERO**			
2.23	2.09	2.00	-4.50	6.96	1.56	1.54	-1.23
4.46	1.98	2.00	1.00				

8.6. Discussion

To the best of our knowledge, only two models were proposed in the literature. Lente et al. [9] and Leifer [10] to interpret the mathematical equation to describe photochemical reactions for both the AB $(1\Phi)_{\varepsilon_{B\neq0}}$ and AB (2Φ) systems. Lente et al. [9] proposed a model for the photochemical reactions of the AB $(1\Phi)_{\varepsilon_{B\neq0}}$type that was used in several studies [11–14]. Leifer [10] on the other hand tackled the AB (2Φ) photochemical kinetics and the approached was employed in various studies [15–22]. Both models [9,10] were based on the rate equation (8-1), below.

$$rate = \frac{dC_A}{dt} = -\Phi_{A\rightarrow B}\sum_{\lambda_{irr}\,min}^{\lambda_{irr}\,max}\frac{\varepsilon_A^{\lambda_{irr}}C_A(t)}{\varepsilon_A^{\lambda_{irr}}C_A(t)+\varepsilon_B^{\lambda_{irr}}C_{B,i}(t)}P_{0,\lambda_{irr}}\left(1-10^{-\varepsilon_A^{\lambda_{irr}}C_A(t)l-\varepsilon_B^{\lambda_{irr}}C_{B,i}(t)l}\right) \quad \text{Eq.8-1}$$

Equation 8-1 is the same differential equation used for the photochemical reaction driven by monochromatic irradiation for AB $(1\Phi)_{\varepsilon_{B\neq0}}$, but in Eq. 8-1 the polychromatic irradiation is indicates by the summation over the wavelength of $P_{\lambda_{irr}}$and the molar absorption coefficients ($\varepsilon_A^{\lambda_{irr}}$and $\varepsilon_B^{\lambda_{irr}}$). It is important to underline that, in both models, the quantum yields were considered independent of the wavelength [9,10].

In the model was proposed by Lente et al. [9], the quantification of the quantum yield at the maximum observation wavelength used Eq. (8-2):

$$\Phi_{A\rightarrow B} = \frac{\alpha V}{\left(\varepsilon_A^{\lambda_{obs}}-\varepsilon_B^{\lambda_{obs}}\right)l_{obs}} \quad \text{Eq.8-2}$$

where α is the slope obtained from the linear correlation of ν_0 against photon count N. Eq. (8-2) was correlated to Eq. (8-1). Eq. (8-2) also seems to be correlated to the differential quantum yield equation ($\Phi_{A\rightarrow B} = \frac{rate}{P_{abs,\lambda_{irr}}}$). According to the Beer-Lambert law, if absorbance is used rather than concentration, and ($\frac{dA_{tot\,(t)}}{dt} = \left(\varepsilon_A^{\lambda_{obs}} - \varepsilon_B^{\lambda_{obs}}\right) l_{obs} \frac{dC_A}{dt}$), this will then add $\left(\left(\varepsilon_A^{\lambda_{obs}} - \varepsilon_B^{\lambda_{obs}}\right) l_{obs}\right)$ to the simple form equation. If one uses the number of photons absorbed by the system per volume, the mathematical expression of the $P_{abs,\lambda_{irr}}$ will be equal to ($\frac{P_{0,\lambda_{irr}}\left(1-10^{-A_{tot}^{\lambda_{irr}}}\right)}{V} = \frac{N}{V}$). Thus, the equation can be written in a simple form as ($-\frac{dA}{dt} = \left(\varepsilon_A^{\lambda_{obs}} - \varepsilon_B^{\lambda_{obs}}\right) l_{obs} \Phi_{A\rightarrow B} \frac{N}{V}$). The factor α is a result of the relation between the initial rate ($\frac{dA}{dt}$) and N and can be rewritten as $\alpha = \frac{\left(\varepsilon_A^{\lambda_{obs}} - \varepsilon_B^{\lambda_{obs}}\right) l_{obs}\, \Phi_{A\rightarrow B}}{V}$ (see Appendix VI-D).

This approach stipulates that, in order to calculate the value of α, one has to achieved the ν_0 and N values of the photochemical reactions. Hence, the initial rate of the reaction is inversely proportional to the volume of solution as described in the previous paragraph, which means less light being absorbed per a unit volume is equivalent to having a larger volume [9,12].

In this context, the effect of the light intensity on the reaction was obtained by using a constant light intensity and different volumes of the sample solutions. Hence, the rate of the reaction is proportional to the number of photons absorbed [9,12], where N can be represented by:

$$N = \int_{\lambda_{irr}\,min}^{\lambda_{irr}max} P_{0,\lambda_{irr}} \left(1 - 10^{-A_{tot}^{\lambda_{irr}}}\right) d\lambda_{irr} \qquad \text{Eq.8-3}$$

However, due to the difficulty in solving reported the system's the differential equation (Eq.8-1), and numerical method were required. Also, the molar absorption coefficient of the photoproduct (as example of trichlorophenol (TCP)) was calculated from the commercially available of photoproduct [12]. This model [9] was used to determine the quantum yield, of dichloroquinone and its derivatives in aqueous solution [11–14]. It was concluded that the quantum yield was both pH dependent and wavelength independent, and that the α value depended on the substituents on the quinone.

This approached [9] has however some limitations for instance, different photoproducts usually formed during the photochemical reaction of the TCP or its derivatives [11–14]. This means that the mechanism of these compounds is not that adopted to AB $(1\Phi)_{\varepsilon_{B\neq 0}}$. In this case the equations described here Eq. 8-1 and 8-2 do not correspond to the physical system studied (i.e. TCP). Rather, the photochemical reactions in these compounds obeyed consecutive photoreactions mechanism not unimolecular AB $(1\Phi)_{\varepsilon_{B\neq 0}}$. This model [9] is therefore not accurate to describe the photochemical reaction of TCP due to the formation several photoproducts.

Moreover, one study [13] reported a variation between the values of the quantum yields obtained from ν_0 and those estimated by fitted from the experimental curve using numerical methods. The author's suggested that the observed difference was due to the assumption that compound (A) is the alone light absorbing species in the reactive medium[13]. One can also assume that due to the irradiation path length not being

considered in the equations (Eqs. 8-1, 8-2), there might be an inconsistency when the volume increases the I_{irr} will increase, and hence ν_0 should also increase.

Even though, the quantum yield of TCP in aqueous solutions ($\Phi_{A\rightarrow B}$= 0.057 at 312 nm), was considered independent of wavelength [11–14], it important to stress that in previous studies [23,24] it was reported to vary between 0.022 and 0.03 at 452 nm and in the UV range (185-436 nm), respectively. Therefore, such a significant difference between the quantum yield values tends to confirm that the quantum yields of TCP are rather wavelength dependent. This contradicts the original assumption in Lente approach [9] that quantum yield is wavelength independent.

Therefore, in this method the initial rate of the absorbance was used to determine the quantum yield of the photochemical reaction. However, by doing so one cannot indicate the reduction in the rate of the reaction. The photostabilisation of the compound can be observed as a reduction in the rate constant of the photochemical reaction, which is difficult to obtain from this method due to difficulties in integrating the differential equation (Eq.8-1). The rate constant can inform about the factors that affect or reductions of the reaction such as photon absorbed by the system.

The second photokinetic model used to study the AB (2Φ) photodegradation kinetics of the different compounds in the aquatic environment [10], relates to the kinetic method proposed by Zepp [25] and which itself was used in several studies [15–22]. The modification to Zepp's model was the addition of the sum on the wavelength dependent

parameters such as $P_{0,\lambda_{irr}}\ and\ \varepsilon_A^{\lambda_{irr}}$, whereas, here as well $\Phi_{A\to B}$ was assumed to be constant [10].

The model used the differential equation (8-1) but imposed that, the total absorbance at all wavelengths must be lower than 0.02, which means that light absorption is weak. This allowed to consider a Simpson expansion of Eq. (8-1), that was then simplified to:

$$\frac{dC_A}{dt} = -2.303\Phi_{A\to B} l C_A(t) \sum_\lambda P_{0,\lambda_{irr}} \varepsilon_A^{\lambda_{irr}} \qquad \text{Eq.8-4a}$$

Eq.8-4a was integrated to lead to a first-order kinetics model.

$$\ln\frac{C_0}{C_t} = kt = \left(2.303\Phi_{A\to B} l \sum_\lambda P_{0,\lambda_{irr}} \varepsilon_A^{\lambda_{irr}}\right)t \qquad \text{Eq.8-4b}$$

Where k is the apparent pseudo first-order photoreaction rate constant.

The value of the quantum yield can then be quantified by Eq. (8-5)

$$\Phi_{A\to B} = \frac{k}{2.303 l \sum_\lambda P_{0,\lambda_{irr}} \varepsilon_A^{\lambda_{irr}}} \qquad \text{Eq.8-5}$$

In order to apply this method to calculate the quantum yield, the experimental traces were observed using various analytical methods, such as, HPLC. The photokinetic traces were then fitted to first-order kinetics Eq. (8-4b) to obtain the apparent rate constant (k). After that, the quantum yield was quantified using Eq. (8-5) [15–22].

Nevertheless, there was some issues in this model [10] which resulted from the use of the expansion in Eq. (8-1) in order to get Eq. (8-4a), wherein Eq. (8-4a) has simplified variant of Eq. (8-1). However, the use of the expansion in Eq. (8-4a) will make it difficult to find the amount of the light absorbed by compound (A). In other words, when the concentration of compound (A) changes during the reaction, then the amount of light

absorbed by the compound (A) will also change in accordance with the photoproduct that has been formed, which in turn will itself absorb the incident light [26]. Therefore, using Eq. (8-4a) results in that only compound (A) apparently absorbing all the incident light. The results suggest that Eq. (8-4a) cannot be considered due to the loss of the indicator factor of light absorbed by the compound when using the expansion, which is called the photokinetic factor.

It is interesting to observe that while, mathematically, k is concentration independent as suggested in Eq.8-4b. Previous studies [27,28], using this method [10], found that experimental rate constant of the photodegradation of naphthalene and oxytetracycline varied with concentration. This contradiction between theory (Eq.8-4b) and experiment might be due to approximation adopted in the derivation of Eq.8- 4 as discussed above.

From the experimental observations, the application of the photochemical reaction method from [10] was not particularly consistent because the model does not consider the amount light absorbed by both compounds, which has certain limitations in terms of representing essential parameters in the photochemical reaction with regard to the light absorbed.

The analysis presented here for the two models [9,10], shows a lack in the literature for a comprehensive method that has physical chemistry background does not rely on assumptions, and whose predications are observed experimentally.

The model proposed in this work indicated that the overall rate constant of unimolecular and reversible photochemical reactions depends on photochemical reaction parameters

such as $\Phi_{A\to B}^{\lambda_{irr}}$, $\Phi_{B\to A}^{\lambda_{irr}}$,$\varepsilon_{A}^{\lambda_{irr}}$, $\varepsilon_{B}^{\lambda_{irr}}$, and $P_{\lambda_{irr}}$, as per experimental conditions. Also, the mathematical formulation of Eqs. (6-10) and (6-11) indicated that the overall rate constant was concentration independent. In addition, there was a distinct correlation between the findings for the mathematical and experimental overall rate constants, where the overall rate constant was concentration independent. When compared with reference [10], the experimental rate constant in the second method [10] does not correlate with the mathematical prediction, as mention above [27,28]. The experimental values for the rate constant are thus meaningful for the experiment under particular conditions because they are, in this instance, representative of the photochemical reaction parameters. However, it is difficult to use a rate constant to compare different experiments on the same compound due to the difficulty in obtaining the same $P_{\lambda_{irr}}$ for each experiment. From this perspective, it is important to quantify all fundamental photochemical parameters before comparing experiments.

Furthermore, in this study, the quantum yields were wavelength dependent due to the quantum yield being depend on parameters such as $\varepsilon_{A}^{\lambda_{irr}}$, $\varepsilon_{B}^{\lambda_{irr}}$ and $F_{\lambda_{irr}}$, which are themselves inherently wavelength dependent; by comparison, quantum yield was considered wavelength independent in the first and second models [9,10], without providing tangible experimental proof for it.

The study results suggested that a good fit to all photokinetic traces for both systems AB $(1\Phi)_{\varepsilon_{B\neq 0}}$ and AB (2Φ) can be achieved with the η-order kinetics model. This finding confirmed that the study compounds obeys η-order kinetics. The method applied here

was useful to studying those compounds selected (AB $(1\Phi)_{\varepsilon_{B\neq0}}$ and AB (2Φ)) systems, and will helpfully describe and rationalise photostability and photokinetics.

8.7. Conclusion

A new kinetic order (η-order) was designed to describe the photodegradation of systems AB $(1\Phi)_{\varepsilon_{B\neq0}}$and AB (2Φ) as driven by polychromatic light. These results strongly suggest that the photodegradation reactions of studies compounds in ethanol are better described by the η-order kinetics than classical thermal kinetic orders (which are, in a practical sense, not useful in these instances). The overall rate constant, k_η, was found to be dependent on $\Phi_{\mathrm{A}\rightarrow\mathrm{B}}$, $\Phi_{\mathrm{B}\rightarrow\mathrm{A}}$,$\varepsilon_A^{\lambda_{irr}}$, $\varepsilon_B^{\lambda_{irr}}$, and $P_{\lambda_{irr}}$, but was concentration independent. This study strongly suggests that studies compounds should be protected from light under all circumstances.

8.8. References

1. ICH. ICH Guidance on Analytical Method Validation. Proceedings of the International Conference on Harmonisation. 1996; (November). Available at: DOI:10.1136/bmj.333.7574.873-a
2. Piechocki JT., Thoma K. Pharmaceutical photostability and stabilization technology. Informa Healthcare; 2007. 445 p.
3. Maafi W., Maafi M. Modelling nifedipine photodegradation, photostability and actinometric properties. International Journal of Pharmaceutics. Elsevier B.V.; 2013; 456(1): 153–164. Available at: DOI:10.1016/j.ijpharm.2013.07.075
4. Maafi M., Maafi W. Montelukast photodegradation: Elucidation of Φ-order kinetics, determination of quantum yields and application to actinometry. International Journal of Pharmaceutics. 2014; 471(1–2): 544–552. Available at: DOI:10.1016/j.ijpharm.2014.05.016
5. Maafi W. Modelling and elucidation of photoreaction kinetics - Applications and actinometry using nifedipine, nisoldipine, montelukast, fluvoxamine and

riboflavin. De Montfort University; 2016; Available at: https://www.dora.dmu.ac.uk/handle/2086/13110

6. Lee LY. Study Of The Photodegradation And Photostability Of Anti-Cancer Drugs In Different Media Towards The Development Of Both New Actinometers And Liquid Formulations. De Montfort University; 2016; Available at: https://www.dora.dmu.ac.uk/handle/2086/12188

7. Maafi M., Maafi W. Quantitative assessment of photostability and photostabilisation of Fluvoxamine and its design for actinometry. Photochemical and Photobiological Sciences. 2015; 14(5): 982–994. Available at: DOI:10.1039/c5pp00022j

8. Maafi M., Lee LY. Determination of Dacarbazine Φ-Order Photokinetics, Quantum Yields, and Potential for Actinometry. Journal of Pharmaceutical Sciences. Elsevier Masson SAS; 2015; 104(10): 3501–3509. Available at: DOI:10.1002/jps.24568

9. Fábián I., Lente G. Light-induced multistep redox reactions: The diode-array spectrophotometer as a photoreactor. Pure and Applied Chemistry. 2010; 82(10): 1957–1973. Available at: DOI:10.1351/PAC-CON-09-11-16

10. Leifer A. The kinetics of environmental aquatic photochemistry : theory and practice. American Chemical Society; 1988. 304 p.

11. Gombár M., Józsa É., Braun M., Ösz K. Construction of a photochemical reactor combining a CCD spectrophotometer and a LED radiation source. Photochemical and Photobiological Sciences. 2012; 11(10): 1592–1595. Available at: DOI:10.1039/c2pp25166c

12. Pino-Chamorro JÁ., Ditrói T., Lente G., Fábián I. A detailed kinetic study of the direct photooxidation of 2,4,6-trichlorophenol. Journal of Photochemistry and Photobiology A: Chemistry. Elsevier B.V.; 2016; 330: 71–78. Available at: DOI:10.1016/j.jphotochem.2016.07.025

13. Józsa É., Kiss V., Ősz K. Photochemical processes of 1,4-benzoquinones in aqueous medium. Journal of Photochemistry and Photobiology A: Chemistry. 2018; 360(December 2017): 166–173. Available at: DOI:10.1016/j.jphotochem.2018.04.024

14. Lente G., Espenson JH. Photoreduction of 2,6-dichloroquinone in aqueous solution: Use of a diode array spectrophotometer concurrently to drive and detect a photochemical reaction. Journal of Photochemistry and Photobiology A: Chemistry. 2004; 163(1–2): 249–258. Available at: DOI:10.1016/j.jphotochem.2003.12.005

15. Apell JN., McNeill K. Updated and validated solar irradiance reference spectra for estimating environmental photodegradation rates. Environmental Science:

Processes & Impacts. Royal Society of Chemistry; 2019; : 427–437. 8a

16. Oliveira C., Lima DLD., Silva CP., Calisto V., Otero M., Esteves VI. Photodegradation of sulfamethoxazole in environmental samples: The role of pH, organic matter and salinity. Science of the Total Environment. Elsevier B.V.; 2019; 648: 1403–1410. Available at: DOI:10.1016/j.scitotenv.2018.08.235

17. Yassine M., Fuster L., Dévier MH., Geneste E., Pardon P., Grélard A., et al. Photodegradation of novel oral anticoagulants under sunlight irradiation in aqueous matrices. Chemosphere. 2018; 193: 329–336.

18. Mazellier P., Méité L., De Laat J. Photodegradation of the steroid hormones 17β-estradiol (E2) and 17α-ethinylestradiol (EE2) in dilute aqueous solution. Chemosphere. Elsevier Ltd; 2008; 73(8): 1216–1223.

19. Calisto V., Domingues MRM., Esteves VI. Photodegradation of psychiatric pharmaceuticals in aquatic environments - Kinetics and photodegradation products. Water Research. 2011; 45(18): 6097–6106.

20. Wols BA., Harmsen DJH., Beerendonk EF., Hofman-Caris CHM. Predicting pharmaceutical degradation by UV (MP)/H2O2 processes: A kinetic model. Chemical Engineering Journal. Elsevier B.V.; 2015; 263: 336–345.

21. Stefan MI., Bolton JR. Fundamental approach to the fluence-based kinetic and electrical energy efficiency parameters in photochemical degradation reactions: Polychromatic light. Journal of Environmental Engineering and Science. 2005; 4(SUPPL. 1): 13–18. Available at: DOI:10.1139/s04-026

22. Galbavy ES., Ram K., Anastasio C. 2-Nitrobenzaldehyde as a chemical actinometer for solution and ice photochemistry. Journal of Photochemistry and Photobiology A: Chemistry. 2010; 209(2–3): 186–192.

23. Hu M., Wang Y., Xiong Z., Bi D., Zhang Y., Xu Y. Iodine-sensitized degradation of 2,4,6-trichlorophenol under visible light. Environmental Science and Technology. 2012; 46(16): 9005–9011. Available at: DOI:10.1021/es301577p

24. Benitez FJ., Beltran-Heredia J., Acero JL., Rubio FJ. Chemical decomposition of 2,4,6-trichlorophenol by ozone, Fenton's reagent, and UV radiation. Industrial and Engineering Chemistry Research. 1999; 38(4): 1341–1349.

25. Zepp RG. Quantum Yields for Reaction of Pollutants in Dilute Aqueous Solution. Environmental Science and Technology. 1978; 12(3): 327–329. Available at: DOI:10.1021/es60139a010

26. Mauser H (Heinz)., Gauglitz G (Günter). Photokinetics : theoretical fundamentals and applications. Elsevier; 1998. 555 p.

27. Jing L., Chen B., Zhang B., Zheng J., Liu B. Naphthalene degradation in seawater by UV irradiation: The effects of fluence rate, salinity, temperature and initial concentration. Marine Pollution Bulletin. Elsevier Ltd; 2014; 81(1): 149–156.

28. Jin X., Xu H., Qiu S., Jia M., Wang F., Zhang A., et al. Direct photolysis of oxytetracycline: Influence of initial concentration, pH and temperature. Journal of Photochemistry and Photobiology A: Chemistry. Elsevier B.V.; 2017; 332: 224–231.

Chapter 9

Development of actinometers

9.1. Introduction

The rates at which photochemical reactions proceed are related to the number of photons absorbed. Therefore, it is important to determine the number of the photons absorbed by a molecule during any given photochemical reaction. The number of photons absorbed is obtained using actinometry [1].

Chemical actinometry is achieved by the irradiation of the sample at a fixed concentration and maintaining all other conditions, with the except that light intensity is varied. The rate at which the molecule reacts can thus be determined, as is normally quantified via determining the change in concentration of the principal reagent and photoproduct after irradiation for given length of time. Once the rate of the photoreaction actinometer has been quantified, using the known quantum yield (Φ) of the specific chemical actinometer, the photon flux (N) can then be determined using Eq.9-1 [1].

$$P_{abs,\lambda_{irr}} = \frac{rate}{\Phi} \qquad \text{Eq. 9-1}$$

According to the limitations of chemical actinometers, as ferrioxalate requires working in dark and time consuming due to it is need to special analytical procedure, and physical actinometers (which is need to calibrated), as described in chapter 2, the aim of this chapter is to use the Φ-order and η-order kinetics to develop new, accurate and easy to implement actinometers for monochromatic and polychromatic studies.

9.2. Results and discussion

9.2.1. Development of actinometry under irradiation by monochromatic light

In order to test the validity of this new procedure, freshly prepared ORVT solutions were subject to irradiation using beams of different radiant powers at one of the six UVA monochromatic wavelengths (λ_{irr} =295, 310, 328, 340, 350 and 360 nm). For a specified λ_{irr}, the experimental photokinetic traces obtained for the sequence values of radiant power (Fig. 9-1) were each fitted with the model described by Eq. 5-4. A good fit was observed for these photokinetic traces, further confirming that ORTV as example obeys Φ-order kinetics. Linear relationships were obtained for the variation of the overall rate constant (k) and radiant power values (P) for each λ_{irr} (inset in Fig.9-1).

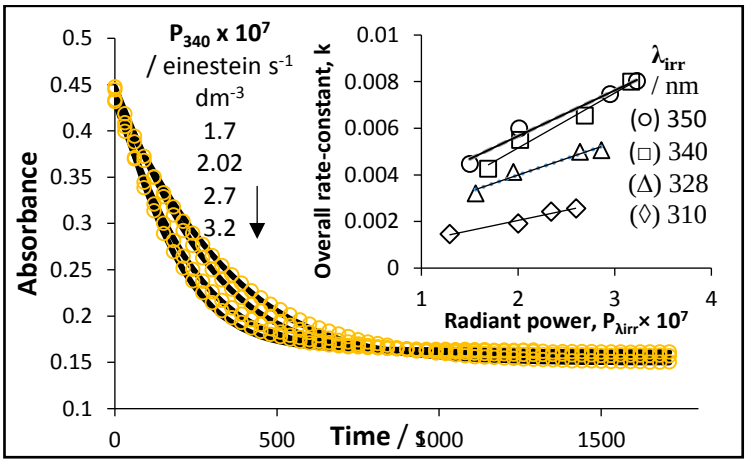

Figure 9- 1: Effect of increasing the radiant power of the monochromatic irradiation beam on the photokinetic traces of t-ORVT (2 × 10^{-5} M) at 340 nm. The experimental data (circles) were fitted by Eq. 5-3. Inset: Linear correlation of $k_{A\rightleftharpoons B}^{\lambda_{irr}}$ (in s^{-1}) with $P_{\lambda_{irr}}$ (in einstein s^{-1} dm^{-3}) for each.

The $\beta_{\lambda_{irr}}$ factor values were calculated from the experimental data, as described in Table 5, Chapter 5, as based on Eq.5-4. By plotting the $\beta_{\lambda_{irr}}$ factor values against the

corresponding wavelengths, a sigmoid-shaped graph is obtained (Fig.1, Eq.9-2), except the O-DAE is triangle-shape graph.

$$k_{A\leftrightarrows B}^{\lambda_{irr}} = \left(\Phi_{A\to B}^{\lambda_{irr}} \times \varepsilon_A^{\lambda_{irr}} + \Phi_{B\to A}^{\lambda_{irr}} \times \varepsilon_B^{\lambda_{irr}}\right) \times l_{\lambda_{irr}} \times P_{\lambda_{irr}} \times F_{\lambda_{irr}}(pss) = \beta_{\lambda_{irr}} \times P_{\lambda_{irr}}$$ Eq.5-4

The advantages of Eq.9-2 are both to allow the $\beta_{\lambda_{irr}}$ values to be obtained at any wavelength in the range studied, and to facilitate the determination of the radiant power ($P_{\lambda_{irr,x}}$) of an unknown source, assuming a monochromatic wavelength ($\lambda_{irr,x}$) is used. $\beta_{\lambda_{irr}}$ allows us then to develop a new actinometric method. This can be simply obtained using the ratio $P_{\lambda_{irr,x}} = k_{A\rightleftharpoons B}^{\lambda_{irr,x}}/\beta_{\lambda_{irr}}$, where these parameters correspond to the $\beta_{\lambda_{irr}}$ value calculated using Eq. (9-2) for $\lambda_{irr,x}$, and $k_{A\rightleftharpoons B}^{\lambda_{irr,x}}$, as obtained by irradiating ethanolic solutions in studies of stilebinods compounds by the monochromatic beam (at $\lambda_{irr,x}$) and by fitting its trace to Eq. 5-3 (chapter 5).

$$\beta_{\lambda_{irr,X}} = A + \frac{B}{1+C\times e^{-D(\lambda_{irr}-E)}}$$ Eq. 9-2a

Where the values of A, B, C, D and E are given in Table 9-1.

Table 9- 1: *Values of equation 9-2a.*

Compound (X)	A	B	C	D	E
t-STIL	1550	38900	62	0.1	251
PINO	5500	14400	1.35	0.11	297
RVT	2303	38500	79	0.101	256
ORVT	2220	23900	139	0.088	260
PTERO	700	38500	96	0.084	242
C-DEA	3100	4000	0.12	0.08	510

In the case of DAE, the following equations were obtained:

$$\beta_{\lambda_{irr,O-DAE\,(280-350)}} = 32.32 \times \lambda_{irr} - 3236.1 \qquad \text{Eq. 9-2b}$$

$$\beta_{\lambda_{irr,O-DAE\,(350-380)}} = -93.65 \times \lambda_{irr} + 41018 \qquad \text{Eq. 9-2c}$$

The linear trend for DAE is characterised by a positive gradient for O-DAE and a negative slope for C-DAE.

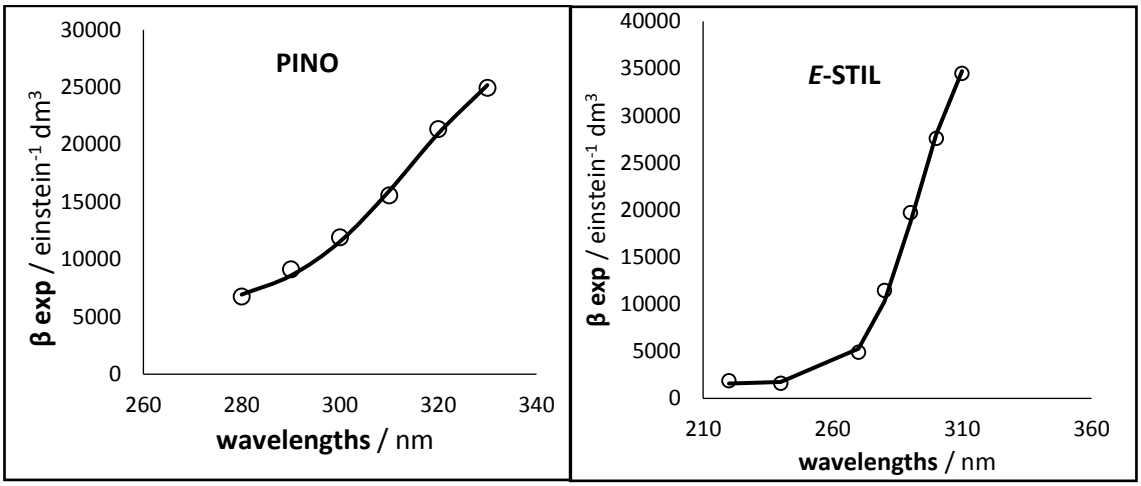

Figure 9- 2: Calculated $\beta_{\lambda_{irr}}$ values (circles) for E-STIL and PINO using Eq. 5-4 and the values of $k_{A\rightleftharpoons B}^{\lambda_{irr}}$ and $P_{\lambda_{irr}}$ provided in Table 5-5, Chapter 5. The sigmoid model, Eq.9-2 (line) was used to fit the experimental data.

For the purposes of this study, the several radiant power values of these experiments were considered unknown and were determined as stated above (using the Φ-order rate constants found for each irradiation). The reliability of the method is indicated by a good correlation between the experimental $P_{cld.}$ and the calculated $P_{\text{exp.}}$ values of the radiant power (Fig.9-3). The straight line is characterised by a slope close to unity and a small intercept (see Appendix V).

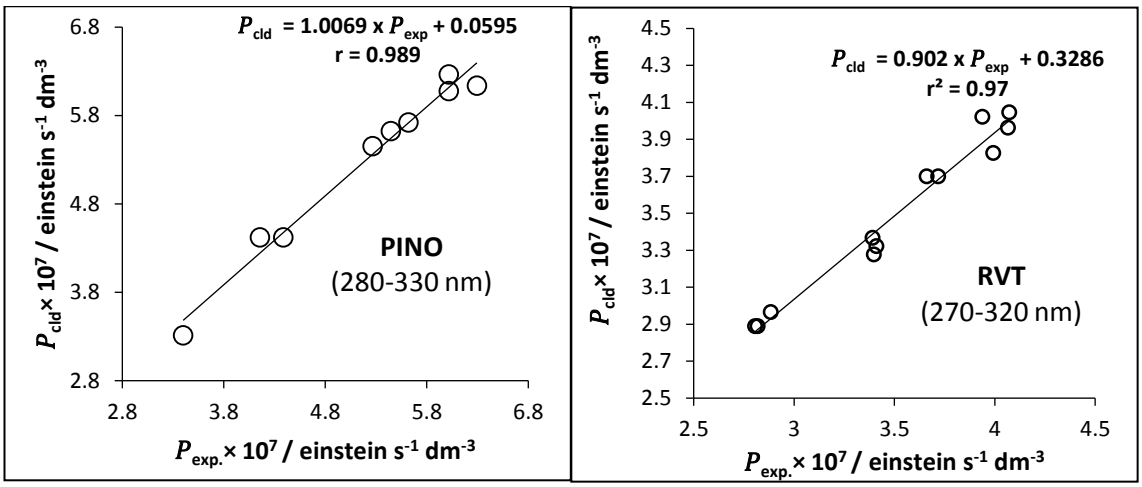

Figure 9- 3: Linear correlation of experimental $P_{exp.}$ with calculated $P_{cld.}$ values of the radiant power for PINO and RVT as example of stilebinods.

9.2.2. Development of actinometry for the studies of compounds irradiated under polychromatic light

In the polychromatic light irradiation studies, the orders Φ and η can be used to develop new actinometers under polychromatic light.

These experiments were exposed to different radiation power such as 400-600 nm for AB $(1\Phi)_{\varepsilon_{B=0}}$, and 200-400 nm for systems AB $(1\Phi)_{\varepsilon_{B\neq0}}$ and AB (2Φ). The kinetic traces are fitted by a particular order kinetic, as Φ- and η-order, which are dependent on the type of photoreaction, as described in Chapters 7 and 8. The $\sum \beta_{AB}$ factor values can be calculated from the gradient of the linear relationship between the overall rate constant and the sum of the radiant powers (Eq. 9-3).

$$\boldsymbol{k} = \sum \boldsymbol{\beta_{AB}} \times \sum \boldsymbol{P}\,(\lambda_i) \qquad \text{Eq.9-3}$$

9.2.2.1. C-DAE actinometric potential

The actinometric potential of C-DAE can be developed by exposing fresh solutions of 4.33 x 10^{-6} M to several polychromatic light intensities in the range 400-800 nm. A good fit with Eq.6-1 was observed for the experimental traces (Fig. 9-4), confirming that the C-DAE obeys Φ-order kinetics. A straight line was found when plotting $k_{AB,cld}$ against $\sum \boldsymbol{P}(\lambda_i)$, with the intercept around zero and a correlation coefficient of 0.998 (Fig. 5a). The value of the gradient of the straight line was expressed as factor called $\sum \beta_{AB}$ (Eq.6-2) [2–6].

$$C_A(t) = \frac{1}{\left(\frac{l_{\lambda_{irr}}}{l_{obs}} \times \sum \varepsilon_A\right)} \times \log\left(1 + \left(-1 + 10^{\left(\frac{l_{\lambda_{irr}}}{l_{obs}} \times \sum A_0\right)}\right) \times e^{(-k_{AB}t)}\right) \quad \text{Eq.6-1}$$

$$k_{AB} = \ln 10 \times l_{\lambda_{irr}} \times \sum(\Phi_{AB} \times \varepsilon_A \times P) = \sum \beta_{AB} \times \sum P(\lambda_i) \quad \text{Eq.6-2}$$

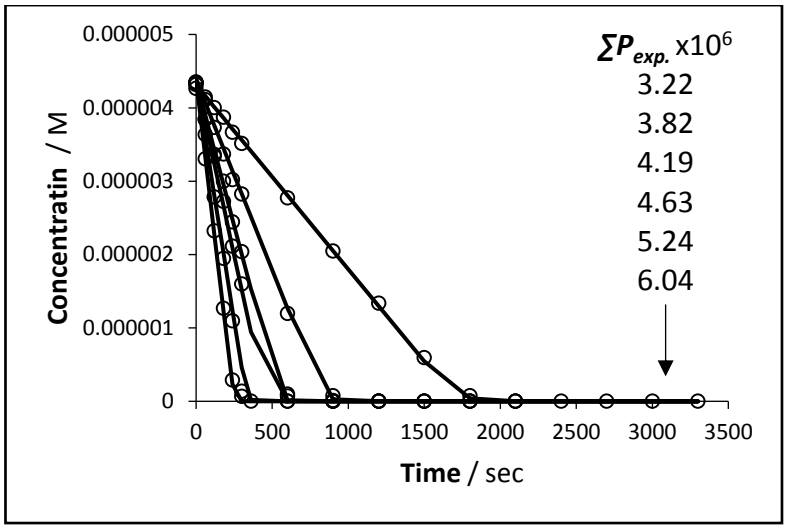

Figure 9- 4: Effect of increasing the radiant power of the polychromatic irradiation beam using LED torch lamp on the photokinetic traces of C-DAE (4.35 × 10^{-6} M) between range 400-600 nm. The experimental data (circles) were fitted by Eq. 6-1.

In addition, the actinometry study can be achieved using the initial velocity (gradient of the linearity of the first point of the experiments data against time) of each experimental

trace. A good linear relationship between the initial velocity and the radiation power (Fig. 9-5b) was observed. This finding confirms that the Φ-order model described the AB $(1\Phi)_{\varepsilon_{B=0}}$ photoreaction under polychromatic light well. The gradient achieved from the equation of the linear relationship between the ν_0 and $\sum P_{exp.}(\lambda_i)$ was expressed as $\sum \delta$ (Eq.9-4) [6].

$$\upsilon_0 = \frac{\ln 10 \times l_{\lambda_{irr}} \times \sum(\Phi_{AB} \times \varepsilon_A \times P)}{\sum \varepsilon_A \times l_{\lambda_{irr}} \times \ln 10} = \sum \delta \times \sum P(\lambda_i) \qquad \text{Eq.9-4}$$

Table 9- 2: Actinometry study of C-DAE

$C_A\ (0) \times 10^6$ / M	$\sum P_{exp.}(\lambda_i) \times 10^6$ / einstein s^{-1} dm^{-3}	k / sec^{-1}	-Slope $\times 10^7$ / sec^{-1}
4.26	3.22	0.016	0.026
4.35	3.82	0.033	0.057
4.33	4.19	0.048	0.076
4.35	4.63	0.058	0.093
4.34	5.24	0.082	0.127
4.32	6.04	0.107	0.168

* where $\sum \varepsilon_B(\lambda_i)$ is 1323914.19 M^{-1} cm^{-1}

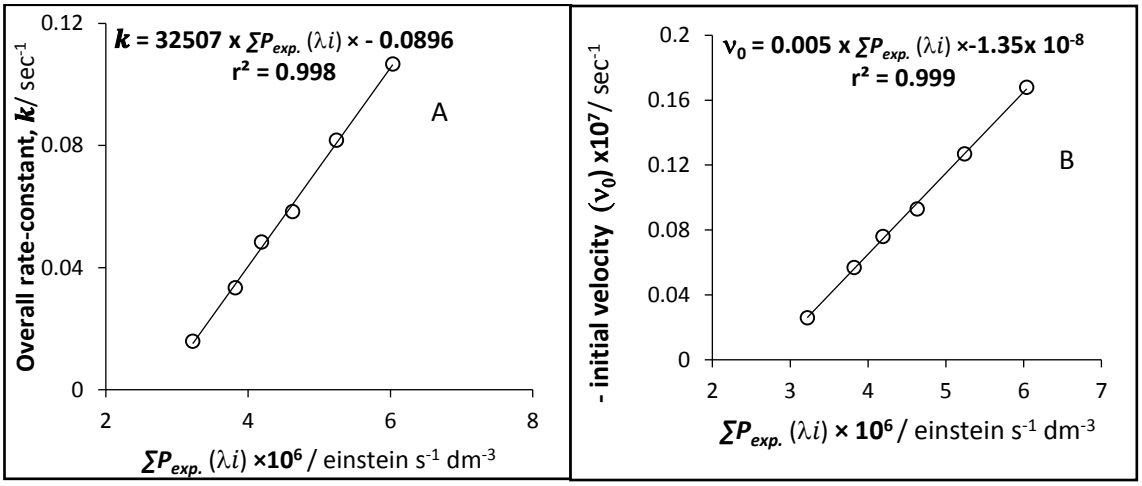

*Figure 9- 5: **(a)** Linear relation between Overall rate-constant (k) of C-DAE with $\sum P_{exp.}(\lambda_i)$. **(b)** Linear relation between initial velocity (gradient) of C-DAE with $\sum P_{exp.}(\lambda_i)$.*

The values of $\sum \beta_{AB}$ and $\sum \delta$ are not related to each other and are obtained differently, as shown by Eqs. 9-3 and 9-4. These values were used to determine the sum of the light intensity of the polychromatic light beam in the range 400-600 nm. By using these factors, the values of $\sum P_{cld.}\,(\lambda_i)$ so quantified were correlated to the experiment with an error of less than 5% and a correlation coefficient of 0.999 with an intercept around zero, which mean that values above correlate well with each other.

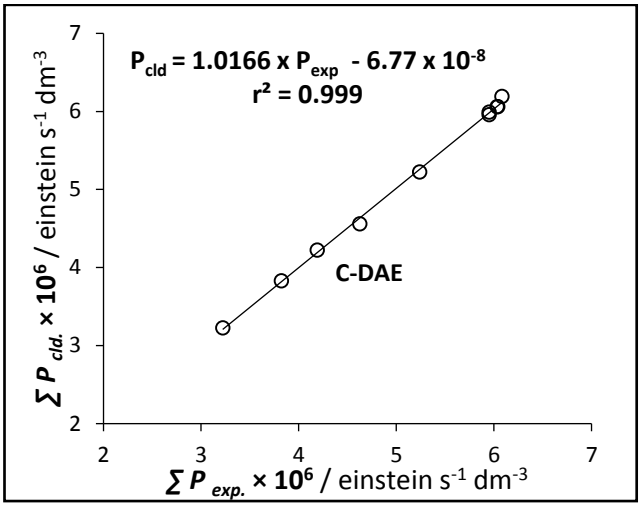

Figure 9- 6: Linear correlation of experimental ($\sum P_{exp.}\,(\lambda_i)$) with calculated ($\sum P_{cld.}\,(\lambda_i)$) values of the radiant power for C-DAE studied under polychromatic light irradiation using LED Torch (visible light).

9.2.2.2. NIF, DBZ, stilebinods group, AXI and O-DAE actinometric potentials

It is interesting to note that the η-order (Chapter 8) was offered to the actinometric method developed for NIF, DBZ (as an example of AB $(1\Phi)_{\varepsilon_{B\neq 0}}$), the stilebinods group, AXI and O-DAE (as an example of AB (2Φ) system).

The potential of the studied compounds, as actinometers, were set out in a series of fresh ethanolic solutions from each compound and subjected to varying intensities of

polychromatic light (in the range 200-400 nm). The photokinetic traces of the studied compounds were well fitted to the η-order equation, and these fits were used to obtain the overall rate-constants. The photochemical reaction became faster with high values of the $\sum P_{exp.}(\lambda_i)$. In addition, as predicted by the pervious equation Eq.9-3, the linear relationship found between the $\boldsymbol{k_\eta}$ and $\sum P_{exp.}(\lambda_i)$ had a correlation coefficient of around 0.99 and an intercept close to zero (Fig. 9-7; Table 9-3).

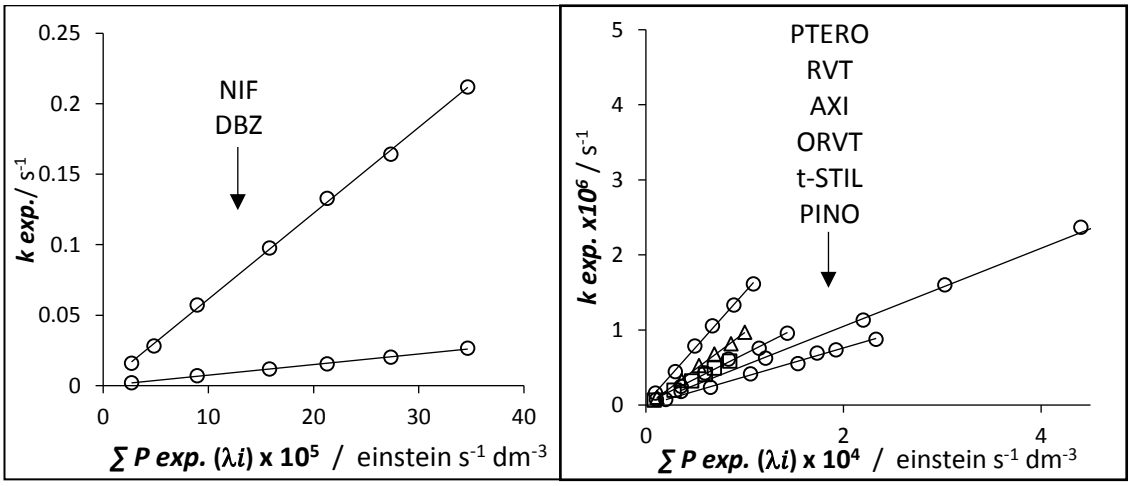

Figure 9- 7: ***a,b.*** *Linear relation between Overall rate-constant (k) and* $\sum P_{exp.}(\lambda_i)$

Furthermore, there is a new and straightforward method by which to quantify the $\sum \beta_{AB}$ factors without follow the reactions to completion. This method was performed by a using a fresh ethanolic solution at same concentrations as the studied compounds (Table 9-3). These concentrations were subject to irradiation under different polychromatic light intensities for the same period of time as each experiment. The concentrations after exposure to this light were obtained by HPLC. Then, by using the Φ- and η-order kinetics, the η function was determined by using Eq.6-5. The overall rate constant (k)

was achieved through rearranging Eqs. (6-4 and 9-5) for the η- and Φ-orders, respectively. Once k was determined for each sum of light intensities, the plot of k against $\sum P_{exp.}(\lambda_i)$ should be found to be linear, as predicated in Eq. 9-3. Therefore, the value of $\sum \beta_{AB}$ can be quantified from the gradient of the linear relationship between k and $\sum P_{exp.}(\lambda_i)$, as per the previous method.

$$\eta(t) = -k_\eta t \qquad \text{Eq.6-4}$$

$$\eta(t) = \left(C_{A_t} - C_{A_0}\right) \times \alpha + \gamma \times Ln\, \frac{C_{A_t}+\delta}{C_{A_0}+\delta} \qquad \text{Eq.6-5}$$

$$k_{AB} = l_{\lambda_{irr}} \times \left(\frac{1}{t} \times ln \frac{\left(-1+10^{C_A\,(t)\times \sum \varepsilon_A}\right)}{\left(-1+10^{\sum A_0)}\right)}\right) \qquad \text{Eq.9-5}$$

where $\boldsymbol{\alpha}$, $\boldsymbol{\gamma}$ and $\boldsymbol{\delta}$ are factors that are dependent on the type of reaction, as described in Chapter 6.

In order to test the validity of this method, the percentage errors between the $\sum \beta_{AB}$ factors calculated by this method and the previous procedure were found to be less than 5%. This indicated that the method was valuable, applicable and time efficient, as illustrated in Fig. (9-8).

Table 9- 3:. Equations for calculation of the radiant power $\sum \beta_{AB}$ using the compounds studied in ethanol under polychromatic light irradiation.

Compound	**Concentration × 10^5** / M	**Linearity Equation of (k) with $\sum \boldsymbol{P_{exp.}}(\lambda_i)$**	**Correlation coefficient, (r^2)**
NIF	2.69	$\boldsymbol{k}$= 1365.3 x $\sum \boldsymbol{P_{exp.}}$+ 6 x 10^{-5}	0.99
DBZ	2.30	$\boldsymbol{k}$ = 211.07 x $\sum \boldsymbol{P_{exp.}}$ - 1 x 10^{-5}	0.99
STIL	1.28	$\boldsymbol{k}$ = 0.0052 x $\sum \boldsymbol{P_{exp.}}$ + 8 x 10^{-9}	0.99

Compound	Concentration × 10^5 / M	Linearity Equation of (k) with $\sum P_{exp.}(\lambda_i)$	Correlation coefficient, (r^2)
PINO	2.12	k = 0.0038 x $\sum P_{exp.}$ - 6 x 10^{-9}	0.99
RVT	2.11	k = 0.0098 x $\sum P_{exp.}$ - 1 x 10^{-8}	0.99
ORVT	2.41	k = 0.0069 x $\sum P_{exp.}$ + 2 x 10^{-9}	0.99
PTERO	2.01	k = 0.0148 x $\sum P_{exp.}$ + 2 x 10^{-8}	0.99
AXI	1.37	k = 0.0066 x $\sum P_{exp.}$ - 2 x 10^{-8}	0.99
O-DAE	0.436	k = -0.01 x $\sum P_{exp.}$ - 1 x 10^{-8}	0.99

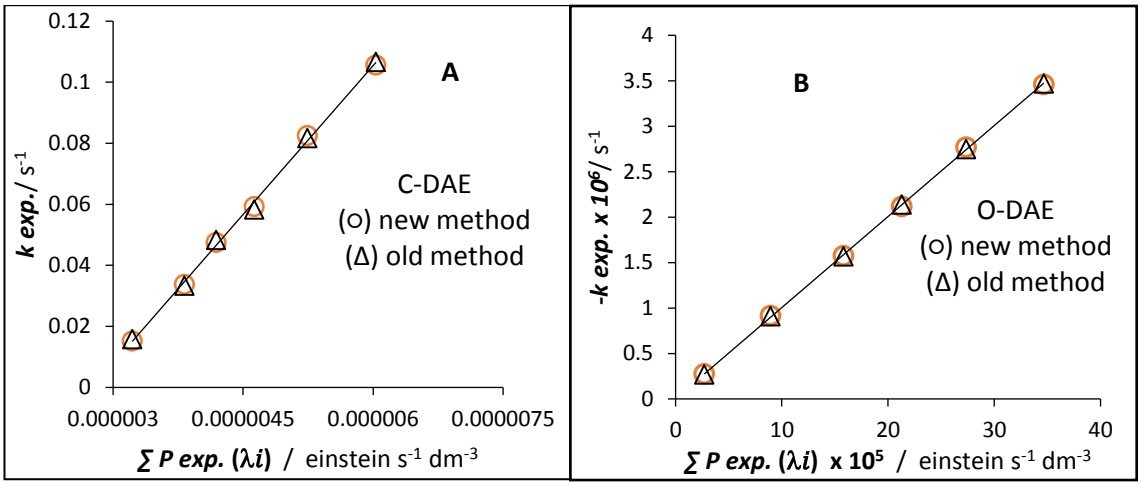

Figure 9- 8: The linear relation between overall rate-constant (k), applying Φ (A) and η (B), with $\sum P_{exp.}(\lambda_i)$; the circles represent the results for the new method and the tringles represent the results for the old method.

The $\sum \beta_{AB}$ factors were obtained from the gradient of the linearity between the k_η and $\sum P_{exp.}(\lambda_i)$. It important to say that the $\sum \beta_{AB}$ factors values for each compound are useful to quantify the sum of the polychromatic light intensity of unknown sources once Eq.9-3 has been rearranged. The accuracy of this method is demonstrated by the excellent correlation between the values of light intensities for the experiment and the

calculations, with a correlation coefficient of 0.99, which means that the two values of light intensities are essentially identical to each other (Fig. 9-9).

$$\sum \boldsymbol{P}(\lambda_i) = \frac{\boldsymbol{k_\eta}}{\sum \boldsymbol{\beta_{AB}}} \qquad \text{Eq.9-3}$$

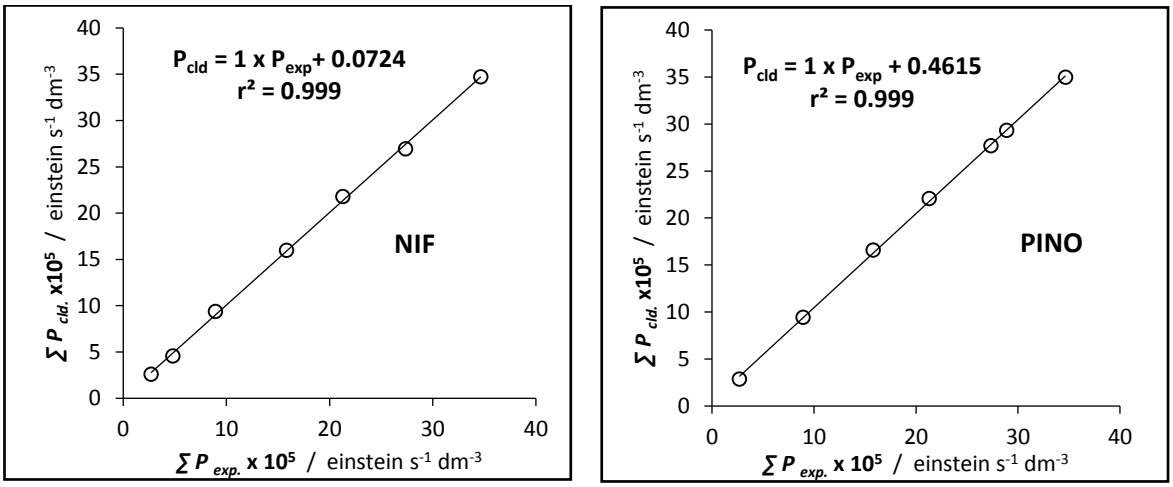

Figure 9- 9: Linear correlation of experimental ($\sum \boldsymbol{P}_{exp.}(\lambda_i)$) and calculated ($\sum \boldsymbol{P}_{cld.}(\lambda_i)$) values for the radiant power for NIF (as an example of system 2) and PINO (as an example of system 3) under irradiation by polychromatic light; for other compounds, see appendix (V).

Moreover, in this study was provided another scale of the photoreactivities for compounds under polychromatic irradiation through the $\sum \beta_{AB}$ factor (Table 9-4) as scale for monochromatic light (Chapter five, Table 5-6). The values of β_{AB} factor of the C-DAE in polychromatic is much bigger than monochromatic light irradiation (Table 5-6), snice they were used same method Φ-order kinetics. This finding shows that the photoreactivity in the polychromatic is much higher than in the mononchromatic light irradiation. However, the $\beta_{\lambda_{irr}}$ factors in other compounds was quantified based on different model (η-order), and it is interesting finding the $\beta_{\lambda_{irr}}$ of AB $(1\Phi)_{\varepsilon_{B\neq 0}}$ is higher

than AB (2Φ), whereas in the scale of the $\beta_{\lambda_{irr}}$ factors for momochromatic light irradiation (Table 5-6) show that the $\beta_{\lambda_{irr}}$ values is larger in major cases of AB (2Φ) than AB $(1\Phi)_{\varepsilon_{B\neq 0}}$.

Table 9- 4: Comparative $\beta_{\lambda_{irr}}$ values for several compounds.

Compound	Pseudo Rate Constant
Polychromatic studies	
C-DAE	32485
Nifidepine	1365.3
Dacarbazine	211.07
O-DAE	0.01
PTERO	0.0148
RVT	0.0098
ORVT	0.0069
Axitinib	0.0066
TSTIL	0.0052
PINO	0.0038

9.3. Study of different lamps on the $\sum \boldsymbol{\beta_{AB}}$ factors

In this section, we will describe the effect of the lamp prolife on the $\sum \beta_{AB}$ factors, where the $\sum \beta_{AB}$ factors are used to quantify the intensity of the light, as discussed previously. By setting up the experiment as described previously, and ensuring identical reaction conditions, the $\sum \mathrm{P}_{\exp}(\lambda_i)$ values for each lamp were found to be same whilst the light profiles were different ($\sum \mathrm{P}_{\exp}(\lambda_i)$ of each light profile for NIF study was 2.97×10^4 einstein s^{-1} dm^{-3}, while, in O-DAE study was 2.98×10^5 einstein s^{-1} dm^{-3}). In this study, four different lamps profiles in the range 200-400 nm were used, one short wavelength with a maximum at 254 nm, the second one mid wavelength (302 nm), the third long wavelength (365 nm) and the fourth was a mix of short with long wavelength (254/365

nm) by using the NIF and O-DAE as experimental examples of systems AB $(1\Phi)_{\varepsilon_{B\neq 0}}$ and AB (2Φ), respectively. Fresh solutions of the selected compounds were exposed to irradiation by the different light intensities of each lamp, as described in the previous section. The $\sum \beta_{AB}$ factors for these compounds were quantified using the new method. The findings indicated that the $\sum \beta_{AB}$ factors for each compound were different from one lamp to another (Fig. 9-10), which suggests that it is important to take into consideration the type of the lamp used when performing photodegradation studies due to it being difficult to replicate the results as it is difficult to obtain the same light profile in each lab. In this study found that there is more variation when plot k_η against $\sum P_{(\lambda_i)}$ in case NIF than O-DAE, and this might be due to the type of the reaction is different, where the NIF is AB $(1\Phi)_{\varepsilon_{B\neq 0}}$ but the O-DAE is reverse reaction.

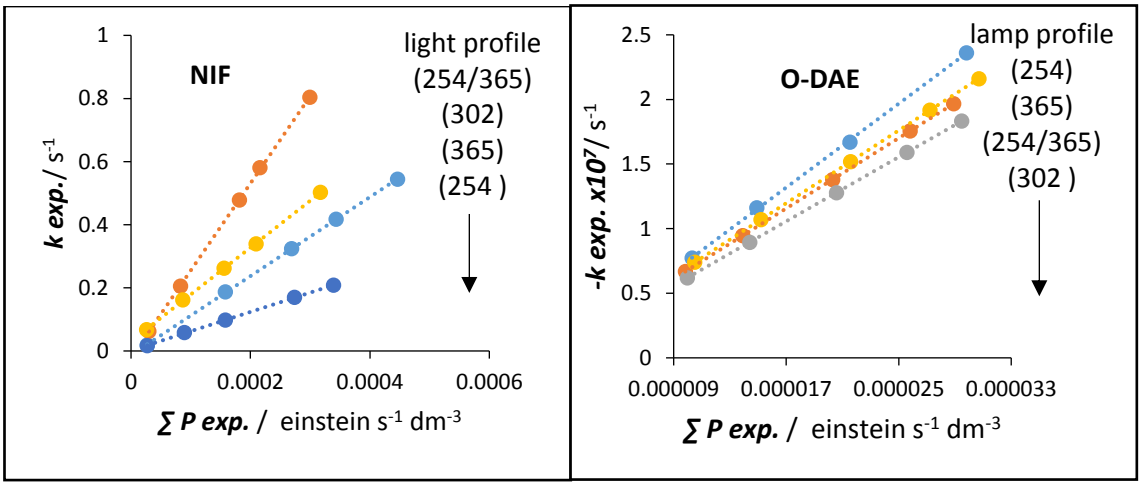

Figure 9- 10: The effect of the $\sum \beta_{AB}$ factors with different lamp profiles with the same $\sum P_{exp}(\lambda_i)$.

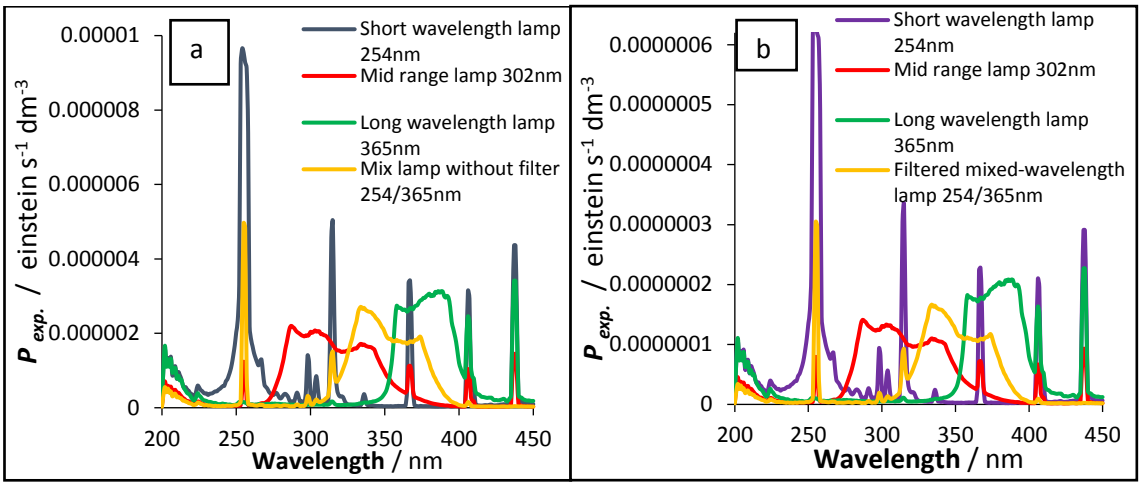

Figure 9- 11: (a) and (b) The light profile used for study effect of different lamp on $\sum \boldsymbol{\beta}_{AB}$ factors for NIF and O-DAE, respectively.

9.4. Discussion

New chemical actinometers have been developed here for both monochromatic and polychromatic light irradiation. The compounds used as new actinometers covered a broad range of the spectrum, namely the UVA, UVB and visible region, such as in the monochromatic and polychromatic studies. These compounds are available commercially, are thermally stable, easy to prepare and follow a known photochemical reaction mechanism.

A comprehensive and easy to implement actinometry technique that can be used for confirmatory purposes in various ways was also suggested. This technique can be applied to the high energy radiant lights that are sometimes needed by radiation experiments in absorption bands with low efficiency, such as λ_{irr} < 250 nm for STIL, RVT, PTERO and ORVT. Such studies complement current actinometric approaches as

they can be easily cover as the UVB, UVA and visible spectrum spans the wide 250–570 nm range.

It is important to note that the type of lamp was effect in replicate the results as describe in the $\beta_{\lambda_{irr}}$ graph (Fig. 9-10), thus when the ferrioxalate, as popular and standard actinometer [1], was used to obtained the light absorbed by the molecule. In this case, it is need to achieved same condition and same type of the lamp that used in the ferrioxalate actinometer because of the data of the ferrioxalate actinometer was obtained from particular light source. Moreover, it is interesting to state that each compound actinometer has different β_{AB} factor, thus lead to it is difficult to use any compound actinometer to determine the light absorbed by another compound due to the original actinometer is special for each compound, and it might be the light absorbed between the compound is different because each compound has different absorption spectra.

However, these methods are definitely not limited to the compounds described above, but can be applied conveniently to many other photoabsorbing molecules whose photoreactions proceed via similar mechanisms.

Finally, it should be pointed out that to apply the actinometric method described in this study, neither the absolute values of the forward and reverse quantum yields, nor the photoisomer spectrum produced must be known. It is possible that this improves actinometry because the new approach proposed in this work reduces two of the most

important parameters relating to the design of actinometers as based on the $\beta_{\lambda_{irr}}$ factors [1].

9.5. Conclusion

Under monochromatic and polychromatic studies, we have developed a new actinometric method for the different compounds. This method is a good actinometric alternative to the ICH-recommended procedure and quinine hydrochloride [11] as a chemical actinometer [4,12] and, indeed, other chemical actinometers such as ferrioxalate [1], which is a standard actinometer and that requires complex reagents such as phenanthroline to form the colour when quantifying the light intensity. The actinometric method using the selected compounds' photoreactions in ethanol could readily be implemented for any unknown source of light radiation for different wavelength ranges. This study has found that when describing the compounds reactivities, there is one parameter that is more significant and broad-ranging than the photochemical quantum yields, which is $\beta_{\lambda_{irr}}$. This method can easily be used to determine $P_{\lambda_{irr}}$ for unknown light sources without knowing the quantum yields of the reactions (Φ) and/or the product photoisomers' spectra ($\varepsilon_B^{\lambda_{irr}}$) by using the $\beta_{\lambda_{irr}}$ factor instead.

9.6. References

1. Kuhn HJ., Braslavsky SE., Schmidt R. Chemical actinometry. Pure and Applied Chemistry. 2007; 61(2): 187–210.
2. Maafi M., Al-Qarni MA. Φ-order spectrophotokinetic characterisation and

quantification of trans-cis oxyresveratrol reactivity, photodegradation and actinometry. Spectrochimica Acta Part A: Molecular and Biomolecular Spectroscopy. Elsevier; 5 January 2018; 188: 64–71.

3. Maafi M. The potential of AB(1Φ) systems for direct actinometry. Diarylethenes as successful actinometers for the visible range. Physical Chemistry Chemical Physics. 2010; 12(40): 13248–13254.

4. Maafi M., Maafi W. Montelukast photodegradation: Elucidation of Φ-order kinetics, determination of quantum yields and application to actinometry. International Journal of Pharmaceutics. 2014; 471(1–2): 544–552.

5. Maafi W., Maafi M. Modelling nifedipine photodegradation, photostability and actinometric properties. International Journal of Pharmaceutics. Elsevier B.V.; 2013; 456(1): 153–164.

6. Maafi M., Maafi W. Quantification of Unimolecular Photoreaction Kinetics: Determination of Quantum Yields and Development of Actinometers—The Photodegradation Case of Cardiovascular Drug Nisoldipine. International Journal of Photoenergy. 2015; 2015: 1–12.

7. Maafi M., Maafi W. Modeling and Elucidation of the Kinetics of Multiple Consecutive Photoreactions AB4(4Φ) With Φ-order Kinetics. Application to the Photodegradation of Riboflavin. Journal of Pharmaceutical Sciences. Elsevier; 1 December 2016; 105(12): 3537–3548.

8. Maafi M., Lee LY. Determination of Dacarbazine Φ-Order Photokinetics, Quantum Yields, and Potential for Actinometry. Journal of Pharmaceutical Sciences. Elsevier Masson SAS; 2015; 104(10): 3501–3509.

9. Maafi M., Maafi W. Quantitative assessment of photostability and photostabilisation of Fluvoxamine and its design for actinometry. Photochemical and Photobiological Sciences. 2015; 14(5): 982–994.

10. Tønnesen HH. Photoreactivity of drugs. In Situ. 2008; : 102–113.

11. ICH. ICH Guidance on Analytical Method Validation. Proceedings of the International Conference on Harmonisation. 1996; (November).

12. Maafi M., Lee LY. Actinometric and Φ-order photodegradation properties of anti-cancer sunitinib. Journal of Pharmaceutical and Biomedical Analysis. Elsevier B.V.; 2015; 110: 34–41.

Chapter 10

General Conclusions

10.1. Conclusion

This research work deals with the absence of detailed photokinetic models explaining kinetics of photochemical reactions. A two-step approach has been developed for the development of new kinetic models (Φ and η), consisting of (i) a model development stage based on optimised closed-form integrated rate-laws and NIM simulation cases, and (ii) the model validation stage which is designed to confirm the validity of the developed model with further NIM simulation kinetical cases within defined applicability limits.

For three types of photoreaction mechanisms, namely unimolecular AB $(1\Phi)_{\varepsilon_{B=0}}$, unimolecular AB $(1\Phi)_{\varepsilon_{B\neq0}}$ and photoreversibles AB (2Φ), the above methodology is used for the development of new photokinetic order.

A confirmation of the validity of the above models was achieved using C-DAE as model example for AB $(1\Phi)_{\varepsilon_{B=0}}$) reaction types, NIF and DBZ as drug examples for AB $(1\Phi)_{\varepsilon_{B\neq0}}$) reaction, and stilbinolid group, AXI and O-DAE as compound examples for photoreversibles AB (2Φ) reaction mechanisms.

Consequently, a precise description of the kinetic evolution of the compounds' photoreactions in solutions was achieved through the utilisation of the models. The benefit of the kinetic models also included the elucidation of the kinetic parameters that defined the mechanisms of the photoreaction studies and the quantitative analysis of the initial concentration effects on the kinetic photoreaction.

In addition, it was also noticed that a new kinetic parameter that could be commonly used to describe the rate of photoreactions, namely the beta factor or the pseudo rate-constant, it is also proved to be a beneficial tool for analysis and comparison of photoreactivity rates independently of the intensity of the monochromatic and polychromatic light used.

The models above could be used to describe the kinetics of any molecules that follow the above mechanisms of photoreaction. As is common in thermal studies, for comparative and photoprotective purposes, the kinetic parameters underlying these photoreactions are also identified and used for the shelf-life determination by the proposed kinetic elucidation methods.

Finally, these studies provide simple, accurate and universally reproducible experiments for carrying photostability studies, as well as analysing the resulting kinetic data. The study also offers both quantitative and qualitative photostability data for molecules and may also be used by extrapolation in the quantitative analysis of variables, as well as for predictive purposes.

10.2. Future work and limitation

Notably, the research presented within this thesis offers approach for the exploration and analysis of photoreactions kinetics. As well as this, it opens new research perspectives in the field of photochemistry.

Through the utilisation of the NIM-based methodology, the development of further kinetic models for molecules and drugs photo-degrading, via different mechanism of

reaction from the ones described in this thesis, is possible. Nevertheless, a step-by-step method to the study of other photoreaction mechanisms has the possibility of progressively leading to the development of photoreactions' kinetic models, which could ultimately cover most eventualities and that could contribute to the development of photo-protective strategies. This method should be performed in combination with practical photostability studies on molecules that have been studies as reaction mechanisms. The photoreactive mechanism of drugs has limited information, which is useful for the determination of photo-products, and for elucidation and verification of the reaction mechanisms by advanced analytical methods such as Liquid Chromatography Mass Spectrometry (LC-MS). Consequently, this would provide an overview of reliable reactions, as well as the effects of various variables, such as excipients and solvents. When such mechanisms are combined with a quantitative data treatment technique such as Φ-kinetics, accurate conclusions can be drawn about the photostability of compounds and informed decisions can be concerning over protective means and shelf-life.

Different studies have shown the dependence of the quantum yield of the photoreactions on irradiation wavelength and it has been confirmed in these studies. Therefore, the result itself should be explored further within the same and new mechanisms. As well as, the variation of this essential parameter with wavelength should be carefully examined, because a mathematical relationship between the quantum yield and the wavelength could be defined in all cases.

Appendix I

Results of the photokinetic studies of some stilbenoid and diarylethene derivatives under monochromatic light

(Chapter 5)

Results of the photokinetic studies of some stilbenoid and diarylethene derivatives under monochromatic light

i. Results of the identifiability issue:

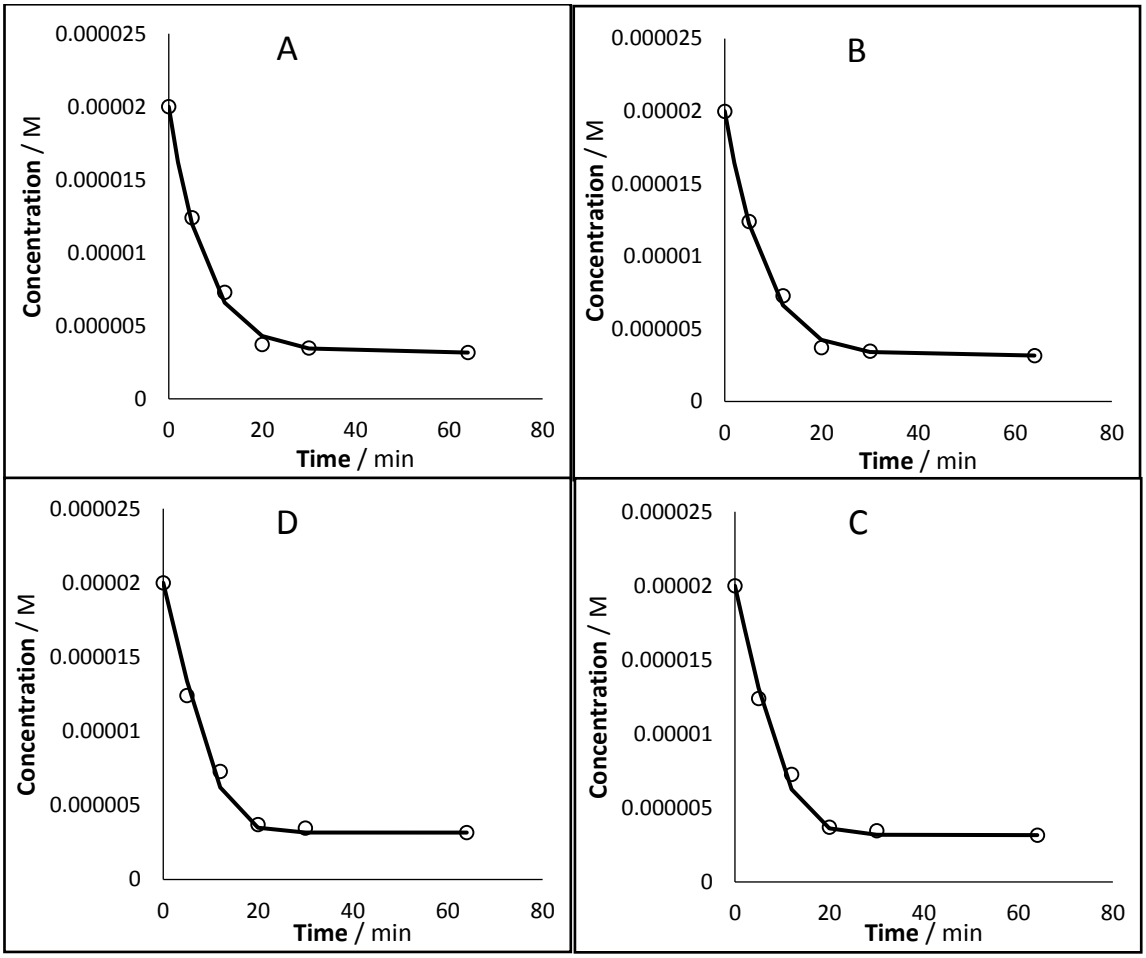

Figure I- 1: The t-ORVT concentration monitored by HPLC when irradiated continuously with a monochromatic beam at 328 nm (2.39 × 10−7 einstein s−1dm−3, 22◦C) and fitted by Eq.36 using random numbers, which in Fig (A,B,C and D) the α values at cases 2,3,5 and 6 respectively.

ii. Spectrum electronic evolution of studied compounds:

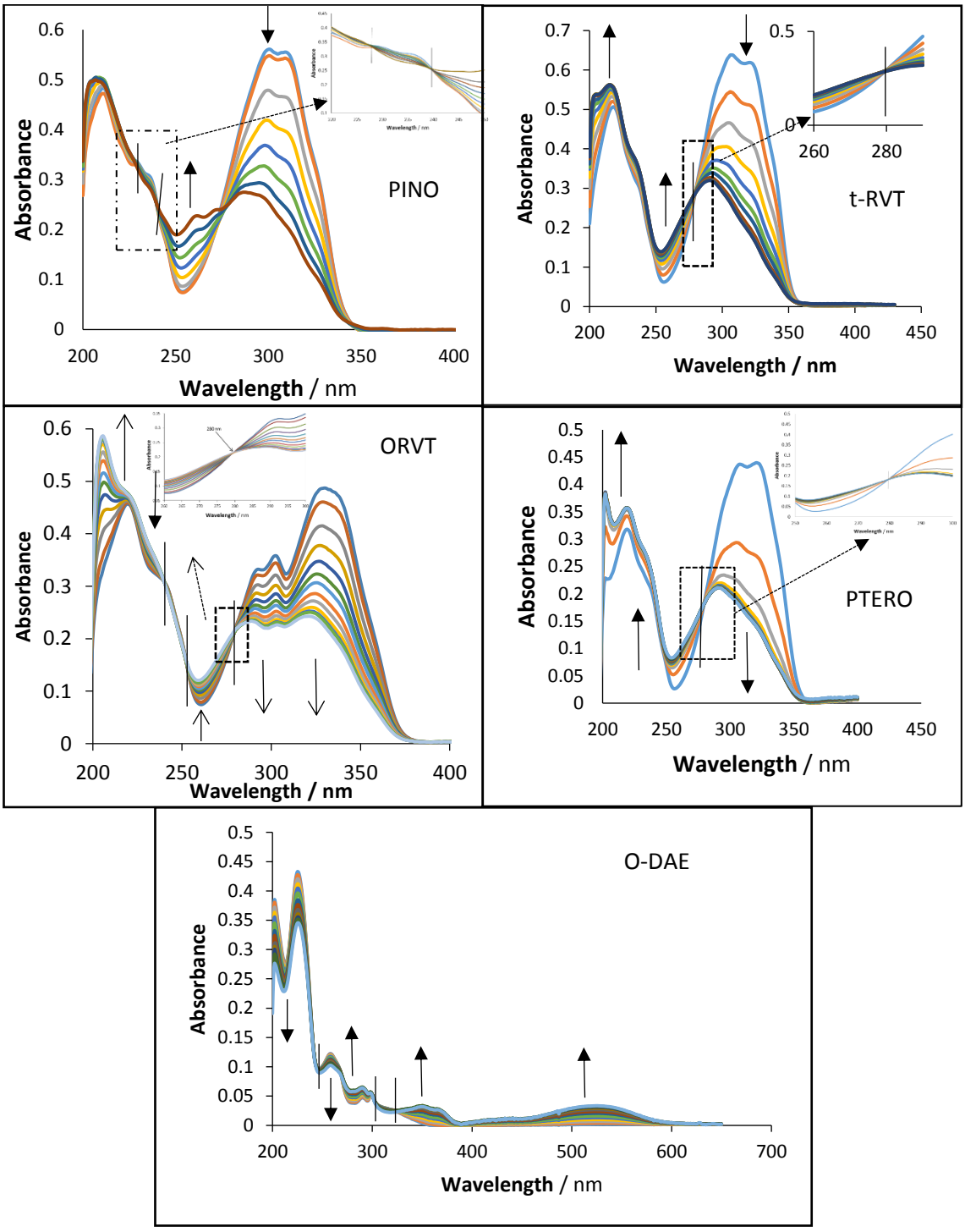

Figure I- 2: Evolution the electronic absorption spectra of PINO, t-RVT, PTERO, ORVT and O-DEA (2.16 × 10^{-5}, 1.88 × 10^{-5}, 1.95 × 10^{-5}, 2 × 10^{-5} and 5.26 x 10^{-6} M, respectively) in ethanol solutions subjected to continuous irradiation with a monochromatic beams at 300, 310, 320, 328 and 350 (5. × 10-7, 7.03× 10-7, 1.06 ×10-6 , 2.64 × 10-7 and 5.4 × 10-7 einstein s-1 dm-3), respectively. The arrows indicate the direction of the evolution of absorption maxima during photoreaction and vertical line cross the spectra at the isosbestic point.

iii. Photokinetic traces of studies compounds

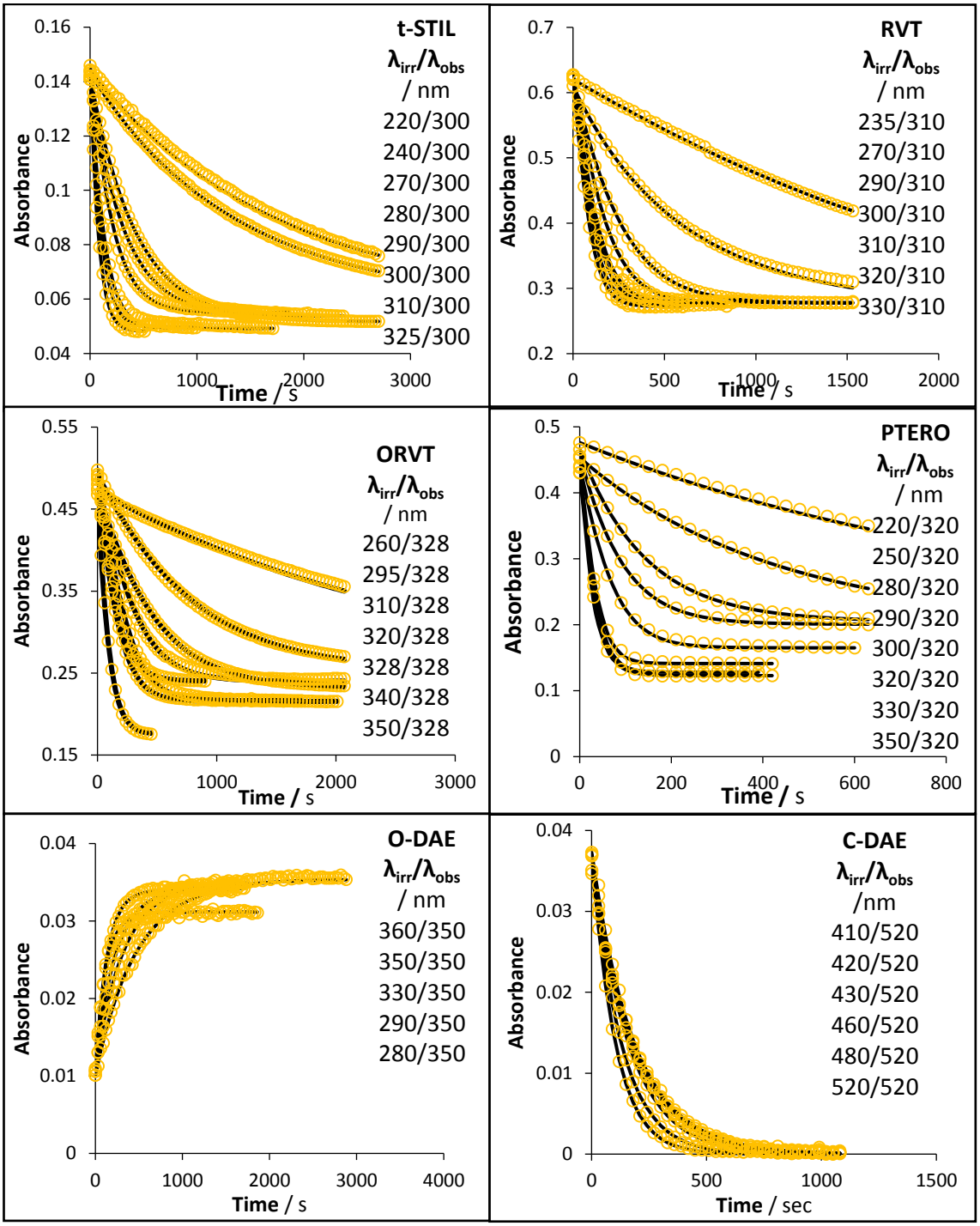

Figure I- 3: Photokinetic traces of t-STIL, RVT, ORVT , PTERO, O-DAE and C-DAE in ethanol solutions at different irradiation wavelengths (λ_{irr}) and λ_{obs}= 300, 310, 320, 328, 350 and 520 nm, respectively. The circles represent the exp. data while the lines represent the fitting traces using Eq.5-3.

iv. Reconstructed electronic absorption spectra of some studies compounds

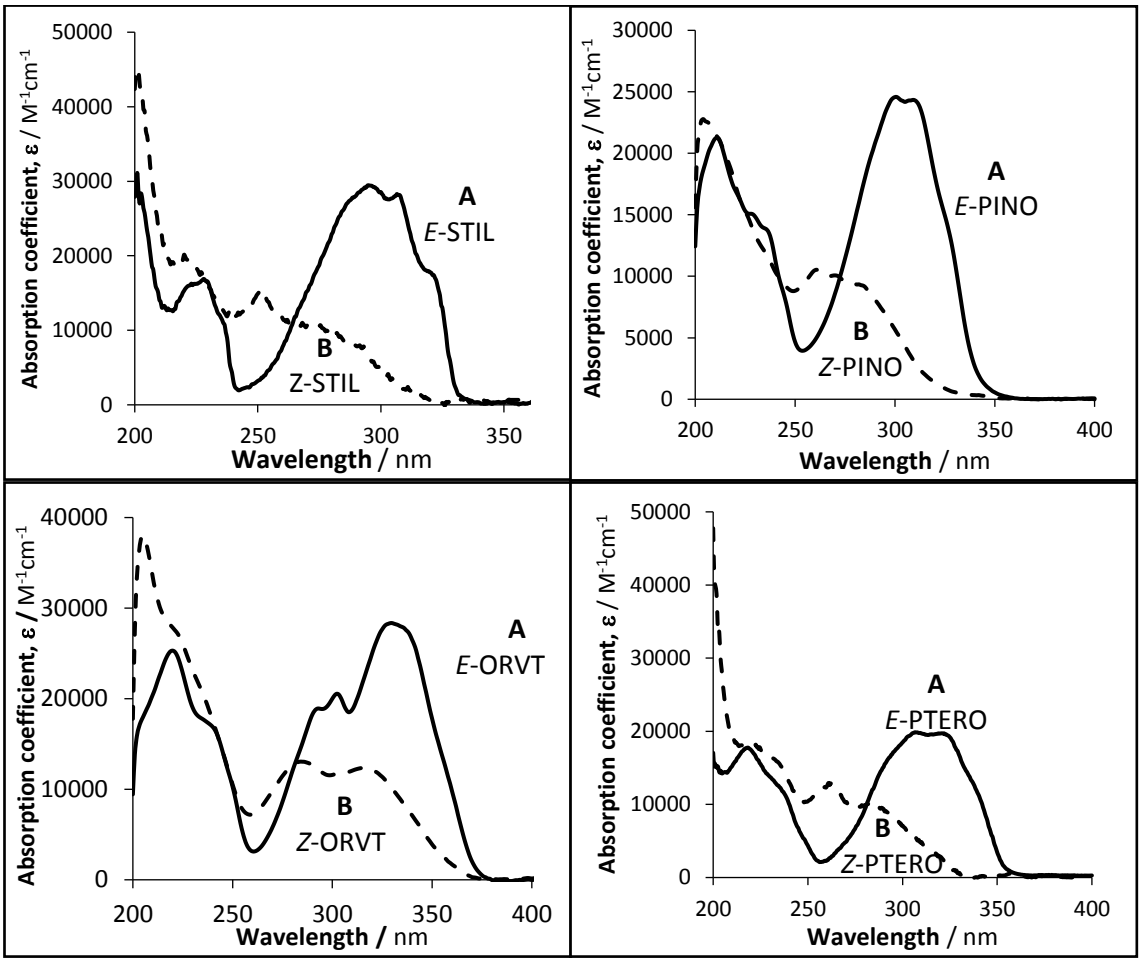

Figure I- 4: Native and reconstructed electronic absorption spectra (absorption coefficient units) of t-ismors and its cis- isomers photoproduct of STIL, PINO, RVT, ORVT and PTERO, respectively.

v. Degradation percentage of A and B compounds

Table I-1: The degradation percentage at each irradiation wavelength.

λ_{irr} /nm	$\mathbf{C_A(0) \times 10^5}$ / M	$\mathbf{C_A(pss) \times 10^6}$ / M	$\mathbf{C_B(pss) \times 10^5}$ / M	$K_{\rightleftharpoons}^{\lambda_{irr}}$	**% DEGRADATION**
t-STIL					
240	0.525	1.27	0.398	3.12	75.73
270	0.585	1.38	0.447	3.25	76.45
280	0.556	1.25	0.430	3.43	77.44
290	0.497	1.09	0.388	3.56	78.07
300	0.539	1.09	0.429	3.92	79.69
310	0.469	0.935	0.375	4.01	80.04
PINO					
280	2.38	10.31	1.35	1.31	56.66
290	2.32	5.80	1.74	2.99	74.96
300	2.16	4.71	1.68	3.57	78.16
310	2.11	3.85	1.72	4.48	81.74
320	1.98	2.94	1.68	5.72	85.13
330	2.31	3.26	1.98	6.09	85.98
RVT					
290	1.84	6.96	1.14	1.64	62.18
300	1.83	6.66	1.17	1.75	63.69
310	1.92	6.87	1.24	1.80	64.30
320	1.92	6.23	1.29	2.08	67.53
330	2.02	5.08	1.52	2.99	74.92
340	1.88	2.88	1.59	5.55	84.74
ORVT					
260	1.79	7.83	1.003	1.28	56.17
295	1.74	3.54	1.36	3.92	79.67
310	1.69	4.65	1.22	2.63	72.47
320	1.74	4.21	1.32	3.15	75.90
328	1.6	4.19	1.18	2.82	73.83
340	1.61	2.7	1.34	4.95	83.2
350	1.91	2.23	1.69	7.59	88.36
360	1.68	0.43	1.64	38.23	97.45
PTERO					
240	1.54	0.14	1.33	0.094	8.63
250	1.24	9.29	3.11	0.34	25.07
270	1.52	9.28	5.96	0.64	39.10
290	1.49	4.92	9.98	2.03	66.97
300	1.48	4.04	0.11	2.65	72.59
310	1.51	4.45	0.11	2.39	70.54
320	1.50	3.92	0.11	2.82	73.81
O-DAE					
290	1.35	5.05	0.85	1.68	62.71
330	1.39	3.95	1.00	2.53	71.71
350	1.16	0.27	1.14	42.39	97.69
360	1.07	0.12	1.06	88.13	98.87
380	0.464	0.081	0.46	56.00	98.24

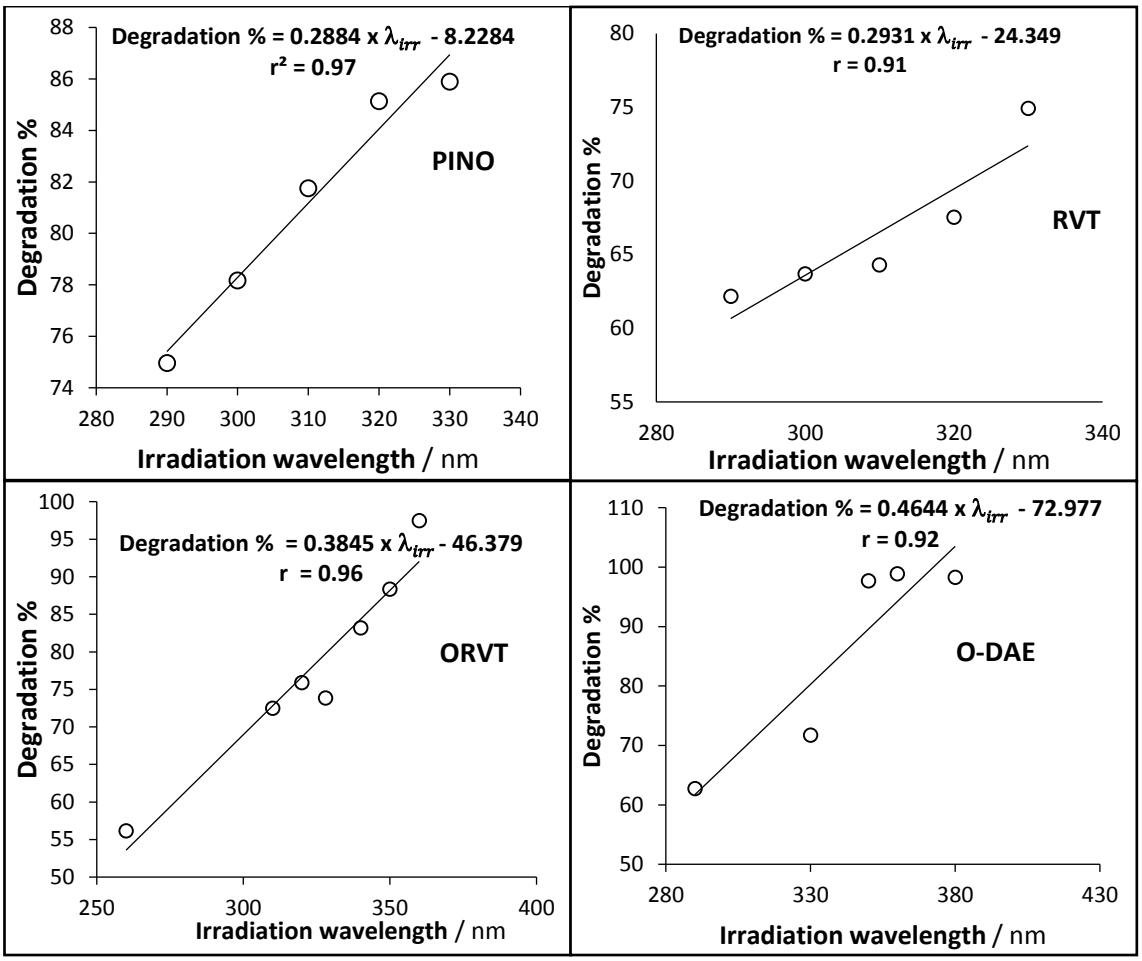

Figure I- 5: Relationship between $Degradation\ \%$ with irradiation wavelength (λ_{irr}) of PINO, RVT, ORVT and O-DAE.

vi. Quantum yields graph of studies compound under monochromatic irradiation

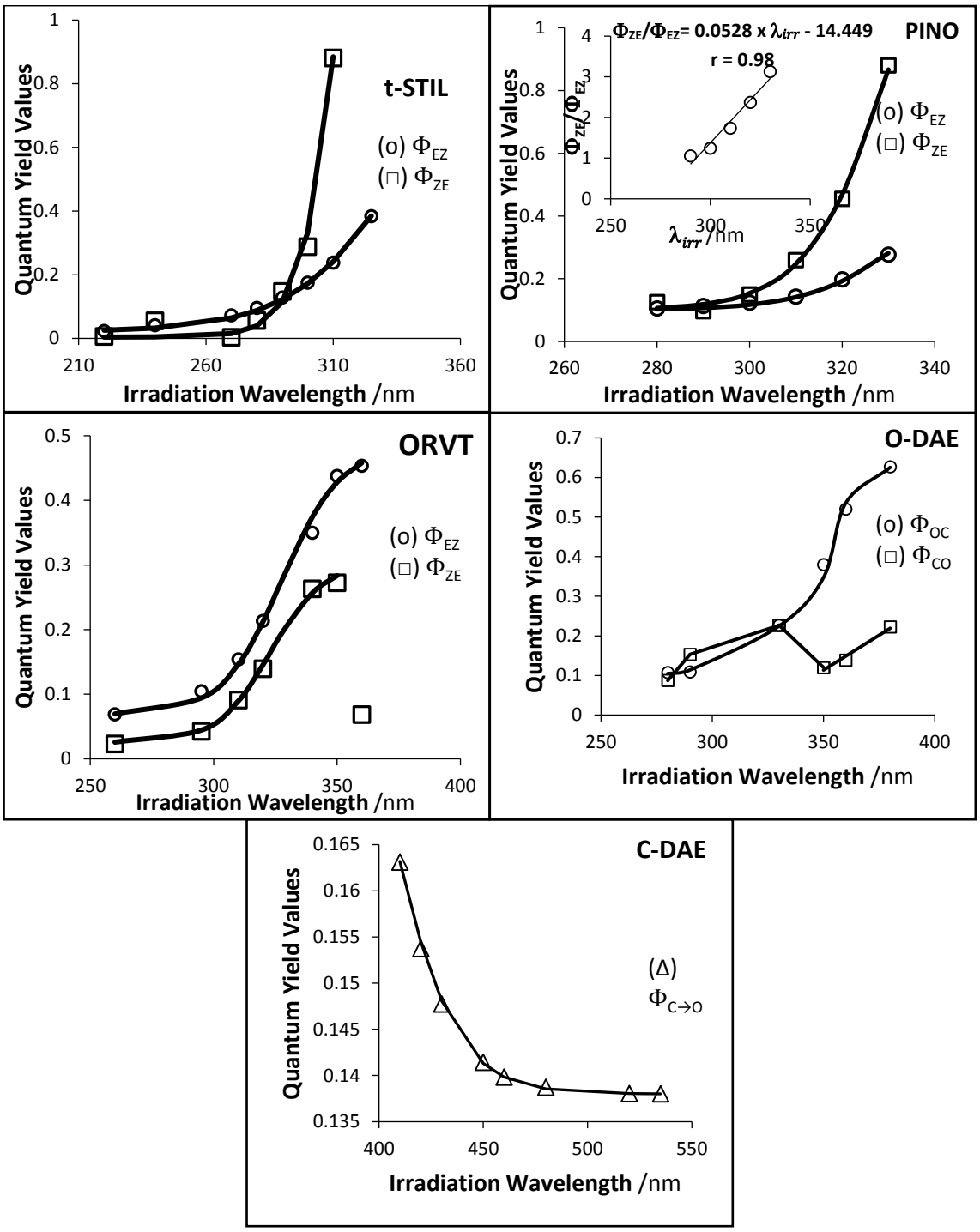

Figure I- 6: t-STIL, PINO, ORVT, O-DAE and C-DAE forward $\Phi_{E\rightarrow Z}^{\lambda_{irr}}$ and reverse $\Phi_{Z\rightarrow E}^{\lambda_{irr}}$ photochemical quantum yield values determined at different irradiation wavelengths. Inset:

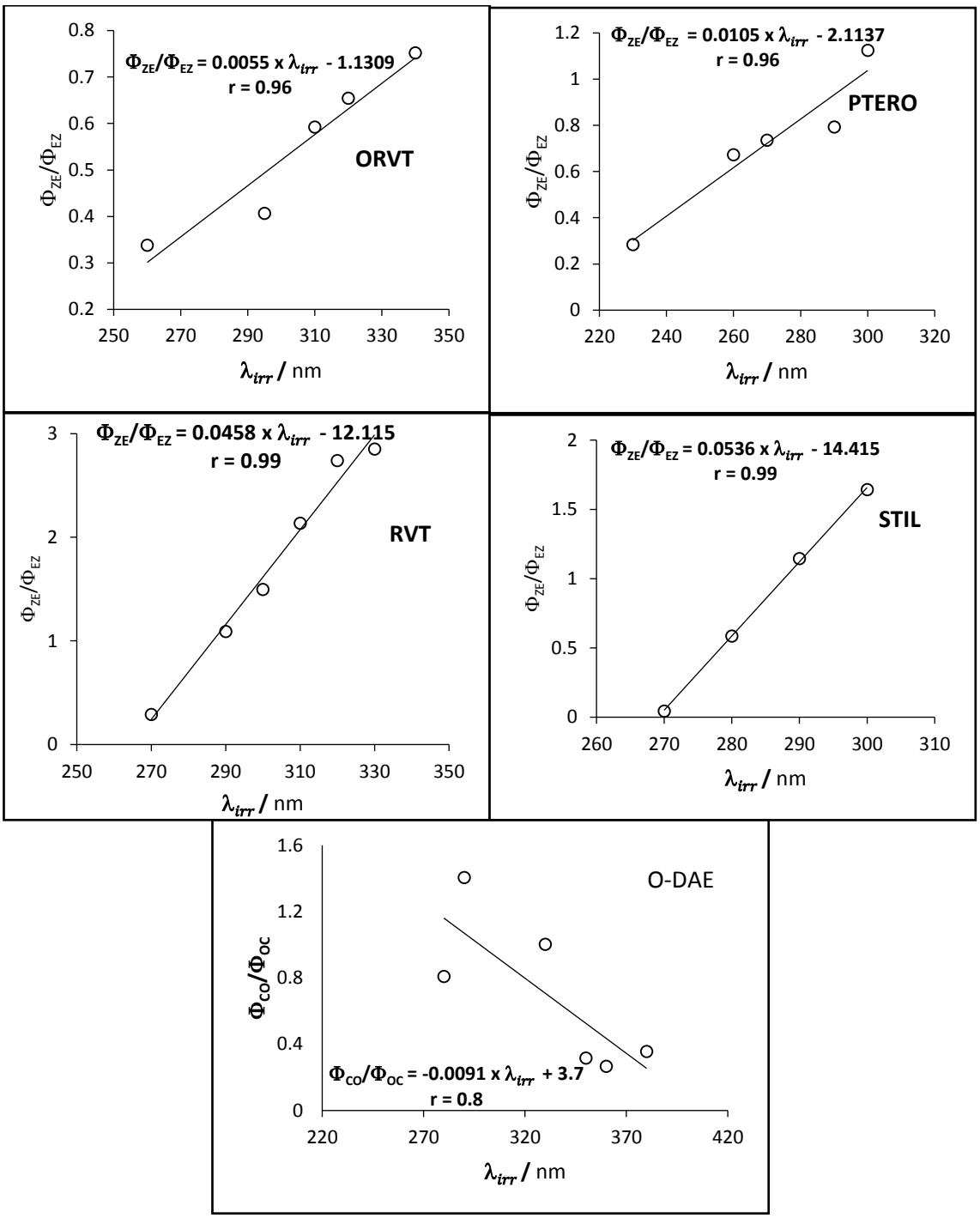

Figure I- 7: The relationship of the quantum yields ratio ($\Phi_{Z\to E}^{\lambda_{irr}}/\Phi_{E\to Z}^{\lambda_{irr}}$) with irradiation wavelength.

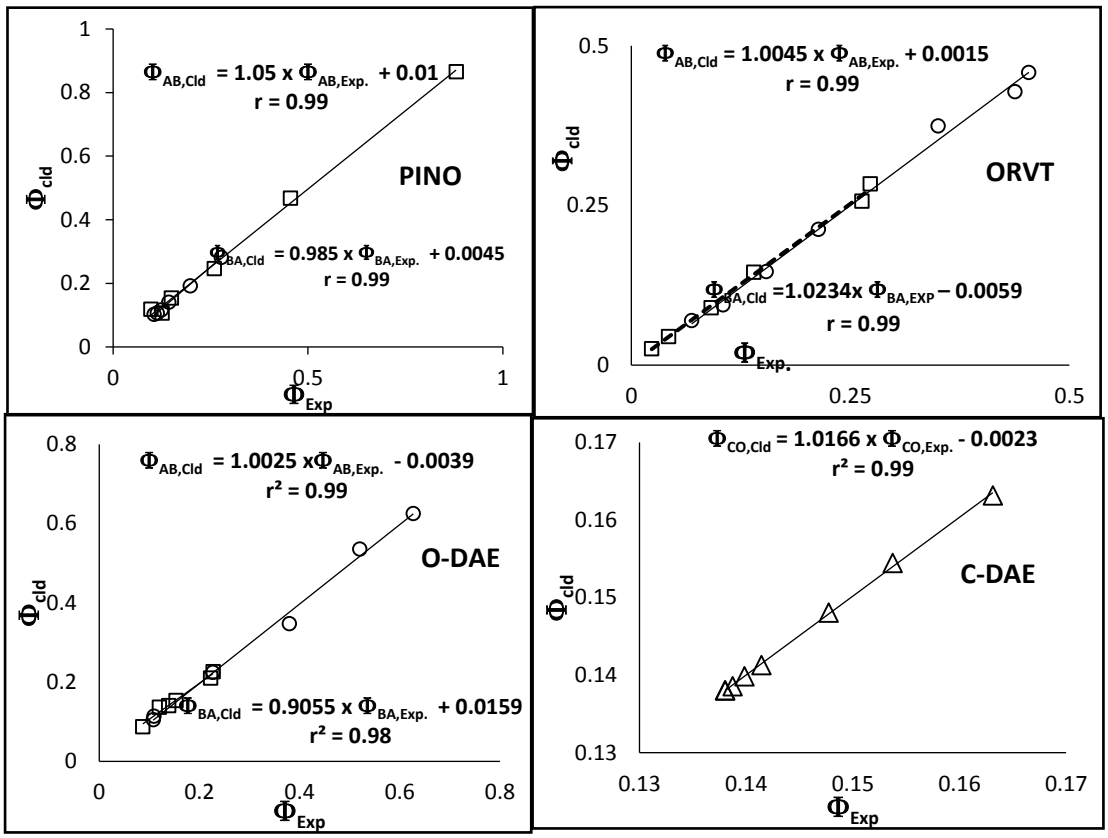

*Figure I- 8: **T**he linear- relationship of the experimental and calculated PINO, ORVT, O-DAE and C-DAE (Eq.5-17 - 5-19) values of the forward ($\Phi_{E\rightarrow Z}^{\lambda_{irr}}$) and the reverse ($\Phi_{Z\rightarrow E}^{\lambda_{irr}}$) quantum yields.*

Table I-2: Quantum yields of Z ⇋E photoismoerisation and photostatsionary state of stilbene and some derivative.

Compound	Solvent	Wavelength nm	$\Phi_{E\rightarrow Z}$	$\Phi_{Z\rightarrow E}$	Ref.
Stilbene	n-Hexane	254	0.67	0.28	63
		313	0.59	0.32	
	cyclohexane	254	0.79		71
		300-313	0.32		
	Benzene	313	0.36		71
		313	0.46	0.33	64,65,66
		405	0.42	0.22	67
	Methanol	313	0.48	0.32	79
Nitrostilbenes					
4-nitro-4' methoxystilbenes (4,4-NMS)	Methylcyclohexane (MCH)-decalin	313	0.60	0.38	78
		405	0.70	0.39	
	Methanol	366	0.13	0.31	79
4-nitro-4'-dimethylaminostilbenes (4,4-NDS)	Cyclohexane	313	0.14	0.45	70
		366	0.20	0.40	
		405	0.16	0.42	
		436	0.16	0.37	
	Benzene	313	0.015	0.42	70
		366	0.016	0.39	
		405	0.015	0.40	
		436	0.013	0.40	
	ethanol	366	0	0.31	70
1,2-diarylethylenes					
3-styrylpyridines (3-azastilbenes) (3-StP)	n-hexane	254	0.52	0.22	72
		313	0.56	0.22	73,75, 77
4-styrylpyridines (4-azastilbenes) (4-StP)	n-hexane	254	0.39	0.34	72,74
		313	0.37	0.34	73,75, 77
1-styrylnaphthalenes (1-StN)	MCH	313	0.16		68
		366	0.30		69
2-styrylnaphthalenes (2-StN)	MCH	313	0.24	0.28	76
		334	0.14	0.12	69,76
2,2'-dinaphthylethylenes (2,2-DNE)	MCH	313	0.04		69
		334	0.05		
		366	0.08		

Table I-3: the effect of the monosubstituted and disubstituted on the value of quantum yield of Stilbene.

Positions			*o*-	*m*-	*p*-	Solvent	Ref.
Monosubstituted							
Stilbene	Φ_{tc}	$-NH_2$	0.12	0.23	0.52	Acetonitrile	[1]
			0.04	0.09	0.49	Cyclohexane	[1]
		-OH		0.32	0.42	Cyclohexane	[6,7]
			0.39	0.25	0.35	Acetonitrile	[10]
			0.30	0.19	0.49	Acetonitrile/H_2O (1:1)	[10]
		$-OCH_3$		0.31	0.40	Cyclohexane	[7]
				0.32	0.39		[8]
				0.39	0.53	Acetonitrile	[8]
		-Cyano		0.39	0.46	Cyclohexane	[11]
	Φ_{ct}	$-NH_2$	0.48	0.07	0.37	Cyclohexane	[3]
			0.44	0.07	0.42	Acetonitrile	
		-Cyano		0.44	0.41	Cyclohexane	[11]

Compound	Positions	Φ_{tc}	Solvent	Ref.
disubstituted				
STILBENE	*m,p*-dimethoxy	0.41	Cyclohexane	[8]
		0.59	Acetonitrile	
	m,m-dimethoxy	0.29	Cyclohexane	[8]
		0.28	Acetonitrile	
	o,o'-dimethyl	0.57	Cyclohexane	[9]
	m,m'-dimethyl	0.55		[9]
	p,p'-dimethyl	0.39		[9]
	o,p,o-trimethyl	0.47	Methylcyclohexane (MCH)-	[11]
	p-CN-p'-NMe_2	0.5	Ethanol	[5]
	p-CN-m'-NMe_2	0.24		[5]
	m,m, m',m'-tetramethox	0.32	Acetonitrile	[12]

	m-nitro-m'-methoxy	0.45	Cyclohexane	[11]
	p-nitro-m'-methoxy	0.61		
	p-nitro-p'-methoxy	0.55		
	p,p'-dinitro	0.27	Benzene	[13]
	p-Nitro-*p'*-dimethylami	0.016		[13]
	p-Nitro-*p'*-methoxy	0.40		[13]
	p-Nitro-*m'*-methoxy	0.38		[13]
	p,p'-diamino	0.39	Acetonitrile	[4]

Appendix II

Results of the simulation studies

(Chapter 6)

1. Rate law of the system $\mathrm{AB}(1\Phi)_{\varepsilon_{B=0}}$

The differential equation of the A → B photoreaction $\mathrm{AB}(1\Phi)_{\varepsilon_{B=0}}$ when irradiated with polychromatic light, has form

$$\frac{dC_A\,(t)}{dt} = -\frac{dC_B\,(t)}{dt} = -l_{\lambda_{irr}} \times C_A\,(t) \times \sum_{\lambda_i}^{\lambda_f} \Phi_{A\to B}(\lambda_i) \times \varepsilon_A\,(\lambda_i) \times P(\lambda_i) \times F(\lambda_i, t)$$

Eq.A2.1

with $l_{\lambda_{irr}}$ (a constant) and $C_A^j(t)$ are wavelength independent. Hence, the summation over the irradiation wavelength domain concerns all remaining parameters, including the photokinetic factor (which involves the total absorbance $A_{tot}(\lambda_i, t) = l_{\lambda_{irr}} \times C_A^j(t) \times \sum_{\lambda_i}^{\lambda_f} \varepsilon_A\,(\lambda_i)$).

Where $F(\lambda_i, t)$ is given as

$$F_{\lambda_{irr}}(t) = \frac{1-10^{-(l_{\lambda_{irr}} \times C_A^j(t) \times \sum_{\lambda_i}^{\lambda_f} \varepsilon_A(\lambda_i)}}{l_{\lambda_{irr}} \times C_A^j(t) \times \sum_{\lambda_i}^{\lambda_f} \varepsilon_A\,(\lambda_i)}$$

Eq.A2.2

Hence we have

$$\frac{dC_A\,(t)}{dt} = -\frac{l_{\lambda_{irr}} \sum_{\lambda_i}^{\lambda_f} \Phi_{A\to B}(\lambda_i) \times \varepsilon_A\,(\lambda_i) \times P(\lambda_i)(1-10^{-(l_{\lambda_{irr}} \times C_A^j(t) \times \sum_{\lambda_i}^{\lambda_f} \varepsilon_A\,(\lambda_i)})}{\sum_{\lambda_i}^{\lambda_f} \varepsilon_A\,(\lambda_i)}$$

E*q.A2.3*

$$\frac{dA_{tot}(\lambda_i,t)}{dt} = -l_{\lambda_{irr}} \sum_{\lambda_i}^{\lambda_f} \Phi_{A\to B}(\lambda_i) \times \varepsilon_A\,(\lambda_i) \times P(\lambda_i)\,(1-10^{-(l_{\lambda_{irr}} \times C_A^j(t) \times \sum_{\lambda_i}^{\lambda_f} \varepsilon_A\,(\lambda_i)})$$

E*q.A2.4*

If we separate the variables of the equation, we find

$$\frac{dA_{tot}(\lambda_i,t)}{(1-10^{-(A_{tot}(\lambda_i,t)})} = -l_{\lambda_{irr}} \sum_{\lambda_i}^{\lambda_f} \Phi_{A\to B}(\lambda_i) \times \varepsilon_A\ (\lambda_i) \times P(\lambda_i)\, dt \qquad \text{Eq.A2.5}$$

To achieved the integration of the left side of Eq. A2.5 it is required to make use of a change of variable, e.g. $d\left(10^{(A_{tot}(\lambda_i,t)}\right)=\left(\ln(10)\ \ \right)10^{(A_{tot}(\lambda_i,t)}\ dA_{tot}(\lambda_i,t)$,

Hence the integration of

and integrating it yields E*q.A2.5 is*

$$\frac{1}{\ln(10)} \int \frac{d\left(10^{(A_{tot}(\lambda_i,t)}\right)}{(10^{(A_{tot}(\lambda_i,t)}-1)} = -\int \left[l_{\lambda_{irr}} \sum_{\lambda_i}^{\lambda_f} \Phi_{A\to B}(\lambda_i) \times \varepsilon_A\ (\lambda_i) \times P(\lambda_i)\right] dt \qquad \text{Eq.A2.6}$$

$$\ln \frac{10^{(A_{tot}(\lambda_i,t)}-1}{10^{(A_{tot}(\lambda_i,0)}-1} = -\ln(10)\, l_{\lambda_{irr}} \sum_{\lambda_i}^{\lambda_f} \Phi_{A\to B}(\lambda_i) \times \varepsilon_A\ (\lambda_i) \times P(\lambda_i)\, t \qquad \text{Eq.A2.7}$$

Reformulate E*q.A2.7*

$$A_{tot}(\lambda_i,t) = \log\left(1 + \left(-1 + \ 10^{(l_{\lambda_{irr}} \times \left(C_A\,(0) \times l_{\lambda_{obs}} \times \sum\ \varepsilon_A\right)}\right) \times\ e^{-\left(\ln(10) l_{\lambda_{irr}} \sum_{\lambda_i}^{\lambda_f} \Phi_{A\to B}(\lambda_i) \times \varepsilon_A\,(\lambda_i) \times P(\lambda_i)\right)t}\right)$$

Eq. A2.8

Rewriting the Eq. A2.8 in form $C_A\,(t)$ is given as

$$C_A\,(t) = \ \frac{1}{\left(l_{\lambda_{irr}} \times \sum\ \varepsilon_A\right)} \times\ \log\left(1 + \left(-1 + \ 10^{(l_{\lambda_{irr}} \times (C_A\,(0) \times l_{\lambda_{obs}} \times \sum\ \varepsilon_A)}\right) \times\ e^{(-k_{AB}t)}\right) \qquad \text{Eq. A2.9}$$

with the rate-constant has the following expression.

$$k_{AB} = \ln(10)\, l_{\lambda_{irr}} \sum_{\lambda_i}^{\lambda_f} \Phi_{A\to B}(\lambda_i) \times \varepsilon_A\,(\lambda_i) \times P(\lambda_i) \qquad \text{Eq.A2.10}$$

2. Rate law of the for AB $(1\Phi)_{\varepsilon_{B\neq 0}}$ and AB (2Φ)

For the two other reaction systems

$$\frac{dC_A\,(t)}{dt} = \sum_{\lambda_i}^{\lambda_f}\left[\left(\Phi_{B\to A}(\lambda_i)\times\varepsilon_B\,(\lambda_i)\times C_B\,(t) - \Phi_{A\to B}(\lambda_i)\times\varepsilon_A\,(\lambda_i)\times C_A\,(t)\right)\times P(\lambda_i)\times F(\lambda_i,t)\right]\times l_{\lambda_{irr}} \qquad \text{Eq. A2.11}$$

If the section irradiated is relatively large (a very tens of nm) or the concentration is not too low, the total absorbance is relatively high ($A_A\,(\lambda_i,t) > 3$) which means that the power number in the $F(\lambda_i,t)$ becomes very small.

$$F(\lambda_i,t) = \frac{1-10^{-A_{tot}(\lambda_i,t)}}{A_{tot}(\lambda_i,t)} \approx \frac{1}{A_{tot}(\lambda_i,t)} \approx \frac{1}{l_{\lambda_{irr}}\times C_A\,(t)\times\sum_{\lambda_i}^{\lambda_f}\varepsilon_A\,(\lambda_i)} \qquad \text{Eq. A2.12}$$

Similarly as above, the power number in the photokinetic factor is small.

$$F(\lambda_i,t) = \frac{1-10^{-A_{tot}(\lambda_i,t)}}{A_{tot}(\lambda_i,t)} \approx \frac{1}{A_{tot}(\lambda_i,t)} \approx \frac{\alpha_{AB}(\lambda)}{C_A^j(t)+\beta_{AB}(\lambda)} \qquad \text{Eq.A2.13}$$

with $\alpha_{AB}(\lambda)$ and $\beta_{AB}(\lambda)$ (both expressed in M) are defined as

$$\alpha_{AB}(\lambda) = \frac{1}{l_{\lambda_{irr}}\times\sum_{\lambda_i}^{\lambda_f}\left[\varepsilon_A\,(\lambda_i)-\varepsilon_B\,(\lambda_i)\right]} \qquad \text{Eq.A2.14}$$

$$\beta_{AB}(\lambda) = C_A\,(0)\times\frac{\sum_{\lambda_i}^{\lambda_f}\varepsilon_B\,(\lambda_i)}{\sum_{\lambda_i}^{\lambda_f}\left[\varepsilon_A\,(\lambda_i)-\varepsilon_B\,(\lambda_i)\right]} \qquad \text{Eq.A2.15}$$

Hence, introducing these equations in Eq.A2.11 gives the following differential equation.

$$\frac{dC_A\ (t)}{dt} = \frac{1}{C_A\ (t) + \beta_{AB}(\lambda)} \times \alpha_{AB}(\lambda) \times \left(-C_A\ (t) \times \left(l_{\lambda_{irr}} \times \sum_{\lambda_i}^{\lambda_f} \left[\left(\Phi_{B\to A}(\lambda_i) \times \varepsilon_B\ (\lambda_i) + \Phi_{A\to B}(\lambda_i) \times \varepsilon_A\ (\lambda_i) \right) \times P(\lambda_i) \right] \right) + C_A\ (0) \times \left(l_{\lambda_{irr}} \times \sum_{\lambda_i}^{\lambda_f} \left[\Phi_{B\to A}(\lambda_i) \times \varepsilon_B\ (\lambda_i) \times P(\lambda_i) \right] \right) \right)$$

Eq.A2.16

Rearranging it gives

$$\frac{C_A\ (t)+\beta_{AB}(\lambda)}{C_A\ (t)+\rho_1} dC_A\ (t) = \alpha_{AB}(\lambda) \times \rho_2 \times dt$$

Eq.A2.17

with the constants ρ_1 and ρ_2 have the forms

$$\rho_1 = \frac{1}{\rho_2} \times C_A\ (0) \times \left(l_{\lambda_{irr}} \times \sum_{\lambda_i}^{\lambda_f} \left[\Phi_{B\to A}(\lambda_i) \times \varepsilon_B\ (\lambda_i) \times P(\lambda_i) \right] \right)$$

Eq.A2.18

$$\rho_2 = -\left(l_{\lambda_{irr}} \times \sum_{\lambda_i}^{\lambda_f} \left[\left(\Phi_{B\to A}(\lambda_i) \times \varepsilon_B\ (\lambda_i) + \Phi_{A\to B}(\lambda_i) \times \varepsilon_A\ (\lambda_i) \right) \times P(\lambda_i) \right] \right)$$

Eq.A2.19

The closed-form integration leads to the following integrated rate-law

$$\left(C_A\ (t) - C_A\ (0) \right) + \rho_3\ ln \frac{C_A\ (t)+\rho_1}{C_A\ (0)+\rho_1} = -k_\eta t$$

Eq.A2.20

or

$$\eta(t) = -\ k_\eta \times t$$

Eq.A2.21

With

$$\rho_3 = \beta_{AB}(\lambda) - \rho_1$$

Eq.A2.22

And k_η has the expression

$$k_\eta = -\alpha_{AB}(\lambda) \times \rho_2 = \frac{l_{\lambda_{irr}} \times \sum_{\lambda_i}^{\lambda_f} \left[\left(\left[\Phi_{B\to A}(\lambda_i) \times \varepsilon_B\ (\lambda_i) + \Phi_{A\to B}(\lambda_i) \times \varepsilon_A\ (\lambda_i)\right]\right) \times P(\lambda_i)\right]}{l_{\lambda_{irr}} \times \sum_{\lambda_i}^{\lambda_f} \left[\varepsilon_A\ (\lambda_i) - \varepsilon_B\ (\lambda_i)\right]} \quad \text{Eq. A2.23}$$

Simulation study

3. Φ-order kinetic model for AB$(1\Phi)_{\varepsilon_{B=0}}$system

Table II-1. Example sets of data used to generate unimolecular photokinetic traces and fitting by using the Φ-order method Eq. 6-1 and to calculate k_{AB} using Eq.6-2.

Case	$C_A(0)$ x 10^6	$\sum \varepsilon_A$ / $M^{-1}cm^{-1}$	ℓ_{irr} / cm	$\sum \Phi_{AB}$	$\sum P$ x10^8 / einstein s^{-1} dm^{-3}	$k_{AB,mod}$ / s^{-1}	$k_{AB,cld}$ / s^{-1}
1	2.50	225980	2	0.31	2.50	0.0081	0.0081
2	0.851	601543	2	0.23	1.5	0.0096	0.0096
3	4.32	118970	2	0.78	2.00	0.0085	0.0085
4	9.14	65650	2	0.48	5.5	0.0079	0.0079
5	3.65	151230	2	0.15	7	0.0073	0.0073
6	24.0	24560	2	0.062	150	0.011	0.011
7	3.25	180100	0.5	0.041	80	0.0068	0.0068
8	0.851	601543	2	0.23	3.5	0.0223	0.0223
9	18.9	31520	3	0.023	200	0.01	0.01
10	4.15	136504	3	0.072	25	0.0169	0.0169
11	5.10	106230	2	0.34	5	0.00831	0.00831
12	8.51	66500	2	0.4	6	0.00771	0.00771
13	4.51	128950	2	0.154	8	0.00732	0.00732
14	7.45	78450	2	0.45	5	0.00813	0.00813
15	6.15	95320	2	0.58	3	0.00764	0.00764
16	5.25	110620	2	0.36	4	0.00734	0.00734
17	4.25	138960	2	0.45	3	0.00864	0.00864
18	3.25	182350	2	0.68	2	0.0114	0.0114
19	6.50	89560	2	0.45	4	0.00742	0.00742
20	9.86	55890	2	0.23	2	0.0118	0.0118
21	9.51	62350	2	0.45	6	0.00775	0.00775
22	7.45	80350	2	0.78	3	0.00866	0.00866
23	5.68	103560	2	0.89	20	0.0849	0.0849
24	7.48	78950	2	0.45	4.8	0.00785	0.00785
25	9.82	55620	2	0.74	4	0.00758	0.00758
26	1.24	482300	2	0.31	1	0.00689	0.00689
27	7.48	75800	2	0.36	6	0.00754	0.00754
28	1.56	378400	2	0.64	0.7	0.00781	0.00781
29	1.56	35600	2	0.73	0.6	0.00718	0.00718
30	2.13	278400	2	0.081	7	0.00727	0.00727
31	23.5	21543	2	0.023	400	0.00913	0.00913
32	31.4	15986	2	0.038	300	0.00839	0.00839
33	45.7	10235	2	0.084	200	0.00792	0.00792
34	62.5	9545	2	0.047	400	0.00826	0.00826
35	51.5	10235	2	0.062	300	0.00877	0.00877
36	78.4	7648	2	0.071	400	0.010	0.010
37	81.4	7215	2	0.041	600	0.00814	0.00814

38	95.6	6210	2	0.064	500	0.00915	0.00915
39	42.3	14023	2	0.022	600	0.00852	0.00852
40	61.2	9623	2	0.052	350	0.00807	0.00807
41	63.2	9456	2	0.045	450	0.00882	0.00882
42	74.5	8014	2	0.078	300	0.00864	0.00864
43	10.1	58960	2	0.022	150	0.00896	0.00896
44	33.6	16895	2	0.051	200	0.00794	0.00794
45	90.1	6586	2	0.072	400	0.00873	0.00873
46	71.4	8325	2	0.033	700	0.00886	0.00886
47	66	9068	2	0.055	400	0.00919	0.00919
48	59	10120	2	0.041	500	0.00955	0.00955
49	47.8	12330	2	0.061	300	0.0104	0.0104
50	91.2	6012	2	0.021	1500	0.00872	0.00872
51	83.2	7124	2	0.056	500	0.00919	0.00919
52	77	7710	2	0.032	750	0.00852	0.00852
53	30.1	19850	2	0.051	200	0.00932	0.00932
54	5.94	98560	1	0.29	15	0.00987	0.00987
55	7.45	80530	1	0.87	5	0.00807	0.00807
56	4.87	112560	1	0.61	5	0.0079	0.0079
57	4.21	124500	1	0.321	7.8	0.00718	0.00718
58	3.25	184500	1	0.621	3	0.00791	0.00791
59	1.45	412500	1	0.52	1.5	0.00741	0.00741
60	2.31	235600	1	0.45	3	0.00732	0.00732
61	2.89	201500	1	0.61	2.5	0.00708	0.00708
62	1.25	452300	1	0.71	0.9	0.00665	0.00665
63	3.48	16500	1	0.52	4	0.00794	0.00794
64	4.51	125620	1	0.042	60	0.00729	0.00729
65	8.95	65230	1	0.032	150	0.00721	0.00721
66	4.44	125860	1	0.052	50	0.00753	0.00753
67	7.77	74520	1	0.056	80	0.00769	0.00769
68	8.88	65890	1	0.064	75	0.00728	0.00728
69	6.66	89560	0.5	0.62	15	0.00959	0.00959
70	5.62	98560	0.5	0.47	15	0.008	0.008
71	7.15	75620	0.5	0.31	30	0.0081	0.0081
72	3.45	145230	0.5	0.61	6.8	0.00694	0.00694
73	5.26	95630	0.5	0.54	15	0.00892	0.00892
74	6.25	92030	0.5	0.68	9.8	0.00706	0.00706
75	9.56	56210	0.5	0.29	40	0.00751	0.00751
76	7.46	80120	0.5	0.036	250	0.00830	0.00830
77	6.85	85200	0.5	0.045	200	0.00883	0.00883
78	8.56	70150	0.5	0.074	150	0.00896	0.00896
79	6.24	85620	0.5	0.042	200	0.00828	0.00828
80	4.15	142300	0.5	0.052	85	0.00724	0.00724
81	4.12	123500	0.5	0.071	70	0.00707	0.00707
82	1.2	490200	0.5	0.032	38	0.00686	0.00686
83	2.3	256200	0.5	0.051	45	0.00677	0.00677
84	22.4	25621	3	0.32	15	0.0085	0.0085

85	64.2	9325	3	0.51	28	0.0092	0.0092
86	74.8	7941	3	0.23	68	0.00858	0.00858
87	48.7	11451	3	0.81	15	0.00961	0.00961
88	7.95	74510	3	0.44	3.5	0.00793	0.00793
89	3.2	184500	3	0.41	1.5	0.00784	0.00784
90	2.14	275600	3	0.32	1.5	0.00914	0.00914
91	1.14	512000	3	0.71	0.3	0.00753	0.00753
92	1.36	420100	3	0.51	0.5	0.0074	0.0074
93	20.1	28840	3	0.045	90	0.00807	0.00807
94	23.6	25220	3	0.044	150	0.0115	0.0115
95	2.87	201200	3	0.061	9	0.00763	0.00763
96	3.01	198502	3	0.031	20	0.0085	0.0085
97	4.15	136504	3	0.072	15	0.0102	0.0102
98	3.50	165209	3	0.023	30	0.00787	0.00787
99	3.8	154210	3	0.061	15	0.00975	0.00975
100	1.59	374120	3	0.052	5.5	0.00739	0.00739

* where ℓ_{obs} is 1 cm.

4. η-order kinetic model for AB$(1\Phi)_{\varepsilon_{B\neq 0}}$ and AB(2Φ) systems

Table II-2. Sets of data used to generate some unimolecular AB$(1\Phi)_{\varepsilon_{B\neq 0}}$ photokinetic traces and fitted by using η-order method Eq. 6-5 and to calculate k_{AB}.

Case	$\sum \varepsilon_A$ / $M^{-1}cm^{-1}$	$\sum \varepsilon_B$ / $M^{-1}cm^{-1}$	$\frac{\sum \varepsilon_A}{\sum \varepsilon_B}$	ℓ_{irr} / cm	$\sum \Phi_{AB}$	$\sum P$ / einstein s^{-1} dm^{-3}	$\sum \Phi_{AB} \times \varepsilon_A \times P$ (k_{AB}cld.)	$\left(\sum \varepsilon_A - \sum \varepsilon_B\right)$ / $M^{-1}cm^{-1}$	Average k_{AB}mod. / s^{-1}	Average ν_0 mod. X10^6 / s^{-1}
1	1684678.98	758105.54	2.22	2	45.73	0.0019	1.04	926573.44	1.04	-0.61
2	827826.45	372521.90	2.22	2	18.89	0.00012	0.04	455304.55	0.04	-0.051
3	1012855.50	743938.39	1.36	2	69.98	0.0005	0.96	268917.1	0.96	-0.94
4	1692277.54	2290528.68	0.74	2	91.48	0.0005	2.21	-598251.13	2.21	-1.30
5	1329572.21	1434053.79	0.93	2	74.59	0.00196	4.89	-104481.59	4.89	-3.67
6	1343694.32	417261.63	3.22	2	20.10	0.0162	11.04	926432.69	11.04	-8.13
7	673050.02	727065.49	0.93	2	18.49	0.0162	4.94	-54015.47	4.94	-7.10
8	658414.37	727065.49	0.91	2	8.44	0.392	4.16	-68651.12	4.16	-6.10
9	880339.54	798558.57	1.10	2	21.01	0.0161	3.63	81780.97	3.63	-4.00
10	932108.35	335035.46	2.78	2	5.71	0.0167	2.22	597072.89	2.22	-2.36
11	795819.61	798558.57	0.99	2	48.64	0.0090	8.65	-2738.96	8.65	-10.80
12	1070863.36	930534.27	1.15	2	53.44	0.0079	9.45	140329.08	9.45	-8.80
13	1079447.47	291978.29	3.69	2	58.16	0.0078	7.13	787469.18	7.13	-6.60
14	1079447.28	1509972.65	0.715	2	102.36	0.0078	10.25	-430525.37	10.25	-9.50
15	1241520.37	571941.89	2.17	2	27.70	0.0084	5.91	669578.48	5.91	-4.76
16	1578375.59	1141445.57	1.38	2	20.48	0.0083	7.96	436930.02	7.96	-5.03
17	1409815.78	1013813.01	1.39	2	22.23	0.0083	6.49	396002.76	6.49	-4.61
18	1335639.17	1013813.01	1.32	2	19.16	0.018	11.70	321826.16	11.70	-8.76
19	589188.65	464362.32	1.27	2	10.86	0.018	2.90	124826.33	2.90	-4.93
20	740465.81	467124.60	1.56	2	10.82	0.008	1.54	273341.21	1.54	-2.08

21	998674.77	940878.83	1.06	2	10.86	0.047	12.61	57795.94	12.61	-12.50
22	868338.64	258743.11	3.36	2	73.54	0.0002	0.19	609595.54	0.19	-0.22
23	705182.11	809532.59	0.87	2	60.36	0.0005	0.58	-104350.46	0.58	-0.82
24	984038.49	1701212.77	0.58	2	77.39	0.0017	3.24	-717174.26	3.24	-3.30
25	10075018.39	17009730.94	0.59	2	108.58	0.0002	5.27	-6934712.55	5.27	-0.52
26	1079447.47	291978.29	3.69	2.3	58.16	0.0078	7.13	787469.18	7.13	-6.60
27	1335639.17	1013813.01	1.32	2.7	19.16	0.018	11.70	321826.16	11.70	-8.76
28	795819.61	798558.57	0.99	3.1	48.64	0.0090	8.65	-2738.96	8.65	-10.80
29	998674.77	940878.83	1.06	2.5	10.86	0.047	12.61	57795.94	12.61	-12.60
30	1012855.50	743938.39	1.36	3	69.98	0.0005	0.96	268917.1	0.96	-0.93

* where ℓ_{obs} is 1 cm.

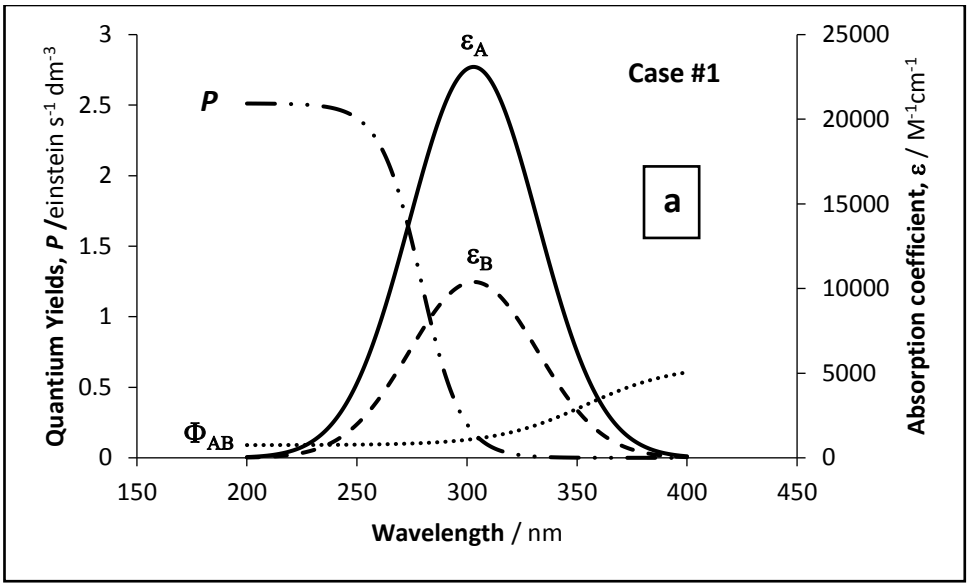
Case #1
a
P
ε_A
ε_B
Φ_{AB}
Quantium Yields, P /einstein s-1 dm-3
Absorption coefficient, ε / M-1cm-1
Wavelength / nm
0
0.5
1
1.5
2
2.5
3
0
5000
10000
15000
20000
25000
150
200
250
300
350
400
450

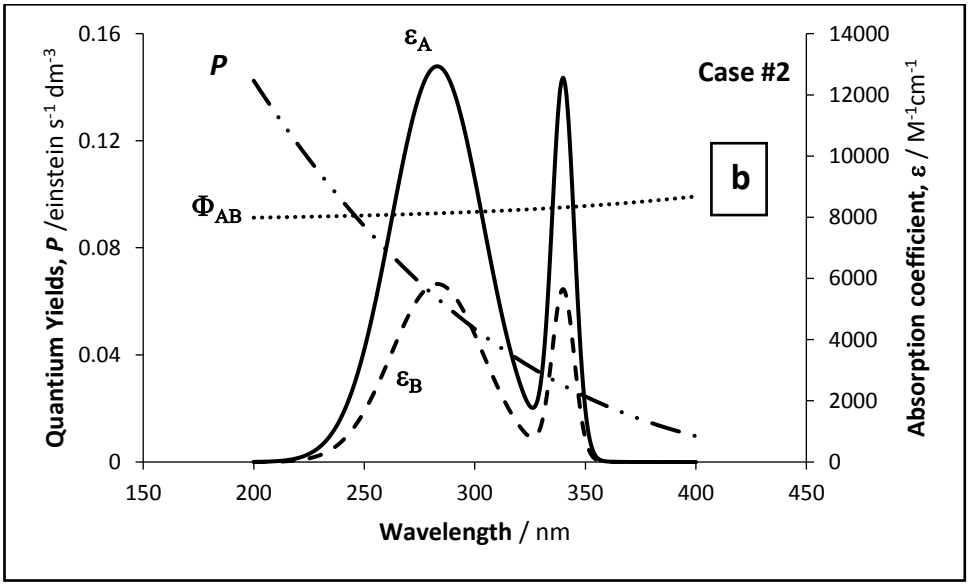
Case #2
b
P
ε_A
ε_B
Φ_{AB}
Quantium Yields, P /einstein s-1 dm-3
Absorption coefficient, ε / M-1cm-1
Wavelength / nm
0
0.04
0.08
0.12
0.16
0
2000
4000
6000
8000
10000
12000
14000
150
200
250
300
350
400
450

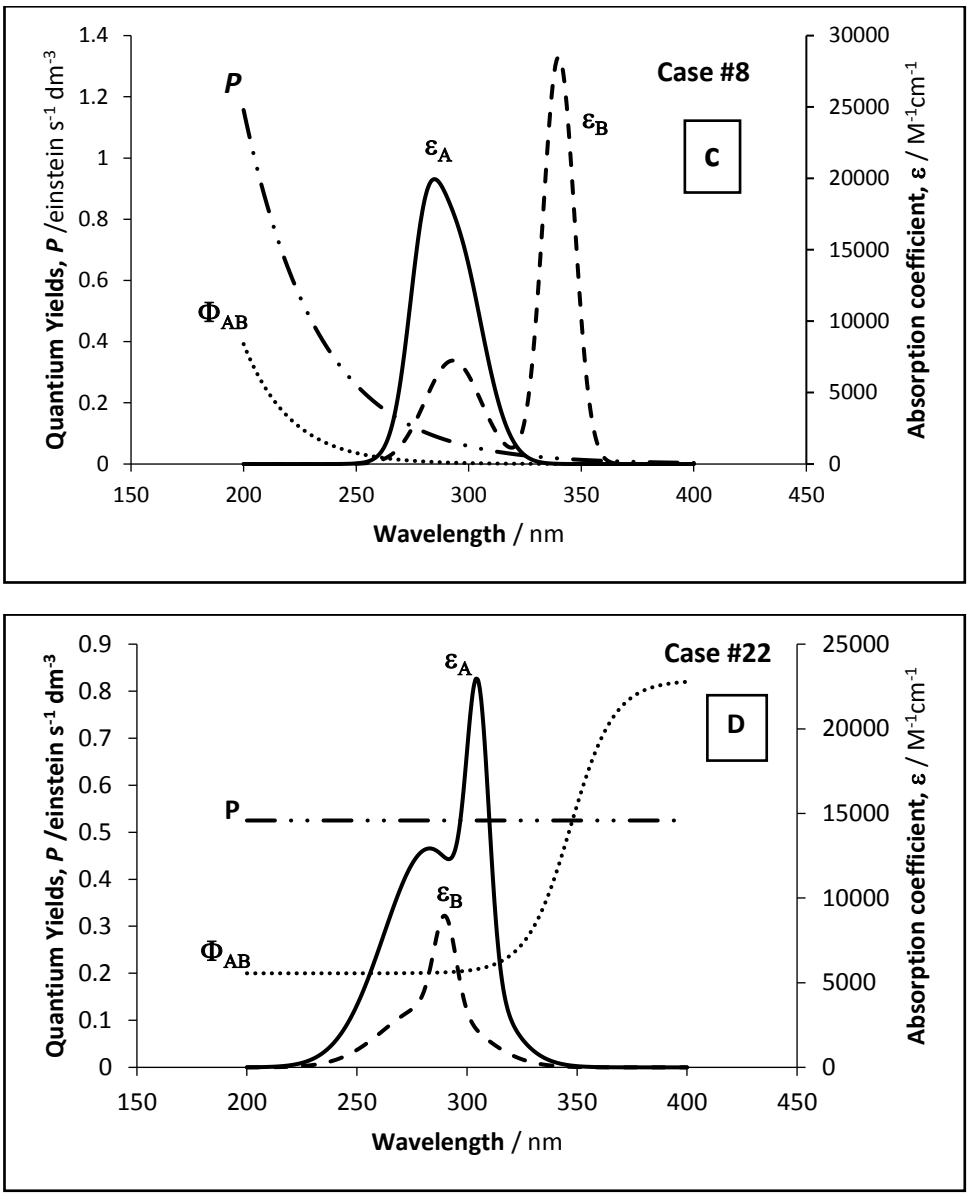

Figure II- 1: a, b, c, D. Examples of simulation profiles of ε_A, ε_B,P, Φ_{AB}.

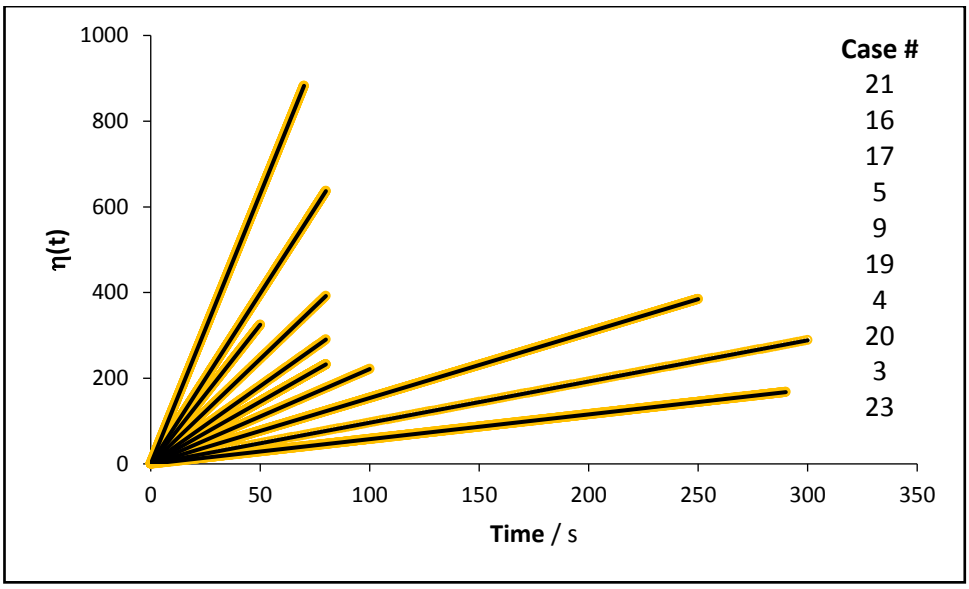

Figure II- 2: applied η–order on the photokinetic traces of simulated date under polychromatic light, circle corresponding to experimental data and line corresponding to the fitting traces using Eq.6-4.

Table II-3. $k_{\eta,\,mod.}$ and $k_{\eta,\,cld.}$

Conc. x 10^4 / M	k_{AB} cld. / s^{-1}	k_{AB} mod. /s^{-1}	Conc. x 10^4 / M	k_{AB} cld. / s^{-1}	k_{AB} mod. /s^{-1}	Conc. x 10^4 / M	k_{AB} cld. / s^{-1}	k_{AB} mod. /s^{-1}
Case 1*			**Case 10***			**Case 19***		
0.5	1.04	1.04	**0.621**	2.22	2.22	**0.511**	2.90	2.90
0.05	1.04	1.04	**0.0685**	2.22	2.22	**0.0545**	2.90	2.90
0.005	1.04	1.04	**0.00412**	2.22	2.22	**0.00541**	2.90	2.90
2	1.04	1.04	**1.45**	2.22	2.22	**1.22**	2.90	2.90
0.212	1.04	1.04	**0.305**	2.22	2.22	**0.45**	2.90	2.90
0.0322	1.04	1.04	**0.0412**	2.22	2.22	**0.0415**	2.90	2.90
0.007	1.04	1.04	**0.00689**	2.22	2.22	**0.00814**	2.90	2.90
0.71	1.04	1.04	**0.856**	2.22	2.22	**0.855**	2.90	2.90
0.0831	1.04	1.04	**0.0912**	2.22	2.22	**0.0944**	2.90	2.90
Case 2*			**Case 11***			**Case 20***		
0.5	0.04	0.04	**0.745**	8.65	8.65	**0.585**	1.54	1.54
0.05	0.04	0.04	**0.0721**	8.65	8.65	**0.0577**	1.54	1.54
0.005	0.04	0.04	**0.00712**	8.65	8.65	**0.00556**	1.54	1.54
0.21	0.04	0.04	**1.12**	8.65	8.65	**1.1**	1.54	1.54
0.005	0.04	0.04	**0.258**	8.65	8.65	**0.405**	1.54	1.54
0.0322	0.04	0.04	**0.0314**	8.65	8.65	**0.0463**	1.54	1.54
0.007	0.04	0.04	**0.00945**	8.65	8.65	**0.00811**	1.54	1.54
0.684	0.04	0.04	**0.814**	8.65	8.65	**0.822**	1.54	1.54
0.0831	0.04	0.04	**0.0955**	8.65	8.65	**0.0901**	1.54	1.54
Case 3*			**Case 12***			**Case 21***		

0.412	0.96	0.96	**0.865**	9.45	9.45	**0.511**	12.60	12.60
0.0652	0.96	0.96	**0.0548**	9.45	9.45	**0.0501**	12.60	12.60
0.00845	0.96	0.96	**0.00451**	9.45	9.45	**0.0057**	12.60	12.60
1.12	0.96	0.96	**1.47**	9.45	9.45	**1.05**	12.60	12.60
0.658	0.96	0.96	**0.213**	9.45	9.45	**0.422**	12.60	12.60
0.0145	0.96	0.96	**0.0579**	9.45	9.45	**0.0432**	12.60	12.60
0.00445	0.96	0.96	**0.00881**	9.45	9.45	**0.00874**	12.60	12.60
0.914	0.96	0.96	**0.715**	9.45	9.45	**0.835**	12.60	12.60
0.0784	0.96	0.96	**0.0844**	9.45	9.45	**0.091**	12.60	12.60
Case 4*			**Case 13***			**Case 22***		
0.745	2.21	2.21	**0.547**	7.13	7.13	**0.574**	0.19	0.19
0.0812	2.21	2.21	**0.0743**	7.13	7.13	**0.0585**	0.19	0.19
0.00923	2.21	2.21	**0.00915**	7.13	7.13	**0.00547**	0.19	0.19
1.45	2.21	2.21	**0.988**	7.13	7.13	**1.19**	0.19	0.19
0.312	2.21	2.21	**0.219**	7.13	7.13	**0.419**	0.19	0.19
0.0415	2.21	2.21	**0.0397**	7.13	7.13	**0.0462**	0.19	0.19
0.00526	2.21	2.21	**0.00714**	7.13	7.13	**0.00848**	0.19	0.19
0.813	2.21	2.21	**0.812**	7.13	7.13	**0.801**	0.19	0.19
0.0632	2.21	2.21	**0.0847**	7.13	7.13	**0.0926**	0.19	0.19
Case 5*			**Case 14***			**Case 23***		
0.512	4.89	4.89	**0.635**	10.25	10.25	**0.515**	0.58	0.58
0.0321	4.89	4.89	**0.0678**	10.25	10.25	**0.0552**	0.58	0.58
0.00624	4.89	4.89	**0.00624**	10.25	10.25	**0.00562**	0.58	0.58
3.47	4.89	4.89	**1.14**	10.25	10.25	**1.25**	0.58	0.58
0.189	4.89	4.89	**0.325**	10.25	10.25	**0.425**	0.58	0.58
0.0458	4.89	4.89	**0.0487**	10.25	10.25	**0.0444**	0.58	0.58
0.00861	4.89	4.89	**0.00974**	10.25	10.25	**0.00856**	0.58	0.58
0.871	4.89	4.89	**0.874**	10.25	10.25	**0.82**	0.58	0.58
0.0743	4.89	4.89	**0.0954**	10.25	10.25	**0.0901**	0.58	0.58
Case 6*			**Case 15***			**Case 24***		
0.417	11.04	11.04	**0.641**	5.91	5.91	**0.585**	3.24	3.24
0.0325	11.04	11.04	**0.0652**	5.91	5.91	**0.0552**	3.24	3.24
0.00742	11.04	11.04	**0.00741**	5.91	5.91	**0.00562**	3.24	3.24
1.45	11.04	11.04	**1.01**	5.91	5.91	**1.24**	3.24	3.24
0.235	11.04	11.04	**0.385**	5.91	5.91	**0.441**	3.24	3.24
0.0412	11.04	11.04	**0.0484**	5.91	5.91	**0.0449**	3.24	3.24
0.00526	11.04	11.04	**0.00956**	5.91	5.91	**0.00854**	3.24	3.24
0.845	11.04	11.04	**0.878**	5.91	5.91	**0.822**	3.24	3.24
0.0941	11.04	11.04	**0.0903**	5.91	5.91	**0.0952**	3.24	3.24
Case 7*			**Case 16***			**Case 25***		
0.00621	4.94	4.94	**0.589**	7.96	7.96	**0.519**	5.27	5.27
0.00812	4.94	4.94	**0.0547**	7.96	7.96	**0.0525**	5.27	5.27
0.0214	4.94	4.94	**0.00574**	7.96	7.96	**0.00535**	5.27	5.27
0.0526	4.94	4.94	**1.35**	7.96	7.96	**1.02**	5.27	5.27
0.0784	4.94	4.94	**0.401**	7.96	7.96	**0.411**	5.27	5.27
0.341	4.94	4.94	**0.0452**	7.96	7.96	**0.0432**	5.27	5.27
0.451	4.94	4.94	**0.00889**	7.96	7.96	**0.00878**	5.27	5.27

0.91	4.94	4.94	**0.814**	7.96	7.96	**0.825**	5.27	5.27
2.22	4.94	4.94	**0.0932**	7.96	7.96	**0.0923**	5.27	5.27
Case 8*			**Case 17***			**Case 26***		
0.487	4.16	4.16	**0.521**	6.49	6.49	**0.547**	7.13	7.13
0.0625	4.16	4.16	**0.0541**	6.49	6.49	**0.0743**	7.13	7.13
0.00514	4.16	4.16	**0.00595**	6.49	6.49	**0.00915**	7.13	7.13
3.14	4.16	4.16	**1.11**	6.49	6.49	**0.988**	7.13	7.13
0.121	4.16	4.16	**0.425**	6.49	6.49	**0.219**	7.13	7.13
0.0233	4.16	4.16	**0.0441**	6.49	6.49	**0.0397**	7.13	7.13
0.00745	4.16	4.16	**0.00871**	6.49	6.49	**0.00714**	7.13	7.13
0.812	4.16	4.16	**0.885**	6.49	6.49	**0.812**	7.13	7.13
0.0854	4.16	4.16	**0.0832**	6.49	6.49	**0.0847**	7.13	7.13
Case 9*			**Case 18***			**Case 27***		
0.478	3.63	3.63	**0.545**	11.70	11.70	**0.545**	11.70	11.70
0.0601	3.63	3.63	**0.0514**	11.70	11.70	**0.0514**	11.70	11.70
0.00524	3.63	3.63	**0.00525**	11.70	11.70	**0.00525**	11.70	11.70
2.58	3.63	3.63	**1.24**	11.70	11.70	**1.24**	11.70	11.70
0.354	3.63	3.63	**0.412**	11.70	11.70	**0.412**	11.70	11.70
0.0212	3.63	3.63	**0.0489**	11.70	11.70	**0.0489**	11.70	11.70
0.00981	3.63	3.63	**0.00813**	11.70	11.70	**0.00813**	11.70	11.70
0.745	3.63	3.63	**0.822**	11.70	11.70	**0.822**	11.70	11.70
0.0901	3.63	3.63	**0.0902**	11.70	11.70	**0.0902**	11.70	11.70

*using same set of data in table II-2.

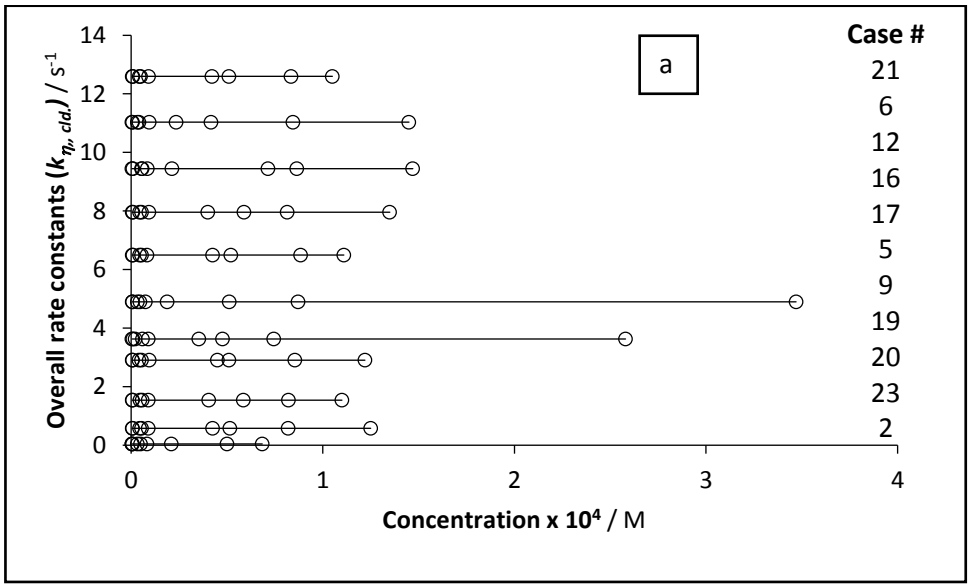

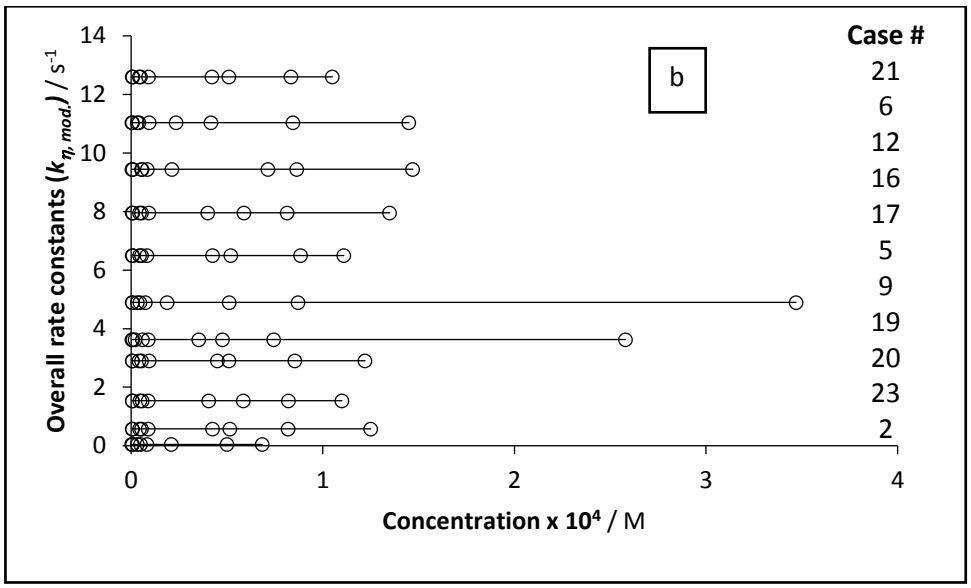

Figure II- 3: a,b. Concentration ($\boldsymbol{C}_A(0)$) independent $k_{\eta,\,mod.}$ and $k_{\eta,\,cld.}$ as predicted by the ▯ model (E.q.6-10) using date in table II-2.

Table II-4. $\upsilon_{0,mod.}$ and $\upsilon_{0,cld.}$

Conc. x 10^4 / M	**(-) ν_0 cld. x10^6** /s^{-1}	**(-) ν_0 mod x10^6** /s^{-1}	**Conc. x 10^4** / M	**(-) ν_0 cld. x 10^6** /s^{-1}	**(-) ν_0 mod x 10^6** /s^{-1}	**Conc. x 10^4** / M	**(-) ν_0 cld. x 10^6** /s^{-1}	**(-) ν_0 mod x10^6** /s^{-1}
Case 1*			**Case 10***			**Case 19***		
0.5	0.62	0.61	**0.621**	2.38	2.36	**0.511**	4.93	4.94
0.05	0.62	0.61	**0.0685**	2.38	2.35	**0.0545**	4.93	4.93
0.005	0.62	0.61	**0.00412**	2.38	2.35	**0.00541**	4.93	4.93
2	0.62	0.61	**1.45**	2.38	2.35	**1.22**	4.93	4.92
0.212	0.62	0.61	**0.305**	2.38	2.35	**0.45**	4.93	4.92
0.0322	0.62	0.61	**0.0412**	2.38	2.35	**0.0415**	4.93	4.92
0.007	0.62	0.61	**0.00689**	2.38	2.35	**0.00814**	4.93	4.93
0.71	0.62	0.61	**0.856**	2.38	2.36	**0.855**	4.93	4.93
0.0831	0.62	0.61	**0.0912**	2.38	2.36	**0.0944**	4.93	4.93
Case 2*			**Case 11***			**Case 20***		
0.5	0.052	0.051	**0.745**	10.87	10.80	**0.585**	2.08	2.08
0.05	0.052	0.051	**0.0721**	10.87	10.70	**0.0577**	2.08	2.08
0.005	0.052	0.051	**0.00712**	10.87	10.55	**0.00556**	2.08	2.08
0.21	0.052	0.051	**1.12**	10.87	10.57	**1.1**	2.08	2.08
0.005	0.052	0.051	**0.258**	10.87	10.50	**0.405**	2.08	2.08
0.0322	0.052	0.051	**0.0314**	10.87	10.50	**0.0463**	2.08	2.08
0.007	0.052	0.051	**0.00945**	10.87	10.63	**0.00811**	2.08	2.08
0.684	0.052	0.051	**0.814**	10.87	10.63	**0.822**	2.08	2.08

0.0831	0.052	0.051	**0.0955**	10.87	10.75	**0.0901**	2.08	2.08
Case 3*			**Case 12***			**Case 21***		
0.412	0.95	0.94	**0.865**	8.82	8.80	**0.511**	12.60	12.50
0.0652	0.95	0.94	**0.0548**	8.82	8.80	**0.0501**	12.60	12.50
0.00845	0.95	0.94	**0.00451**	8.82	8.81	**0.0057**	12.60	12.50
1.12	0.95	0.94	**1.47**	8.82	8.81	**1.05**	12.60	12.50
0.658	0.95	0.94	**0.213**	8.82	8.77	**0.422**	12.60	12.50
0.0145	0.95	0.94	**0.0579**	8.82	8.80	**0.0432**	12.60	12.50
0.00445	0.95	0.94	**0.00881**	8.82	8.80	**0.00874**	12.60	12.50
0.914	0.95	0.94	**0.715**	8.82	8.80	**0.835**	12.60	12.50
0.0784	0.95	0.94	**0.0844**	8.82	8.80	**0.091**	12.60	12.50
Case 4*			**Case 13***			**Case 22***		
0.745	1.31	1.30	**0.547**	6.61	6.60	**0.574**	0.22	0.22
0.0812	1.31	1.30	**0.0743**	6.61	6.60	**0.0585**	0.22	0.22
0.00923	1.31	1.30	**0.00915**	6.61	6.60	**0.00547**	0.22	0.22
1.45	1.31	1.30	**0.988**	6.61	6.61	**1.19**	0.22	0.22
0.312	1.31	1.30	**0.219**	6.61	6.60	**0.419**	0.22	0.22
0.0415	1.31	1.30	**0.0397**	6.61	6.60	**0.0462**	0.22	0.22
0.00526	1.31	1.30	**0.00714**	6.61	6.60	**0.00848**	0.22	0.22
0.813	1.31	1.30	**0.812**	6.61	6.60	**0.801**	0.22	0.22
0.0632	1.31	1.30	**0.0847**	6.61	6.60	**0.0926**	0.22	0.22
Case 5*			**Case 14***			**Case 23***		
0.512	3.68	3.67	**0.635**	9.50	9.50	**0.515**	0.82	0.82
0.0321	3.68	3.67	**0.0678**	9.50	9.50	**0.0552**	0.82	0.82
0.00624	3.68	3.67	**0.00624**	9.50	9.50	**0.00562**	0.82	0.82
3.47	3.68	3.67	**1.14**	9.50	9.50	**1.25**	0.82	0.82
0.189	3.68	3.67	**0.325**	9.50	9.54	**0.425**	0.82	0.82
0.0458	3.68	3.67	**0.0487**	9.50	9.54	**0.0444**	0.82	0.82
0.00861	3.68	3.67	**0.00974**	9.50	9.50	**0.00856**	0.82	0.82
0.871	3.68	3.67	**0.874**	9.50	9.50	**0.82**	0.82	0.82
0.0743	3.68	3.67	**0.0954**	9.50	9.54	**0.0901**	0.82	0.82
Case 6*			**Case 15***			**Case 24***		
0.417	8.21	8.13	**0.641**	4.76	4.76	**0.585**	3.30	3.30
0.0325	8.21	8.04	**0.0652**	4.76	4.77	**0.0552**	3.30	3.30
0.00742	8.21	8.07	**0.00741**	4.76	4.76	**0.00562**	3.30	3.30
1.45	8.21	8.10	**1.01**	4.76	4.76	**1.24**	3.30	3.30
0.235	8.21	8.07	**0.385**	4.76	4.76	**0.441**	3.30	3.30
0.0412	8.21	8.08	**0.0484**	4.76	4.65	**0.0449**	3.30	3.30
0.00526	8.21	8.08	**0.00956**	4.76	4.76	**0.00854**	3.30	3.30
0.845	8.21	8.14	**0.878**	4.76	4.76	**0.822**	3.30	3.30
0.0941	8.21	8.16	**0.0903**	4.76	4.77	**0.0952**	3.30	3.30
Case 7*			**Case 16***			**Case 25***		
0.00621	7.34	7.05	**0.589**	5.04	5.03	**0.519**	0.52	0.52
0.00812	7.34	7.10	**0.0547**	5.04	5.03	**0.0525**	0.52	0.52
0.0214	7.34	7.08	**0.00574**	5.04	5.04	**0.00535**	0.52	0.52
0.0526	7.34	7.10	**1.35**	5.04	5.04	**1.02**	0.52	0.52
0.0784	7.34	7.06	**0.401**	5.04	5.04	**0.411**	0.52	0.52

0.341	7.34	7.01	**0.0452**	5.04	5.05	**0.0432**	0.52	0.52
0.451	7.34	7.09	**0.00889**	5.04	5.04	**0.00878**	0.52	0.52
0.91	7.34	7.075	**0.814**	5.04	5.04	**0.825**	0.52	0.52
2.22	7.34	7.10	**0.0932**	5.04	5.04	**0.0923**	0.52	0.52
Case 8*			**Case 17***			**Case 26***		
0.487	6.31	6.10	**0.521**	4.61	4.60	**0.547**	6.61	6.60
0.0625	6.31	6.14	**0.0541**	4.61	4.60	**0.0743**	6.61	6.60
0.00514	6.31	6.11	**0.00595**	4.61	4.60	**0.00915**	6.61	6.60
3.14	6.31	6.05	**1.11**	4.61	4.60	**0.988**	6.61	6.61
0.121	6.31	6.1	**0.425**	4.61	4.61	**0.219**	6.61	6.60
0.0233	6.31	6.03	**0.0441**	4.61	4.61	**0.0397**	6.61	6.60
0.00745	6.31	6.03	**0.00871**	4.61	4.61	**0.00714**	6.61	6.60
0.812	6.31	6.05	**0.885**	4.61	4.61	**0.812**	6.61	6.60
0.0854	6.31	6.06	**0.0832**	4.61	4.61	**0.0847**	6.61	6.60
Case 9*			**Case 18***			**Case 27***		
0.478	4.12	4.00	**0.545**	8.76	8.75	**0.545**	8.76	8.75
0.0601	4.12	4.00	**0.0514**	8.76	8.75	**0.0514**	8.76	8.75
0.00524	4.12	4.00	**0.00525**	8.76	8.74	**0.00525**	8.76	8.74
2.58	4.12	4.00	**1.24**	8.76	8.76	**1.24**	8.76	8.76
0.354	4.12	4.00	**0.412**	8.76	8.75	**0.412**	8.76	8.75
0.0212	4.12	4.00	**0.0489**	8.76	8.77	**0.0489**	8.76	8.77
0.00981	4.12	4.00	**0.00813**	8.76	8.77	**0.00813**	8.76	8.77
0.745	4.12	4.04	**0.822**	8.76	8.76	**0.822**	8.76	8.76
0.0901	4.12	4.00	**0.0902**	8.76	8.75	**0.0902**	8.76	8.75

*using same set of data in table II-2.

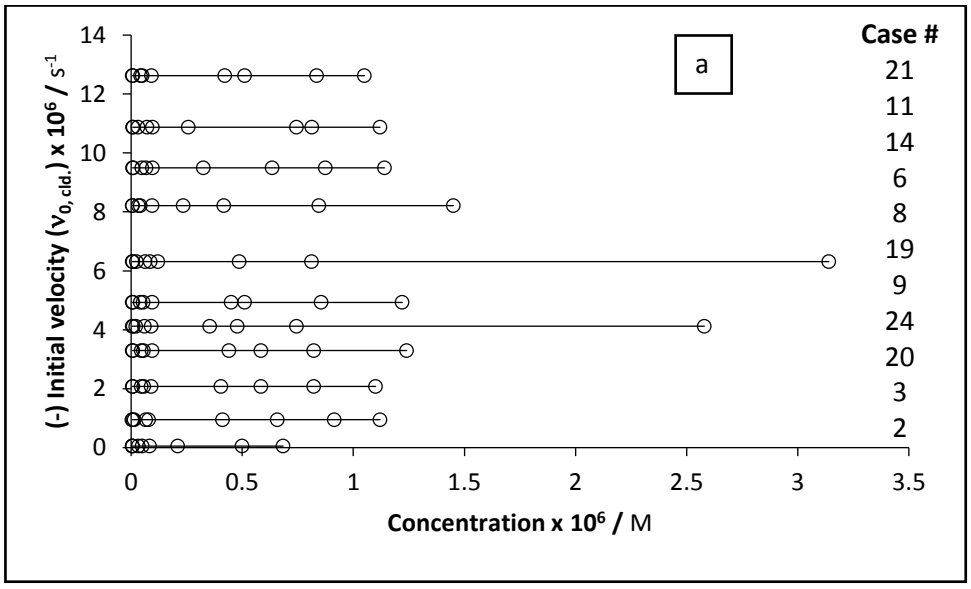

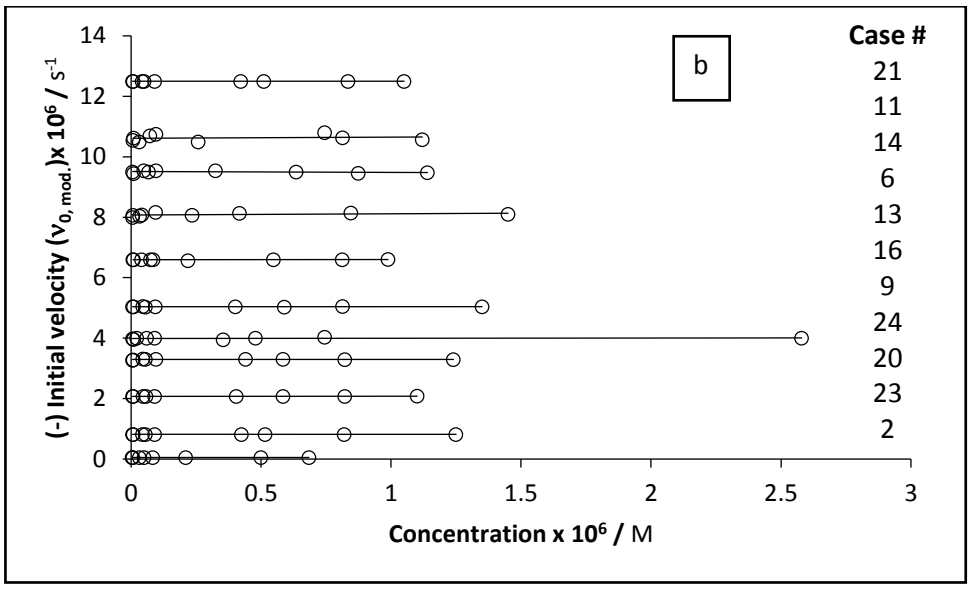

Figure II- 4: a,b. Concentration ($\boldsymbol{C_A}(0)$) independent $v_{0,mod.}$ and $v_{0,cld.}$ as predicted by the model (E.q.6-12) using date in table II-2.

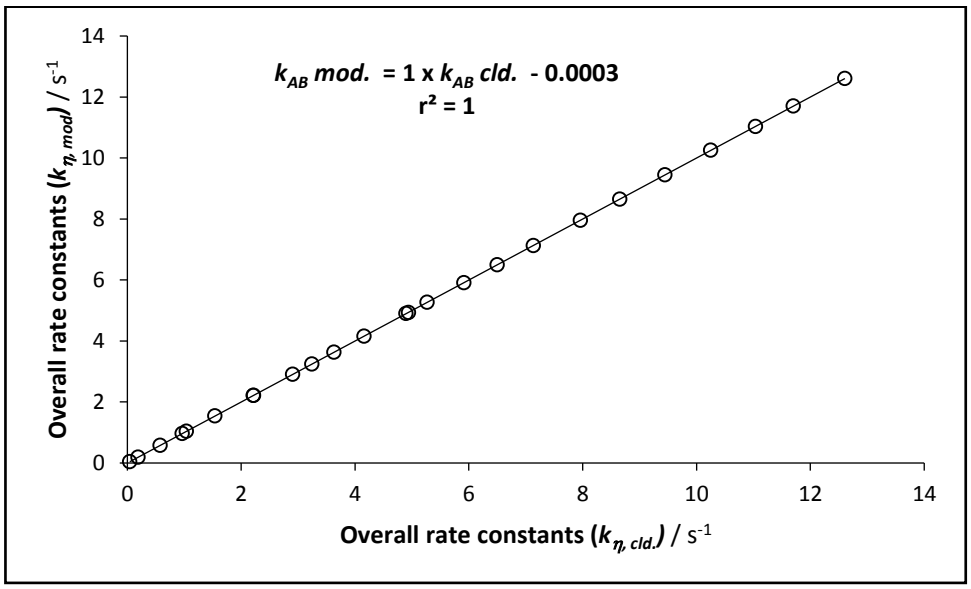

Figure II- 5: Linear correlation between $k_{\eta,\,mod.}$ and $k_{\eta,\,cld.}$ for all different cases in table II-2.

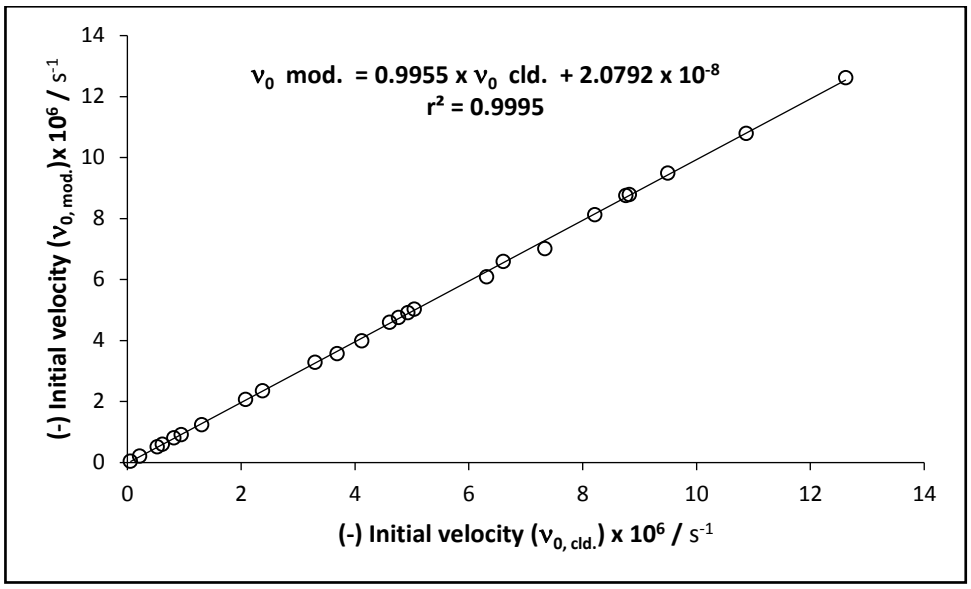

Figure II- 6: Linear correlation between $\upsilon_{0,mod.}$ and $\upsilon_{0,cld.}$ for all different cases in table II-2.

Table II-5. Sets of data used to generate some photoreversible AB (2Φ) photokinetic traces and fitting by using η-order method Eq.6-5.

Case	$\sum \boldsymbol{\varepsilon_A}$ / $M^{-1}cm^{-1}$	$\sum \boldsymbol{\varepsilon_B}$ / $M^{-1}cm^{-1}$	$\frac{\sum \boldsymbol{\varepsilon_A}}{\sum \boldsymbol{\varepsilon_B}}$	ℓ_{irr} / cm	$\sum \boldsymbol{P}$ /einstein s^{-1} dm^{-3}	$\sum(\boldsymbol{\Phi_{AB}} \times \boldsymbol{\varepsilon_A} \times \boldsymbol{P})$	$\sum(\boldsymbol{\Phi_{BA}} \times \boldsymbol{\varepsilon_B} \times \boldsymbol{P})$	$(\sum \boldsymbol{\varepsilon_A} - \sum \boldsymbol{\varepsilon_B})$ / $M^{-1}cm^{-1}$
1	1684678.98	758105.54	2.22	2	0.0019	1.04	0.65	926573.44
2	827826.45	372521.90	2.22	2	0.00012	0.04	0.02	455304.55
3	1012855.50	743938.39	1.36	2	0.0005	0.96	0.21	268917.1
4	1692277.54	2290528.68	0.74	2	0.0005	2.21	0.53	-598251.13
5	1329572.21	1434053.79	0.93	2	0.00196	4.89	0.76	-104481.59
6	1343694.32	417261.63	3.22	2	0.0162	11.04	1.81	926432.69
7	673050.02	727065.49	0.93	2	0.0162	4.94	20.51	-54015.47
8	658414.37	727065.49	0.91	2	0.392	4.16	94.71	-68651.12
9	880339.54	798558.57	1.10	2	0.0161	3.63	24.74	81780.97
10	932108.35	335035.46	2.78	2	0.0167	2.22	14.69	597072.89
11	795819.61	798558.57	0.99	2	0.0090	8.65	11.86	-2738.96
12	1070863.36	930534.27	1.15	2	0.0079	9.45	3.43	140329.08
13	1079447.47	291978.29	3.69	2	0.0078	7.13	2.77	787469.18
14	1079447.28	1509972.65	0.715	2	0.0078	10.25	3.21	-430525.37
15	1241520.37	571941.89	2.17	2	0.0084	5.91	10.05	669578.48
16	1578375.59	1141445.57	1.38	2	0.0083	7.96	5.542	436930.02
17	1409815.78	1013813.01	1.39	2	0.0083	6.49	12.07	396002.76
18	1335639.17	1013813.01	1.32	2	0.018	11.70	12.48	321826.16
19	589188.65	464362.32	1.27	2	0.018	2.90	6.90	124826.33

20	**740465.81**	**467124.60**	**1.56**	**1**	**2**	**0.008**	**1.54**	**4.36**	**273341.21**
21	998674.77	940878.83	1.06	1	2.3	0.047	12.61	6.42	57795.94
22	868338.64	258743.11	3.36	1	2.7	0.0002	0.19	0.03	609595.54
23	705182.11	809532.59	0.87	1	3.1	0.0005	0.58	0.01	-104350.46
24	984038.49	1701212.77	0.58	1	2.5	0.0017	3.24	1.32	-717174.26
25	10075018.39	17009730.94	0.59	1	3	0.0002	5.27	1.85	-6934712.55

* where ℓ_{obs} is 1 cm.

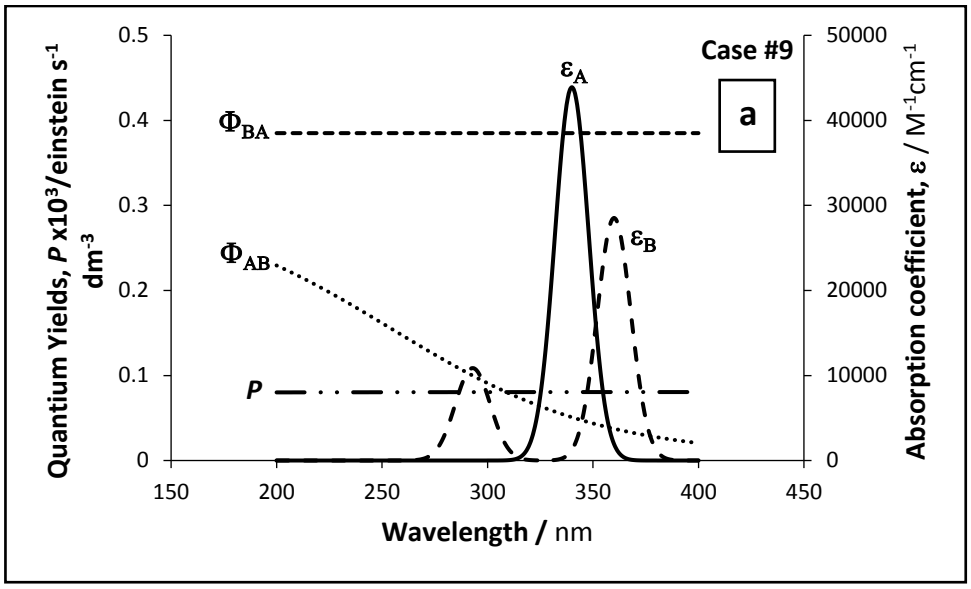
Case #9
a
Quantium Yields, P x10³/einstein s⁻¹ dm⁻³
Absorption coefficient, ε / M⁻¹cm⁻¹
Wavelength / nm
ΦBA
ΦAB
P
εA
εB
0.5
0.4
0.3
0.2
0.1
0
50000
40000
30000
20000
10000
0
150
200
250
300
350
400
450

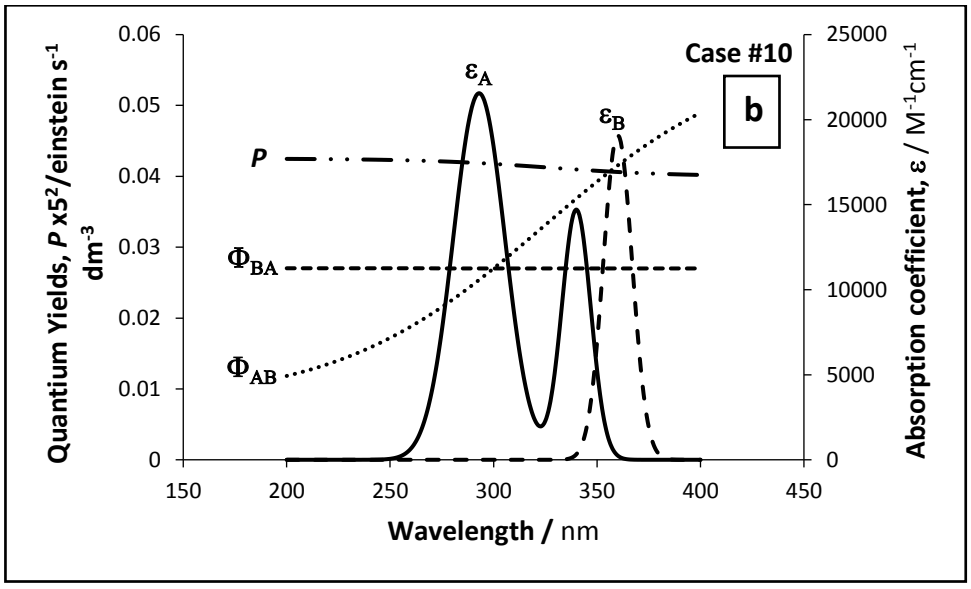
Case #10
b
Quantium Yields, P x5²/einstein s⁻¹ dm⁻³
Absorption coefficient, ε / M⁻¹cm⁻¹
Wavelength / nm
ΦBA
ΦAB
P
εA
εB
0.06
0.05
0.04
0.03
0.02
0.01
0
25000
20000
15000
10000
5000
0
150
200
250
300
350
400
450

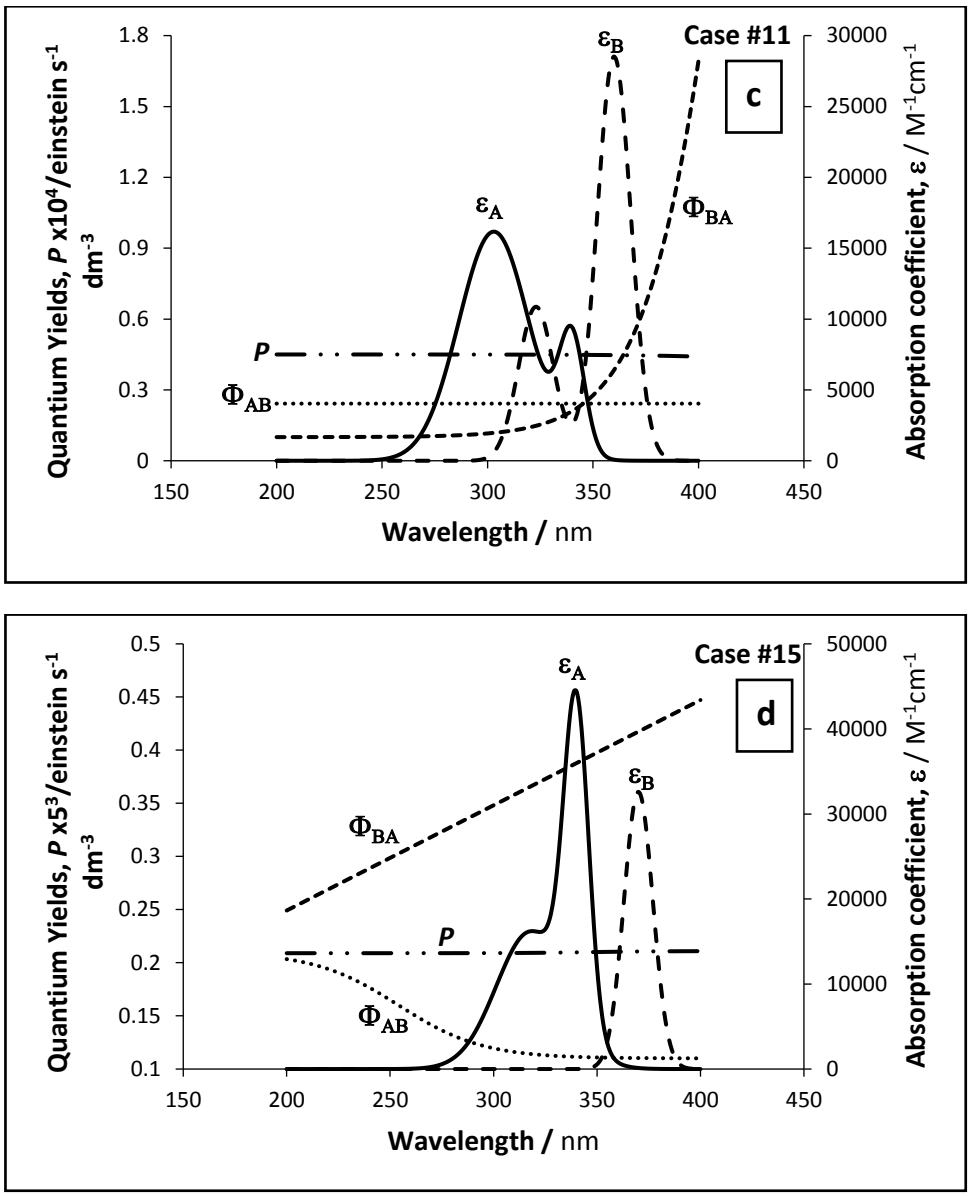

Figure II- 7: a, b, c, Examples of simulation profiles of ε_A, ε_B,P, Φ_{AB} and Φ_{BA}

Table II-6. $k_{\eta,\,mod.}$ and $k_{\eta,\,cld.}$

$C_A(0)$ x 10^5 / M	k_{AB} cld. / s^{-1}	k_{AB} mod. /s^{-1}	$C_A(0)$ x 10^5 / M	k_{AB} cld. / s^{-1}	k_{AB} mod. /s^{-1}	$C_A(0)$ x 10^5 / M	k_{AB} cld. / s^{-1}	k_{AB} mod. /s^{-1}
Case 1*			**Case 10***			**Case 19***		
5.1	0.18	0.18	**5.23**	2.83	2.83	**5.25**	7.86	7.86
0.625	0.18	0.18	**0.501**	2.83	2.83	**0.523**	7.86	7.86
0.0525	0.18	0.18	**0.0541**	2.83	2.83	**0.0532**	7.86	7.86
0.874	0.18	0.18	**3.45**	2.83	2.83	**3.45**	7.86	7.86
0.0725	0.18	0.18	**0.311**	2.83	2.83	**0.352**	7.86	7.86
8.25	0.18	0.18	**0.0624**	2.83	2.83	**0.0625**	7.86	7.86
0.354	0.18	0.18	**7.96**	2.83	2.83	**8.01**	7.86	7.86
0.0545	0.18	0.18	**0.815**	2.83	2.83	**0.81**	7.86	7.86
1.21	0.18	0.18	**0.0907**	2.83	2.83	**0.0901**	7.86	7.86
0.1535	0.18	0.18	**0.1535**	2.83	2.83	**0.1535**	7.86	7.86
0.1014	0.18	0.18	**0.1014**	2.83	2.83	**0.1014**	7.86	7.86
Case 2*			**Case 11***			**Case 20***		
5.41	0.01	0.01	**5.55**	-749	-749	**5**	2.16	2.16
0.422	0.01	0.01	**0.512**	-749	-749	**0.501**	2.16	2.16
0.0541	0.01	0.01	**0.0512**	-749	-749	**0.0514**	2.16	2.16
2.32	0.01	0.01	**3.05**	-749	-749	**3.2**	2.16	2.16
0.352	0.01	0.01	**0.245**	-749	-749	**0.302**	2.16	2.16
0.0756	0.01	0.01	**0.0625**	-749	-749	**0.0601**	2.16	2.16
8.52	0.01	0.01	**7.52**	-749	-749	**8.01**	2.16	2.16
0.954	0.01	0.01	**0.701**	-749	-749	**0.805**	2.16	2.16
0.0874	0.01	0.01	**0.0922**	-749	-749	**0.0874**	2.16	2.16
0.1535	0.01	0.01	**0.1535**	-749	-749	**0.1535**	2.16	2.16
0.1014	0.01	0.01	**0.1014**	-749	-749	**0.1014**	2.16	2.16
Case 3*			**Case 12***			**Case 21***		
5.21	0.43	0.43	**5.25**	9.17	9.17	**5.52**	32.91	32.91
0.463	0.43	0.43	**0.515**	9.17	9.17	**0.523**	32.91	32.91
0.0562	0.43	0.43	**0.0544**	9.17	9.17	**0.0521**	32.91	32.91
1.98	0.43	0.43	**2.05**	9.17	9.17	**3.52**	32.91	32.91
0.301	0.43	0.43	**0.314**	9.17	9.17	**0.285**	32.91	32.91
0.066	0.43	0.43	**0.0625**	9.17	9.17	**0.0624**	32.91	32.91
8.74	0.43	0.43	**7.14**	9.17	9.17	**7.84**	32.91	32.91
0.845	0.43	0.43	**0.801**	9.17	9.17	**0.774**	32.91	32.91
0.0952	0.43	0.43	**0.0901**	9.17	9.17	**0.0856**	32.91	32.91
0.1535	0.43	0.43	**0.1535**	9.17	9.17	**0.1535**	32.91	32.91
0.1014	0.43	0.43	**0.1014**	9.17	9.17	**0.1014**	32.91	32.91
Case 4*			**Case 13***			**Case 22***		
5.01	-0.46	-0.46	**5.74**	1.26	1.26	**5.32**	0.04	0.04
0.42	-0.46	-0.46	**0.525**	1.26	1.26	**0.523**	0.04	0.04
0.0512	-0.46	-0.46	**0.0545**	1.26	1.26	**0.0514**	0.04	0.04
2.41	-0.46	-0.46	**3.25**	1.26	1.26	**2.23**	0.04	0.04

0.3	-0.46	-0.46	**0.351**	1.26	1.26	**0.301**	0.04	0.04
0.0612	-0.46	-0.46	**0.0624**	1.26	1.26	**0.0602**	0.04	0.04
8.65	-0.46	-0.46	**8.04**	1.26	1.26	**7.85**	0.04	0.04
0.841	-0.46	-0.46	**0.814**	1.26	1.26	**0.745**	0.04	0.04
0.0952	-0.46	-0.46	**0.0952**	1.26	1.26	**0.0874**	0.04	0.04
0.1535	-0.46	-0.46	**0.1535**	1.26	1.26	**0.1535**	0.04	0.04
0.1014	-0.46	-0.46	**0.1014**	1.26	1.26	**0.1014**	0.04	0.04
Case 5*			**Case 14***			**Case 23***		
5.3	-5.41	-5.41	**5.52**	-3.13	-3.13	**5.23**	-0.57	-0.57
0.399	-5.41	-5.41	**0.521**	-3.13	-3.13	**0.525**	-0.57	-0.57
0.0558	-5.41	-5.41	**0.0523**	-3.13	-3.13	**0.0521**	-0.57	-0.57
3.25	-5.41	-5.41	**3.45**	-3.13	-3.13	**3.21**	-0.57	-0.57
0.256	-5.41	-5.41	**0.315**	-3.13	-3.13	**0.325**	-0.57	-0.57
0.0362	-5.41	-5.41	**0.0614**	-3.13	-3.13	**0.0632**	-0.57	-0.57
7.8	-5.41	-5.41	**7.84**	-3.13	-3.13	**7.45**	-0.57	-0.57
0.841	-5.41	-5.41	**0.784**	-3.13	-3.13	**0.745**	-0.57	-0.57
0.0745	-5.41	-5.41	**0.0901**	-3.13	-3.13	**0.0901**	-0.57	-0.57
0.1535	-5.41	-5.41	**0.1535**	-3.13	-3.13	**0.1535**	-0.57	-0.57
0.1014	-5.41	-5.41	**0.1014**	-3.13	-3.13	**0.1014**	-0.57	-0.57
Case 6*			**Case 15***			**Case 24***		
5.85	1.39	1.39	**5.41**	2.38	2.38	**5.62**	-0.64	-0.64
0.423	1.39	1.39	**0.512**	2.38	2.38	**0.541**	-0.64	-0.64
0.0451	1.39	1.39	**0.0541**	2.38	2.38	**0.0542**	-0.64	-0.64
2.01	1.39	1.39	**2.25**	2.38	2.38	**2.86**	-0.64	-0.64
0.223	1.39	1.39	**0.336**	2.38	2.38	**0.301**	-0.64	-0.64
0.066	1.39	1.39	**0.0641**	2.38	2.38	**0.0625**	-0.64	-0.64
7.41	1.39	1.39	**7.45**	2.38	2.38	**7.45**	-0.64	-0.64
0.841	1.39	1.39	**0.785**	2.38	2.38	**0.732**	-0.64	-0.64
0.0912	1.39	1.39	**0.0925**	2.38	2.38	**0.0865**	-0.64	-0.64
0.1535	1.39	1.39	**0.1535**	2.38	2.38	**0.1535**	-0.64	-0.64
0.1014	1.39	1.39	**0.1014**	2.38	2.38	**0.1014**	-0.64	-0.64
Case 7*			**Case 16***			**Case 25***		
5.23	-47.10	-47.10	**5.22**	3.09	3.09	**5.32**	-0.10	-0.10
0.521	-47.10	-47.10	**0.541**	3.09	3.09	**0.534**	-0.10	-0.10
0.0478	-47.10	-47.10	**0.0541**	3.09	3.09	**0.0536**	-0.10	-0.10
3.56	-47.10	-47.10	**2.23**	3.09	3.09	**3.25**	-0.10	-0.10
0.425	-47.10	-47.10	**0.301**	3.09	3.09	**0.315**	-0.10	-0.10
0.0614	-47.10	-47.10	**0.0621**	3.09	3.09	**0.0612**	-0.10	-0.10
8.52	-47.10	-47.10	**8.01**	3.09	3.09	**7.41**	-0.10	-0.10
0.814	-47.10	-47.10	**0.801**	3.09	3.09	**0.752**	-0.10	-0.10
0.077	-47.10	-47.10	**0.0912**	3.09	3.09	**0.0912**	-0.10	-0.10
0.1535	-47.10	-47.10	**0.1535**	3.09	3.09	**0.1535**	-0.10	-0.10
0.1014	-47.10	-47.10	**0.1014**	3.09	3.09	**0.1014**	-0.10	-0.10
Case 8*			**Case 17***					
5.23	-144	-144	**5.52**	4.69	4.69			
0.403	-144	-144	**0.523**	4.69	4.69			
0.0454	-144	-144	**0.0545**	4.69	4.69			

3.45	-144	-144	**2.95**	4.69	4.69
0.235	-144	-144	**0.314**	4.69	4.69
0.0614	-144	-144	**0.062**	4.69	4.69
7.84	-144	-144	**7.85**	4.69	4.69
0.789	-144	-144	**0.741**	4.69	4.69
0.0847	-144	-144	**0.0902**	4.69	4.69
0.1535	-144	-144	**0.1535**	4.69	4.69
0.1014	-144	-144	**0.1014**	4.69	4.69
Case 9*			**Case 18***		
6.21	34.69	34.69	**5.14**	7.51	7.51
0.512	34.69	34.69	**0.415**	7.51	7.51
0.0501	34.69	34.69	**0.0554**	7.51	7.51
3.45	34.69	34.69	**2.45**	7.51	7.51
0.341	34.69	34.69	**0.325**	7.51	7.51
0.0614	34.69	34.69	**0.0614**	7.51	7.51
7.54	34.69	34.69	**8.14**	7.51	7.51
0.774	34.69	34.69	**0.874**	7.51	7.51
0.0874	34.69	34.69	**0.0947**	7.51	7.51
0.1535	34.69	34.69	**0.1535**	7.51	7.51
0.1014	34.69	34.69	**0.1014**	7.51	7.51

*using same set of data in table 1.

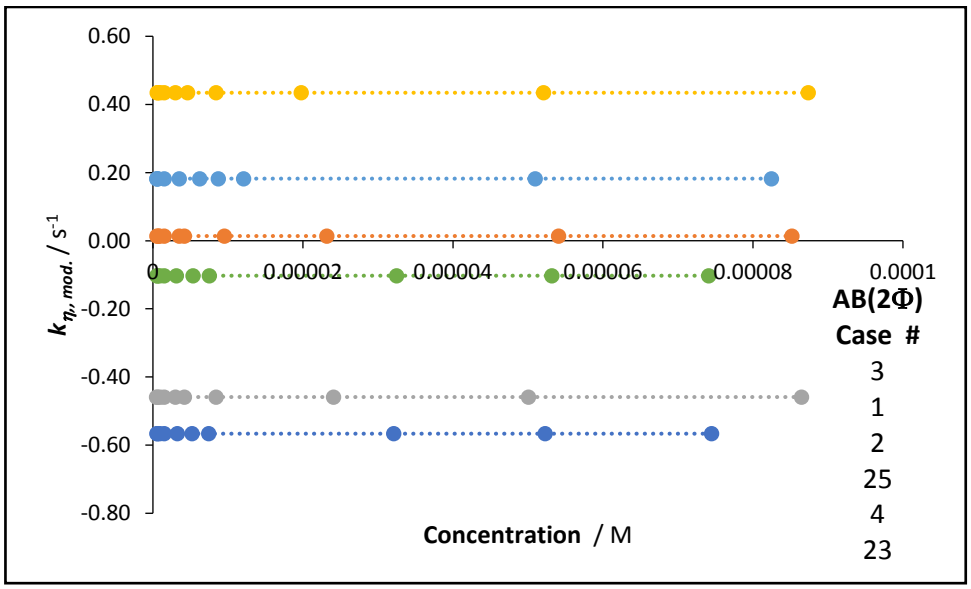

Figure II- 8: Concentration ($\boldsymbol{C_A}(0)$) independent $k_{\eta,\,mod.}$ and $k_{\eta,\,cld.}$ as predicted by the η–model (E.q.6-11) using date in table II-5.

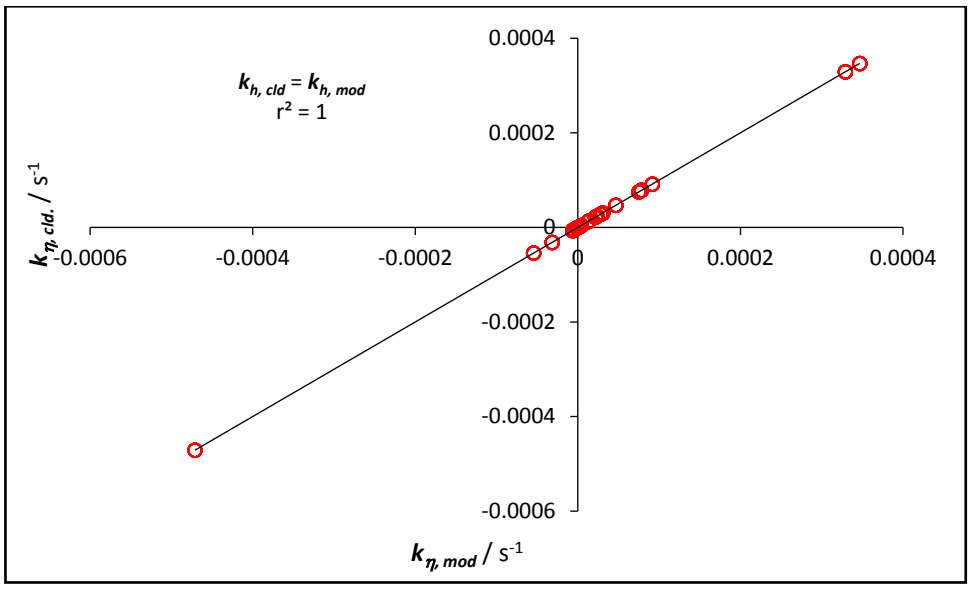

Figure II- 9: Linear correlation between $k_{\eta,\,mod.}$ and $k_{\eta,\,cld.}$ for all different cases in table II-5.

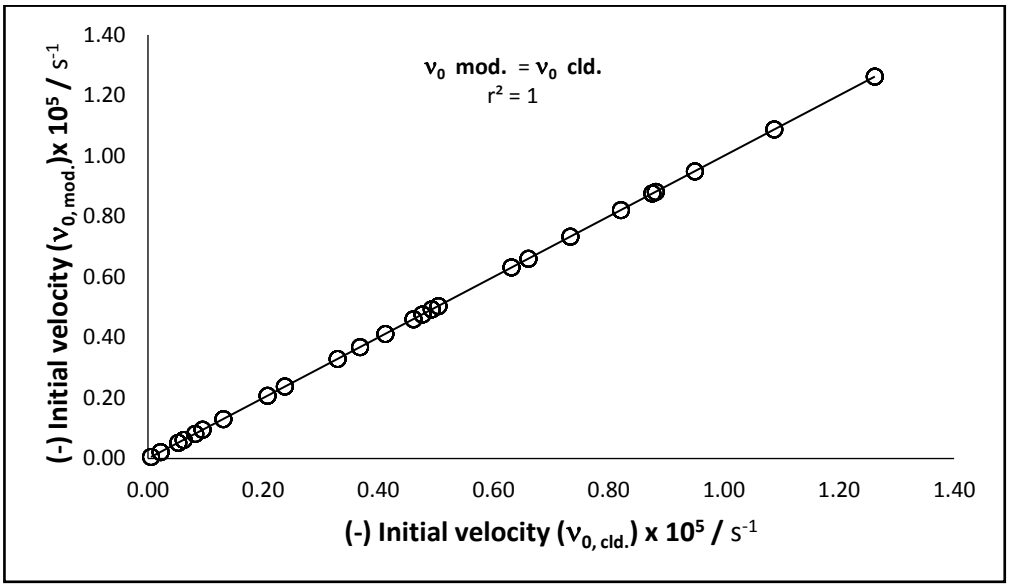

Figure II- 10: Linear correlation between $\upsilon_{0,mod.}$ and $\upsilon_{0,cld.}$ for all different cases in table II-5.

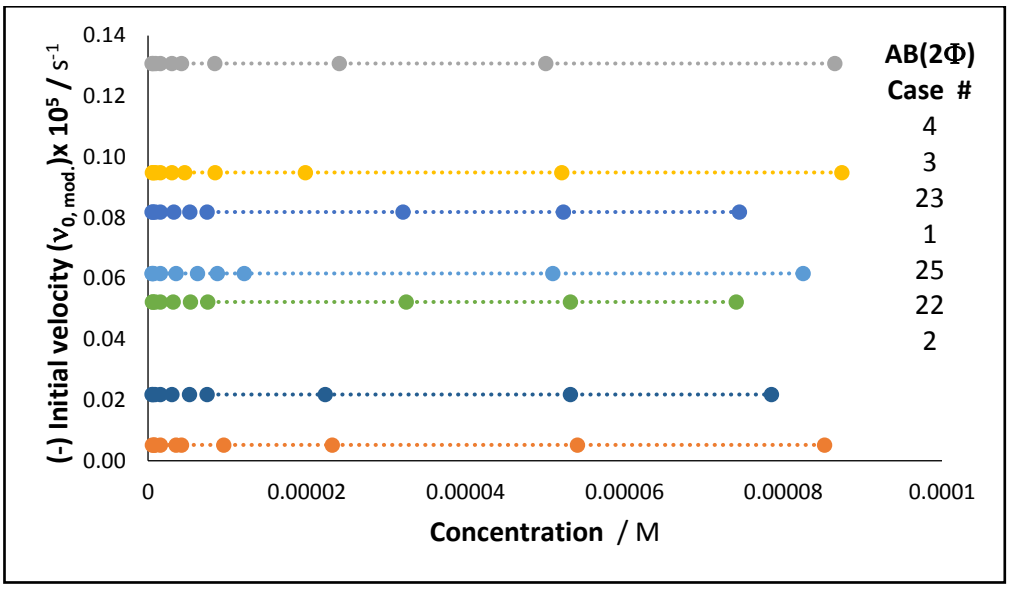

Figure II- 11: Concentration ($C_A(0)$) independent $v_{0,mod.}$ and $v_{0,cld.}$ as predicted by the η–model (E.q.6-13) using date in table II-5.

5. Actinometry

5.1. AB$(1\Phi)_{\varepsilon_{B=0}}$ system actinometry study

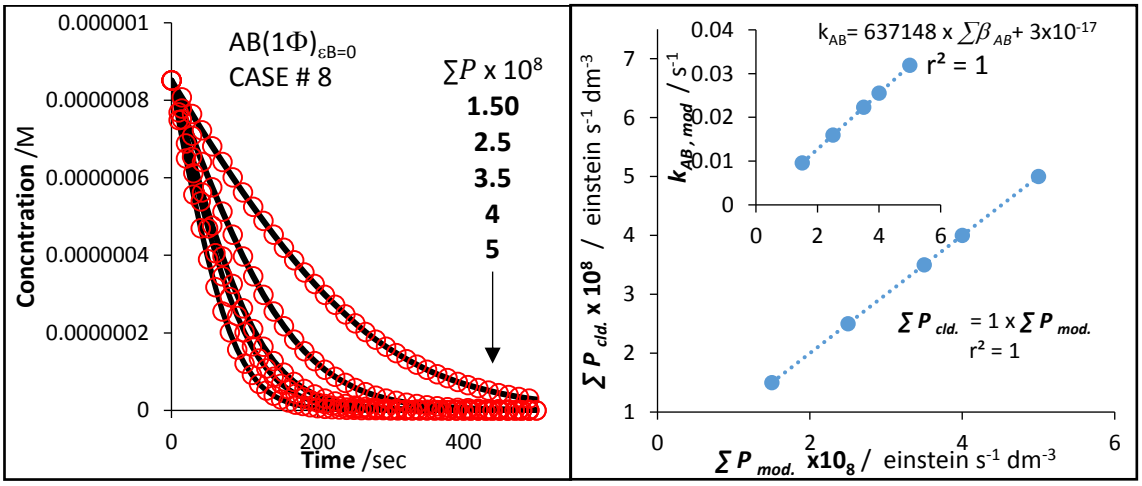

Figure II- 12: (a) Effect of increasing the radiant power of the polychromatic irradiation beam on the photokinetic traces of simulated date at range 400-600nm. The experimental data (circles) were fitted by Eq. 6-1. (b) Linear correlation of $k_{A\rightleftharpoons B}^{\lambda_{irr}}$ (in s-1) with $\sum P_{\lambda_{irr}}$ (in einstein s^{-1} dm^{-3}) for each.

5.2. AB$(1\Phi)_{\varepsilon_{B\neq0}}$ and AB(2Φ) systems actinometry study

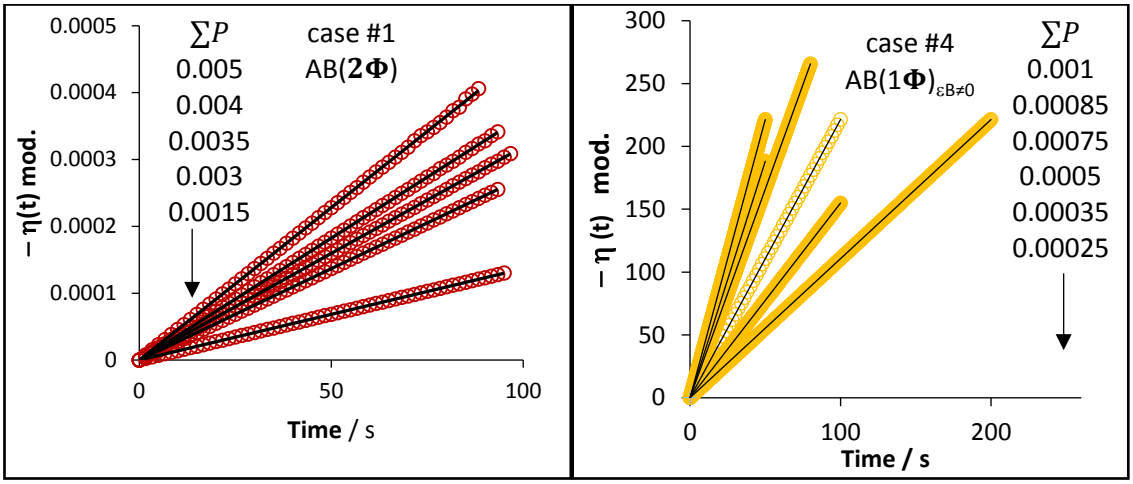

Figure II- 13: Effect of increasing the radiant power of the polychromatic irradiation beam on the photokinetic traces of simulated date at range 200-400nm. The experimental data (circles) were fitted by Eq. 6-4.

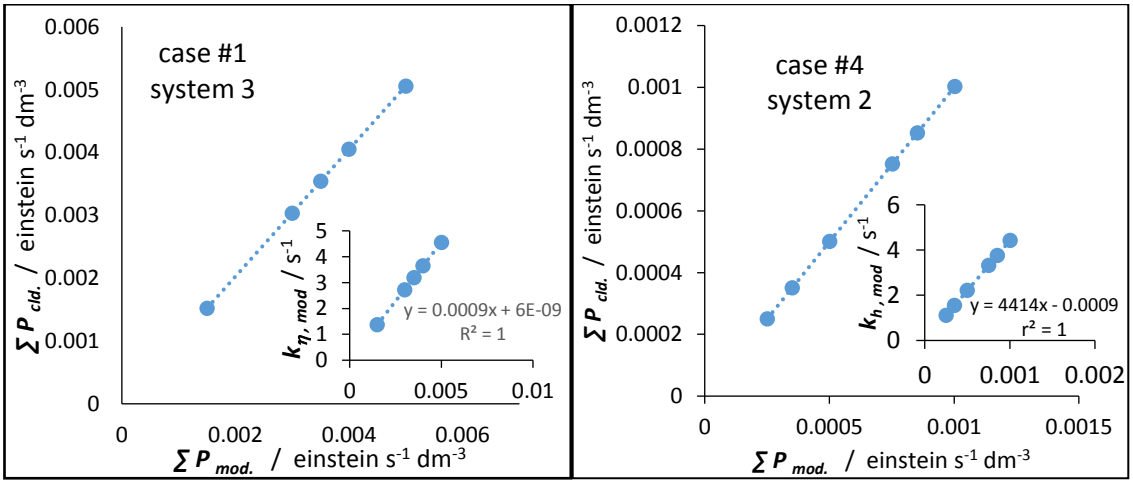

Figure II- 14:. Linear correlation of experimental ($\sum P$) and calculated ($\sum P$) values of the radiant power showing simulation cases. Inset: the linear relationship between the $k_{\eta,mod.}$ and $\sum P$.

Appendix III

Result of the study C-DAE under polychromatic irradiation light and fitting by using Φ-order model

(Chapter 7)

Result of the study C-DAE under polychromatic irradiation light and fitting by using Φ-order model

1. **Preparation the C-DAE from under irradiation O-DAE under UV light and photokinetic study of C-DAE**

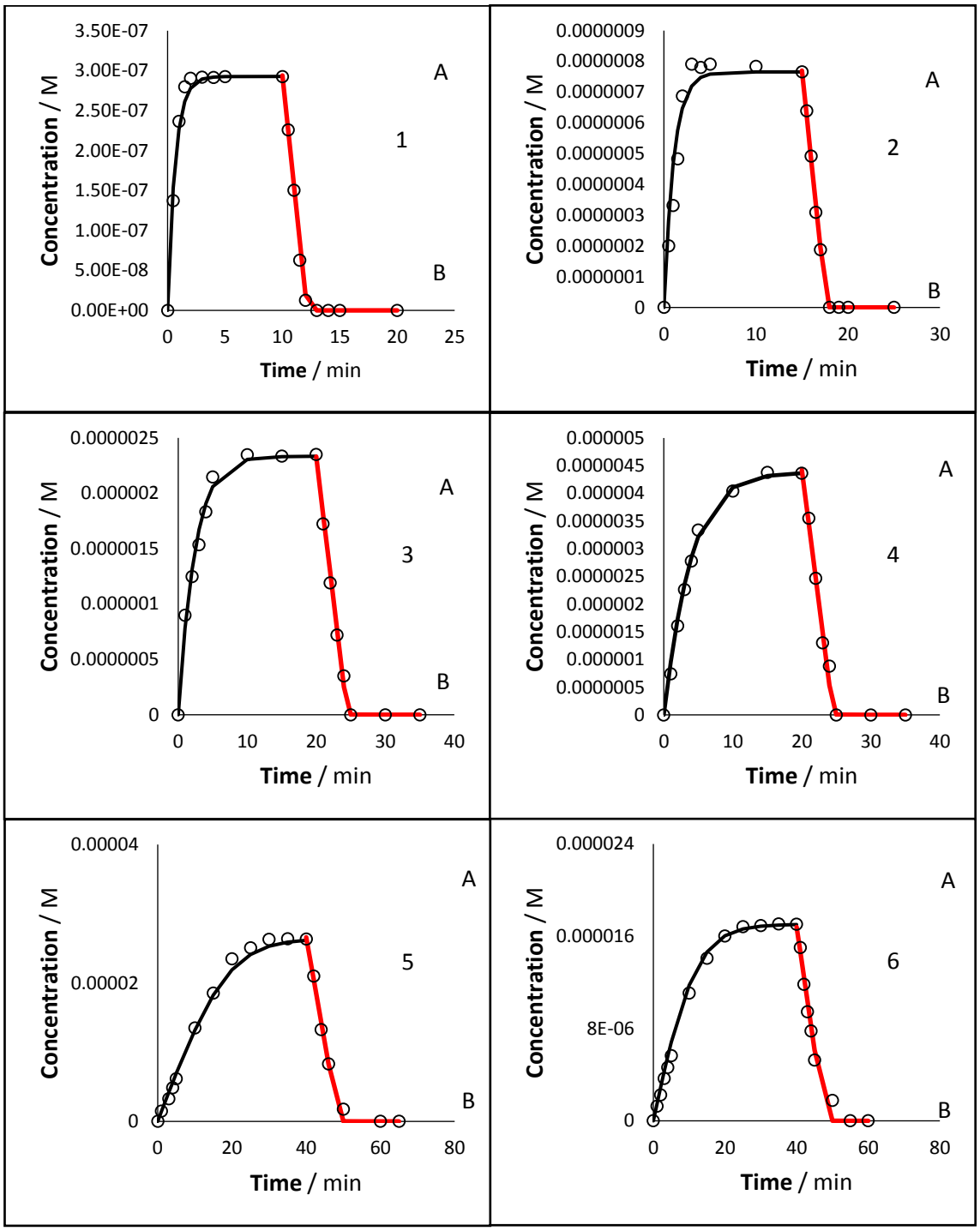

Figure III- 1: 1,2,3,4,5,6 HPLC traces of C-DAE at different concentration (red line fitting by using Eq.7-1, chapter seven).

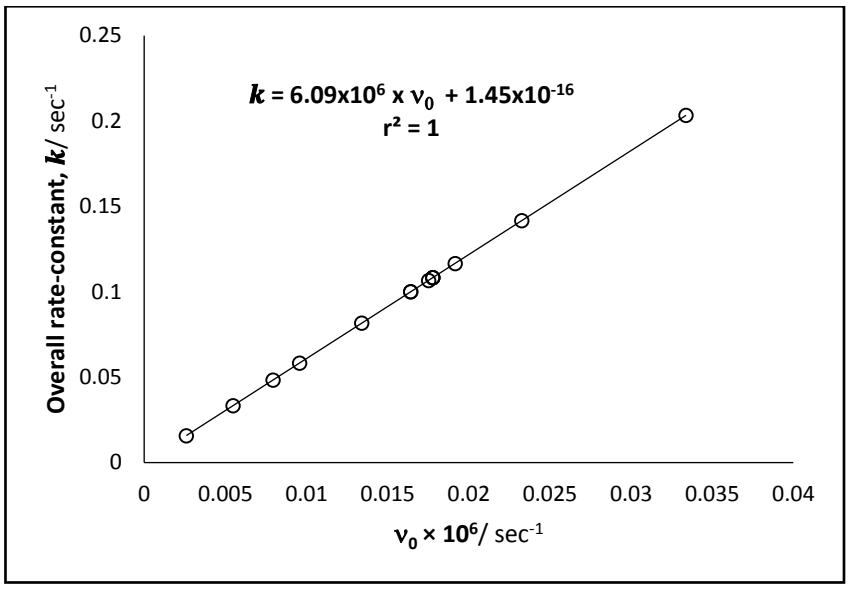

Figure III- 2: Linear relation between Overall rate-constant (k) and -$v_{0,exp}$ for both study concentration effect and actinometry.

Appendix IV

Result of study photodegradation of studies compounds under polychromatic irradiation light and applied η-order model

(Chapter 8)

Result of study photodegradation of studies compounds under polychromatic irradiation light and applied η-order model

i. **Spectrum electronic evolution of studied compounds under polychromatic light irradiation**:

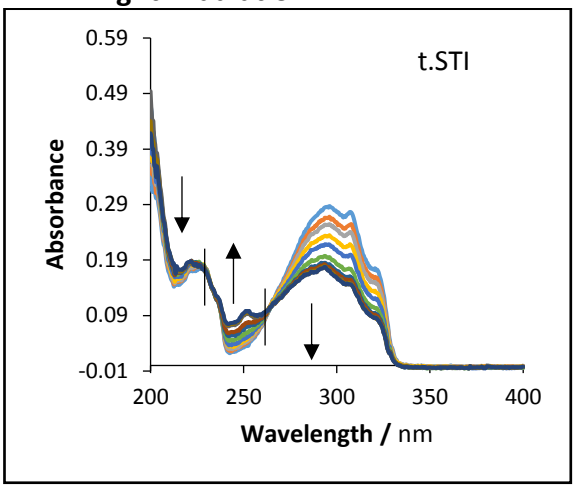

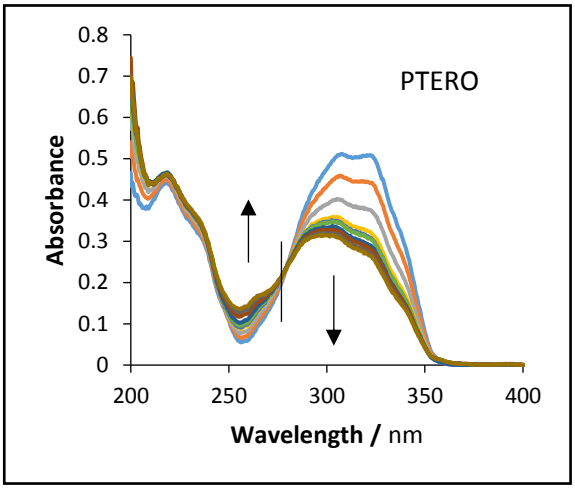

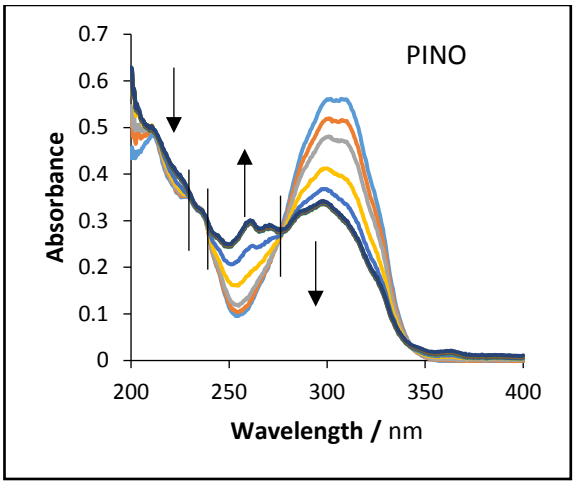

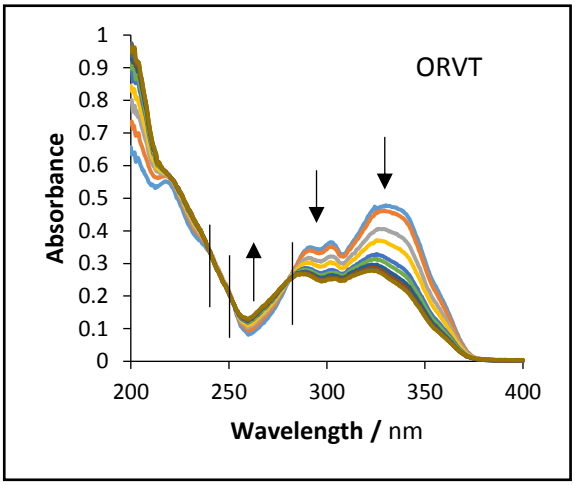

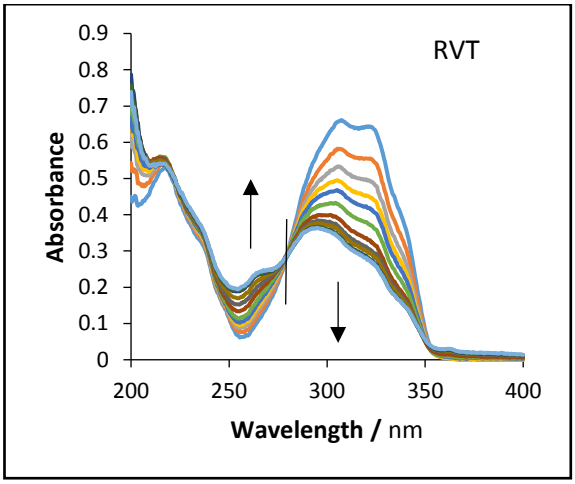

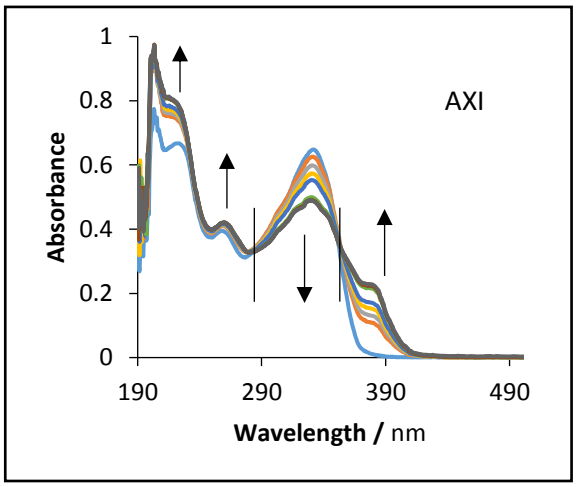

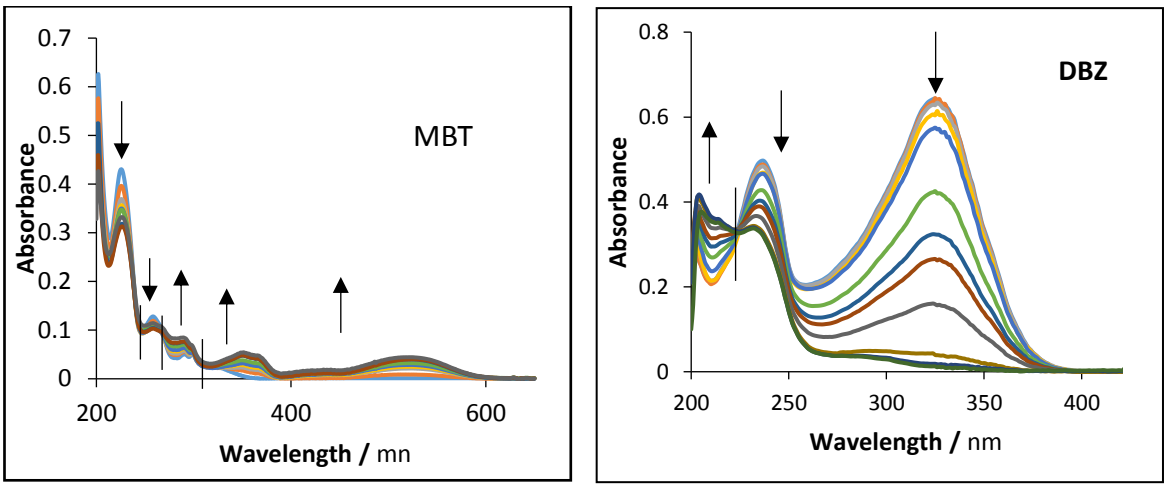

Figure IV- 1: Evolution of the absorption spectra of t-STIL, PINO, RVT, ORVT, PTERO, AXI, O-DAE and DBZ (1.26×10-5 , 1.83×10-5 , 2.17×10-5 , 1.81×10-5 , 2.08×10-5 , 2.23×10-5, 1.36 x 105 and 5.41×10-5 M) in ethanol, when subjected to a polychromatic steady irradiation (200-400 nm) using mix wavelength lamp (254/365 nm). Arrows indicate direction of evolution; vertical lines cross the spectra at the isosbestic points.

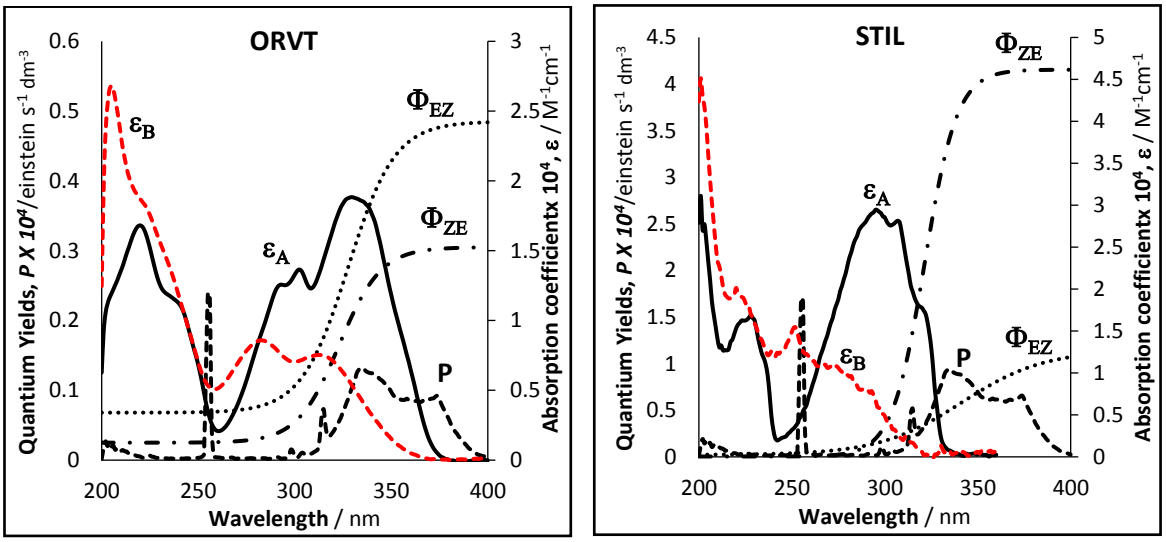

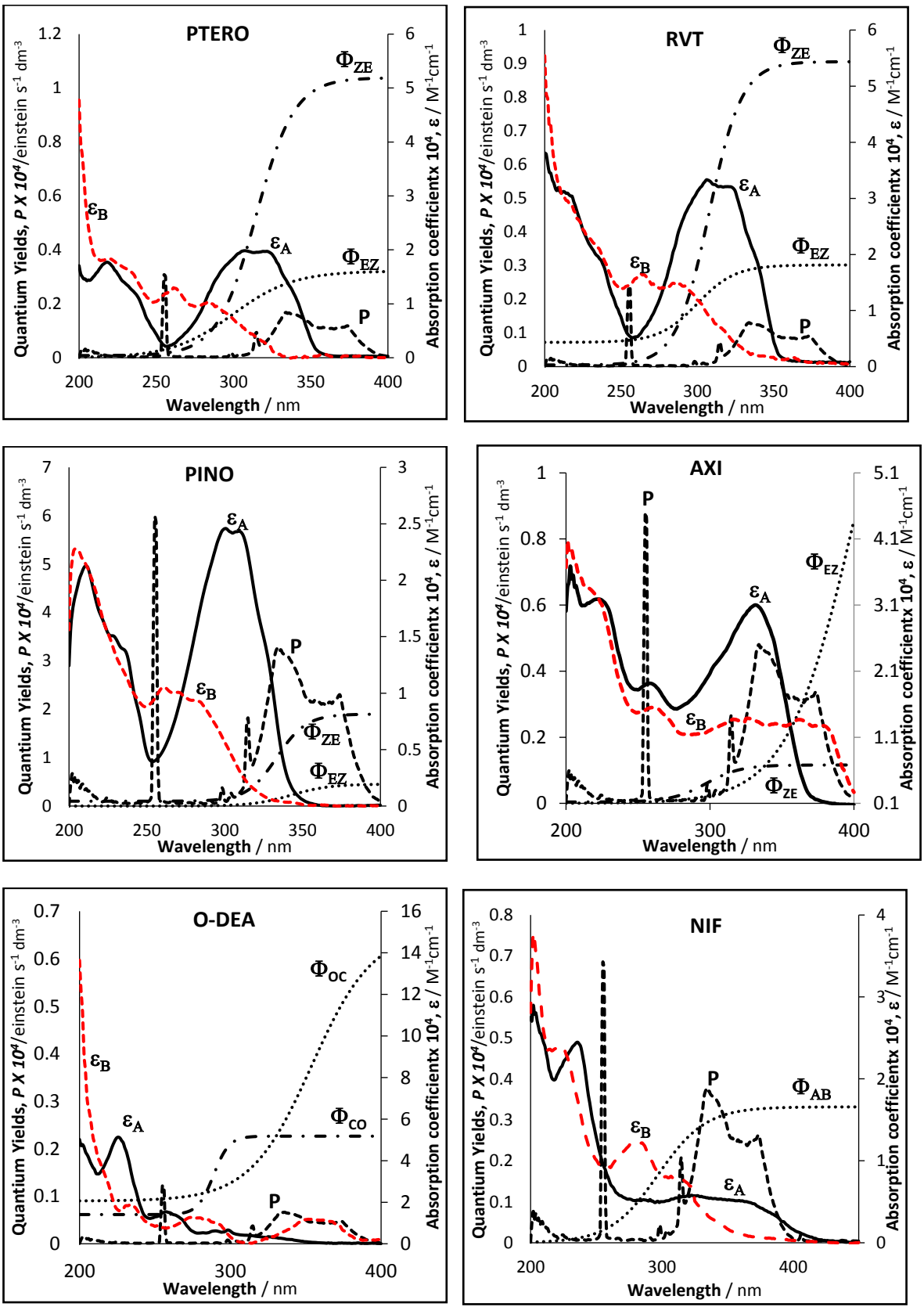

Figure IV- 2: *Profiles of experimental ε_A, ε_B, P, Φ_{AB} and Φ_{BA} of studies compounds using mix wavelength lamp (254/365 nm).*

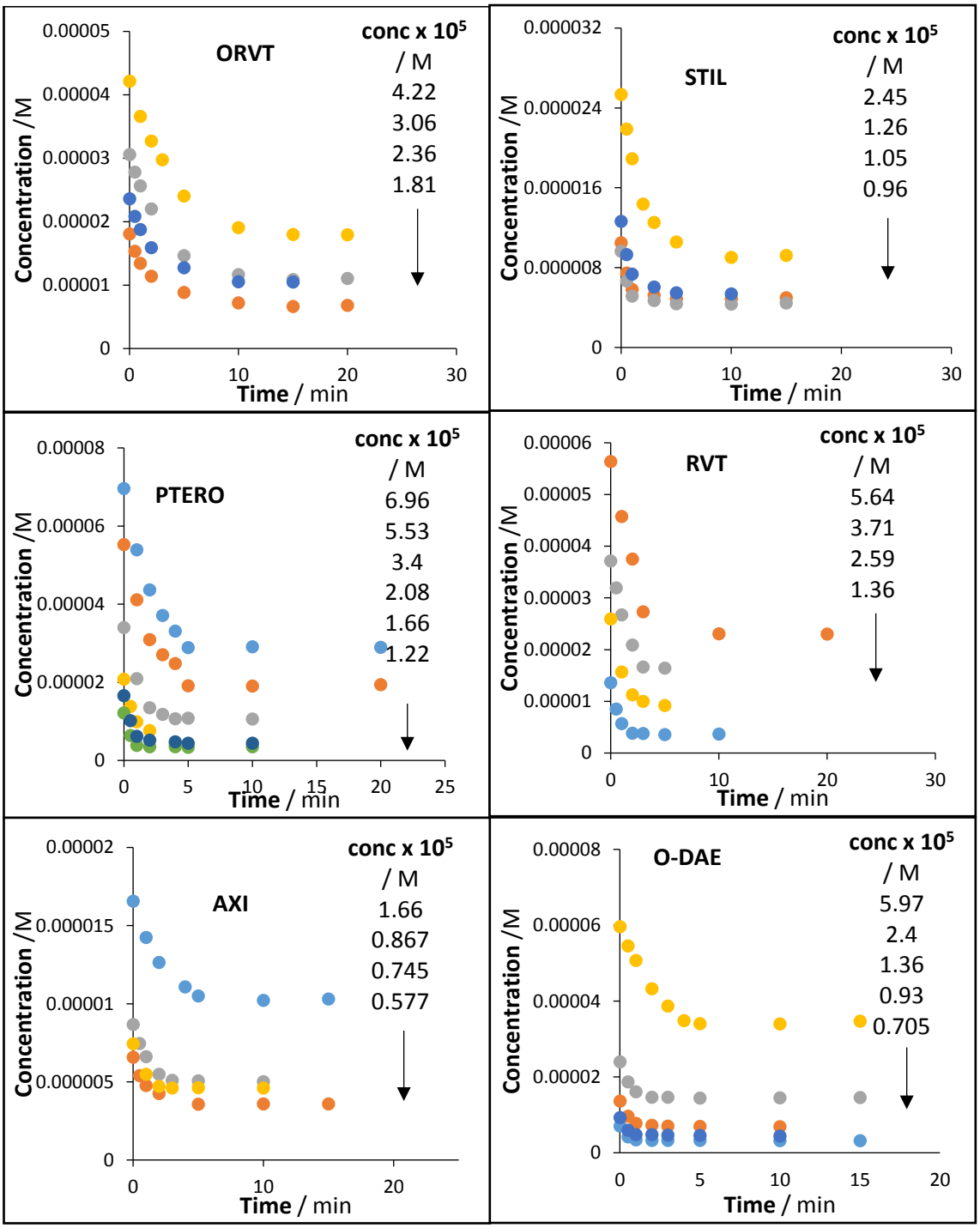

Figure IV-3: *Photokinetic traces of studies compounds under polychromatic light* using mix wavelength lamp (254/365 nm) and monitoring by using HPLC.

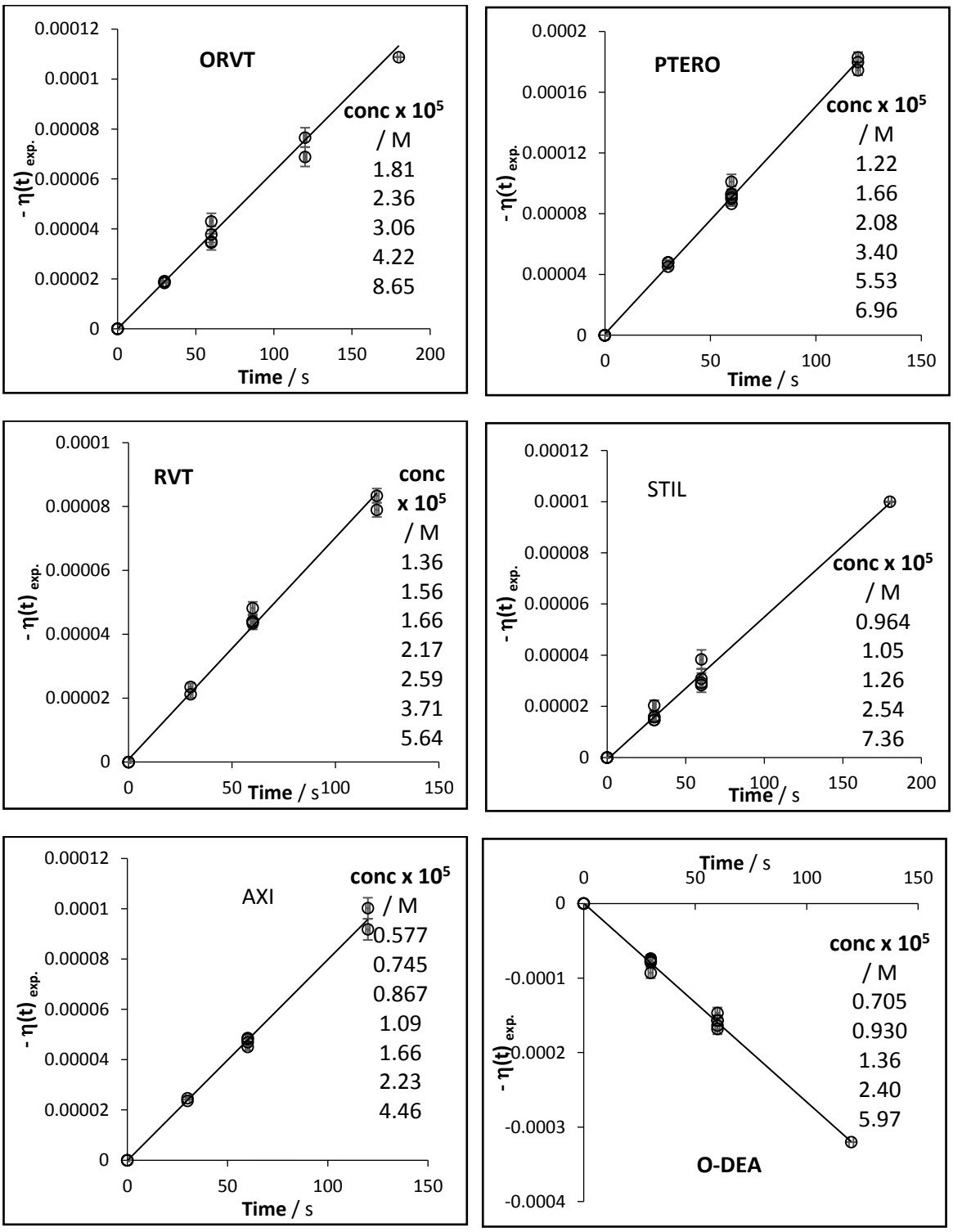

Figure IV- 4: Applied η-order on p*hotokinetic traces of studies compounds under polychromatic light using mix wavelength lamp (254/365 nm)., circle corresponding to experimental data and line corresponding to the fitting traces using Eq.6-4.*

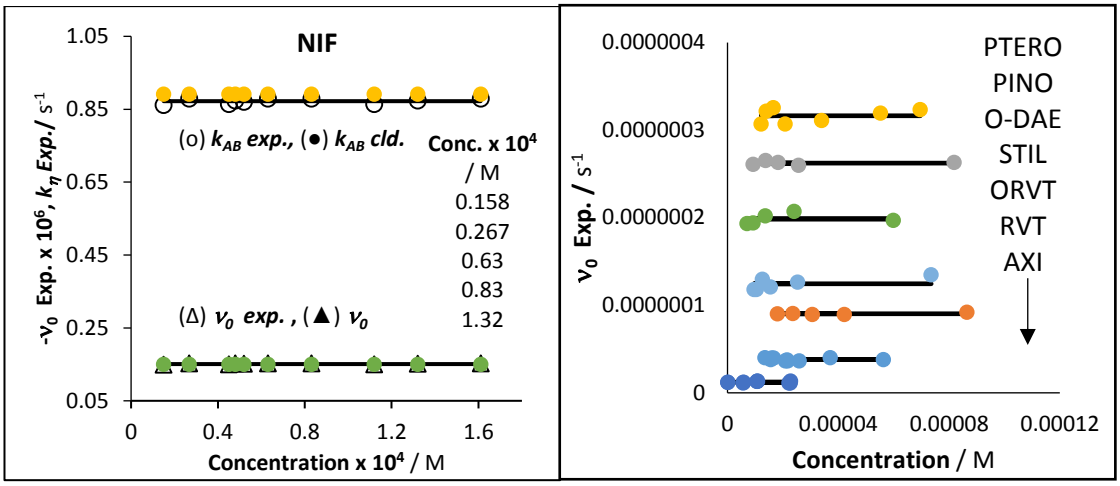

Figure IV- 5: Constant $\upsilon_{0,exp.}$ of studies compounds with different initial concentration ($\boldsymbol{C_A}(0)$). The open and solid symbols represent the experimental and calculated values of $\upsilon_{0,cld.}$.

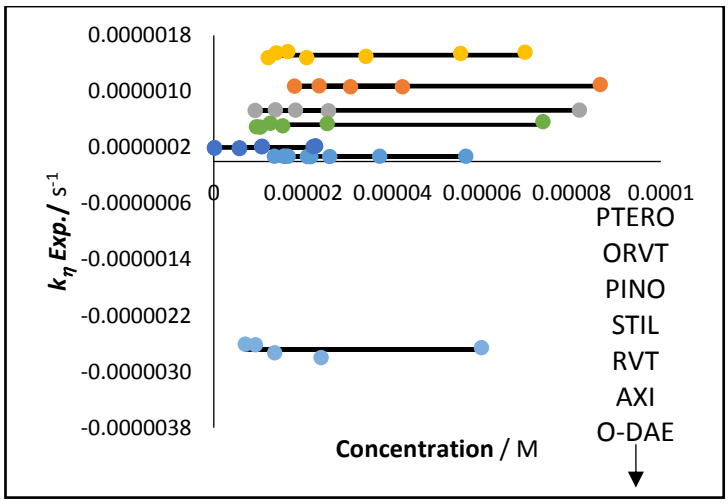

Figure IV- 6: Constant $k_{\eta,\,exp.}$ of studies compounds of AB (2Φ) system with different initial concentration ($\boldsymbol{C_A}(0)$).

Appendix V

This appendix shows the results of (Development of actinometers) under monochromatic and polychromatic light irradiation.
(Chapter 9)

This appendix shows the results of chapter 9 (Development of actinometers) under monochromatic and polychromatic light irradiation.

1. Actinometry under Monochromatic irradiation study

Table V-1: *Correlation equations for the variation of the three drug's photodegradation overall rate-constants ($k_{A\leftrightharpoons B}^{\lambda_{irr}}$) with radiant power ($P_{\lambda_{irr}}$) and the area of radiant power employed for various monochromatic irradiations.*

Irradiation wavelength λ_{irr} /nm	Equation of the line $k_{A\leftrightharpoons B}^{\lambda_{irr}} = \beta_{\lambda_{irr}} \times P_{\lambda_{irr}} + \text{Intercept}$	Correlation coefficient, r^2	$P_{\lambda_{irr}}$ x 10^7 / einsteins^{-1} dm^{-3}
310	8751.1 × P_{310} + 0.0003	0.965	1.29 – 2.34
328	14171 × P_{328} + 0.0012	0.953	1.56 – 2.86
340	23587 × P_{340} + 0.0004	0.977	1.69 – 3.17
350	19590 × P_{350} + 0.0017	0.980	1.5 – 3.28
360	6317.5× P_{360} + 0.0102	0.991	4.47 – 7.61

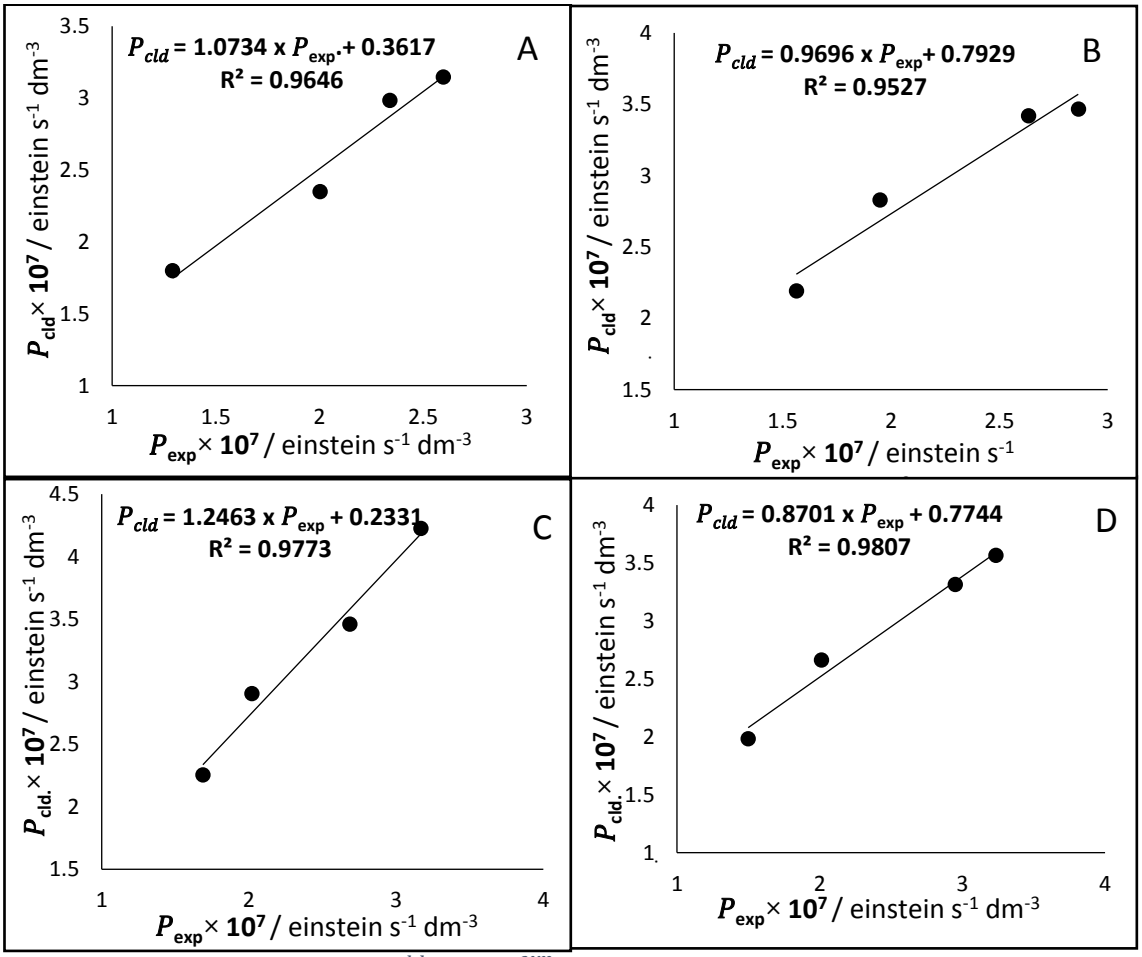

Figure V- 1: Linear correlation of $P_{\lambda_{irr}}^{cld.}$ with $P_{\lambda_{irr}}^{exp.}$ for each wavelength, which Fig. A at 310 nm, B at 328 nm, C at 340 nm and D at 350 nm by using line Equation Table V-1.

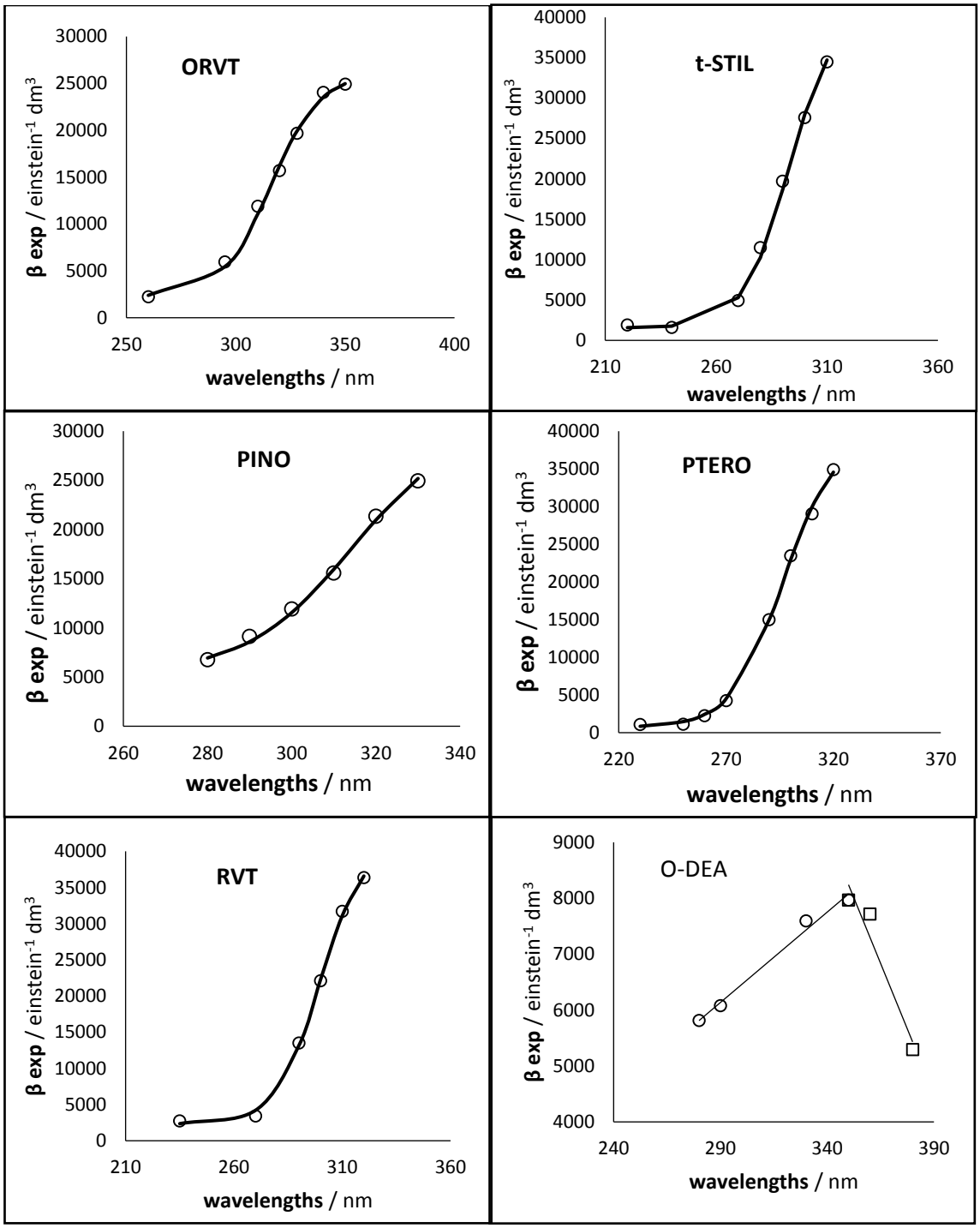
ORVT
β exp / einstein-1 dm3
wavelengths / nm
t-STIL
β exp / einstein-1 dm3
wavelengths / nm
PINO
β exp / einstein-1 dm3
wavelengths / nm
PTERO
β exp / einstein-1 dm3
wavelengths / nm
RVT
β exp / einstein-1 dm3
wavelengths / nm
O-DEA
β exp / einstein-1 dm3
wavelengths / nm

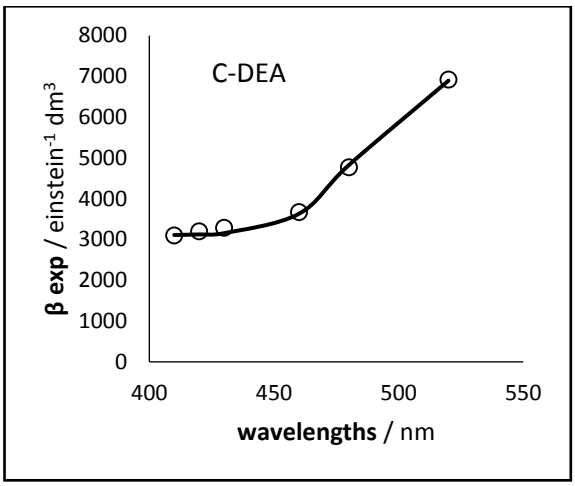

Figure V- 2: Calculated $\beta_{\lambda_{irr}}$ values (circles) for t-STIL, PINO, RVT, ORVT, PTERO, O-DAE and C-DAE using Eq. 5-3 and the values of $k_{A\rightleftharpoons B}^{\lambda_{irr}}$ and $P_{\lambda_{irr}}$ provided in Table 5-4, Chapter 5. The sigmoid model, Eq. 9-1 (line) and linear equation (tringle shape, Eq.9-2) of studies compounds and O-DAE, respectively, were used to fit the experimental data.

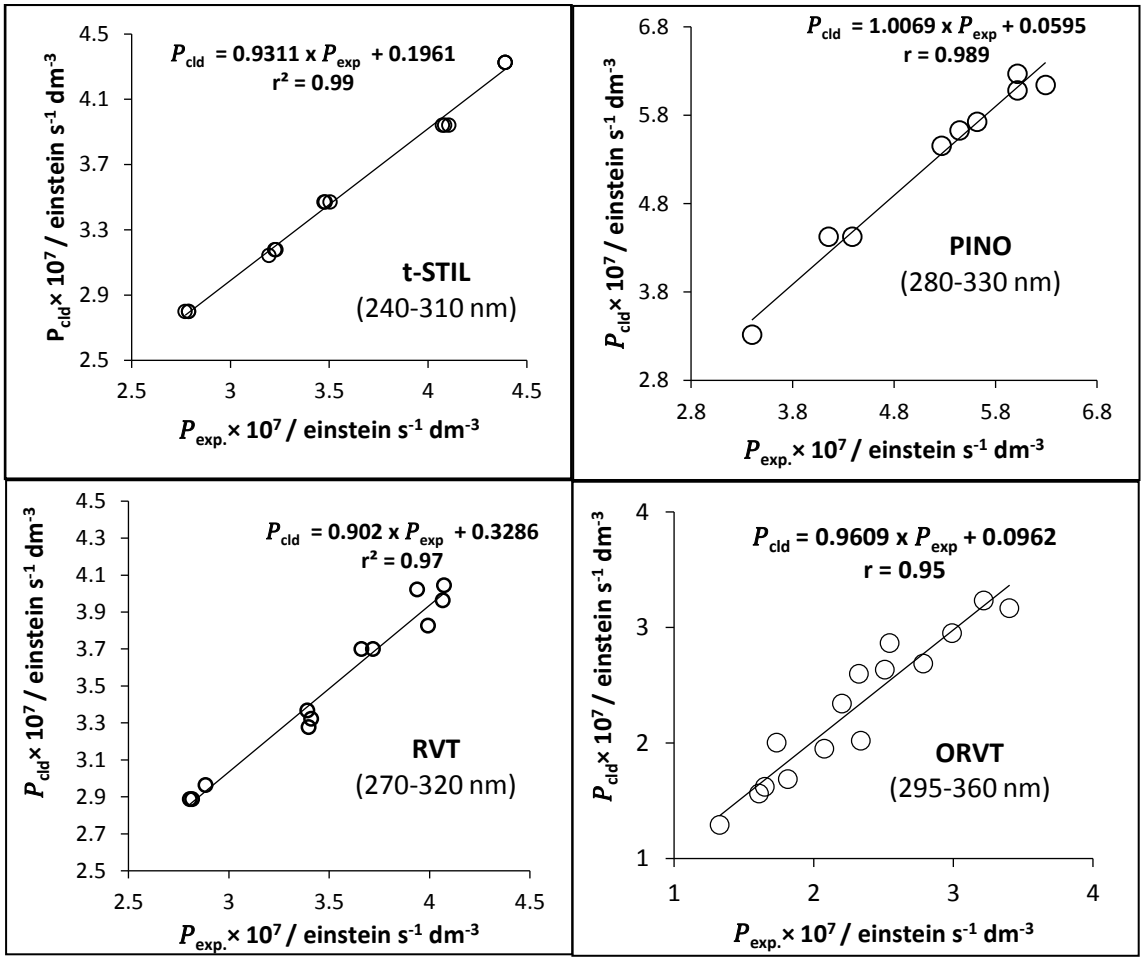

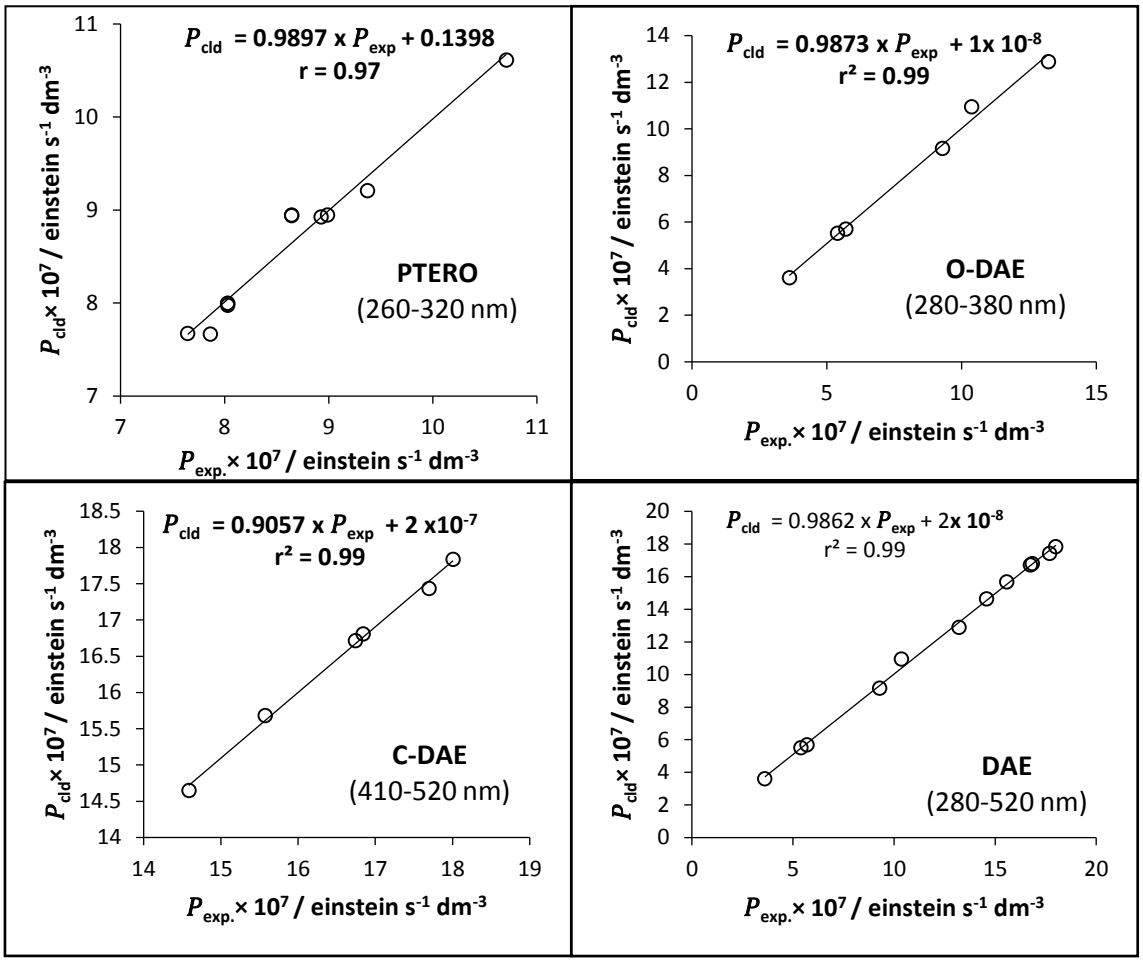

Figure V- 3: Linear correlation of experimental $P_{exp.}$ with calculated $P_{cld.}$ values of the radiant power for studied compounds after using a new method Eq. 9-1 to calculate $\beta_{\lambda_{irr}}$ values.

2. Actinometry under polychromatic irradiation study

2.1. Φ-order kinetic

Table V-2. Actinometry study of C-DAE

C_A (0)× 10^6 / M	$P_{exp.}$× 10^6 / einstein s^{-1} dm^{-3}	- Slope× 10^7 / min^{-1}	- Slope× 10^7 / sec^{-1}	k / min^{-1}	k / sec^{-1}	α× 10^7 / min^{-1}	α× 10^7 / sec^{-1}
4.26	3.22	1.57	0.026	0.95	0.016	1.56	0.026
4.35	3.82	3.39	0.057	2	0.033	3.28	0.055
4.33	4.19	4.58	0.076	2.9	0.048	4.76	0.079
4.35	4.63	5.59	0.093	3.5	0.058	5.75	0.096
4.34	5.24	7.59	0.127	4.9	0.082	8.05	0.134
4.32	6.04	10.10	0.168	6.4	0.107	10.51	0.172

*$\sum \varepsilon_B$ is 1323914.19 M^{-1} cm^{-1}

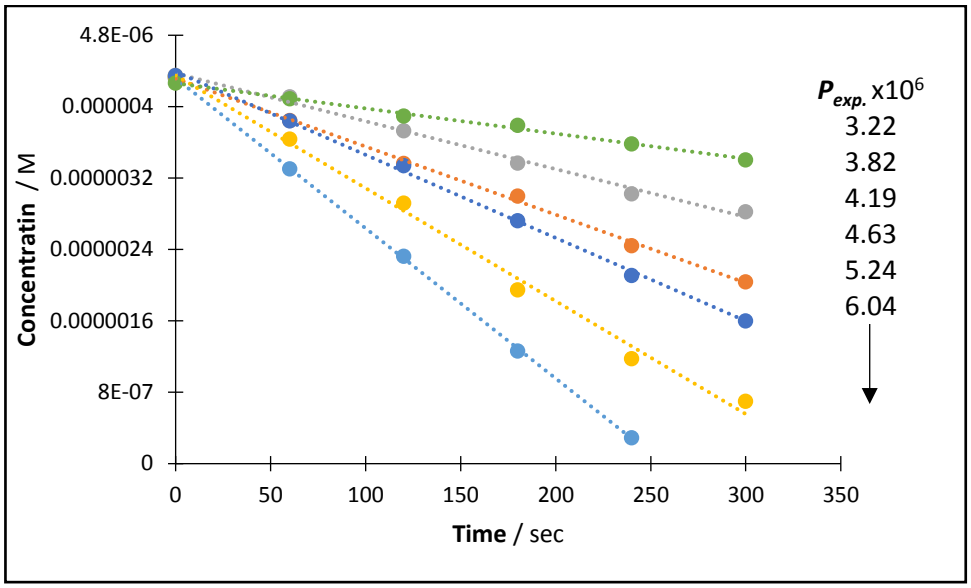

Figure V- 4: Photokinetic traces of C-DAE at different $\sum_{400}^{600} P_{exp.}$ with similar concentration.

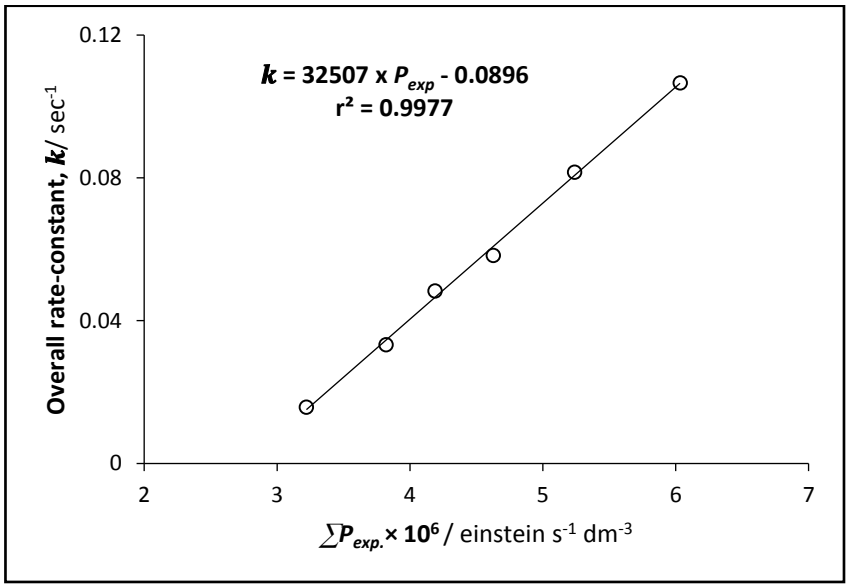

Figure V- 5: Linear relation between Overall rate-constant (k) and $\sum P_{exp.}$ of C-DAE under polychromatic light irradiation.

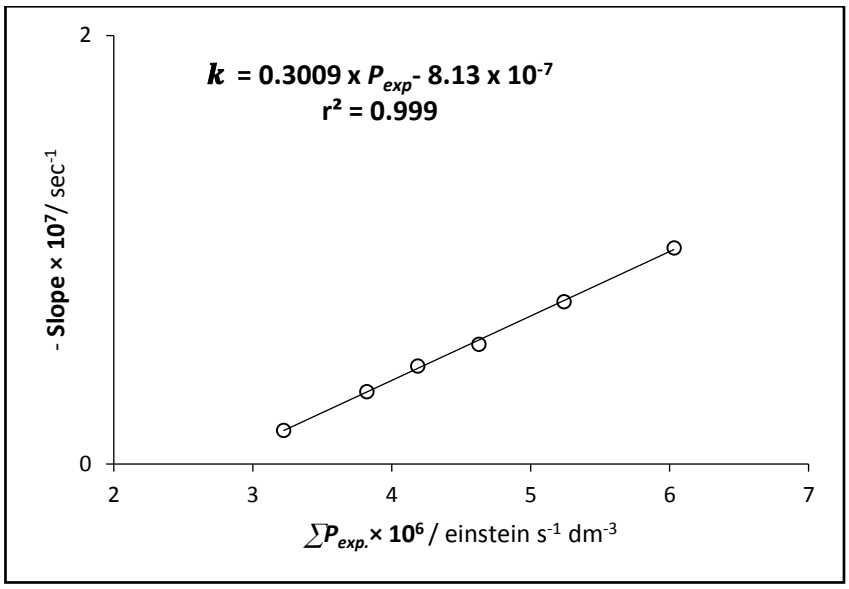

Figure V- 6: Linear relation between initial slope of photokinetic traces of C-DAE under polychromatic light irradiation with $\sum P_{exp.}$

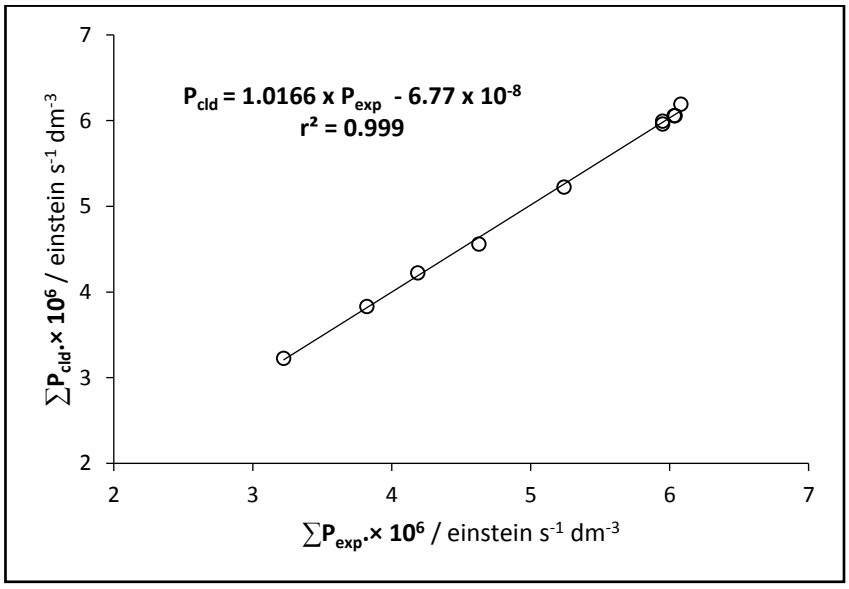

Figure V- 7: Linear relation between $\sum P_{cld.}$ *and* $\sum P_{exp.}$ *values of the radiant power for C-DAE after using method Eq. 9-4 to calculate* $\sum \beta_{\lambda_{irr}}$ *values.*

Table V-3. *$\sum \beta_{\lambda_{irr}}$ factor values with different simulated lamps profiles with same summation of the light intensity value ($P_{simulation.}$).*

#	$\sum_{400}^{600} P_{simulation.}$ × 10^6 / einstein s^{-1} dm^{-3}	k / s^{-1}	Factor	β / einstein^{-1} dm^3	$\sum_{400}^{600} P_{cld.}$ × 10^6 / einstein s^{-1} dm^{-3}
Exp.	5.95	0.009310789	-	1564.29	5.95
1	5.95	0.018651	2.767	3134.9	5.95
2	5.95	0.015611	2.767	2623.7	5.95
3	5.95	0.0035	2.767	588.28	5.95
4	5.95	0.018513	2.767	3111.8	5.95
5	5.95	0.001928	2.767	323.97	5.95
6	5.95	0.009459	2.7665	1590	5.95
7	5.95	0.015096	2.767	2537.5	5.95
8	5.95	0.01149	2.767	1931.3	5.95
9	5.95	0.014813	2.767	2489.8	5.95

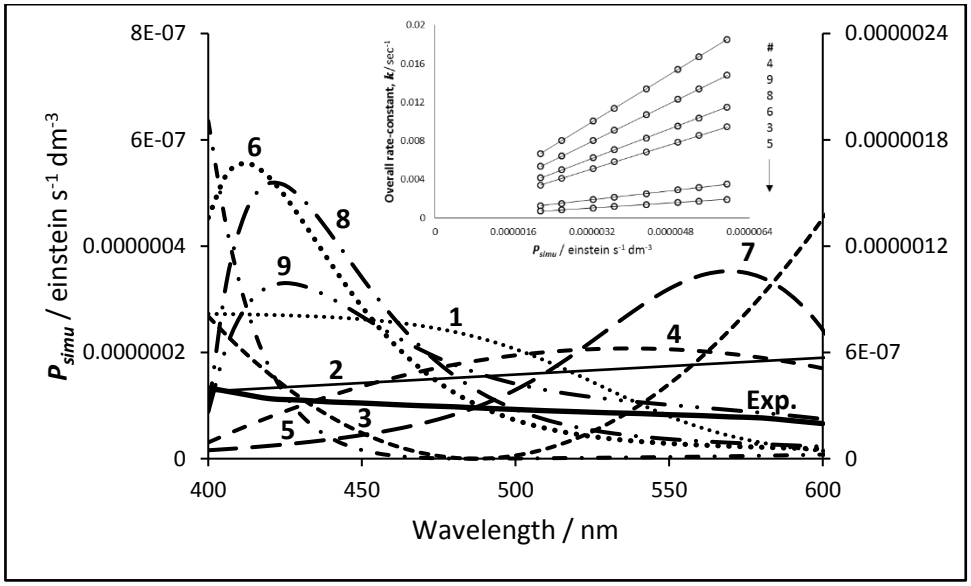

Figure V-8: light profile of different simulated lamps.

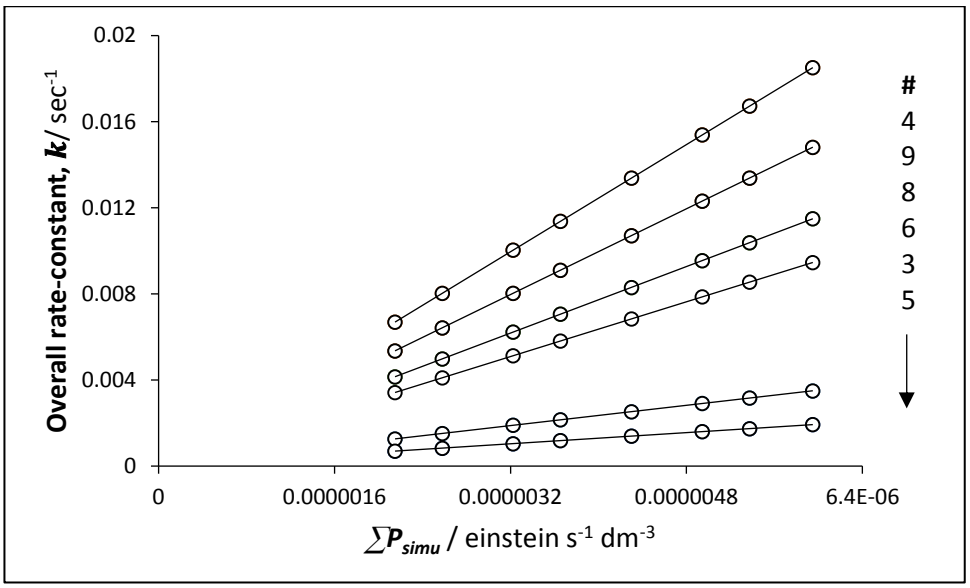

Figure V- 9: Linear relation between Overall rate-constant (k) and $\sum P_{simu}$. values of the radiant power for simulated lamps.

2.2. η-order

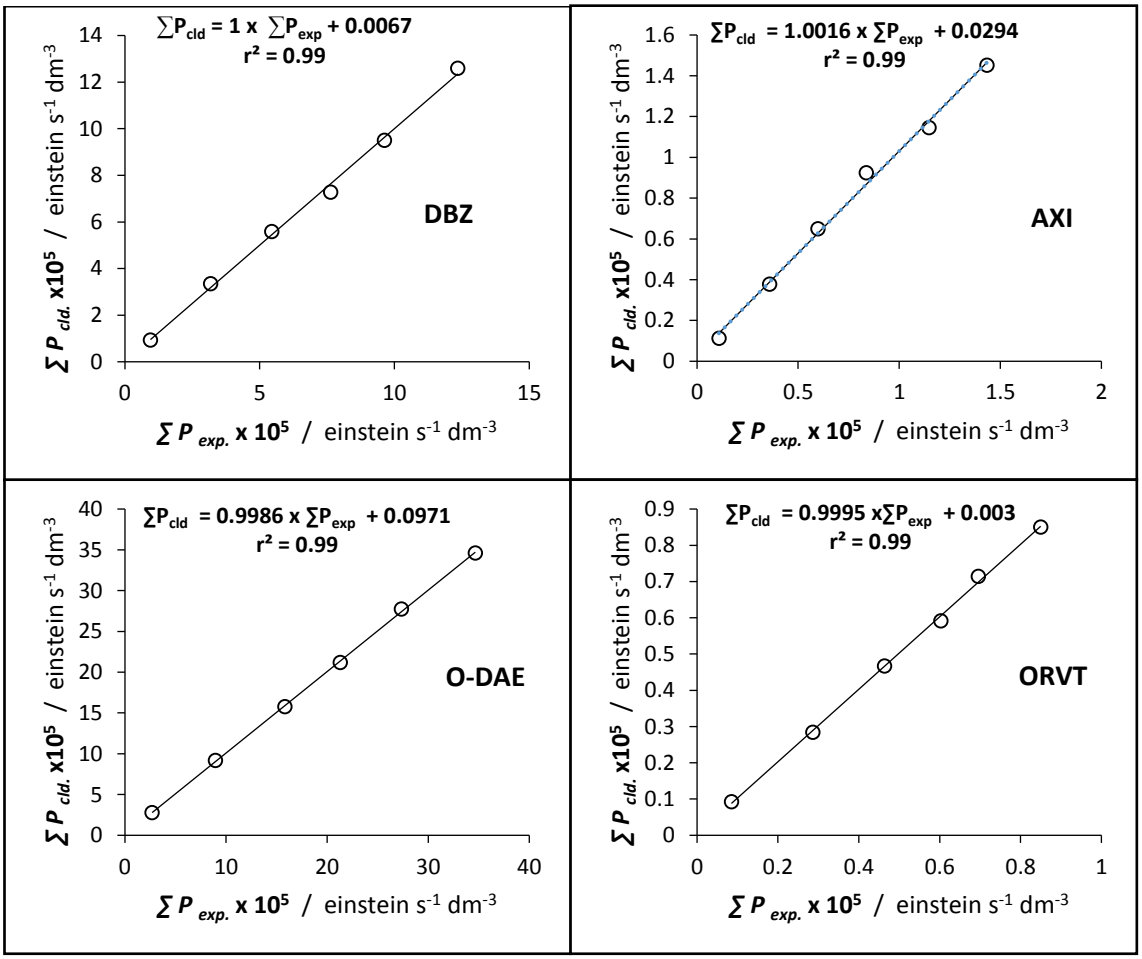

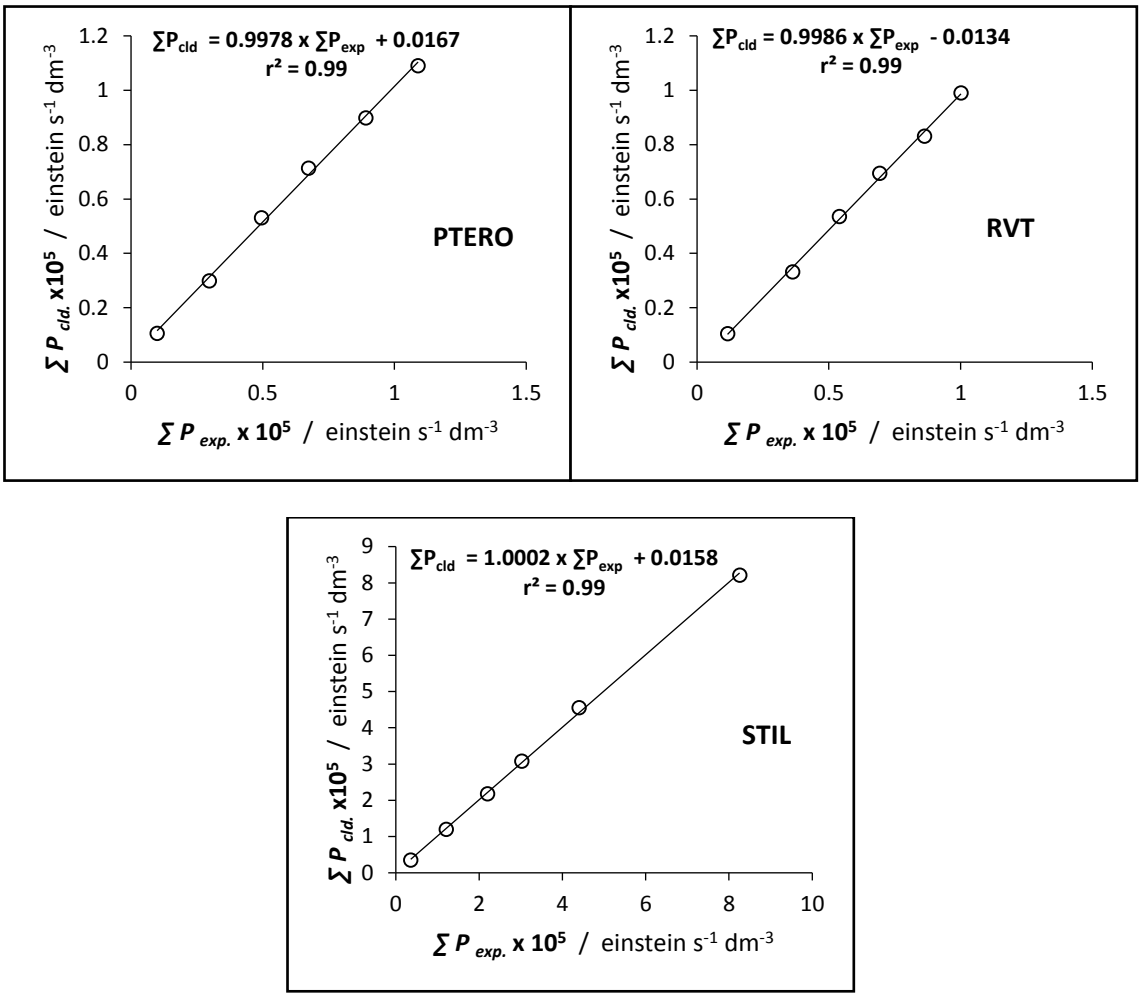

Figure V- 10: Linear correlation of experimental (∑ P exp..) and calculated (∑ P cld..) values for the radiant power for studied compounds under irradiation by polychromatic light using mix wavelength lamp (254/365 nm).

Appendix VI-A

The model proposed by Mazellier et al. for photochemical reaction of the AB $(1\Phi)_{\varepsilon_{B\neq 0}}$ system under monochromatic light irradiation

The photochemical reaction of the AB $(1\Phi)_{\varepsilon_{B\neq 0}}$system under monochromatic light irradiation:

In the model proposed was first proposed by Zepp [1] and a similar method was proposed by Mazellier et al. [2] was used the same differential equation (Eq. 5-21) that is the general photochemical rate law for an AB $(1\Phi)_{\varepsilon_{B\neq 0}}$.

$$-\frac{dC_A}{dt} = \Phi_{A\to B} P_{abs,\lambda_{irr}} \qquad \text{Eq.VI-A1}$$

Or by expressing, fully the rate law,

$$-\frac{dC_A}{dt} = \Phi_{A\to B} P_{0,\lambda_{irr}} \frac{\left(1-10^{-\left(\varepsilon_A^{\lambda_{irr}} C_A(t)+\varepsilon_B^{\lambda_{irr}} C_B(t)\right)l}\right)}{\left(\varepsilon_A^{\lambda_{irr}} C_A(t)+\varepsilon_B^{\lambda_{irr}} C_B(t)\right)l} \varepsilon_A^{\lambda_{irr}} C_A(t) l \qquad \text{Eq.VI-A2}$$

Then, if the total absorbance is lower than 0.02 [2], which can mean that the concentration of the compound is low, a Simpson expansion can be performed.

$$e^{-x} = 1 - x + \frac{x^2}{2!} - \frac{x^3}{3!} + \cdots \qquad \text{Eq.VI-A3}$$

So, if we consider

$$x = 1 - e^{-2.303-\left(\varepsilon_A^{\lambda_{irr}} C_A(t)+\varepsilon_B^{\lambda_{irr}} C_B(t)\right)l} = 1 - e^{-x} \qquad \text{Eq.VI-A4}$$

When x is less than 0.02, then the higher order terms $\frac{x^2}{2!}, \frac{x^3}{3!}, \ldots$ in Eq. (Eq.VI-A4) can be assumed small. So, Eq.VI-A4 become

$$1 - e^{-2.303-\left(\varepsilon_A^{\lambda_{irr}} C_A(t)+\varepsilon_B^{\lambda_{irr}} C_B(t)\right)l} = -2.303 - \left(\varepsilon_A^{\lambda_{irr}} C_A(t) + \varepsilon_B^{\lambda_{irr}} C_B(t)\right) l \qquad \text{Eq.VI-A5}$$

Therefore, Eq.VI-A2 gives

$$\frac{dC_A}{dt} = 2.303\ \Phi_{A\rightarrow B} P_{0,\lambda_{irr}} l \varepsilon_A^{\lambda_{irr}} C_A(t) \qquad \text{Eq.VI-A6}$$

The author's considered the quantum yield to be constant during the photoreaction. So, by integrating Eq.VI-A7

$$\ln \frac{C_A(t)}{C_A(0)} = -2.303\ \Phi_{A\rightarrow B} P_{0,\lambda_{irr}} l \varepsilon_A^{\lambda_{irr}} t = -kt \qquad \text{Eq.VI-A7}$$

In this procedure, the author's relied on the expansion of the exponential term because they considered that a closed form integration of Eq.VI-A2 is impossible; which is true. However, using the expansion of the e^{-x} comes at equation. That is, the find integrated rate- law is the same to the one that would be obtained for an AB $(1\Phi)_{\varepsilon_{B=0}}$ system using the same procedure. In other word, the two systems should, according to this approach, have the same kinetic behaviour. This is not correct in absolute, because it was, for instances, proved [3] that the rate of AB $(1\Phi)_{\varepsilon_{B=0}}$ depends only on A_A(t) while that of AB $(1\Phi)_{\varepsilon_{B\neq 0}}$ depends on both (A_A(t) + A_B(t)). This limits the usefulness of the proposed equation

VI-A. References:

1- Zepp RG. Quantum Yields for Reaction of Pollutants in Dilute Aqueous Solution. Environmental Science and Technology. 1978; 12(3): 327–329.
2- Nassar R., Trivella A., Mokh S., Al-Iskandarani M., Budzinski H., Mazellier P. Photodegradation of sulfamethazine, sulfamethoxypiridazine, amitriptyline, and clomipramine drugs in aqueous media. Journal of Photochemistry and Photobiology A: Chemistry. Elsevier B.V.; 2017; 336: 176–182.
3- Maafi M., Brown RG. The kinetic model for AB(1φ) systems. Journal of Photochemistry and Photobiology A: Chemistry. April 2007; 187(2–3): 319–324.

Appendix VI-B

The model proposed by Stadler et al. for photochemical reaction of the AB $(1\Phi)_{\varepsilon_{B\neq 0}}$ system under monochromatic light irradiation.

The photochemical reaction of the AB $(\mathbf{1\Phi})_{\varepsilon_{B\neq 0}}$system under monochromatic light irradiation.

In the model proposed in 2018 by Stadler et al. [1] was used the same differential equation (Eq. 5-21) is came from general photochemical rate law.

$$\frac{dC_A}{dt} = -\Phi_{A\to B} P_{abs,\lambda irr} \quad \text{Eq.VI-B1}$$

By using the absorbance rather than the concentration.

$$A_{tot}^{\lambda_{irr}}(t) = A_A^{\lambda_{irr}}(t) + A_B^{\lambda_{irr}}(t) \quad \text{Eq.VI-B2}$$

According to beer's lambert law

$$A_{tot}(t) = \varepsilon_A\, C_A(t) l + \varepsilon_B\, C_B(t) l \quad \text{Eq.VI-B2}$$

And

$$C_{tot}(0) = C_A(0) = C_A(t) + C_B(t) \quad \text{Eq.VI-B3}$$

$$C_B(t) = C_A(0) - C_A(t) \quad \text{Eq.VI-B4}$$

By using Eq.VI-B4 into Eq.VI-B2 is given

$$A_{tot}(t) = \varepsilon_A\, C_A(t) l + \varepsilon_B\, C_A(0) l - \varepsilon_B\, C_A(t) \quad \text{Eq.VI-B5}$$

$$A_{tot}(t) = C_A(t) l(\varepsilon_A - \varepsilon_B) + \varepsilon_B\, C_A(0) l \quad \text{Eq.VI-B6}$$

By differentiating over time Eq.VI-B6 is given

$$\frac{dA_{tot}(t)}{dt} = l(\varepsilon_A - \varepsilon_B)\frac{dC_A(t)}{dt} + \varepsilon_B\, l \frac{dC_A(0)}{dt} \quad \text{Eq.VI-B7}$$

Then,

$$\frac{dA_{tot}(t)}{dt} = l(\varepsilon_A - \varepsilon_B)\frac{dC_A(t)}{dt} \quad \text{Eq.VI-B8}$$

Using Eq.VI-B8 into Eq.VI-B1,

$$\frac{dA_{tot}(t)}{dt} = -\Phi_{A\to B} P_{abs,\lambda irr} l(\varepsilon_A - \varepsilon_B) \quad \text{Eq.VI-B9}$$

When compound A completely transform to B at (∞)

$A_{tot}(\infty) = \varepsilon_B\, C_A(0) l$,and $A_{tot}(0) = \varepsilon_A\, C_A(0) l$ Eq.VI-B10

Using Eq.VI-B10 into Eq.VI-B9

$\frac{dA_{tot}(t)}{dt} = -\Phi_{A\to B} P_{abs,\lambda irr} l(\frac{A_{tot}(0)-A_{tot}(\infty)}{C_A(0)})$ Eq.VI-B11

Eq.VI-B11 is the differential equation derived by the Stadler et al. [1] at time (t). The author's proposed to use the initial phase of the reaction in ordered to determine the quantum yield by:

$\Phi_{A\to B} = \frac{k_{fit} C_A(0)}{P_{0,\lambda_{irr}}\left(1-10^{-\varepsilon_A C_A(0) l_{irr}}\right)}$ Eq.VI-B12

Where k_{fit} represents the initial slope of the trace of the reaction. This Eq.VI-B12 is, however not correlated in an observes way to Eq.VI-B11. So, let us derives the expression of k_{fit} from the Eq.VI-B11 as shown by the authors.

Accordingly, at t=0 we have,

$\left(\frac{dA_{tot}(t)}{dt}\right)_{t=0} = -\Phi_{A\to B} P_{0,\lambda_{irr}}\left(1-10^{-\varepsilon_A C_A(0) l_{irr}}\right)(\frac{A_{tot}(0)-A_{tot}(\infty)}{C_A(0)})$ Eq.VI-B13

By rearrange the Eq.VI-B13 to obtained the quantum yield is give as

$\Phi_{A\to B} = \left(\frac{dA_{tot}(t)}{dt}\right)_{t=0} \times \frac{-1}{(A_{tot}(0)-A_{tot}(\infty)))} \times \frac{C_A(0)}{P_{0,\lambda_{irr}}\left(1-10^{-\varepsilon_A C_A(0) l_{irr}}\right)}$ Eq.VI-B14

Comparing Eq.VI-B13 and Eq.VI-B11

$k_{fit} = \frac{-\left(\frac{dA_{tot}(t)}{dt}\right)_{t=0}}{(A_{tot}(0)-A_{tot}(\infty)))}$ Eq.VI-B15

The author's state that the k_{fit} was obtained from the fitting of the experimental date by using first order model.

$$A_{tot}(t) = A_{tot}(0) - (1 - (A_{tot}(\infty) - A_{tot}(0))e^{-k_{fit}t}) \quad \text{Eq.VI-B16}$$

with k_{fit} here represents the rate-constant of the 1st- order reaction.

By derivative over time Eq.VI-B16 is given

$$\frac{dA_{tot}(t)}{dt} = (A_{tot}(\infty) - A_{tot}(0)k_{fit}\, e^{-k_{fit}t} \quad \text{Eq.VI-B17}$$

Accordingly, at t=0 we have,

$$\left(\frac{dA_{tot}(t)}{dt}\right)_{t=0} = \left(A_{tot}(\infty) - A_{tot}(0)\right) k_{fit} \quad \text{Eq.VI-B18}$$

By rearrange Eq.VI-B18,

$$k_{fit} = \frac{\left(\frac{dA_{tot}(t)}{dt}\right)_{t=0}}{(A_{tot}(\infty) - A_{tot}(0))} \quad \text{Eq.VI-B19}$$

According to deviation proposed above by the author's, it is clear that the equation of the rate for the photochemical reaction equation as given by Eq.VI-B1 and Eq.VI-B9 is effectively equal to the first order rate equation Eq.VI-B17 since their rate-constant are equal using the value obtained from Eq.VI-B18 and Eq.VI-B11. This identity is not valid. Therefore, such an approximation cannot doubt on the validity of the result obtained.

VI-B. References:

1- Stadler E., Eibel A., Fast D., Freißmuth H., Holly C., Wiech M., et al. A versatile method for the determination of photochemical quantum yields: Via online UV-Vis spectroscopy. Photochemical and Photobiological Sciences. Royal Society of Chemistry; 2018; 17(5): 660–669.

Appendix VI-C

The model proposed for photochemical reaction of the AB (2Φ) system under monochromatic light irradiation

The photochemical reaction of the AB (2Φ) system under monochromatic light irradiation:

Method was reported by Irie group [1]:

$$\frac{dC_B}{dt} = \frac{1000 \times P_{0,\lambda_{irr}}}{l}\left(\Phi_{A\to B}^{\lambda_{irr}}\left(1-10^{-\varepsilon_A^{\lambda_{irr}}C_A(t)l}\right)-\Phi_{B\to A}^{\lambda_{irr}}\left(1-10^{-\varepsilon_B^{\lambda_{irr}}C_B(t)l}\right)\right) \quad \text{Eq.VI-C1a}$$

By using the expansion (assuming $\varepsilon_A^{\lambda_{irr}}C_A(t)l$ must be less than 0.2) in Eq.VI-C1a

$$\frac{dC_B}{dt} = 2.303 \times 1000 \times P_{0,\lambda_{irr}}(\Phi_{A\to B}^{\lambda_{irr}}\varepsilon_A^{\lambda_{irr}}C_A(t) - \Phi_{B\to A}^{\lambda_{irr}}\varepsilon_B^{\lambda_{irr}}C_B(t)) \quad \text{Eq.VI-C1b}$$

In this proposed (Eq.VI-C1a) the reactive system looks like having two independent compounds (A and B). this means that according to the above equation A absorbs of $P_{0,\lambda_{irr}}$ independently of B and vice versa. But this does not correspond to the physical systems where $P_{0,\lambda_{irr}}$ is absorbed by both A and B. Accordingly there is a missing factor in Eq. IC1a to indicate that the light is simultaneously absorbed by both species A and B (i.e. $P_{0,\lambda_{irr}}\left(1-10^{-\varepsilon_A^{\lambda_{irr}}C_A(t)l}\right)$). Thus, Eq.VI-C1a does not correspond to the physical system studied.

VI-C. References:

1- Nakashima H., Irie M. Synthesis of silsesquioxanes having photochromic dithienylethene pendant groups. Macromolecular Chemistry and Physics. John Wiley & Sons, Ltd; 1 April 1999; 200(4): 683–692.

Appendix VI-D

The model proposed for photochemical reaction of the AB $(\mathbf{1\Phi})_{\varepsilon_{B\neq 0}}$ system under polychromatic light irradiation

The photochemical reaction of the AB $(\mathbf{1\Phi})_{\varepsilon_{B\neq 0}}$system under polychromatic light irradiation:

In the model was proposed by Lente et al. [1], according to the quantification of the quantum yield at the maximum observation wavelength used Eq. (VI-D2):

$$\frac{dC_A}{dt} = -\Phi_{A\to B} P_{abs,\lambda irr} \quad \text{Eq.VI-D1a}$$

$$\frac{dC_A}{dt} = -\Phi_{A\to B} \sum_{\lambda_{irr}\,min}^{\lambda_{irr}\,max} \frac{\varepsilon_A^{\lambda_{irr}} C_A(t)}{\varepsilon_A^{\lambda_{irr}} C_A(t) + \varepsilon_B^{\lambda_{irr}} C_{B,i}(t)} P_{0,\lambda_{irr}} \left(1 - 10^{-\varepsilon_A^{\lambda_{irr}} C_A(t) l - \varepsilon_B^{\lambda_{irr}} C_{B,i}(t) l}\right) \quad \text{Eq.VI-D1b}$$

$$\Phi_{A\to B} = \frac{\alpha V}{\left(\varepsilon_A^{\lambda_{obs}} - \varepsilon_B^{\lambda_{obs}}\right) l_{obs}} \quad \text{Eq.VI-D2}$$

In order to driven the Eq.VI-D2 form Eq.III-A1, by using the absorbance rather than the concentration.

$$A_{tot}^{\lambda_{irr}}(t) = A_A^{\lambda_{irr}}(t) + A_B^{\lambda_{irr}}(t) \quad \text{Eq.VI-D3}$$

According to beer's lambert law

$$A_{tot}(t) = \varepsilon_A\, C_A(t) l + \varepsilon_B\, C_B(t) l \quad \text{Eq.VI-D4}$$

And

$$C_{tot}(0) = C_A(0) = C_A(t) + C_B(t) \quad \text{Eq.VI-D5}$$

$$C_B(t) = C_A(0) - C_A(t) \quad \text{Eq.VI-D6}$$

By using Eq.VI-D6 into Eq.VI-D4 is given

$$A_{tot}(t) = \varepsilon_A\, C_A(t) l + \varepsilon_B\, C_A(0) l - \varepsilon_B\, C_A(t) \quad \text{Eq.VI-D7}$$

$$A_{tot}(t) = C_A(t) l(\varepsilon_A - \varepsilon_B) + \varepsilon_B\, C_A(0) l \quad \text{Eq.VI-D8}$$

By differentiating over time Eq.VI-D8 is given

$$\frac{dA_{tot}(t)}{dt} = l(\varepsilon_A - \varepsilon_B)\frac{dC_A(t)}{dt} + \varepsilon_B\, l \frac{dC_A(0)}{dt} \quad \text{Eq.VI-D9}$$

Then,

$$\frac{dA_{tot}(t)}{dt} = l(\varepsilon_A - \varepsilon_B)\frac{dC_A(t)}{dt}$$ Eq.VI-D10

Using Eq.VI-D10 into Eq.VI-D1,

$$\frac{dA_{tot}(t)}{dt} = -\Phi_{A\to B}P_{abs,\lambda irr}l(\varepsilon_A - \varepsilon_B)$$ Eq.VI-D11

where α in Eq.VI-D2 is the slope obtained from the linear correlation of ν_0 against photon count N.

Where $N = \int_{\lambda_{irr}\,min}^{\lambda_{irr}max} P_{0,\lambda_{irr}}\left(1 - 10^{-A_{tot}^{\lambda_{irr}}}\right)d\lambda_{irr}$ Eq.VI-D12

Accordingly, at t=0 we have,

$$\left(\frac{dA_{tot}(t)}{dt}\right)_{t=0} = -\Phi_{A\to B}l(\varepsilon_A - \varepsilon_B)\sum_{\lambda_{irr}\,min}^{\lambda_{irr}\,max} P_{0,\lambda_{irr}}\left(1 - 10^{-\varepsilon_A^{\lambda_{irr}}C_A(0)l}\right)$$ Eq.VI-D13

By using photons absorbed by the system per volume (V)

$$\left(\frac{dA_{tot}(t)}{dt}\right)_{t=0} = -\Phi_{A\to B}l(\varepsilon_A - \varepsilon_B)\frac{\sum_{\lambda_{irr}\,min}^{\lambda_{irr}\,max} P_{0,\lambda_{irr}}\left(1-10^{-\varepsilon_A^{\lambda_{irr}}C_A(0)l}\right)}{V}$$ Eq.VI-D14

Then α was given as

$$\alpha = \frac{-\Phi_{A\to B}l(\varepsilon_A - \varepsilon_B)}{V}$$ Eq.VI-D15

By rearrange Eq.III-A15, we will get Eq.III-A2.

Given the complexity of the basic of Eq.VI-D1b, the authors have avoided these issues by only using the initial rates.

If reformate write

$$\frac{dC_A}{dt} = -\Phi_{A\to B}\left[\alpha_1 P_{0,\lambda_{irr}(1)}(1 - 10^{-\gamma_1}) + \alpha_2 P_{0,\lambda_{irr}(2)}(1 - 10^{-\gamma_2})\right]$$ Eq.VI-D16

$$\frac{dC_A(1)}{dt} = -\Phi_{A\to B}\left[\alpha_1 P_{0,\lambda_{irr}(1)}(1-10^{-\gamma_1})\right] \quad \text{Eq.VI-D17}$$

$$\frac{dC_A(2)}{dt} = -\Phi_{A\to B}\left[\alpha_2 P_{0,\lambda_{irr}(2)}(1-10^{-\gamma_2})\right] \quad \text{Eq.VI-D18}$$

$$\frac{dC_A}{dt} = \frac{dC_A(1)}{dt} + \frac{dC_A(2)}{dt} \quad \text{Eq.VI-19}$$

If the kinetic at λ_{irr} (1) is done and then in second experiment the kinetics at λ_{irr}(2) is done as well independently, and if we add the two kinetics we should find the kinetics of the sample irradiated with both λ_{irr} (1) and λ_{irr} (2). But this does not correspond to the physical system where the kinetic was happen in the same time and we cannot know the kinetic start from each experiment. It is clear that the closed form integration of the Eq.VI-D1b is difficult.

VI-D. References:

1- Fábián I., Lente G. Light-induced multistep redox reactions: The diode-array spectrophotometer as a photoreactor. Pure and Applied Chemistry. 2010; 82(10): 1957–1973.